

2013-01-01

Geochemical Characterization Of Mineral Dust Sources In The Chihuahuan Desert And Southern High Plains Regions

Porfirio Peinado

University of Texas at El Paso, ppeinado@miners.utep.edu

Follow this and additional works at: https://digitalcommons.utep.edu/open_etd

 Part of the [Environmental Engineering Commons](#), and the [Environmental Sciences Commons](#)

Recommended Citation

Peinado, Porfirio, "Geochemical Characterization Of Mineral Dust Sources In The Chihuahuan Desert And Southern High Plains Regions" (2013). *Open Access Theses & Dissertations*. 1903.
https://digitalcommons.utep.edu/open_etd/1903

This is brought to you for free and open access by DigitalCommons@UTEP. It has been accepted for inclusion in Open Access Theses & Dissertations by an authorized administrator of DigitalCommons@UTEP. For more information, please contact lweber@utep.edu.

GEOCHEMICAL CHARACTERIZATION OF MINERAL DUST SOURCES
IN THE CHIHUAHUAN DESERT AND SOUTHERN HIGH PLAINS REGIONS

PORFIRIO PEINADO

Environmental Science and Engineering Program

APPROVED:

Thomas E. Gill, Ph.D., Chair

Jeffrey A. Lee, Ph.D.

Russell R. Chianelli, Ph. D.

Charles D. Turner, Ph.D.

William S. Walker, Ph. D.

Benjamin C. Flores, Ph.D.
Dean of the Graduate School

Copyright ©

By

Porfirio Peinado

2013

Dedication

Instituto Tecnológico de Los Mochis

Juan de Dios Bátiz 81259. Los Mochis, Sinaloa.

‘Everything passes and everything stays,

But our fate is to pass,

To pass making paths,

Paths on the sea’

----- Antonio Machado’s Cantares

GEOCHEMICAL CHARACTERIZATION OF MINERAL DUST SOURCES
IN THE CHIHUAHUAN DESERT AND SOUTHERN HIGH PLAINS REGIONS

by

PORFIRIO PEINADO, M.S.

DISSERTATION

Presented to the Faculty of the Graduate School of

The University of Texas at El Paso

in Partial Fulfillment

of the Requirements

for the Degree of

DOCTOR OF PHILOSOPHY

Environmental Science and Engineering Program

THE UNIVERSITY OF TEXAS AT EL PASO

May 2013

Acknowledgements

I would like to express my gratitude to my Committee Chair Dr. Thomas E. Gill, for having given me the opportunity to pursue the terminal degree of my academic career under his tutelage. I am grateful to Dr. Jeffrey A. Lee, Dr. Russell R. Chianelli, Dr. Charles D. Turner, and Dr. William S. Walker for consenting to be part of my Ph. D. dissertation committee.

I express my sincere gratitude to Dr. Arturo Woocay for his guidance and patience with all my questions regarding to ordinary analysis techniques. I am really thankful to Dr. Irasema Coronado for her support, positive vibes and cheerfulness that brought hope to me during challenging times. I wish to thank Dr. Minghua Ren for assistance with ICP-OES analyses and sample preparation techniques.

The completion of my studies would not been possible without the generous funding from the ESE Ph.D. program, and the National Council of Science and Technology grant scholarship for graduate studies in foreign countries.

I thank my friends for their care. But most importantly, this momentous achievement would not have been possible without the love and support showered on me by my mother, father, sisters and brothers.

Abstract

The Chihuahuan Desert (northern Chihuahua, southern New Mexico, and far west Texas) and the southern High Plains (west Texas and eastern New Mexico) regions have been identified as one of the most persistent dust producing regions of North America. Regional-scale dust storms have been observed by satellite imagery to identify sources of dust, resulting in collection and examination of physical soil samples to better understand the source signatures (geochemical characteristics) of dust origins in these two regions.

The soil characteristics were examined through several techniques: Particle Size Distribution, X-Ray Diffraction (XRD), Inductively Coupled Plasma Optical Emission Spectrometry (ICP-OES), and Total Organic Carbon. Numerous ordination analysis techniques were applied to the data. These results were used to interpret associations between elemental, mineral, and geological content on the dust-producing soil samples and the associated dust emission “hotspots” in the Chihuahuan Desert and Southern High Plains regions, and develop a database of the geochemical and physical attributes of dust producing soils in these adjacent regions.

Granulometric data emphasized that dust source soils from the Chihuahuan Desert were less sandy textured when compared to those soil samples from the Southern High Plains region. Potassium, iron, aluminum, and titanium concentrations showed strong connectivity to anthropogenic activity (land use for farming). A cluster of samples with enhanced concentrations of heavy metals (arsenic, lead, copper, and chromium) appeared in rangeland sites, where land development and oil field activities were observed. The clay soil fraction emitted from dust storm sites was significantly associated with alkali earth metals (calcium, magnesium, and

strontium) prone to traveling across the region in this fine particle fraction. Calcite, dolomite and gypsum were characteristic of dust storm sites in the Chihuahuan Desert, gypsum in the USA and the carbonates in the Mexican region of the Chihuahuan Desert. Southern High Plains region samples were dominated by quartz. Contoured mapping confirmed concentration affinities on the components mentioned above.

Overall, this study shows an intricate linkage between the Southern High Plains and the Chihuahuan Desert regions as one regional-scale geoenvironmental system with combined effects on populations as a mineral aerosol source. These results can be used as a source apportionment tool to better understand and trace the environmental impacts of mineral dust storms locally, regionally, and continentally.

Table of Contents

	Page
Acknowledgements.....	v
Abstract.....	vi
Table of Contents.....	viii
List of Figures.....	xiv
List of Tables.....	xix
Chapter 1 Introduction.....	1
1.1 Problem Statement.....	2
1.2 Hypothesis.....	4
Chapter 2 Literature Review.....	5
2.1 The Chihuahuan Desert.....	5
2.1.1 Location and Limits.....	5
2.1.2 Climate.....	6
2.1.3 Soils.....	7
2.1.4 Aeolian Processes.....	7
2.1.5 Previous Work.....	8
2.2 The Southern High Plains.....	9
2.2.1 Locations and Limits.....	9
2.2.2 Climate.....	10
2.2.3 Soils.....	10
2.2.4 Aeolian Processes.....	12

Chapter 3 Technologies to be used for Analysis	14
3.1 Laser Diffractometry	14
3.2 Total Organic Carbon.....	15
3.3 X – Ray Diffraction.....	16
3.4 Inductively Coupled Plasma Optical Emission Spectrometry (ICP-OES).....	16
3.5 Experimental Design	17
3.5.1 Geographical Information System (GIS) mapping.	17
3.5.2 Land Use/Land cover soilborne dust sources mapping.	18
3.5.3 Particle Size Distribution.	18
3.5.4 X – Ray Diffraction.	19
3.5.5 Inductively Coupled Plasma Optical Emission Spectroscopy (ICP-OES).	19
3.5.6 Total Organic Carbon.	20
3.5.7 Statistical Analysis.....	20
Chapter 4 Laser Diffractometry	22
4.1 Granulometric results of the Southern High Plains region	22
4.1.1 Soil Texture Triangle – Southern High Plains dust source sites.....	38
4.2 Granulometric results of the Chihuahuan Desert region.....	39
4.2.1 Soil Texture Triangle – Chihuahuan Desert dust source sites	42
Chapter 5 Total Organic Carbon.....	43
5.1 Calibration Curve	43
5.2 Total Organic Carbon Methodology	45
5.2.1 Total Organic Carbon Methodology	45
5.3 TOC Results for Southern High Plains samples	46

5.4	TOC Results for the Chihuahuan Desert USA region	49
5.5	TOC Results for the Chihuahuan Desert MEX region.....	51
Chapter 6 Development of Land Use Classes and Geomorphic Surface Types.....		71
6.1	Developing Land Use Categories.....	72
6.2	Dust Sources Characterization	75
6.2.1	Land Use Categories	75
6.2.2	Geomorphic Surfaces Classification.....	78
Chapter 7 X-Ray Diffraction		95
7.1	Preliminary Data Processing	95
7.2	Mineral analyses.....	98
7.2.1	Preliminary Results	98
7.2.2	Overlaying scan analysis.....	105
7.2.2.1	Quartz overlaid specimens.....	105
7.2.2.2	Quartz 2 θ peak matching chart.....	110
7.2.2.3	Pattern Overlays 3D view for quartz	111
7.2.2.4	2D contour plots for quartz.....	112
7.2.2.5	Gypsum overlaid specimens	113
7.2.2.6	Gypsum 2 θ peak matching chart	117
7.2.2.7	Pattern overlays 3D view for gypsum	118
7.2.2.8	2D contour plots for gypsum	119
7.2.2.9	Quartz + Calcite overlaid specimens	120
7.2.2.10	Quartz + Calcite 2 θ peak matching chart	126
7.2.2.11	Pattern overlays 3D view for quartz + calcite	127

7.2.2.12	2D contour plots for quartz + calcite	128
7.2.2.13	Quartz + Gypsum overlaid specimens	129
7.2.2.14	Quartz + Gypsum 2 θ peak matching chart	135
7.2.2.15	Pattern overlays 3D view for quartz + gypsum	136
7.2.2.16	2D contour plots for quartz + gypsum	137
7.2.2.17	Quartz + Calcite Magnesian + Dolomite overlaid specimens	138
7.2.2.18	Quartz + Calcite Magnesian + Dolomite 2 θ peak matching chart	145
7.2.2.19	Pattern overlays 3D view for quartz + calcite magnesian + dolomite	146
7.2.2.20	2D contour plots for quartz + calcite magnesian + gypsum	147
7.2.2.21	Quartz + Calcite + Sodium Plagioclase overlaid specimens	148
7.2.2.22	Quartz + Calcite + Sodium Plagioclase 2 θ peak matching chart	155
7.2.2.23	Pattern overlays 3D view for quartz + calcite + sodium plagioclase	156
7.2.2.24	2D contour plots for quartz + calcite + sodium plagioclase	157
Chapter 8 Inductively Coupled Plasma Optical Emission Spectrometry (ICP-OES)		158
8.1	Metallic Characterization	159
8.1.1	Relationships among standardized values of elemental concentrations and soil textures	160
8.1.2	Discussions	164
8.2	Relationship between standardized values of elemental concentrations and land use classes	166
8.2.1	Discussions	167
Chapter 9 Statistical Analysis		177
9.1	Cluster Analysis	177

9.1.1	Elemental Concentrations	178
9.1.1.1	Discussions	180
9.1.2	Dust Source Sites	182
9.1.2.1	Discussions	184
9.1.3	Narrowing Variables	191
9.1.3.1	Discussions after variables reduction	193
9.1.4	Narrowing Cases Observations	195
9.1.4.1	Discussions after cases reduction	199
9.2	Principal Component Analysis	206
9.2.1	Ordination analysis on original correlation matrix	207
9.2.2	Detecting Outliers	210
9.2.3	Ordination analysis on reduced correlation matrix	212
9.2.3.1	Detecting disrupted observations.....	216
9.2.3.2	Eliminating disrupted observations	217
9.2.4	Final ordination analysis on reduced correlation matrix.....	218
9.2.5	Mapping factors loading groups	221
9.2.6	Conclusions	222
Chapter 10	Summary and Conclusions.....	227
10.1	Particle Size Distribution.....	227
10.2	Land use codes and Land use categories association	230
10.3	Mineral Composition	235
10.4	Standardized value range analysis	240
10.5	Ordination Analysis	243

10.5.1	Preliminary Statistical Relationship.....	243
10.5.2	Refining Statistical Relationship.....	245
10.5.3	Narrowing Statistical Relationship	247
10.5.4	Principal Component Analysis	249
10.6	Connectivity Results Acquirement.....	256
10.6.1	Box Plot Analysis	259
10.6.2	Contour Plotting.....	272
	References Cited	275
Appendix A	X-Ray Diffraction Peak ID Reports	282
	Curriculum Vita	288

List of Figures

	Page
Figure 2.1 – The Chihuahuan Desert region.	5
Figure 2.2 – Southern High Plains region.	9
Figure 4.1 – Granulometric distribution of three soil texture classes.	25
Figure 4.2 – Granulometric distribution for Silt Loam soil texture.	26
Figure 4.3 – Granulometric distribution for Sandy Loam soil texture.	27
Figure 4.4 – Granulometric distribution for Loamy sand soil texture. Part 1 of 3.	28
Figure 4.5 – Granulometric distribution for Loamy sand soil texture. Part 2 of 3.	29
Figure 4.6 – Granulometric distribution for Loamy sand soil texture. Part 3 of 3.	30
Figure 4.7 – Granulometric distribution for Sand soil texture. Part 1 of 6.	31
Figure 4.8 – Granulometric distribution for Sand soil texture. Part 2 of 6.	32
Figure 4.9 – Granulometric distribution for Sand soil texture. Part 3 of 6.	33
Figure 4.10 – Granulometric distribution for Sand soil texture. Part 4 of 6.	34
Figure 4.11 – Granulometric distribution for Sand soil texture. Part 5 of 6.	35
Figure 4.12 – Granulometric distribution for Sand soil texture. Part 6 of 6.	36
Figure 4.13 – Southern High Plains Ternary Graph.	38
Figure 4.14 – Granulometric distribution for loamy sand, loam, and sand textures.	40
Figure 4.15 – Chihuahuan Ternary Graph.	42
Figure 5.1 – Total Organic Carbon calibration curve.	44
Figure 5.2 – Total Organic Carbon measurement results: SHP region.	53
Figure 5.3 – Total Organic Carbon measurement results: CHD USA region.	64

Figure 5.4 – Total Organic Carbon measurement results: CHD MEX region.....	68
Figure 6.1 – Land Use Classification.....	74
Figure 6.2 – Land use of dust sources.....	76
Figure 6.3 – Land use categories for dust source samples.....	77
Figure 6.4 – Geomorphic surfaces percentage.....	79
Figure 6.5 – Geomorphic surfaces dust source samples.	80
Figure 6.6 – Geomorphic surfaces dust source samples map.	82
Figure 7.1 – Quartz indexed (card No. 46-1045) compared to experimental patterns	106
Figure 7.2 – Quartz overlaid powder diffraction patterns.....	109
Figure 7.3 – Quartz 2 θ peak matching in overlaid patterns.	110
Figure 7.4 – 3D view of quartz XRD patterns with major high peaks illustrated.	111
Figure 7.5 – 2D contour plot of 3D quartz overlaid scans.....	112
Figure 7.6 – Gypsum indexed (card No. 33-0311) compared to experimental patterns.....	114
Figure 7.7 – Gypsum overlaid powder diffraction patterns.....	116
Figure 7.8 – Gypsum 2 θ peak matching in overlaid patterns.	117
Figure 7.9 – 3D view of gypsum XRD patterns with major high peaks illustrated.....	118
Figure 7.10 – 2D contour plot of 3D gypsum overlaid scans.	119
Figure 7.11 – Quartz indexed (card No. 46-1045) compared to experimental patterns.	121
Figure 7.12 – Calcite indexed (card No. 5-0586) compared to experimental patterns.....	122
Figure 7.13 – Quartz + Calcite overlaid powder diffraction patterns.	125
Figure 7.14 – Quartz + Calcite 2 θ peak matching in overlaid patterns.	126
Figure 7.15 – 3D view of quartz + calcite XRD patterns with major high peaks illustrated.....	127
Figure 7.16 – 2D contour plot of 3D quartz + calcite overlaid scans.	128

Figure 7.17 – Quartz indexed (card No. 46-1045) compared to experimental patterns.	130
Figure 7.18 – Gypsum index (card No. 33-0311) compared to experimental patterns.	131
Figure 7.19 – Quartz + Gypsum overlaid powder diffraction patterns.	134
Figure 7.20 – Quartz + Gypsum 2 θ peak matching in overlaid patterns.	135
Figure 7.21 – 3D view of quartz + calcite XRD patterns with major high peaks illustrated.	136
Figure 7.22 – 2D contour plot of 3D quartz + gypsum overlaid scans.	137
Figure 7.23 – Quartz indexed (card No. 46-1045) compared to experimental patterns.	139
Figure 7.24 – Calcite Magnesian indexed (card No. 43-0697) compared to experimental patterns.	140
Figure 7.25 – Dolomite indexed (card No. 36-0426) compared to experimental patterns.	141
Figure 7.26 – Quartz + Calcite Magnesian + Dolomite overlaid powder diffraction patterns. ..	144
Figure 7.27 – Quartz + Calcite Magnesian + Dolomite 2 θ peak matching in overlaid patterns.	145
Figure 7.28 – 3D view of quartz + calcite m. + dolomite XRD patterns with major high peaks.	146
Figure 7.29 – 2D contour plot of 3D quartz + calcite magnesian + dolomite overlaid scans. ...	147
Figure 7.30 – Quartz indexed (card No. 46-1045) compared to experimental patterns.	149
Figure 7.31 – Calcite indexed (card No. 47-1743) compared to experimental patterns.	150
Figure 7.32 – Sodium Plagioclase (card No. 47-1743) compared to experimental patterns.	151
Figure 7.33 – Quartz + Calcite + Sodium Plagioclase overlaid powder diffraction patterns.	154
Figure 7.34 – Quartz + Calcite + Sodium Plagioclase 2 θ peak matching in overlaid patterns. .	155
Figure 7.35 – 3D view of quartz + calcite m. + sodium plagioclase XRD patterns with major high peaks.	156
Figure 7.36 – 2D contour plot of 3D quartz + calcite + sodium plagioclase overlaid scans.	157

Figure 9.1 – Tree diagram of 58 variables with complete linkage and geometric distance.	179
Figure 9.2 – Tree diagram of 70 cases with complete linkage and geometric distance.	183
Figure 9.3 – SHP ArcGIS Clustering Map 1.	190
Figure 9.4 – 2D scatter plots of K:Al, K:Mn, and Pb:Ga	192
Figure 9.5 – Tree diagram of 54 variables with complete linkage and geometric distance.	194
Figure 9.6 – 2D Plot of Column Coordinates Part 1.....	196
Figure 9.7 – 2D Plot of Column Coordinates Part 2.....	197
Figure 9.8 – 2D Plot of Column Coordinates Part 3.....	198
Figure 9.9 – Tree diagram of 59 cases with complete linkage and geometric distance.	200
Figure 9.10 – SHP ArcGIS Clustering Map 2.	205
Figure 9.11 – Factor loadings: Factor 1 vs Factor 2 on original database.	211
Figure 9.12 – Factor loadings: Factor 2 vs Factor 4 on reduced database.....	216
Figure 9.13 – Factor loadings: Factor 3 vs Factor 4 on reduced database.....	217
Figure 9.14 – Factor loadings: Factor 2 vs Factor 4 on final reduced database.	218
Figure 9.15 – SHP ArcGIS final factorial loading Map.	221
Figure 10.1 – Soil Texture classification resulted from USDA texture triangle.	228
Figure 10.2 – Satellite imagery: The Chihuahuan Desert and Southern High Plains regions.	229
Figure 10.3 – Land Use Codes of 125 dust source sites.	230
Figure 10.4 – Land Use Categories of 125 dust source sites.....	232
Figure 10.5 – Geomorphic surfaces of 125 dust sources sites.....	233
Figure 10.6 – Preliminary Statistical Relationship.	244
Figure 10.7 – Refined Statistical Relationship.	246
Figure 10.8 – Narrowing Statistical Relationship.....	248

Figure 10.9 – PCA factor loadings. First attempt results.....	250
Figure 10.10 – PCA. Factor 3 vs. Factor 4 on Reduced master database matrix.	252
Figure 10.11 – PCA. Factor 2 vs. Factor 4 on reduced master database matrix.....	254
Figure 10.12 – Box Plot Descriptive Statistics for final dataset groups.	261
Figure 10.13 – Box Plot Mean concentration values charts.	262
Figure 10.14 – Box Plot of Arsenic grouped by land use classes.....	264
Figure 10.15 – Box Plot of Potassium grouped by land use classes.....	268
Figure 10.16 – Contoured Mapping of the As-Pb-Cu-Cr metallic set.....	273
Figure 10.17 – Contoured Mapping of the K-Fe-Al-Ti metallic set.....	274
Figure A.1 – Quartz Peak ID Report.	282
Figure A.2 – Gypsum Peak ID Report.....	283
Figure A.3 – Quartz + Calcite Peak ID Report.....	284
Figure A.4 – Quartz + Gypsum Peak ID Report.....	285
Figure A.5 – Quartz + Calcite Magnesian + Dolomite Peak ID Report.....	286
Figure A.6 – Quartz + Calcite + Sodium Plagioclase Peak ID Report.....	287

List of Tables

	Page
Table 4.1 – Weight percent values for clay, silt, and sand fractions – SHP region.....	37
Table 4.2 – Weight percent values for clay, silt, and sand fractions – CHD region.....	41
Table 5.1 – Total Organic Carbon results on SHP samples.....	48
Table 5.2 – Total Organic Carbon results on the Chihuahuan Desert USA region.	50
Table 5.3 – Total Organic Carbon results on the Chihuahuan Desert MEX region.	52
Table 6.1 – SHP dust sources sites original database Part 1.....	83
Table 6.2 – SHP dust sources sites original database Part 2.....	85
Table 6.3 – Chihuahuan Desert dust sources sites original database.....	87
Table 6.4 – Dust sources sites characterized complete matrix	88
Table 6.5 – Geomorphic classification and modifier codes observed for land use characterization.	91
Table 6.6 – Geomorphic categories for the Southern High Plains region	92
Table 6.7 – Geomorphic categories for the Chihuahuan Desert USA region.....	93
Table 6.8 – Geomorphic categories for the Chihuahuan Desert MEX region.....	94
Table 7.1 – Concentration in percent on SHP soil sources.....	102
Table 7.2 – Concentration in percent on Chihuahuan Desert USA soil sources.	103
Table 7.3 – Concentration as fraction of Chihuahuan Desert MEX soil sources.	104
Table 8.1 – Relationships among elemental concentrations and sites.....	161
Table 8.2 – Geomorphology of Southern High Plains dust events soil samples.	169
Table 8.3 – Land use classes for Southern High Plains dust events soil samples.	170

Table 8.4 – Relationships among elemental concentrations values and land use classes.....	171
Table 8.5 – Complete relationship between elemental concentrations on both, soil texture types and land use classes.	172
Table 8.6 – GIS overlay analysis and sampling site characteristics. The Southern High Plains region.	173
Table 8.7 – Metallic concentrations (ppm) on Southern High Plains dust sources. ICP-OES analysis results	175
Table 9.1 – SHP elemental coefficients Factors on original database.....	207
Table 9.2 – Topmost Factor loading values on original database.....	209
Table 9.3 – SHP metallic coefficients Factors on reduced database	213
Table 9.4 – Topmost Factor loading values on reduced database.	215
Table 9.5 – SHP metallic coefficients Factors on final reduced database	219
Table 9.6 – SHP elemental concentration Factors on final reduced database	220
Table 9.7 – Ordination Analysis Final Dataset Groups	223
Table 9.8 – Factorial ordination analysis on original dataset matrix	224
Table 9.9 – Factorial ordination analysis on reduced dataset matrix.....	225
Table 9.10 – Restricted maximum likelihood correlation coefficients of selected elemental concentrations.	226
Table 10.1 – Concentration in percent on SHP soil sources.....	237
Table 10.2 – Concentration in percent on Chihuahuan Desert USA soil sources.	238
Table 10.3 – Concentration in percent on Chihuahuan Desert MEX soil sources.	239
Table 10.4 – Statistical Analysis Results.....	241
Table 10.5 – Standardized values: relationships among elemental concentrations and sites	242

Table 10.6 – PCA factor loading values	251
Table 10.7 – PCA Final factor loading values	253
Table 10.8 – PCA. Component Groups for dust source sites. Final attempt.	255
Table 10.9 – PCA. Connectivity Results Acquirement.	257
Table 10.10 – Box Plot. Connectivity Results Acquirement.	259

Chapter 1

Introduction

Dust tends to be emitted from hot spots or other preferential source regions such as agricultural land and dry lake beds ([Gillette 1999](#); [Lee et al. 2009](#)). Seasonal dust storms are extremely sensitive to high wind speeds, lack of soil aggregation, low vegetation cover, soil moisture, land – surface type, and high particle availability among other factors that cause a region to be a dust source. The fine sediment fraction of clays and fine silts (both as coarse $PM_{10-2.5}$ particulate matter between 10 to 2.5 μm in diameter, and fine $< PM_{2.5}$ particulate matter less than 2.5 μm in diameter) are preferentially entrained to the atmosphere as mineral aerosols and transported from a few kilometers locally to thousands of kilometers at a large scale ([Gill et al. 2006](#)). Fine particle $PM_{2.5}$ are breathed more deeply into the lungs causing detrimental impacts on human health, asthma in particular, especially to children and elderly populations ([Pope; Dockery 2006](#)). Additionally, $PM_{2.5}$ particulate matter generated by dust storm events penetrates more readily into indoor environments and is transported over greater distances causing an infrastructure and transportation hazard ([Novlan et al. 2007](#); [Wilson; Suh 1997](#)). It is also known that soil is the primary sink of semi-volatile organic compounds such as Polycyclic Aromatic Hydrocarbons (PAHs) in the environment as a result of direct gas exchange between soil and air, and wet and dry deposition ([Cousins et al. 1999](#); [Wania; Mackay 1995](#)) where PAHs concentration in soil correlates with the corresponding levels in air when traveling attached to $PM_{2.5}$ ([Levy et al. 2002](#); [Levy et al. 2003](#)).

Mineral (dust) aerosols emitted from wind-erodible dryland surfaces play important roles in the earth's climate system ([Arimoto 2001](#)) and have a significant impact on air quality ([Rivera Rivera et al. 2009](#)). Although dust occurs globally, the major source regions are the drylands

where large quantities of dust may be emitted from relatively natural surfaces ([Engelbrecht; Derbyshire 2010](#); [Washington et al. 2003](#)), particularly arid and semi-arid regions that have decreased vegetation cover and received annual rainfall under 200-255 mm ([Prospero et al. 2002](#)). Other studies, however, state that a large contribution to global dust loads are emitted from sites with significant human disturbance ([Sokolik; Toon 1996](#)) where anthropogenic agricultural and farm activities such as croplands and rangelands may dominate the production of blowing dust locally or regionally ([Lee et al. 2009](#)).

1.1 Problem Statement

Studies in the recent past have used remote sensing and modeling techniques to locate mineral aerosol sources in the Chihuahuan Desert (northern Chihuahua, southern New Mexico, and far West Texas) and the Southern High Plains (west Texas and eastern New Mexico) regions ([Baddock et al. 2011](#); [Bullard et al. 2011](#); [Janugani et al. 2009](#); [Lee et al. 2009](#); [Prospero et al. 2002](#); [Rivera Rivera et al. 2010](#); [Rivera Rivera et al. 2009](#)). It is also known that mineral dust in other regions is composed mostly of quartz, feldspars, micas, various clay minerals, carbonates, oxides, and evaporite minerals ([Engelbrecht; Derbyshire 2010](#)). Respirable dust (RD, particles $\leq 4\mu\text{m}$ in aerodynamic diameter and defined as the major contributor to air pollution/dust storm generation from both silt and clay soil textures) source soils have been assessed for their physical and chemical characteristics not only in California, USA ([Clausnitzer; Singer 1999](#)), but also in different lands of inner Mongolia plateau, China ([Hai et al. 2008](#)) confirming that the compounds and elements comprised in the floating dust are found in the source soil with various relative differences in abundance among them. However, there is limited “ground truth” information about the chemical composition and physical properties of dust and its sources in the Southern High Plains and Chihuahuan Desert regions. Therefore, it becomes imperative to conduct a more

complete geochemical and granulometric characterization of mineral dust sources in these regions to understand its effect on the environment both directly and indirectly by impacting the chemical and physical properties of the atmosphere.

Because dust source characterization and interpretation demands multidisciplinary expertise and a variety of techniques, Particle Induced X-ray Emission (PIXE), Inductively Coupled Plasma Atomic Emission Spectroscopy (ICP-OES), X-Ray Diffraction (XRD), and Laser Granulometer analysis are techniques that will be used to obtain elemental, mineralogical, and granulometric textural data on dust source materials identified from remote sensing and field work. Association between elemental and chemical composition of the samples and their textures will be achieved by descriptive statistics and cluster analysis.

1.2 Hypothesis

The following hypotheses are tested in this study:

- 1) Chemical and physical characteristics of samples taken from specific source areas will be unique markers of dust production in the region.
- 2) Geoenvironmental (chemical and physical) characterization of dust source materials may be used to develop a set of common soil characteristics to predict wind erosion prone locations.
- 3) Geoenvironmental (chemical and physical) characterization of dust source materials may be used for source apportionment of dust events.

Chapter 2

Literature Review

2.1 The Chihuahuan Desert

2.1.1 Location and Limits

The Chihuahuan Desert is the largest of the North American deserts, located between the 20° and 35° N parallels and the meridians 98.45 and 109.15 west of Greenwich, and includes portions of Arizona, New Mexico and Texas in the United States and ten states of Mexico (Coahuila, Nuevo León, Tamaulipas, San Luis Potosí, Guanajuato, Zacatecas, Aguascalientes, Durango, Chihuahua and Sonora), ([Medellin-Leal 1982](#)) . Henrickson and Straw ([1976](#)) state that the entire area of the Chihuahuan Desert is approximately 507,000 square kilometers (Fig. 2.1).

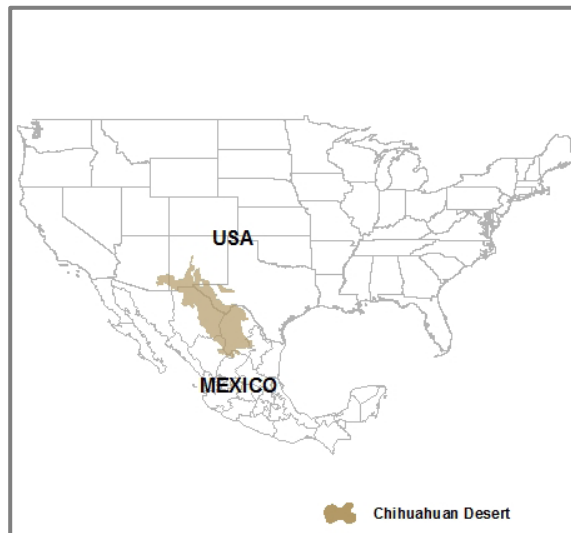


Figure 2.1 – The Chihuahuan Desert region.

2.1.2 Climate

The Chihuahuan Desert is considered to encompass a critical climatic boundary region between the subtropics and the middle latitudes ([Castiglia; Fawcett 2006](#)). In the northwest part of the desert, the annual average temperature is approximately 18°C while the southwest experiences annual average temperature ranges from 22° to 28°C ([Medellin-Leal 1982](#)). Precipitation in the desert varies due to the effects of latitude, topography, and continentality: a minimal annual average precipitation below 200 mm occurs in the center of the desert in comparison to as much as 550 mm annual precipitation at the margins of the Chihuahuan Desert ([McGinnies et al. 1970](#)).

Precipitation in the Chihuahuan Desert usually occurs from isolated showers and thunderstorms, especially during the summertime North American Monsoon ([Douglas et al. 1993](#)). Sometimes very heavy, monsoon precipitation events may cause flash floods especially between July and September where the predominant peaks of rain occur generally. As with precipitation, the wind system in the Chihuahuan Desert is variable because of the topography and different directional forcings imposed by the mountain ranges. Arid lands in western North America periodically experience strong winds and the downwind areas affected vary depending on the type of prevailing weather systems as well as geographic and physiographic setting ([Bach; Brazel 1996](#); [Brazel; Nickling 1986](#)). The strongest winds in the Chihuahuan Desert occur during the dry periods of winter and spring: dust storms are most prevalent during this period when strong pressure gradients cause strong southwesterly wind across the northern part of the desert ([Novlan et al. 2007](#); [Rivera Rivera et al. 2009](#)). The greatest regional (synoptic) wind intensities happen during March and April, although strong localized dust-raising winds associated with

thunderstorm outflows (haboobs) are not unusual, especially during June and July ([Novlan et al. 2007](#)).

2.1.3 Soils

There are few previous soil surveys or soil texture studies in the Chihuahuan Desert Mexican region. In 1971 ([Grande-López; Gómez-González](#)) classified the soils into seven categories: Aridisols, Salt, Lithic, Fluvents, Mollisols, Luvisols and Black Subtropical soils.

2.1.4 Aeolian Processes

Mineral aerosol sources have been identified primarily in the northern Chihuahuan Desert by remote sensing; the region has been identified as one of the major, most intense and regular dust source regions in the Western Hemisphere ([Gill et al. 2008](#); [Janugani et al. 2009](#); [Lee et al. 2009](#); [Prospero 1999](#); [Prospero et al. 2002](#); [Rivera Rivera et al. 2010](#)). The Chihuahuan Desert is prone to emit dust storms due to the presence of erodible sediments in alluvial basins of ephemeral streams (arroyos) and its flat, unvegetated desert basins and playas. A playa is defined as the flat and generally lower portions of arid basins with internal drainage that periodically flood and accumulate sediments ([Neal 1975](#)); they are natural sites of extensive aeolian activity because of the deposition of clastic and chemical sediments in basins by surface water (via fluvial transport) and groundwater (via efflorescence) ([Gill 1996](#)). These surfaces have a supply of particles able to be taken up from surface by wind, and the typical Chihuahuan Desert surfaces have the characteristic factors that cause a region to become a mineral dust producer ([Engelbrecht; Derbyshire 2010](#)): the low threshold velocity, the instability of the atmosphere, proper particle size, appropriate roughness and moisture content of the land surface, the degree of particle exposure, scarce vegetation cover, and the mineralogical composition of loose sediment on the ground surface. Changes in the frequency and extent of natural inundation

occurring in ephemeral lake systems may lead to significant fluctuations in regional dust loadings on a seasonal and inter-annual basis ([Mahowald et al. 2003](#); [Rivera Rivera et al. 2010](#)).

2.1.5 Previous Work

Miguel Dominguez Acosta ([2009](#)) performed preliminary sedimentological, geomorphic, and geochemical investigations delineating dust emissions mechanisms and potency of several individual areas in the Lake Palomas basin for dust storms incidence. Particle Induced X-ray Emission (PIXE), statistical cluster, and enrichment factor coefficients analyses established the geochemical associations between elements, samples and the geological context within the basins. Quartz was the dominant mineral, found in higher concentrations averaging close to 30 percent with maximum values over 40 percent in dust source areas. Adriana Evangelina Pérez ([2008](#)) found similar results for the Salt Flat Basin, at the northeast corner of the Chihuahuan Desert. These results were similar to those of H. Clausnitzer and M. J. Singer ([1999](#)) for dust sources in California. These authors determined that aluminum, calcium and sodium were major elements with a ≥ 10 percent averaged concentration whereas magnesium, titanium, manganese, iron and potassium comprised the major metals group with concentrations of 9 percent and less in dust-producing soil samples.

[Perez \(2008\)](#) analyzed soil characterization to better understand the processes of dust mobilization, provenance and trajectory in the Salt Flat Basin. Proton Induced X-Ray Emission (PIXE), X-Ray Diffraction (XRD), Ion Chromatography (IC), and particulate size distribution were the techniques used to obtain a signature of dust-producing sediments in this one area. The author concluded that silicon, calcium, sulphur, zinc, magnesium, aluminum, iron and sodium were the major elements within samples acquired with various concentration differences among locations. In addition to quartz, sanidine, gypsum, alunite, aragonite, kaolinite, zeolites and

calcite were the minerals found in the X-Ray diffractograms, especially gypsum, aragonite, sanidine and other sulfate minerals, which were consistent with previous studies of evaporites present in the area.

2.2 The Southern High Plains

2.2.1 Locations and Limits

The Southern High Plains (SHP) is an extensive plateau of approximately 130,000 square kilometers in northwestern Texas and eastern New Mexico ([Holliday 1991](#)). The Pecos, Canadian, Red, Brazos and Colorado rivers surround the region at the west, north and east part, respectively whereas the Edwards Plateau at the south merges with the SHP plateau on the southeast diminishing specific demarcation (Fig. 2.2).

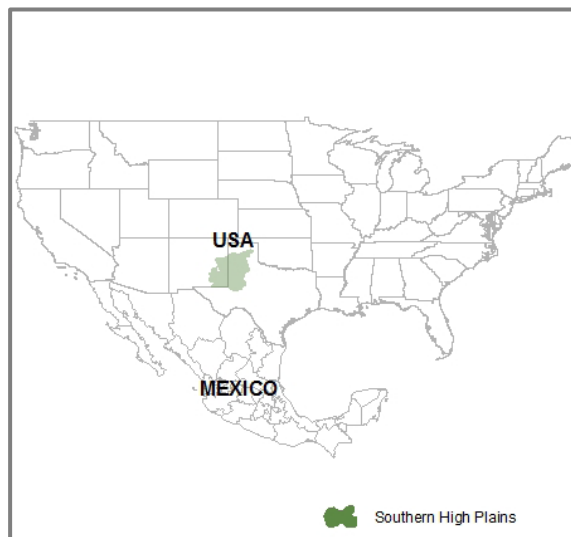


Figure 2.2 – Southern High Plains region.

2.2.2 Climate

Annual maximum average temperatures above 29 °C occur during summer and average winter temperature is above freezing with periods of below freezing temperatures in most years. In Texas, the SHP average annual precipitation ranges from 400 to 500 mm ([Wigner; Peterson 1986](#)), though little rain occurs during the months of November to April. An average of 36 thunderstorm days are annually reported in the region ([Court; Griffiths 1982](#)). The SHP is also recognized as one of the most persistently windy inland regions in the United States and also is one the dustiest areas in the country ([Bomar 1983](#); [Johnson 1965](#); [Orgill; Sehmel 1976](#)). Dust storms in this region are associated with the SHP being an intensive agricultural region and agricultural practices that leave the soil bare and dry during the windy season ([Stout; Lee 2003](#); [Wigner; Peterson 1986](#)). Prevailing winds from the southwest to the northeast across the SHP are associated with the production and transport of dust ([Lee et al. 1994a](#)). Average wind velocities tend to be greatest in the early spring, diminishing to a minimum in summer, and then increasing again in the fall and winter ([Walters 1988](#)), thus the winds are the strongest when the soil is most prone to erosion.

2.2.3 Soils

Initial assessments of the mineralogy and chemistry, and soil texture in the region started several decades ago. In 1972, ([Allen et al.](#)) divided the SHP into three soil texture types: surface soils in the “fine” zone generally consisted of clay loams and silty clay loams. Those in the “medium” zone were primarily fine sandy loams, although sandy clay loams and loams were common. Loamy fine sands and fine sands were the predominant textures in the “coarse” zone. Another study made by Reeves ([1976](#)), classified the region into five soil texture types: clay – clay loam, sandy clay loam – clay loam, sandy loam – sandy clay loam, loamy sand – sandy

loam, and loam type. Most of the research studies that have been made on the eolian sedimentation and soil formation on the Southern High Plains follow the conclusions of [Holliday \(1989\)](#) who stated that the sediments on the surface (known as the Blackwater Draw Formation) fine from southwest to northeast, exhibit a linear relationship of decreasing sand content and sand size and increasing silt content with increasing distance from southwest to northeast, indicating the source area to be the Pecos River valley.

X- ray diffractometry performed on the surface soil in both the coarse (sand and silt) and fine (clay) fractions in areas where the loamy sand, sandy clay loam, and clay textural classes are found, resulted in a uniform mineralogy: Holliday ([1989](#)) evidenced that 80% - 90% of coarse minerals were quartz with the rest of the fraction composed of weatherable feldspar and mica while illite, smectite, smaller amounts of kaolinite, montmorillonite, and interstratified illite-montmorillonite were the clay minerals found in B. L. Allen's ([1972](#)), Dale Martin Rogers's ([1969](#)), and James P. Walters' ([1988](#)) X-ray diffractograms. It is important to mention that quartz or feldspar were X-ray undetectable when analyzing the clay sized grains from any playa soils of the region.

Although the mineralogy and chemistry of the SHP studies have been performed mostly on surface soil, it is confirmed apparently that the mineralogy of the deeper layers is very similar to those of the surface layer because the buried soils were formed under similar conditions. Geochronologically, SHP surface soil has formed throughout the late Quaternary under probably subhumid conditions in the late Pleistocene, becoming semiarid in the Holocene and reached stability with regards to soil formation at present ([Johnson 1986](#)). Yet the geologic processes of formation of these deposits is cyclic: each cycle begins with eolian deposition, continues with landscape stability and soil formation, and ends with erosion.

2.2.4 Aeolian Processes

Composition and characterization of aerosols in the Southern High Plains has been made previously by [Gill et al. \(2009\)](#). This co-authored investigation provides an initial assessment of aerosol chemistry in the west Texas plains to obtain elemental signatures of aerosols occurring within the region: dust storms in the Southern High Plains previously have been investigated mostly with regards to their meteorological characteristics ([Lee et al. 1994b](#); [Wigner; Peterson 1987](#)). Twenty-seven aerosol samples on polycarbonate filters during a variety of aerosol loadings (dust storms, anthropogenic pollution episodes of several kinds, and clear non-polluted conditions) were analyzed by Particle Induced X-ray Emission (PIXE) to determine elemental concentrations in these selected samples. Because the primary motivation for collecting the samples was to document daily aerosol concentrations to evaluate the particulate air quality trends ([Stout 2001](#)), the first two authors maintained a daily log of prevailing weather conditions in the area during the time that samples were collected. As a result, the authors observed that silicon was the dominant element in the coarsest particles during both “dust storm” and “clear non-polluted” air quality conditions with the fraction of crustal elements such as potassium, aluminum, iron and titanium were enhanced during these two air quality conditions. It was also noted that sulfur concentration levels were highest during “pollution episodes” air quality condition, indicating the presence of anthropogenic sulfate aerosols (finer than the dust fraction, PM_{2.5} particulate matter) originated from either fugitive dust entraining from disturbed urban soils (construction sites, etc.) or high winds that cross a livestock feedlot. The authors concluded that the analytical results for major elements may provide some of the first compositional data on aerosols in the Southern High Plains.

A cohort project between Texas Tech University and the University of Texas at El Paso funded by the Texas Norman Hackerman Advanced Research Project Number 003661-0027-2007, allowed already the identification of dust emitting “hot spot” areas through remote sensing techniques, permitting development of an inventory of wind erosion source areas in the Southern High Plains and Chihuahuan Desert regions ([Baddock et al. 2011](#); [Bullard et al. 2011](#); [Lee et al. 2009](#); [Lee et al. 2012](#); [Rivera Rivera et al. 2010](#)). Soil samples from a representative number of remote-sensing-identified dust sources were already collected from the field, through the assistance of Dr. Lee (Texas Tech), Dr. Baddock (USDA-Lubbock), Dr. Gill (UTEP), Dr. Dominguez (UACJ) and others. Those soil samples are analyzed in this project. Additional descriptions of the samples with their site/sample identification numbers discussed in subsequent analytical results and interpretations are given in tables 6.1 through 6.4.

The scope of this project consists of performing physical and chemical analyses using a variety of techniques mentioned previously in this study to obtain elemental, mineralogical, chemical and granulometric textural data that will be used not only to develop knowledge of the geochemical and physical attributes of dust-producing soils in these adjacent regions, but also to be used as a source apportionment to better understand the environmental impacts of mineral dust storms locally, regionally, and continentally.

Chapter 3

Technologies to be used for Analysis

3.1 Laser Diffraction

Dry laser diffraction analysis is a convenient approach to particle size analysis. The ability to measure particles in their dry state (Scirocco 2000 unit of the Malvern Mastersizer laser diffractometer), as collected from a dust trap or as existing at the soil surface, allows to measure the actual size of the often-agglomerated, salt-bearing particles moving in the wind (dry aggregate size distribution), as opposed to other techniques which require the disaggregation of particles and dissolution of salts in liquid. However, cautions must be taken for accurate and reliable results ([Bale 1996](#); [Buurman et al. 1997](#); [Sperazza et al. 2004](#); [Zobeck 2004](#)).

Particle size data was collected with Malvern's Masterziser 2000 software version 5.22. The average of the three successive analytical runs for each sample was then used for particle size distribution analyses. The volume of sample required for particle size analysis for this particular study varied between 0.5 g to 2.0 g depending on the composition of the sample which regulated the rate of sediment flow through the instrument. Sandy samples required greater amounts than loamy soil samples. Grapher 8 statistical software package was used to create soil texture diagrams of the samples from both the Southern High Plains and Chihuahuan Desert regions.

3.2 Total Organic Carbon

Soil organic matter is a crucial component that can be altered by the direct impact of human activities such as deforestation, land use change, biomass burning and environmental pollution ([Bolin 1981](#); [IPCC. 1990](#); [Trabalka; Reichle 1986](#)). Modern agriculture decreases the amount of carbon stored (20 to 40%) in soils due to exposure of organic matter to oxidation from plowing and also due to increased erosion.

Size and dynamics of the carbon in the soils are not well known, remarkably because: (a) limited knowledge of different types of soils; (b) lack of a consistent, complete and uniform data of these soils; (b) spatial variation in carbon content; and (d) the effects of climate, land use, vegetation, and parent material ([Batjes 1996](#)).

Total organic carbon in soil was determined by using the Shimadzu SSM-5000A solid sample module. Soil samples were combusted a high temperature and transformed to carbon dioxide (CO_2), which was then measured with an infrared detector.

Total organic carbon analysis did not require acid treatment, causing to shorten the examination time to about five minute averages per measurement.

3.3 X – Ray Diffraction

Soil mineralogy determines soil functional properties ([Dixon; Schulze 2002](#)). New instrumentation for X-ray powder diffraction (XRD) and improvements in associated mineral identification databases and software have strengthened quantitative determination of soil mineral phases. X-Ray Diffraction (XRD) is a major X-ray-based technique that is well established and widely used with applications in the soil, plant, and environmental sciences ([Schulze; Bertshc 1995](#)). Powder X- Ray diffraction obtains at least four advantages for soil samples: (1) better peak resolution; (2) anomalous scattering effects can be exploited; (3) diffraction patterns can be obtained from small samples; and (4) time-resolved diffraction can be used to follow chemical reactions if needed ([Finger 1989](#)).

3.4 Inductively Coupled Plasma Optical Emission Spectrometry (ICP-OES)

ICP-OES is an analytical technique used especially for the detection of trace metals. It is a type of emission spectroscopy that uses the inductively coupled plasma to produce excited atoms and ions that emit electromagnetic radiation at wavelengths characteristic of a particular element ([Mermet 2005](#); [Stefánsson et al. 2007](#)). Hypothetically, ICP-OES has the ability of simultaneously measuring up to 70 elements but is normally used to measure up to 20-30 elements at a time ([Grave et al. 2005](#)). ICP-OES also has the ability to analyze a wide range of elements and is used for the analysis of light elements such as Na and Mg ([Zhang et al. 2005](#)). ICP-OES is widely used for the characterization of trace metal concentrations in sediments ([Rice 1999](#)). This analytical method has low detection limits for most metals, but one of its drawbacks is the need to digest the solid sample material with a strong acid to produce an aqueous sample for analysis ([Lunderberg et al. 2008](#); [Menzel et al. 2002](#)). A possible disadvantage of ICP technique is this destructive sample preparation method prior to actual analysis ([Smodis 2007](#)).

Improper preparation could lead to contamination of samples, incomplete digestion and/or loss of material by evaporation ([Menzel et al. 2002](#); [Smodis 2007](#)).

3.5 Experimental Design

This proposed study scopes both the Chihuahuan Desert and Southern High Plains regions. A cohort effort between Texas Tech University and the University of Texas at El Paso “Database Development of Wind Erosion Source Areas in the Southern High Plains and Chihuahuan Desert,” funded by the Texas Norman Hackerman Advanced Research Project Number 003661-0027-2007, has allowed for ongoing monitoring, detection, discussion, and evaluation of dust source areas in both regions leading up to my proposed project. This cohort project obtained soil samples taken from “hot spot” dust areas observed by remote sensing techniques in both the Chihuahuan Desert and the Southern High Plains regions ([Baddock et al. 2011](#); [Lee et al. 2009](#); [Rivera Rivera et al. 2010](#)).

The research design and data analyses of this study are multiple, and related to mineral dust source characterization. They include as follows:

3.5.1 Geographical Information System (GIS) mapping.

ESRI ArcGIS within ArcMap version 10.1 was used for mapping soilborne aerosol source distribution. Global Positioning System (GPS) was then used to obtain location of the sites where soil samples are taken which was a subset of the sites determined by ([Dominguez-Acosta et al. 2010](#)) and ([Lee et al. 2012](#)). Hence, the GIS map was created based on the mineral aerosol sources located in the Chihuahuan Desert (northern Chihuahua, southern New Mexico, and far west Texas) and the Southern High Plains (west Texas and eastern New Mexico) regions, respectively.

3.5.2 Land Use/Land cover soilborne dust sources mapping.

Soil type classification for each site above is obtained based on the criteria used by USDA-NRCS Web Soil Survey ([WSS](#)) within the United States, and on the information generated by the Instituto Nacional de Estadística y Geografía ([INEGI](#)) for the northern Chihuahua, Mexico section. Although criteria/classification discrepancies may be present among these two federal agencies when classifying soil by using their respective geospatial vector data and soil classification techniques, the author's interest is based in providing as much detail as possible of pre-existing mapped soil properties for each mineral dust source within the study area of this project.

3.5.3 Particle Size Distribution.

Soil samples are analyzed for particle size using a Malvern Masterziser 2000 laser diffraction instrument (Malvern Instruments Ltd) equipped with the Scirocco 2000 unit for dry analyses and Hydro unit for wet analyses. Both dry and wet analyses are performed on the samples to obtain optimum measurement of dry aggregate size distribution and inherent soil grain size. The particle size analysis was done at the University of Texas at El Paso, Geological Science Department. The particle size distributions generated by the Malvern software are expressed as the measured sample volume spaced logarithmically between 0.01 and 2000 μm ([Rojo 2010](#)). Prior to laser diffractometry, samples are prepared by following the protocols resulting from the detailed study on the use of high-resolution particle size analysis as stated by ([Sperazza et al. 2004](#)). Granulometric (grain size) data results are then used to create soil texture classification in accordance with the United States Department of Agriculture's diameter limits classification (USDA Texture Triangle). Grapher v8 is the modeling software used to compute the texture triangles.

3.5.4 X – Ray Diffraction.

X-Ray Diffraction is used to reveal the chemical (mineral) composition of the soil samples. An average of three to five grams of the source soils are used for mineral characterization analysis. Samples are pulverized in a corundum mortar and pestle using isopropanol alcohol as a solvent/binding agent. A fine powder obtained is then poured in the indented section of the glass sample plate and then compacted by using another glass plate such that the sample surface is aligned with the sample measurement plane. Minerals then are identified by standard XRD at the UTEP Materials Science and Engineering Department using the RIGAKU MiniFlex II X-Ray Diffractometer (RIGAKU Americas Corp., The Woodlands, TX) using Cu-K α radiation at 30 kV and 15 mA and a K β filter. Scans are taken from 10° to 65° in 0.03° increments, at 2.5 s/step.

Once the diffractograms are obtained from soil samples, materials data JADE 9 (XRD pattern processing identification and quantification software package) is loaded for helping identify and quantify minerals found in the prepared soil fine powder. JADE 9 “search/match” option is then used to obtain mineral concentration in percent [Wt%] report.

3.5.5 Inductively Coupled Plasma Optical Emission Spectroscopy (ICP-OES).

This analytical technique is used for the detection of trace metals in the dust source soils. Samples are pulverized in a corundum mortar and pestle, resulting in a powder with an average grain size of 30 μm or smaller. Sample digestion is undertaken following a $\text{Li}_2\text{B}_4\text{O}_7$ fusion procedure. In this case a 0.4000 ± 0.005 sub-sample of powder is mixed with 0.4000 ± 0.0005 g of lithium tetraborate flux. The mixture is fused at 1000 °C for 20 min in a muffle furnace and then dissolved in 50 mL of 5% HNO_3 . ICP-OES instrument precision is monitored by analyzing calibration blank and multi-element standards. Concentration of trace metals in each samples are

then determined. The ICP-OES analysis was performed at the University of Texas at El Paso Geological Sciences Department.

3.5.6 Total Organic Carbon.

Total Organic Carbon analysis determined the organic carbon composition of the soil samples. An average of 61 grams of the source soils are used for organic carbon analysis. Calibration curve was created to achieve equal weighting amounts on both the standard and samples. Samples were then weighed and burned out in the Solid Sample Module SSM-5000A, from which the carbon dioxide (CO_2) emissions were measured by using an infrared detector. Total Organic Carbon analysis was performed in the Environmental and Water Resources Engineering Lab located at the UTEP Civil Engineering Department.

In conclusion, a total of 123 soil samples were analyzed. 72-, 27-, and 24-soil samples comprised the bulk samples taken from the Southern High Plains, the Chihuahuan Desert USA, and the Chihuahuan Desert MEX regions, accordingly.

Once the carbon concentrations [g/kg soil] were calculated, these results were taken into consideration for all the statistical analysis techniques performed in this project.

3.5.7 Statistical Analysis.

Multivariate statistical matrix is prepared for all the mineral dust source samples. Multivariate statistical analysis consists of a collection of methods that can be used when several measurements are made on each individual or object in one or more samples. Statistical techniques including cluster analysis are used to establish the geochemical associations between elements, minerals, sediment textures, and sample sites. Dendrograms are used to correlate geochemical affinity using not only the Pearson correlation to measure the degree to which the same variables of all the soil samples follow a similar pattern of fluctuation through time,

whether or not the mean levels are different, but also Ward's methodology selecting Euclidean distance which is simply the geometric distance in the multidimensional space. It is computed as:

$$\text{distance}(x, y) = \left\{ \sum_i (x_i - y_i)^2 \right\}^{\frac{1}{2}}$$

Grapher 8 and STATISTICA software packages are used to compute and arrange critical soil variable analyses. Classification trees from cluster analysis technique and data mining would result in showing geochemical affinity between Metal/Sites, Mineral/Sites, and Texture/Sites classes.

Elemental concentrations are statistically analyzed to obtain new information on regional atmospheric soil dust source characteristics in the Southern High Plains region, which is an important dust storm source on regional scale. Elemental concentrations then are clustered and principal component analyzed to obtain narrow intervals, so they can be used to determine source apportionment factors that may be useful in tracing long-range transport of dust within the adjacent regions. Soil composition data like those used in this study have been used to obtain geochemical markers of dust from different locations in California ([Ashbaugh et al. 2003](#); [Clausnitzer; Singer 1999](#)) and Asia ([Makra et al. 2002](#); [Suzuki et al. 1993](#)): the methods used in these and other related studies will be consulted to obtain chemical profiles of dust from different source areas and types.

Chapter 4

Laser Diffractometry

Particle size data was collected with Malvern's Mastersizer 2000 software version 5.22. The average of the three successive analytical runs for each sample was then used for particle size distribution analyses. The volume of sample required for particle size analysis for this particular study, varied between 0.5 g to 2.0 g depending on the composition of the sample which regulated the rate of sediment flow through the instrument. Sandy samples required greater amounts than loamy soil samples.

Sodium hexametaphosphate at 5% solution was added into a plastic vessel containing the soil sample. After placing the containers in an automated shaker, samples were dispersed overnight. Samples were then analyzed on Malvern Mastersizer 2000 laser granulometer machine (Hydro unit). Volumetric (equivalent to weight percent) grain size-frequency data distributions were obtained and plots generated for each of the samples.

4.1 Granulometric results of the Southern High Plains region

Clay Loam and Silty Clay Loam soil textures resulted for S(76) 60 and S(59) 46 sites after laser diffractometry completion. In addition, samples S(6) 6 and S(61) 47 were Loam soil texture categorized. In addition, trimodal, bimodal, and unimodal peaks-related distributions were revealed on these samples (Figure 4.1).

The percent clay in the samples fluctuated between 9.8 and 27.8 percent, while the silt percent oscillated from 46 to 59.9 percent. Additionally, the fine sand fraction ranged from 11.9 to 42.8 percent (Table 4.1).

Silt Loam soil texture was indicated for S(18) 15, S(26) 22, S(41) 30, S(44) 33, S(45) 34, S(55) 43, and S(77) 61 dust source samples after particle size examination. Moreover, bimodal and unimodal peaks distributions were observed on granulometric charts of these samples (Figure 4.2).

The percent clay in the samples oscillated from 8.4 to 11.8 percent, while the silt percent by weight ranged from 50.6 to 60.7 percent. Additionally, the fine sand fraction fluctuated from 27.9 to 38.5 percent (Table 4.1).

Sandy Loam soil texture was indicated for S(2) 3, S(3) 4, S(12) 10, S(13) 11, S(21) 18, S(29) 25, and S(72) 56 samples from laser diffraction. All of these samples revealed a very prevailing unimodal distribution, with the exception of S(29) 25 whose grain size distribution revealed a bimodal distribution (Figure 4.3).

Clay size particle fractions resulted with 3.7 – 6.5 percent. The silt fraction of these dust sources ranged from 23.1 to 36.3 percent and the sand size fraction oscillated from 55.4 to 71 percent (Table 4.1).

Loamy sand soil texture was categorized in seventeen samples after laser diffractometry analysis. Here, all of these samples displayed a very dominant bimodal distribution. Clay fraction oscillated from 1.5 to 4.3 percent by weight. The silt fraction rose from 12 to 20 percent by weight and the sand size fraction ranged from 76.1 to 85.9 percent by weight. Site names are shown on Figures 4.4, 4.5, and 4.6, respectively. Also, percent by weight could be found on Table 4.1.

Sand soil texture resulted as the mainstream soil texture class after particle size distribution inquiry. Thirty-seven samples totalized more than 50% of the total number of samples under diffractometry analysis. Here, both, clay and silt fractions resulted with lower

concentrations, that was, 0.0 – 2.0 for clay and 0.0 – 12.2 for silt. On the contrary, sand fraction computed percent by weights from 86.3 to 100 totalized percent, causing to observe a strong unimodal distribution on all the samples. Sites names can be found on Figures 4.7, 4.8, 4.9, 4.10, 4.11, and 4.12. Furthermore, percent by weight of these samples are shown in Table 4.1.

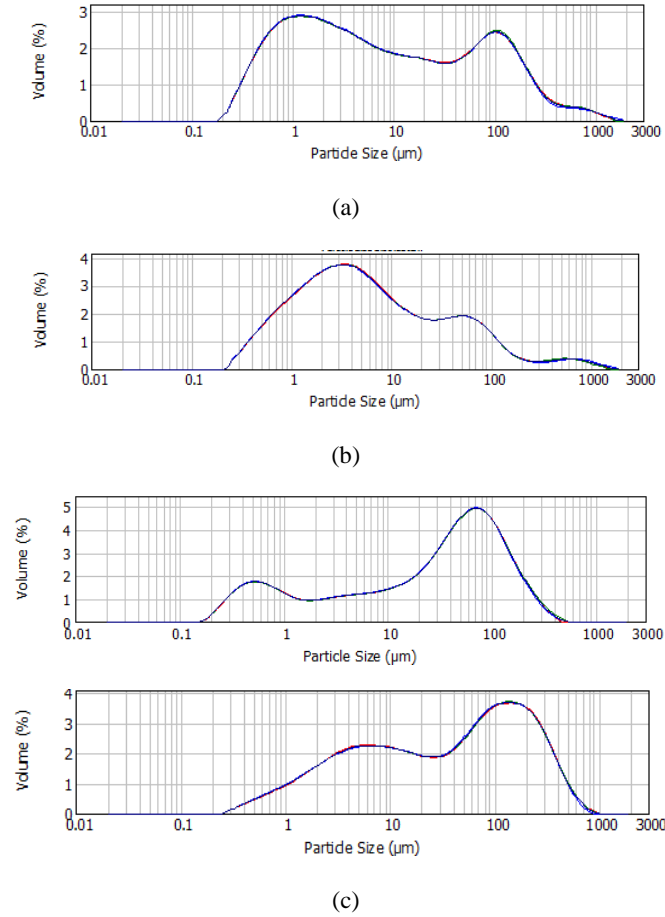


Figure 4.1 – Granulometric distribution of three soil texture classes.

From top to bottom: S(76) 60, S(59) 46, S(6) 6, and S(61) 47, respectively. Soil texture classification as (a) Clay Loam, (b) Silty Clay Loam, and (c) Loam for the samples mentioned above.

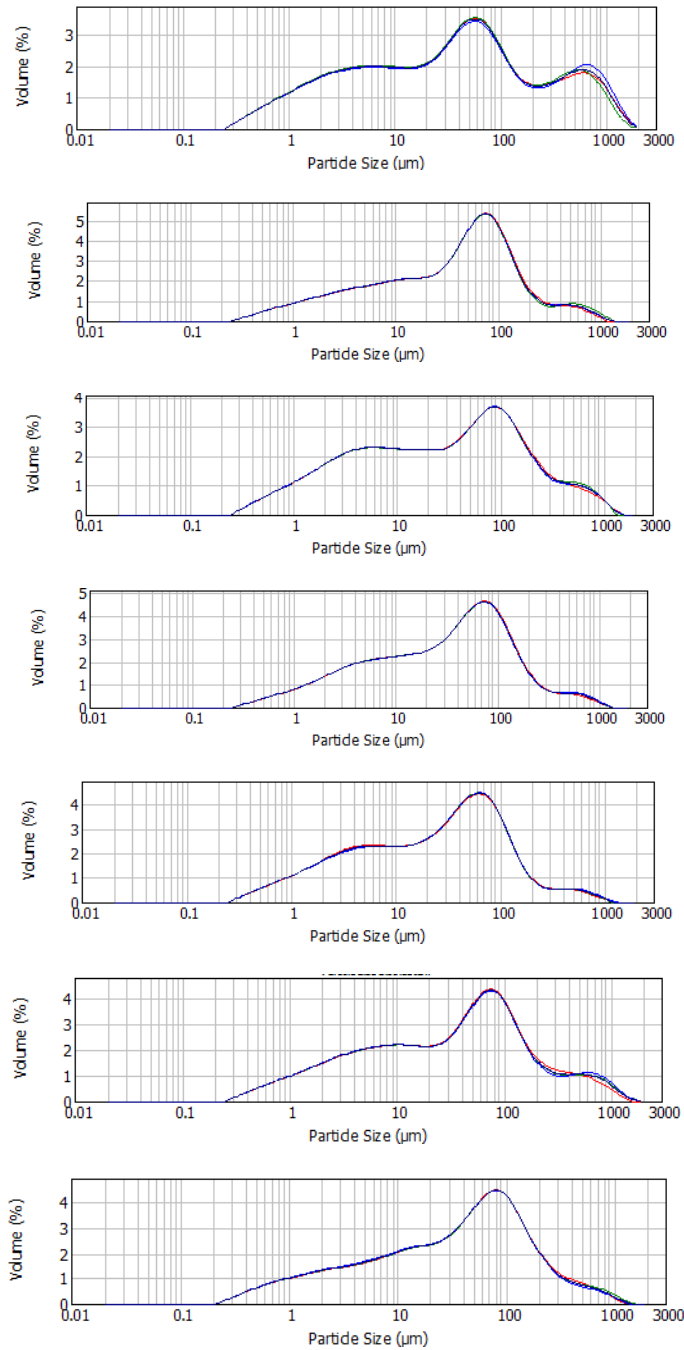


Figure 4.2 – Granulometric distribution for Silt Loam soil texture.

Fom top to bottom: S(18) 15, S(26) 22, S(41) 30, S(44) 33, S(45) 34, S(55) 43, and S(77) 61, accordingly. Soil texture classification as Silt Loam.

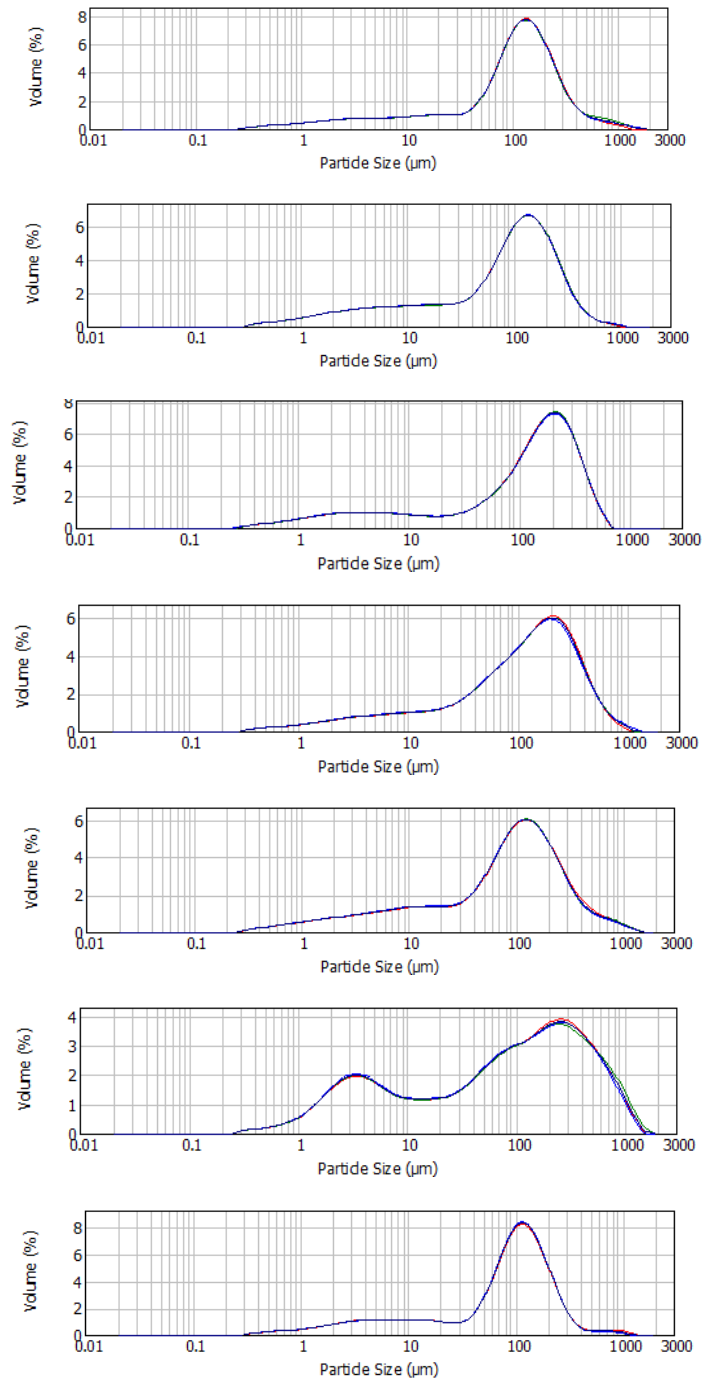


Figure 4.3 – Granulometric distribution for Sandy Loam soil texture.

From top to bottom: S(2) 3, S(3) 4, S(12) 10, S(13) 11, S(21) 18, S(29) 25, and S(72) 56, respectively. Sandy Loam as soil texture classification.

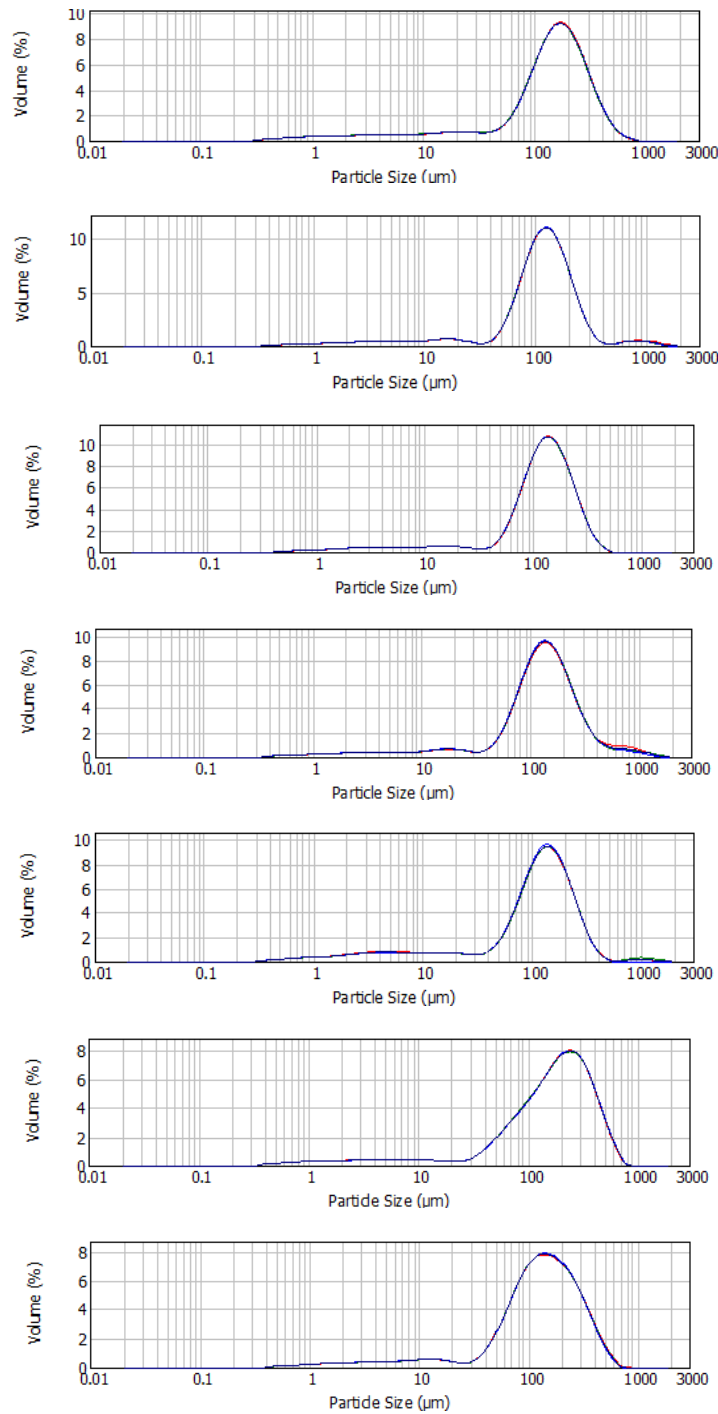


Figure 4.4 – Granulometric distribution for Loamy sand soil texture. Part 1 of 3.

From top to bottom: S(1) 2, S(7) 7, S(10) 9, S(22) 19, S(23) 20, S(30) 26, and S(33) 29, in that order. Loamy Sand classified samples.

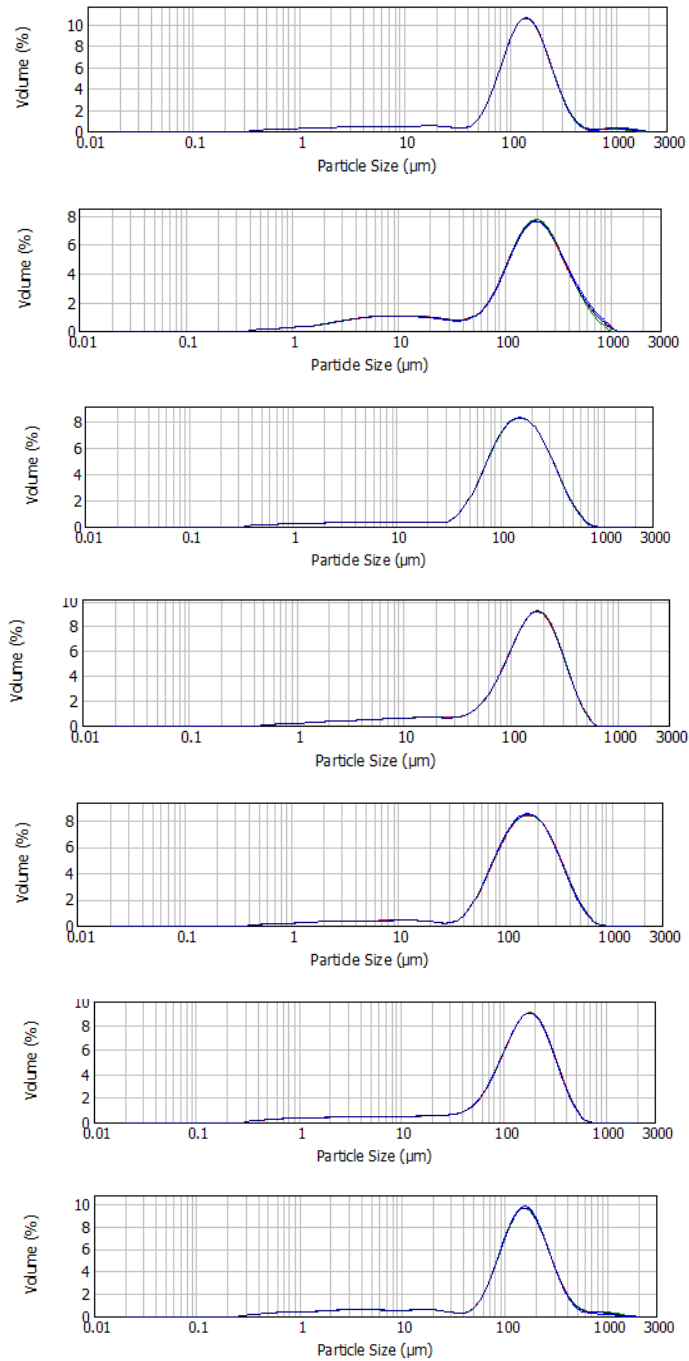


Figure 4.5 – Granulometric distribution for Loamy sand soil texture. Part 2 of 3.

From top to bottom: S(34) 67, S(38) 71, S(52) 40, S(53) 41, S(62) 48, S(71) 55, and S(74) 58, respectively. Loamy Sand classified samples.

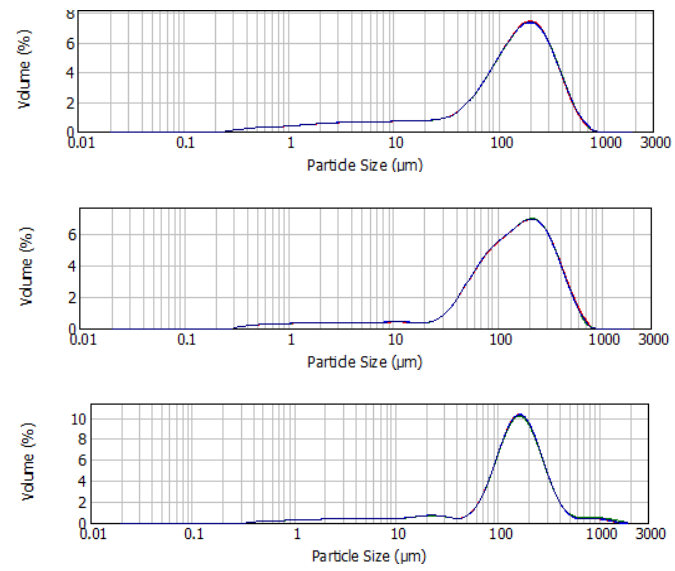


Figure 4.6 – Granulometric distribution for Loamy sand soil texture. Part 3 of 3.

From top to bottom: S(78) 62, S(79) 63, and S(80) 64, in that particular order. Loamy Sand classified samples.

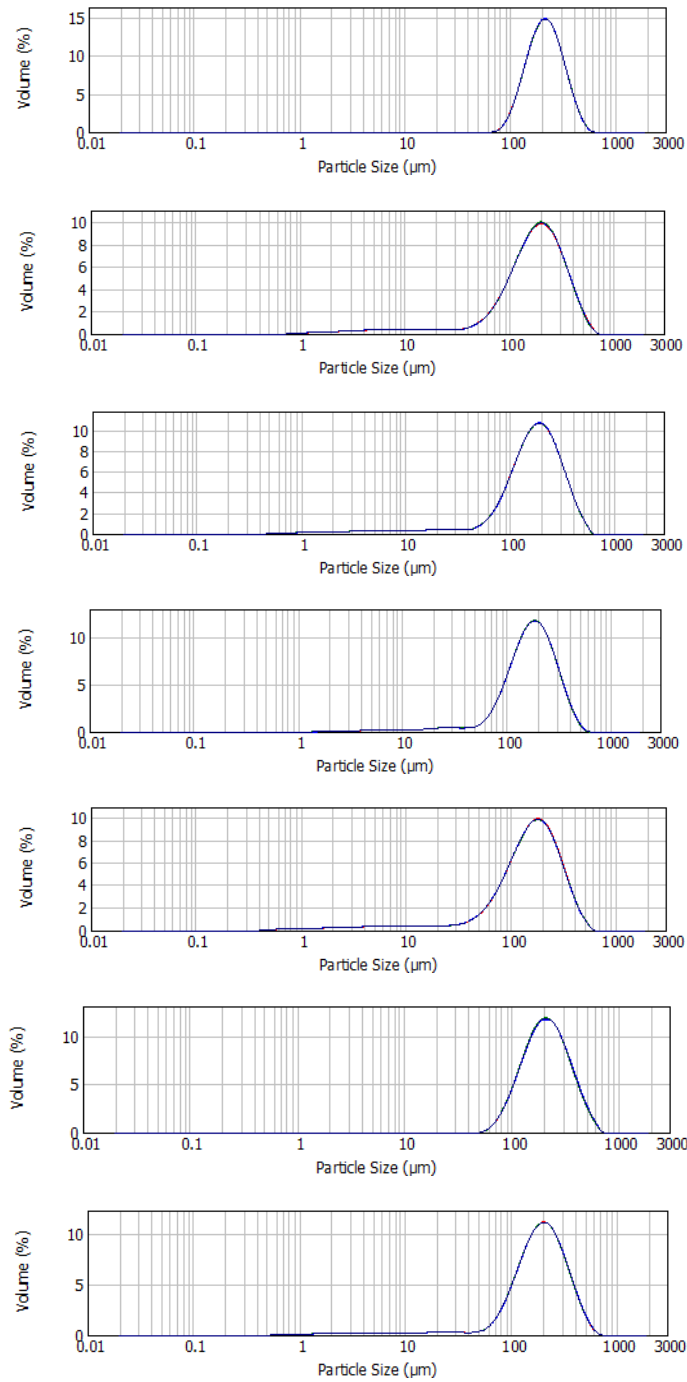


Figure 4.7 – Granulometric distribution for Sand soil texture. Part 1 of 6.

From top to bottom: S(0) 1, S(4) 5, S(9) 8, S(14)12, S(15) 13, S(17) 14, and S(19) 16.

Sand texture classified samples.

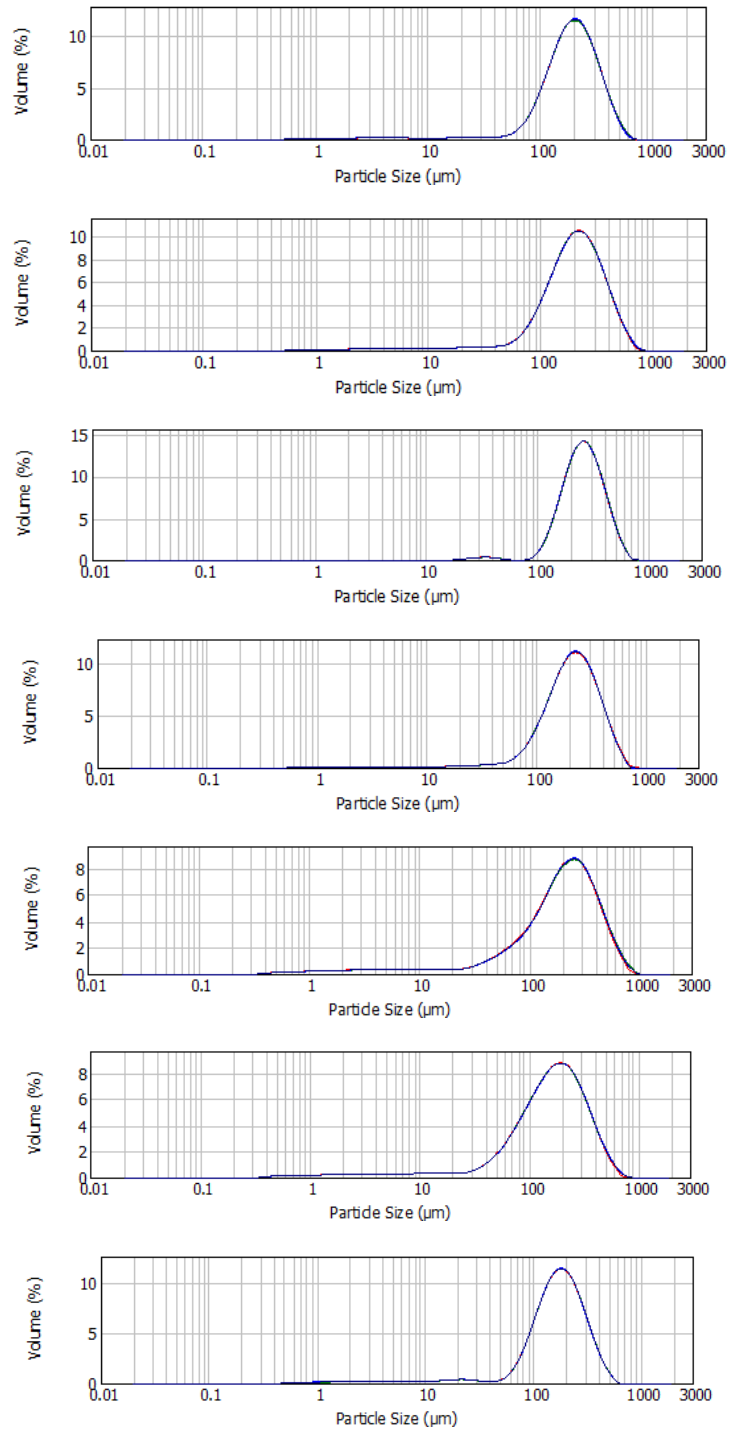


Figure 4.8 – Granulometric distribution for Sand soil texture. Part 2 of 6.

From top to bottom: S(20) 17, S(25) 21, S(27) 23, S(28) 24, S(31) 27, S(32) 28, and S(35) 68. Sand texture classified samples.

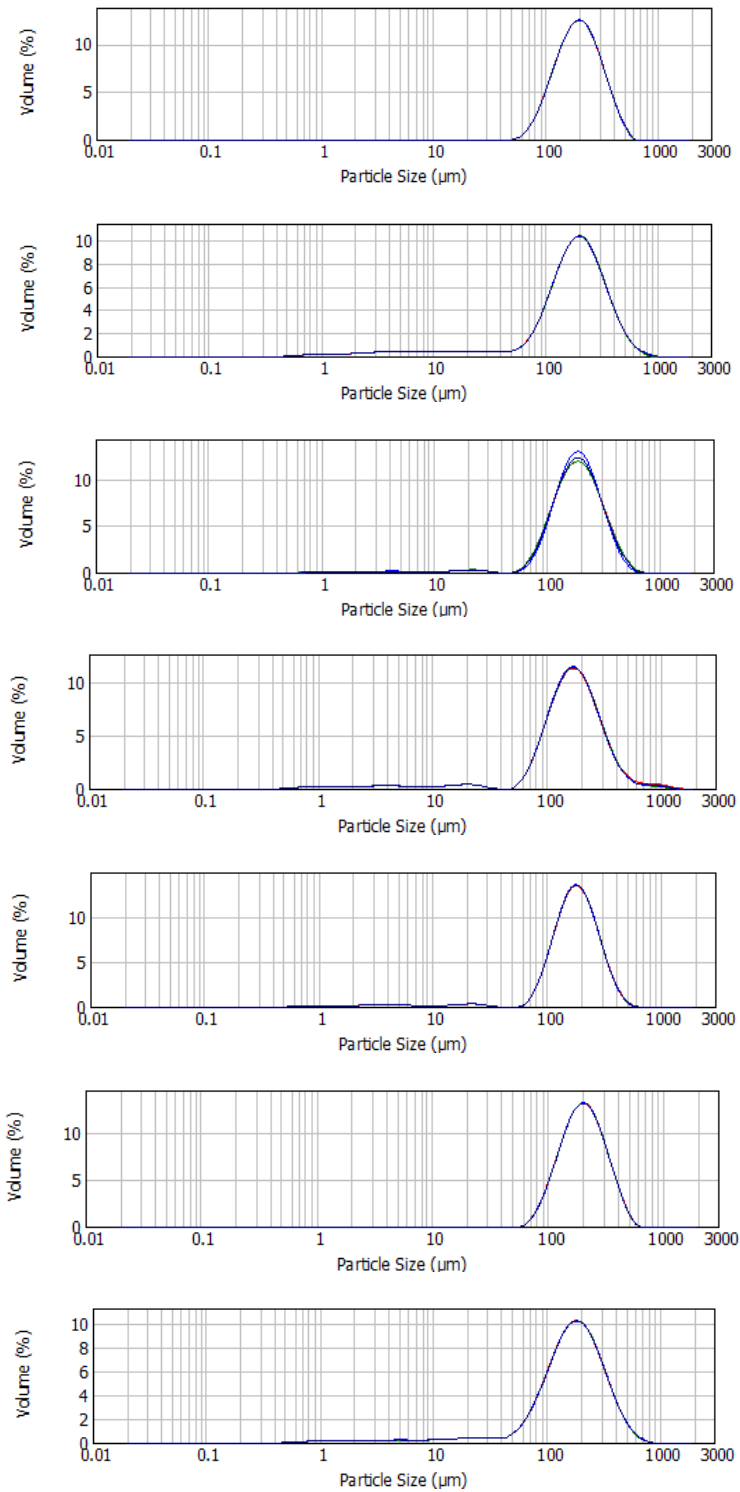


Figure 4.9 – Granulometric distribution for Sand soil texture. Part 3 of 6.

From top to bottom: S(36) 69, S(37) 70, S(39) 72, S(42) 31, S(43) 33, S(47) 35, and S(48) 36. Sand texture classified samples.

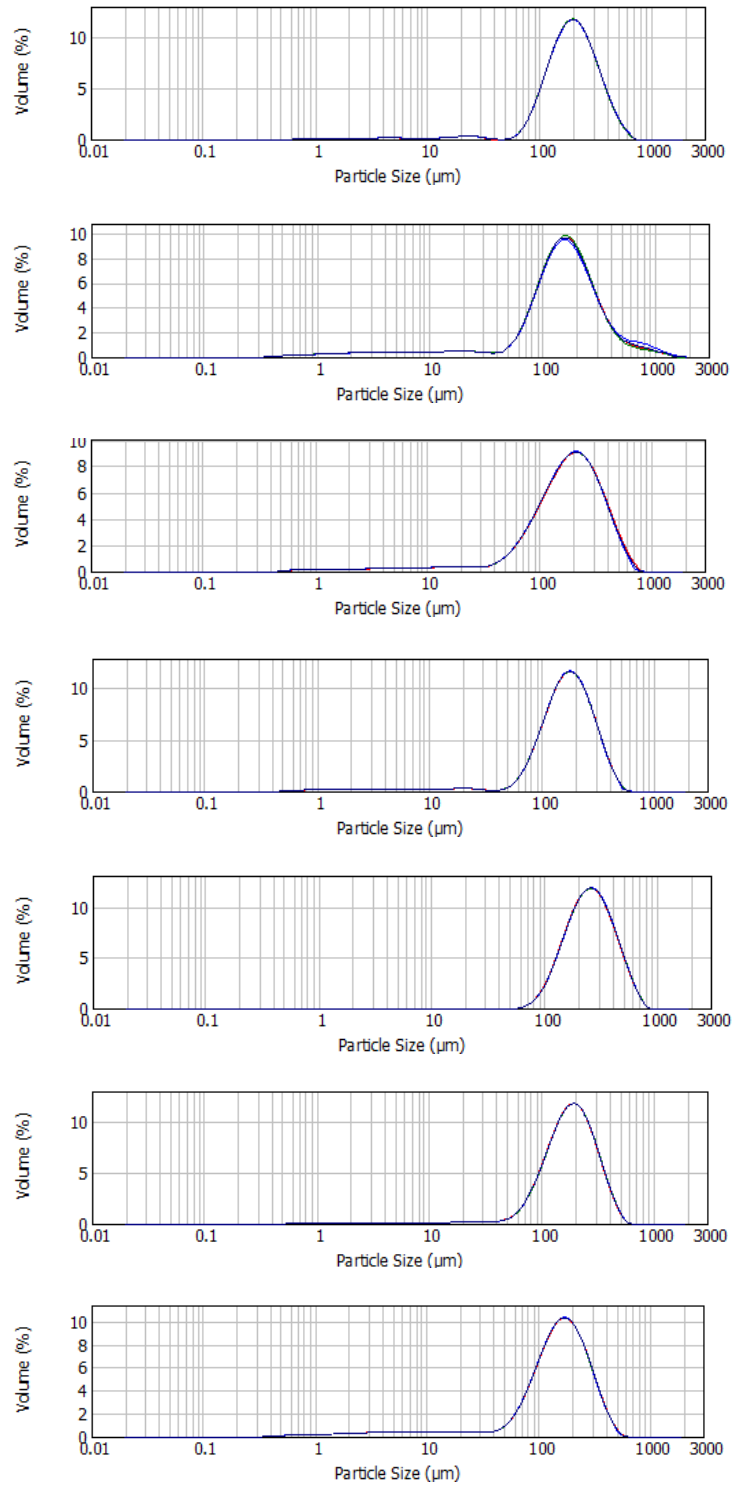


Figure 4.10 – Granulometric distribution for Sand soil texture. Part 4 of 6.

From top to bottom: S(49) 37, S(50) 38, S(51) 39, S(54) 42, S(56) 44, S(57) 45, and S(63) 49. Sand texture classified samples.

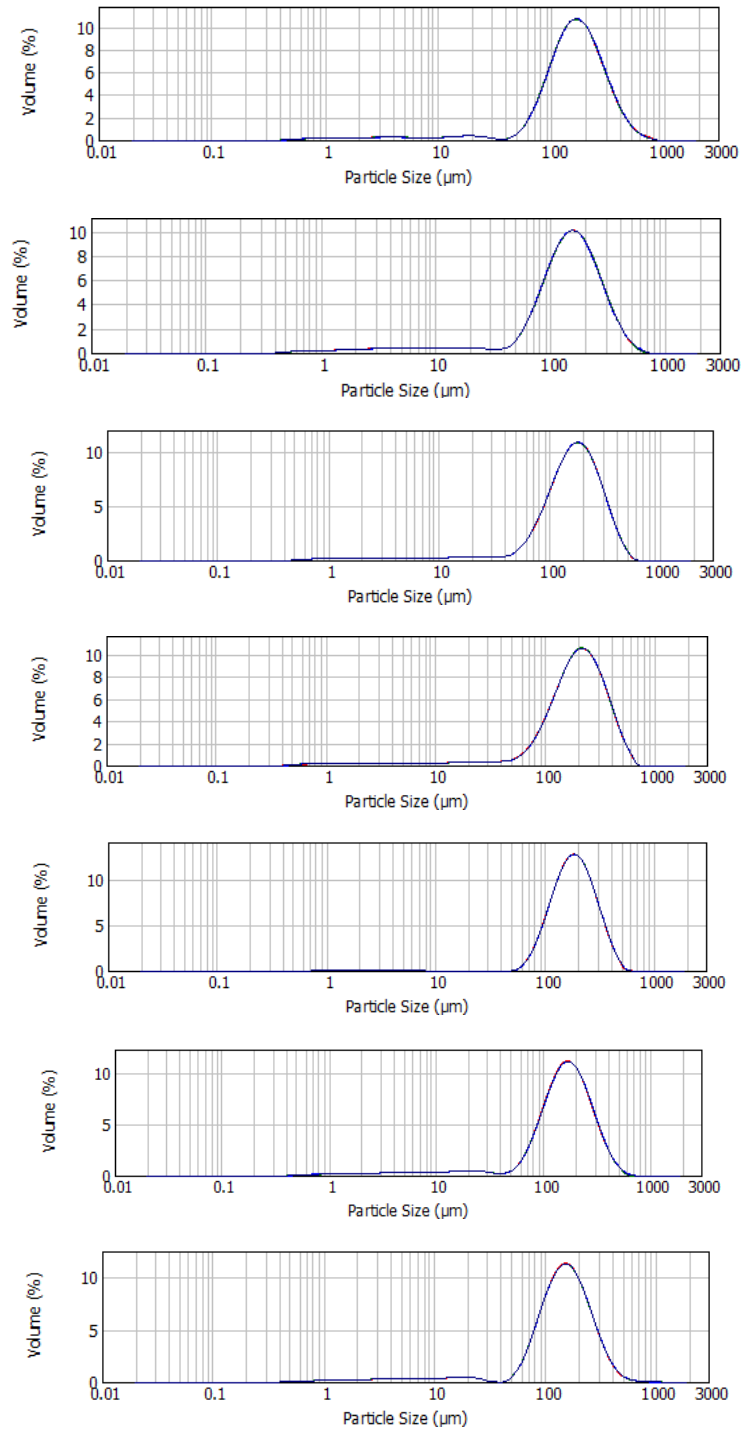


Figure 4.11 – Granulometric distribution for Sand soil texture. Part 5 of 6.

From top to bottom: S(64) 50, S(65) 51, S(66) 52, S(67) 53, S(68) 54, S(73) 57, and S(75) 59. Sand texture classified samples.

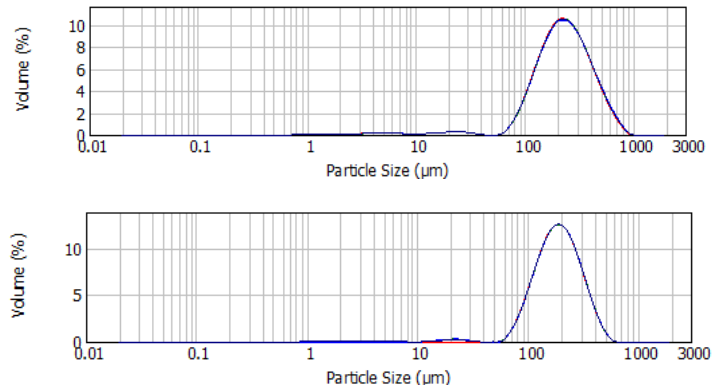


Figure 4.12 – Granulometric distribution for Sand soil texture. Part 6 of 6.

Granulometric distribution. From top to bottom: S(81) 65, and S(82) 66. Sand texture classified samples.

Table 4.1 – Weight percent values for clay, silt, and sand fractions – SHP region.

Clay Loam			
Site	Clay (μm)	Silt (μm)	Sand (μm)
S(76) 60	31.4	45.2	23.4
Silty Clay Loam			
Site	Clay (μm)	Silt (μm)	Sand (μm)
S(59) 46	27.8	59.9	11.9
Silt Loam			
Site	Clay (μm)	Silt (μm)	Sand (μm)
S(18) 15	11.8	50.7	35.0
S(26) 22	9.0	52.3	38.5
S(41) 30	11.4	51.8	36.2
S(44) 33	8.4	56.4	35.0
S(45) 34	11.3	60.7	27.9
S(55) 43	10.2	52.2	36.7
S(77) 61	10.9	50.6	38.2
Loam			
Site	Clay (μm)	Silt (μm)	Sand (μm)
S(6) 6	17.6	46.0	36.4
S(61) 47	9.8	47.4	42.8
Sandy Loam			
Site	Clay (μm)	Silt (μm)	Sand (μm)
S(2) 3	4.7	23.6	71.0
S(3) 4	5.4	31.8	62.7
S(12) 10	5.9	23.1	71.0
S(13) 11	3.7	28.8	67.3
S(21) 18	5.6	33.1	60.8
S(29) 25	6.5	36.3	55.4
S(72) 56	4.7	28.7	66.5
Loamy Sand			
Site	Clay (μm)	Silt (μm)	Sand (μm)
S(1) 2	3.2	15.2	81.6
S(7) 7	2.0	14.4	82.8
S(10) 9	1.8	14.0	84.2
S(22) 19	2.1	14.5	82.5
S(23) 20	3.7	19.8	76.2
S(30) 26	2.7	14.1	83.2
S(33) 29	1.9	16.6	81.4
S(34) 67	2.2	12.0	85.2
S(38) 71	2.3	20.0	77.6
S(52) 40	2.0	12.8	85.2
S(53) 41	1.5	16.1	82.4
S(62) 48	1.6	12.5	85.9
S(71) 55	3.6	15.0	81.5
S(74) 58	4.3	13.7	81.5
S(78) 62	4.2	19.7	76.1
S(79) 63	3.4	17.9	78.6
S(80) 64	2.4	12.5	84.3

Sand			
Site	Clay (μm)	Silt (μm)	Sand (μm)
S(0) 1	0.0	0.0	100.0
S(4) 5	0.6	7.8	91.5
S(9) 8	1.1	8.2	90.7
S(14) 12	0.1	5.8	94.1
S(15) 13	1.5	12.2	86.4
S(17) 14	0.0	0.3	99.7
S(19) 16	0.9	5.3	93.8
S(20) 17	0.8	4.0	95.2
S(25) 21	0.7	5.3	94.0
S(27) 23	0.0	1.4	98.6
S(28) 24	0.7	4.1	95.2
S(31) 27	1.9	11.7	86.5
S(32) 28	1.6	11.7	86.7
S(35) 68	1.0	5.4	93.5
S(36) 69	0.0	0.2	99.8
S(37) 70	1.3	9.8	88.9
S(39) 72	0.5	2.8	96.7
S(42) 31	1.3	5.1	93.3
S(43) 32	0.9	3.0	96.0
S(47) 35	0.0	0.0	100.0
S(48) 36	1.0	7.5	91.5
S(49) 37	0.5	3.0	96.5
S(50) 38	2.0	10.8	86.3
S(51) 39	1.1	8.8	90.1
S(54) 42	1.2	5.1	93.7
S(56) 44	0.0	0.0	100.0
S(57) 45	0.6	3.9	95.5
S(63) 49	1.7	10.9	87.3
S(64) 50	1.3	6.5	92.2
S(65) 51	1.7	10.7	87.7
S(66) 52	1.1	7.1	91.8
S(67) 53	1.3	6.2	92.5
S(68) 54	0.4	1.0	98.6
S(73) 57	1.2	7.6	91.2
S(75) 59	1.3	7.3	91.4
S(81) 65	0.4	2.7	96.8
S(82) 66	0.1	1.2	98.7

4.1.1 Soil Texture Triangle – Southern High Plains dust source sites

Soil texture determination was achieved by plotting the laser diffractometry proportions data scaled to the percentages of sand, silt, and clay. Seven soil texture classes were obtained on the Southern High Plains soils after plotting the proportion values of clay, silt, and sand that resulted from particle size distribution analysis: clay loam, silty clay loam, silt loam, loam, sandy loam, loamy sand, and sand (see Figure 4.13).

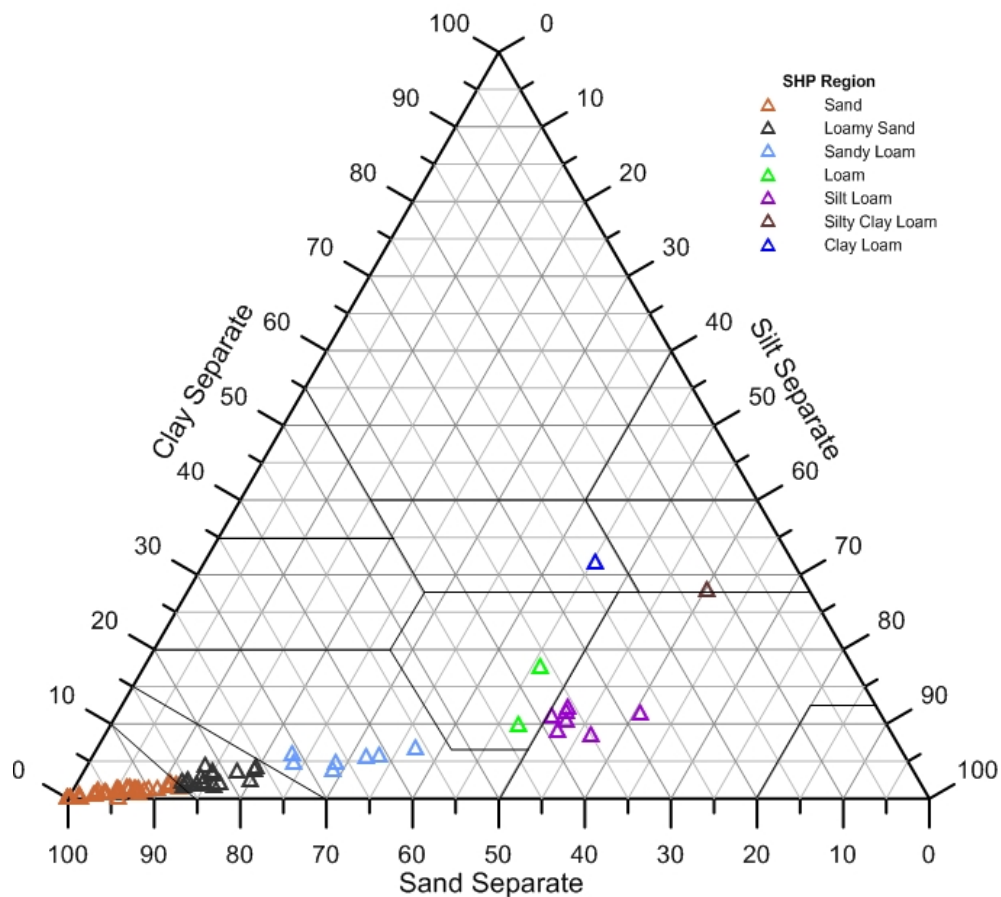


Figure 4.13 – Southern High Plains Ternary Graph.

Soil texture classification for 72 bulk samples. Clay, silt, and sand scaled percentages values included in Table 4.1.

4.2 Granulometric results of the Chihuahuan Desert region

The Chihuahuan Desert region has been sampled recently by several scientists of the University of Texas at El Paso. Dust source sites for these previous doctoral studies were included in 52 bulk samples, from which, 26, 7, and 4 samples were collected and analyzed in *The Pluvial Lake Palomas – Samalayuca Dunes System, Application of Integrated Remote Sensing and GIS Technologies to Geoenvironmental Issues in Far West Texas and Southern New Mexico*, as well as *Evaluating Suspended Dust Particulate Matter from Anthropogenically-Altered Lands* doctoral dissertations by Miguel Dominguez, Ph. D., Adriana Evangelina Perez Ph. D., and Roberto Velarde Ph. D. studies. Continuing with the site selection process, 2 samples from the *Correlation of Dune Geomorphology with Grain Size and Distribution, White Sands National Monument, New Mexico* masters thesis study by Slade Jones, formed part of the samples with available laser diffractometry data. In addition, 7 soil samples were provided from Thomas E. Gill Ph. D.'s UTEP Geology Lab. Percentage of clay, silt, and sand of all the samples were determined, (see Table 4.2).

Six samples from this region were not previously particle size analyzed, however. WRJG001, Jornada Scrap, RL-MV-62A, RL-MV-60B, WRVG007, as well as MRJG006 soil samples, resulted with sand, loam, and loamy sand soil texture classifications, after completing particle size distribution besides soil texture analyses (see Table 4.2).

Minimized weight percent of clay and silt were found on these six samples with values that ranged from 0 to 1.08% on clay, as well as 0 to 6.5% on silt fractions. Sand, on the other hand, fluctuated with weight percent values from 84 to 94.6. Both bimodal and unimodal distributions were observed on granulometric charts. WRVG007 and MRJG006 completed the set of samples with no previous laser diffractometry analysis. As can be seen on Figure 4.14,

unimodal distribution was observed on granulometric charts. The relative proportions of clay, silt, and sand values are included in Table 4.2.

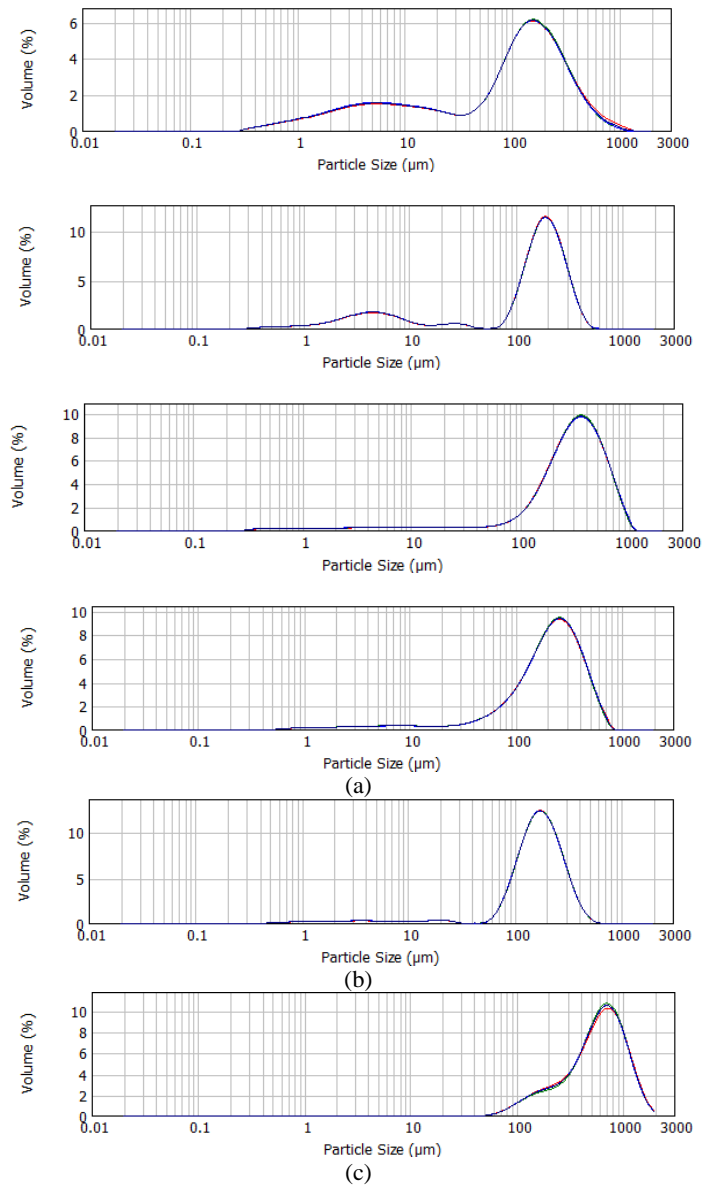


Figure 4.14 – Granulometric distribution for loamy sand, loam, and sand textures.

From top to bottom: (a) MRJG006, MRJG007, MRJG001, and Jornada Scrap, (b) RL-MV-62A, and (c) RL-MV-62B samples. Loamy Sand, Loam, and Sand represented the soil textures classes on samples, in that particular order.

Table 4.2 – Weight percent values for clay, silt, and sand fractions – CHD region.

Sand			
Site	Clay (μm)	Silt (μm)	Sand (μm)
COR 004 ¹	2.6	5.5	91.9
COR 008 ¹	0.0	0.0	100.0
COR 009 ¹	0.0	0.0	100.0
SM 003B ¹	0.0	0.0	100.0
SM 026A ¹	0.0	0.0	100.0
SMD S002 ¹	0.0	0.0	100.0
WRJG001	1.8	4.6	93.3
Jornada	1.0	6.5	92.5
RL-MV-62A	1.3	4.0	94.6
RL-MV-60B	0.0	0.0	84.0
Du1K-u ⁴	0.0	0.5	99.5
Du 1.5K-m ⁴	0.3	2.8	96.9
WS Dune ⁵	0.0	0.1	99.6
WS Interd ⁵	0.0	0.1	99.4
Doña Ana ³	0.8	4.0	94.4
Well 15 ³	1.6	5.1	92.9

Loam			
Site	Clay (μm)	Silt (μm)	Sand (μm)
COR 010 ¹	12.1	42.1	44.9
WRVG007	19.0	36.4	44.6
Coord ²	7.3	40.0	51.4

Clay Loam			
Site	Clay (μm)	Silt (μm)	Sand (μm)
COR 005 ¹	31.5	43.9	24.7

Silty Clay Loam			
Site	Clay (μm)	Silt (μm)	Sand (μm)
ASC 003 ¹	33.2	58.7	8.1
LG 004 ¹	37.7	60.2	2.0
SELP 003 ¹	33.1	56.5	10.2

Silty Clay			
Site	Clay (μm)	Silt (μm)	Sand (μm)
DBM 002 ¹	52.2	41.6	6.2
LF 004 ¹	48.0	43.5	8.5

Clay			
Site	Clay (μm)	Silt (μm)	Sand (μm)
LDP 001 ¹	65.3	33.8	0.8

Loamy Sand			
Site	Clay (μm)	Silt (μm)	Sand (μm)
MRJG006	6.8	10.5	82.3
Dune Surf ²	3.6	18.7	77.7
Sh 1K-m-u ⁴	2.1	19.3	69.8
Sh 400m ⁴	2.8	12.7	84.4
SPHA BOT ³	0.4	17.0	78.0

Sandy Loam			
Site	Clay (μm)	Silt (μm)	Sand (μm)
ASC 002 ¹	8.1	28.3	63.6
COR 001 ¹	4.7	25.0	70.3
LPAL 005 ¹	10.5	16.1	73.4
INBA ³	6.4	26.7	66.8
Hammock ²	5.8	36.0	57.1
SF S36 ²	2.9	42.3	51.3
LSM 002 ¹	4.0	22.5	70.4

Silt Loam			
Site	Clay (μm)	Silt (μm)	Sand (μm)
COR 002 ¹	14.2	54.5	31.3
GV 002 ¹	15.4	50.8	30.0
HWY 45 ¹	16.4	61.1	22.5
TLG 001 ¹	18.0	51.1	29.7
SF S56 ²	6.4	54.8	38.2
SF S2 ²	6.4	71.8	21.8
Well 9 ³	14.6	63.2	21.9
Tula G ³	9.9	57.5	31.6
Old C. Lake ³	1.3	67.6	31.1
ASC 001 ¹	17.4	65.5	16.3
CLP 001 ¹	27.9	63.2	8.9
CLP 002 ¹	26.3	61.2	12.5
B House ²	9.4	74.2	15.9
LSM 003 ¹	27.1	54.8	18.1

¹ Miguel Dominguez, Ph. D. Dissertation samples² Adriana Perez, Ph. D. Dissertation samples³ Thomas E. Gill, Ph. D. UTEP Geology Lab samples⁴ Roberto Velarde, Ph. D. Dissertation samples⁵ Slade Jones, M. S. samples

4.2.1 Soil Texture Triangle – Chihuahuan Desert dust source sites

Soil texture determination was attained by plotting the laser diffractometry proportions data scaled to the percentages of sand, silt, and clay on soil texture triangle, in accordance with the United States Department of Agriculture. Consequently, a total of nine soil texture classes were obtained on the Chihuahuan Desert soils after plotting the proportion values of clay, silt, and sand that resulted from particle size distribution analysis. Sand, loam, clay loam, silty clay loam, silty clay, clay, loamy sand, sandy loam, and silt loam, comprised the soil texture classes after scaling the percentages of clay, silt and sand particle fractions (see Figure 4.15).

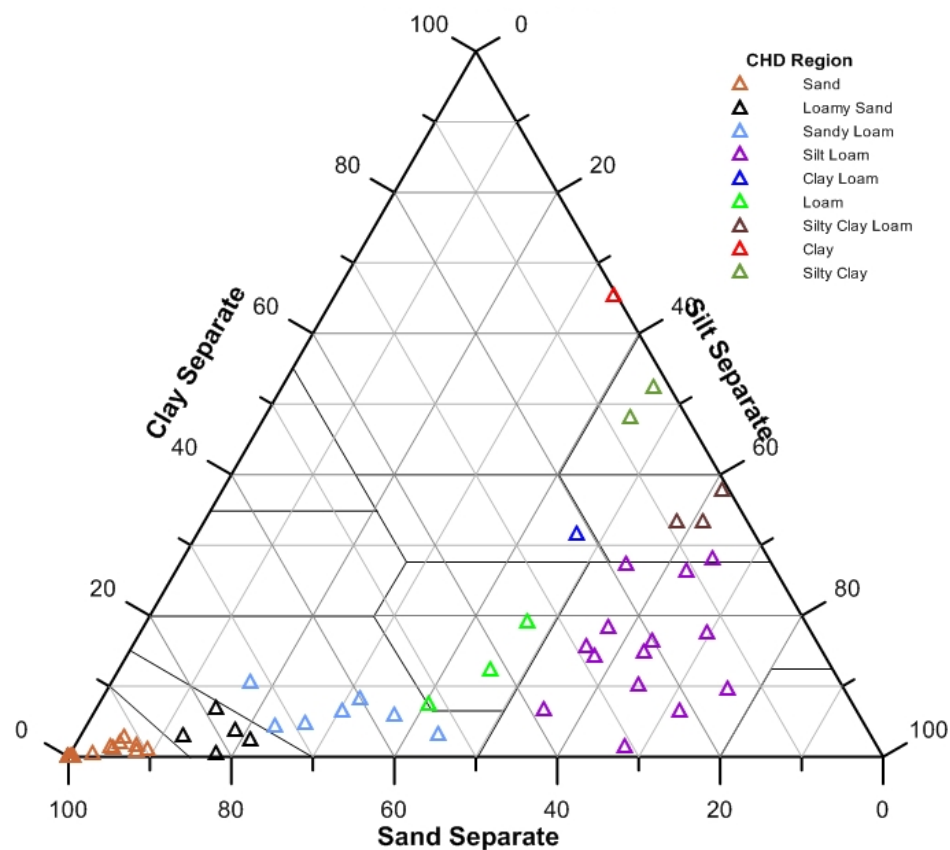


Figure 4.15 – Chihuahuan Ternary Graph.

Chihuahuan Desert Ternary Graph. Soil texture classification for 52 bulk samples. Clay, silt, and sand scaled percentages values included on Table 4.2.

Chapter 5

Total Organic Carbon

Total carbon in soil was determined by using the Shimadzu SSM-5000A solid sample module. (The SSM-5000A is a special accessory for the TOC-V series Total Organic Carbon Analyzer which combines with the TOC-V unit to create a total organic carbon solid sample analysis system capable of analyzing solid samples, such as soil). Performing the direct dry combustion type, that is, soil samples, without any acid treatment, were combusted a high temperature furnace chamber where all forms of carbon (including inorganic carbon, which represented carbonate content in soil) were transformed to carbon dioxide (CO_2), which were then measured with an infrared detector. Dry combustion method shortened the analysis time to about five minutes average per measurement.

5.1 Calibration Curve

Due to the difficulty in weighting out the standard and actual sample to exactly equal amounts, calibration curve was created using the carbon amount (not the carbon concentration) as the reference.

Glucose ($\text{C}_6\text{H}_{12}\text{O}_6$) was used as the total carbon standard. Four samples with different weight of glucose were measured (1.36, 5.00, 20.00, and 40.00 mg) and placed in a ceramic sample boat which were then transmitted into a 900 °C catalytic combustion chamber inside the SSM-5000A to be oxidized into CO_2 with the assistance of oxygen (O_2) gas. The carbon dioxide, was then carried by oxygen gas into the short cell of a non-dispersive infrared (NDIR)

detector in the TOC - V_{CSH} machine, and measured. The total carbon calibration curve results are shown in Figure 5.1.

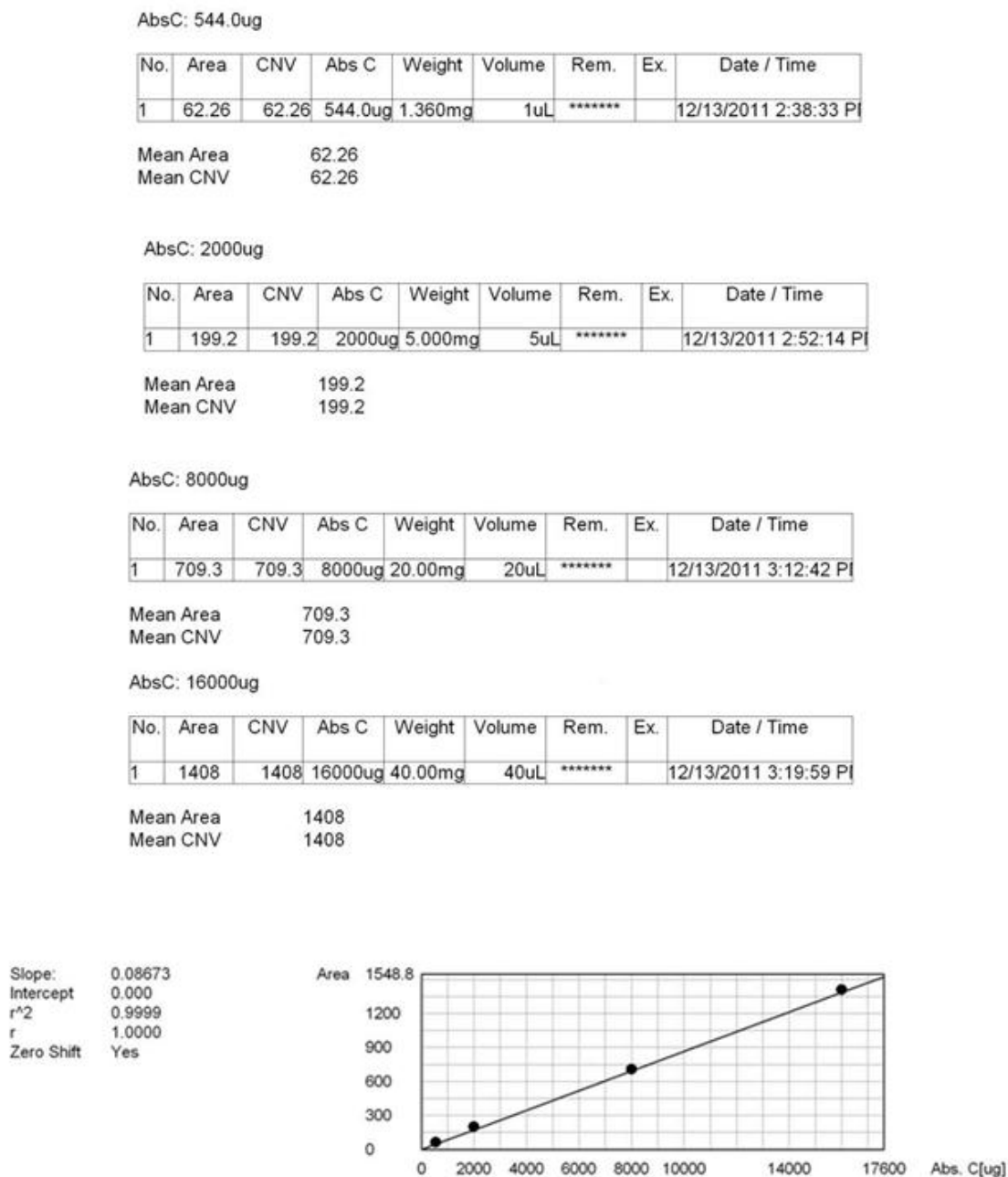


Figure 5.1 – Total Organic Carbon calibration curve.

Glucose as standard. Linearity with a regression value equals to 0.9999.

5.2 Total Organic Carbon Methodology

After creating the total carbon calibration curve, samples from the three regions under study were then combusted inside the SSM-5000A solid sample module by following the methodology described below. A total of 123 soil samples were TOC analyzed: 72-, 27-, and 24-samples from the Southern High Plains, the Chihuahuan Desert USA, and the Chihuahuan Desert MEX regions, in that particular order.

5.2.1 Total Organic Carbon Methodology

1. Powered on the Total Organic Carbon V series (TOC-V) and the SSM-5000A Solid Sample Module.
2. Selected *New System* icon on TOC-V control main menu.
3. Chose the TOC/TN icon so that the total nitrogen measuring instrument turned on.
4. Opened the valve of the carrier gas supply pressure and adjusted to 300 Kpa.
5. Set the TOC-V pressure to 200 Kpa as well as the flow gauge to 500 ml/min.
6. Selected the *SSM Option* after clicking on the *New System* icon on the TOC-V control main menu.
7. Selected the calibration curve "*SHP Calibration Curve. 2011_12_13_14_31_45.cal*" with date of creation *12/13/2011*.
8. Assured the units on *mg* because of solid nature sample by observing the measurements parameters.
9. Edited the soil sample to be analyzed from the *edit point dataset* which was previously created.

10. Adjusted the concentration and weight of the *point* (soil sample to be analyzed), assuring that these values corresponded to the carbon not to the glucose.
11. Corresponding to this study, Glucose and Carbon values were: 1.36mg Glucose – 8mg Carbon; 5mg Glucose – 2 mg Carbon; 20mg Glucose – 8 mg Carbon; and 40mg Glucose – 16 mg Carbon.
12. Added all the *points* (soil samples) to be included on the calibration curve.
13. Started the Total Carbon analysis by connecting the *points* created electronically to the SSM-5000A Solid Sample Module.
14. Followed the instructions that appeared on the computer monitor when single measurement ended.
15. Took the sample boat out and placed next sample boat entering the new concentration on the window that opened on the SSM-5000A software.
16. Performed these steps as many times were needed. Stopped machine when the measurement of the last *point* ended.

5.3 TOC Results for Southern High Plains samples

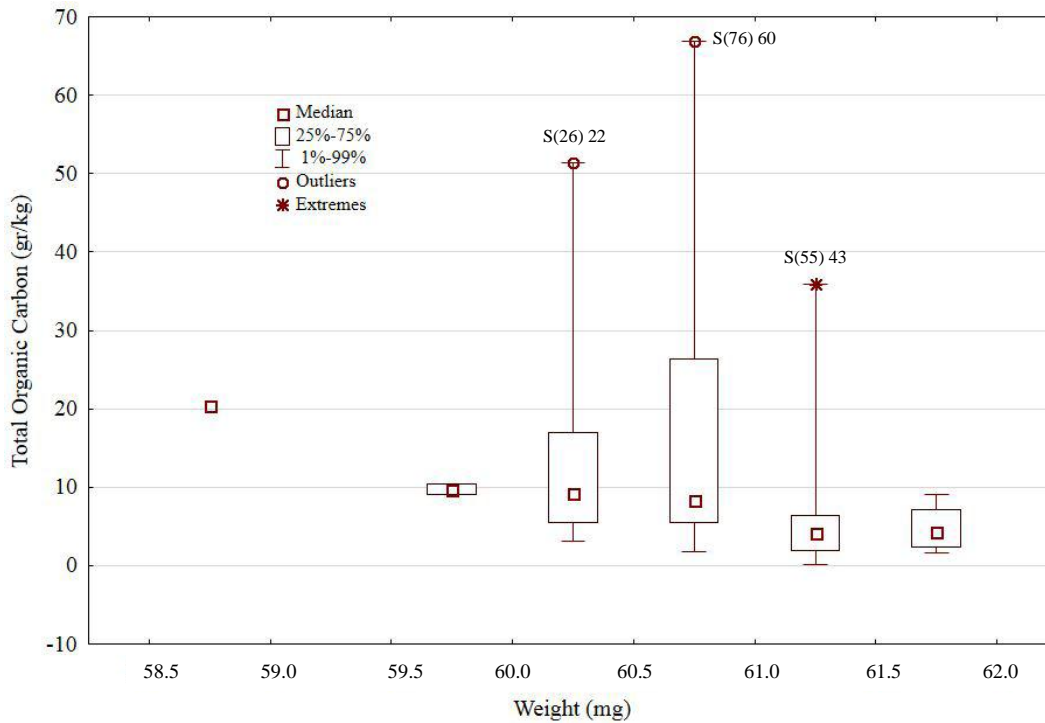
Direct dry combustion was used when obtaining Total Organic Carbon. Samples from the Southern High Plains region scoped a weight range from 58.5 to 62.0 mg of bare soil when performing the TOC analysis. Table 5.1 shows these weight ranges as well as the soil samples considered to be either outliers and/or extreme cases, which in this instance, S(26) 22 and S(76) 60 samples were both outliers categorized, and sample S(55) 43 was considered as an extreme case after comparison completion of its total organic carbon value with those of the same weight range group. The descriptive statistics results computed a total organic carbon mean value of

13.77g/kg-soil; standard deviation value equals to 14.18; in addition to minimum and maximum 0.20 and 66.87 g/kg-soil TOC values, respectively. The results obtained from total organic carbon measurement of each soil sample are shown in Figure 5.2. Since the weight of each sample was entered at the time of the measurement, the measurement results were expressed in milligram units.

Table 5.1 – Total Organic Carbon results on SHP samples.

Box Plots Descriptive Statistics

Weight <= 59 mg	Weight 59.5, 60 mg	Weight 60, 60.5 mg	Weight 60.5, 61 mg	Weight 61, 61.5 mg	Weight 61.5, 62 mg
S(61) 47	S(1) 2 S(23) 20	S(4) 5 S(6) 6 S(9) 8 S(10) 9 S(12) 10 S(13) 11 S(15) 13 S(17) 14 S(19) 16 S(20) 17 S(21) 18 S(22) 19 S(26) 22 S(28) 24 S(29) 25 S(31) 27 S(33) 29 S(36) 69 S(37) 70 S(38) 71 S(65) 51 S(66) 52 S(67) 53 S(74) 58 S(79) 63 S(80) 64	S(2) 3 S(3) 4 S(14) 12 S(18) 15 S(25) 21 S(27) 23 S(30) 26 S(34) 67 S(35) 68 S(42) 31 S(43) 32 S(44) 33 S(48) 36 S(50) 38 S(52) 40 S(53) 41 S(56) 44 S(59) 46 S(63) 49 S(68) 54 S(71) 55 S(72) 56 S(76) 60 S(77) 61 S(78) 62 S(82) 66	S(0) 1 S(32) 28 S(55) 43 S(57) 45 S(62) 48 S(73) 57 S(81) 65	S(7) 7 S(47) 35 S(64) 50 S(75) 59



1 Case	2 Cases	32 Cases	26 Cases	7 Cases	4 Cases
Median = 20.42	Median = 9.69	Median = 9.29	Median = 8.28	Median = 4.11	Median = 4.29
25% = 20.42	25% = 9.04	25% = 5.53	25% = 5.52	25% = 1.88	25% = 2.44
75% = 20.42	75% = 10.34	75% = 17.02	75% = 26.38	75% = 6.44	75% = 7.19
1% = 20.42	1% = 9.04	1% = 3.07	1% = 1.70	1% = 0.21	1% = 1.62
99% = 20.42	99% = 10.34	99% = 51.33	99% = 66.89	99% = 35.95	99% = 9.06

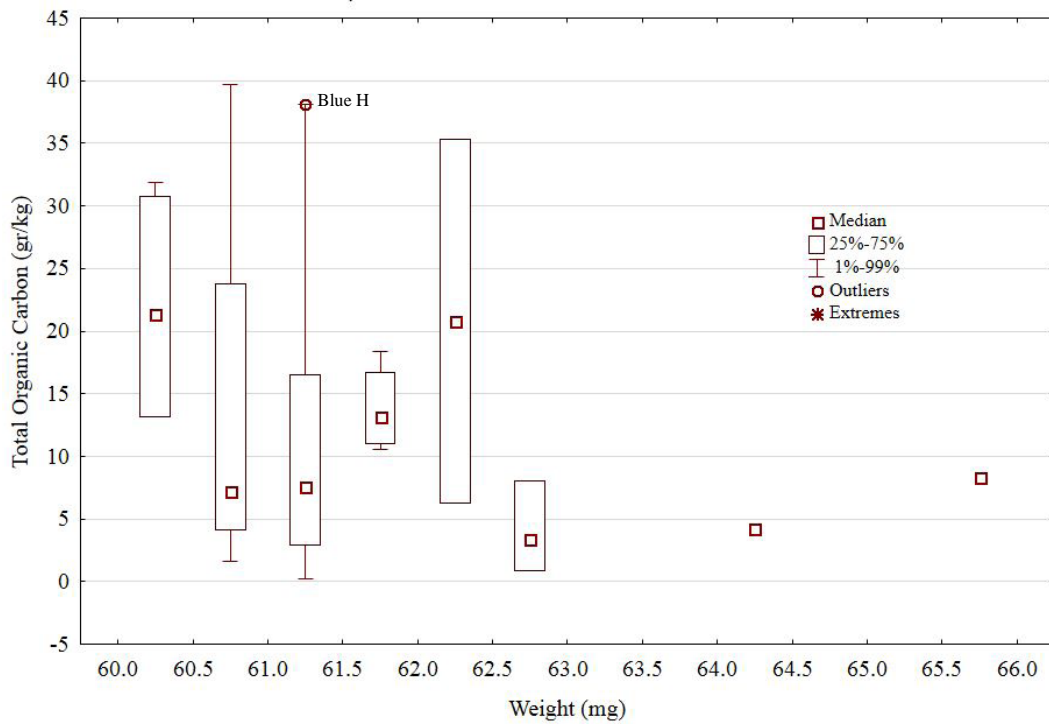
5.4 TOC Results for the Chihuahuan Desert USA region

Direct dry combustion was performed when obtaining Total Organic Carbon. Samples from the Chihuahuan Desert USA region comprised a weight range from 60.0 to 66.0 mg of raw soil when performing the TOC analysis. Table 5.2 illustrates these weight ranges as well as the soil samples considered to be either outliers and/or extreme cases, which in this case, Blue House sample was outlier categorized; no extreme cases were observed. The descriptive statistics results calculated a total organic carbon mean value of 13.24gr/kg-soil; standard deviation value equals to 11.82; in addition to minimum and maximum 0.18 and 39.74 gr/kg-soil TOC values, correspondingly. The results obtained from total organic carbon measurement of each soil sample are shown in Figure 5.3. Since the weight of each sample was entered at the time of the measurement, the measurement results were expressed in milligram units.

Table 5.2 – Total Organic Carbon results on the Chihuahuan Desert USA region.

Box Plots Descriptive Statistics

Weight 60, 60.5 mg	Weight 60.5, 61 mg	Weight 61, 61.5 mg	Weight 61.5, 62 mg	Weight 62, 62.5 mg	Weight 62.5, 63 mg	Weight 64, 64.5 mg	Weight 65.5, 66 mg
McGreg Doña A. SF S36 SF S2	SF S56 WRJ 01 Dul Ku ShlKmu	WS Du OCL SPHA Blue H WRJ06 WRJ07 Du1.5 Jornad	Tula G Well15 Hamm Dune S	Coord Sh400m	WS In Well9 RL62A	RL62B	INBA



	4 Cases	4 Cases	8Cases	4Cases	2Cases	3Cases	1 Case	1 Case
Median =	21.40	7.17	7.54	13.19	20.79	3.38	4.18	8.35
25% =	13.21	4.09	2.94	11.00	6.29	0.88		
75% =	30.73	23.76	16.49	16.67	35.30	8.05		
1% =	13.21	1.62	0.18	10.56	6.28	0.88		
99% =	31.88	39.74	38.14	18.39	35.30	8.05		

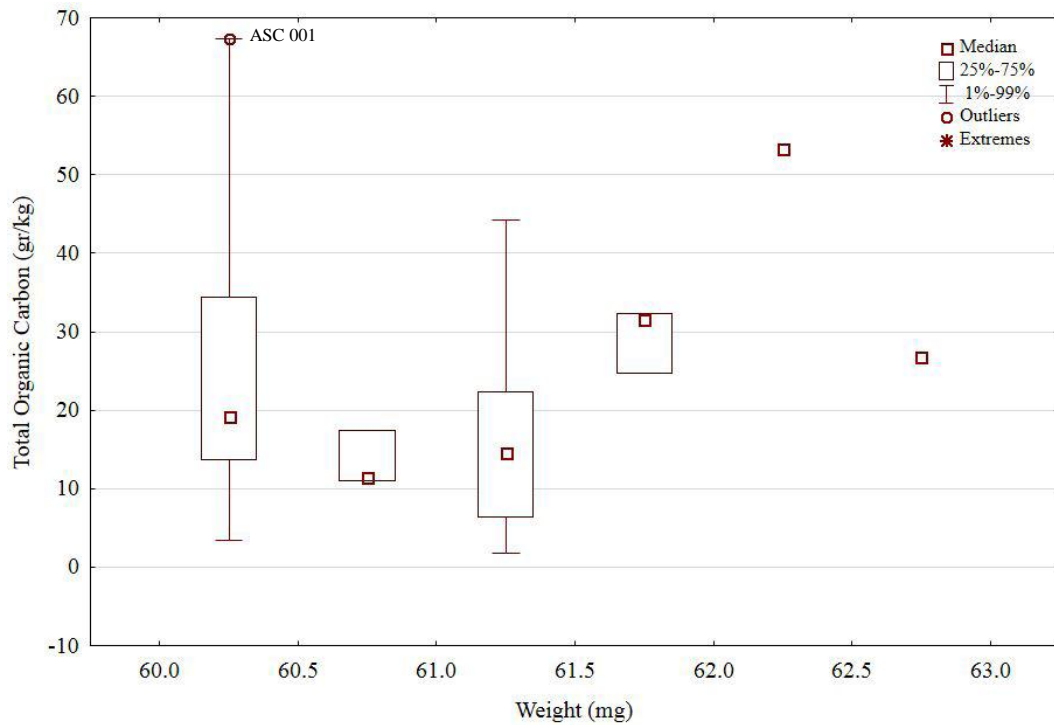
5.5 TOC Results for the Chihuahuan Desert MEX region

Direct dry combustion was used when obtaining Total Organic Carbon. Samples from the Chihuahuan Desert MEX region enclosed a weight range from 60.0 to 63.0 mg of bare soil when implementing the TOC analysis. Table 5.3 demonstrates these weight ranges as well as the soil samples considered to be either outliers and/or extreme cases, which in this case, ASC 001 sample was outlier characterized; no extreme cases were observed. The descriptive statistics results calculated a total organic carbon mean value of 23.25g/kg-soil; standard deviation value equals to 15.84; in addition to minimum and maximum 1.73 and 67.34 g/kg-soil TOC values, correspondingly. The results acquired from total organic carbon measurement of each soil samples are shown in Figure 5.4. Since the weight of each sample was entered at the time of the measurement, the measurement results were expressed in milligram units and converted to g/kg-soil afterwards.

Table 5.3 – Total Organic Carbon results on the Chihuahuan Desert MEX region.

Box Plots Descriptive Statistics

Weight 60, 60.5 mg	Weight 60.5, 61 mg	Weight 61, 61.5 mg	Weight 61.5, 62 mg	Weight 62, 62.5 mg	Weight 62.5, 63 mg
ASC 001 ASC 003 COR 001 COR 004 COR 009 DBM 002 GV 002 LDP 001 LG 004 LSM 003	COR 002 COR 005 LSM 002	CLP 002 COR 008 COR 010 HWY 45 SELP 003 SMD 002	CLP 001 LF 004 TLG 001	ASC 003	LPAL 005



10 Cases	3 Cases	6 Cases	3 Cases	1 Case	1 Case
Median = 19.24	Median = 11.54	Median = 14.61	Median = 31.53	Median = 53.26	Median = 26.79
25% = 13.73	25% = 10.98	25% = 6.46	25% = 24.77	25% =	25% =
75% = 34.38	75% = 17.43	75% = 22.38	75% = 32.29	75% =	75% =
1% = 3.41	1% = 10.98	1% = 1.73	1% = 24.77	1% =	1% =
99% = 67.34	99% = 17.43	99% = 44.19	99% = 32.29	99% =	99% =

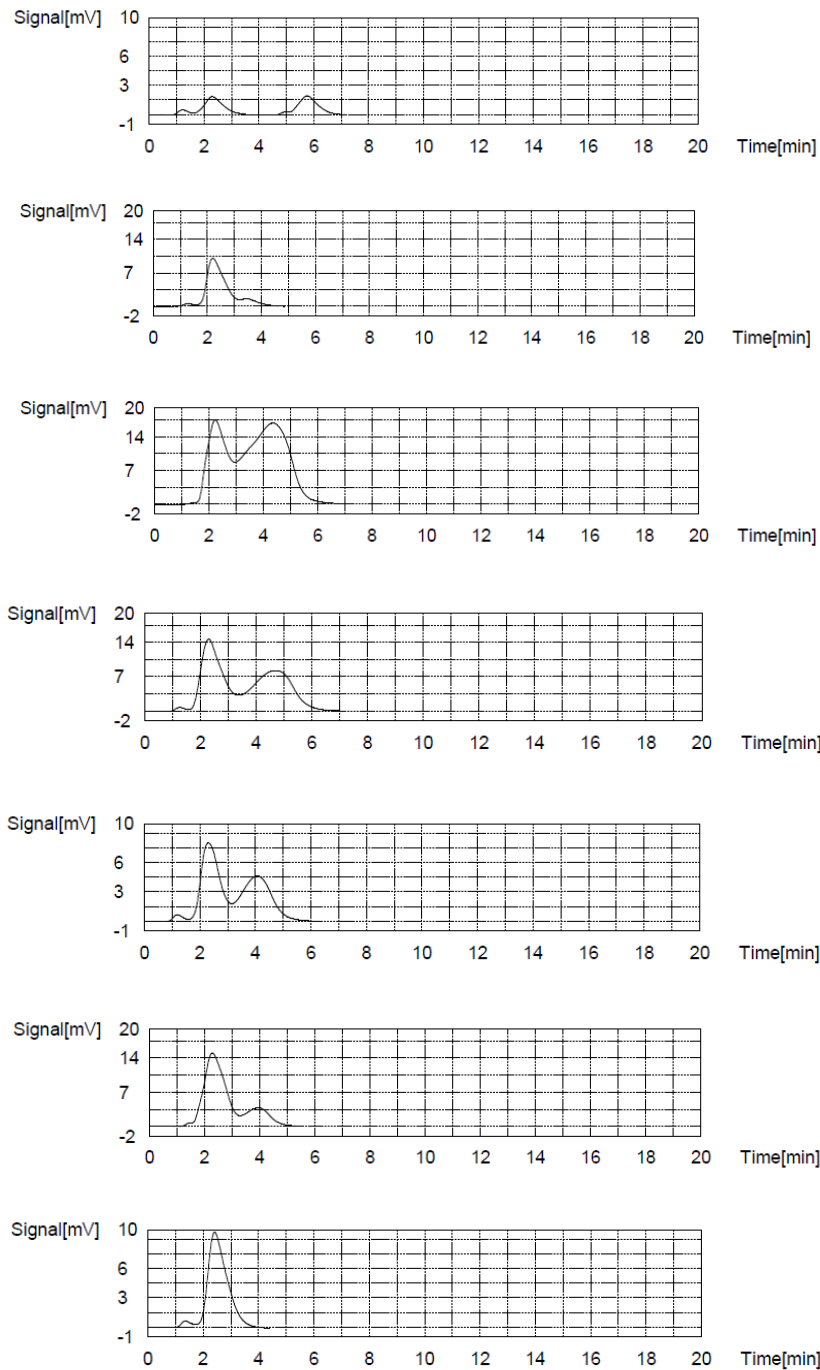


Figure 5.2 – Total Organic Carbon measurement results: SHP region.

From top to bottom: S(0) 1; S(1) 2; S(2) 3; S(3) 4; S(4) 5; S(6) 6; and S(7) 7 samples.

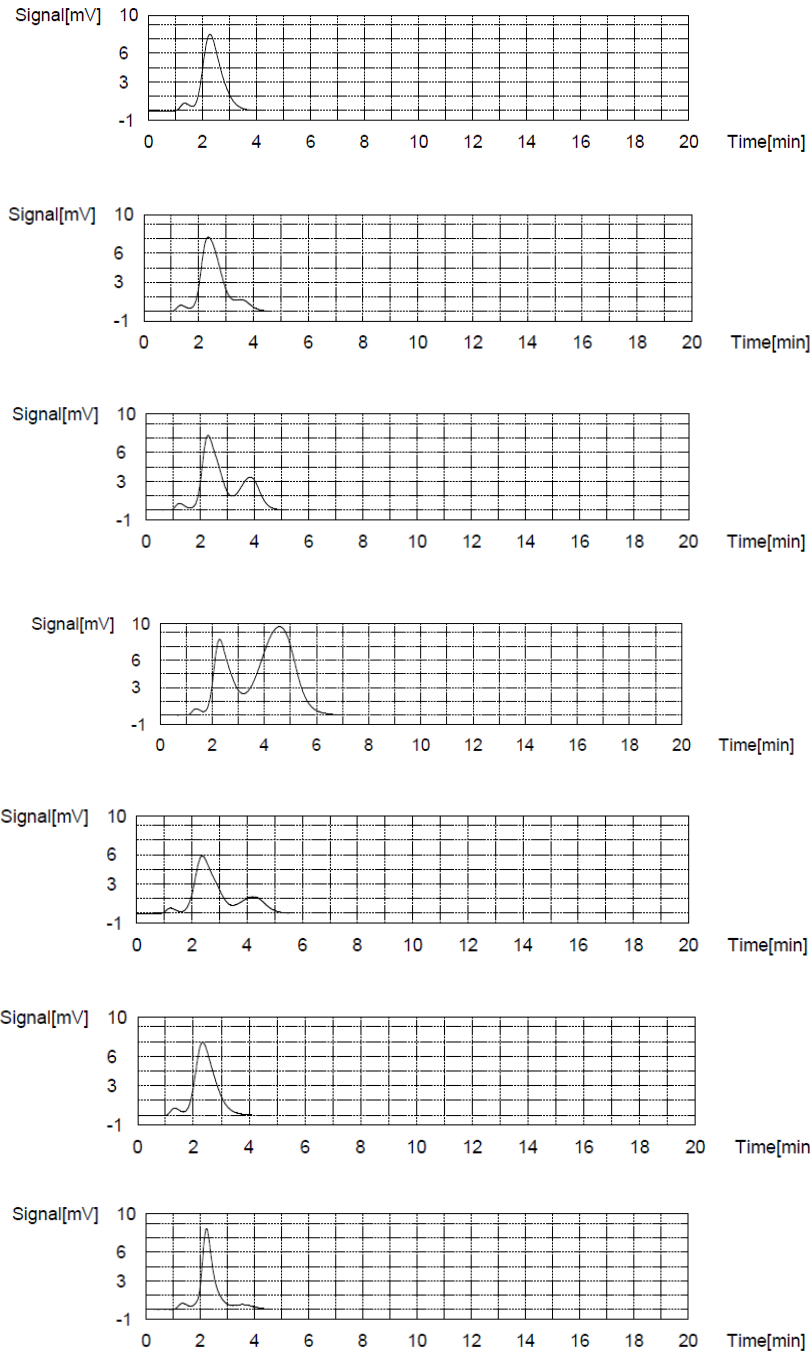


Figure 5.2 (Cont.) Total Organic Carbon measurement results: SHP region.

From top to bottom: S(9) 8; S(10) 9; S(12) 10; S(13) 11; S(14) 12; S(15) 13; and S(17) 14 samples.

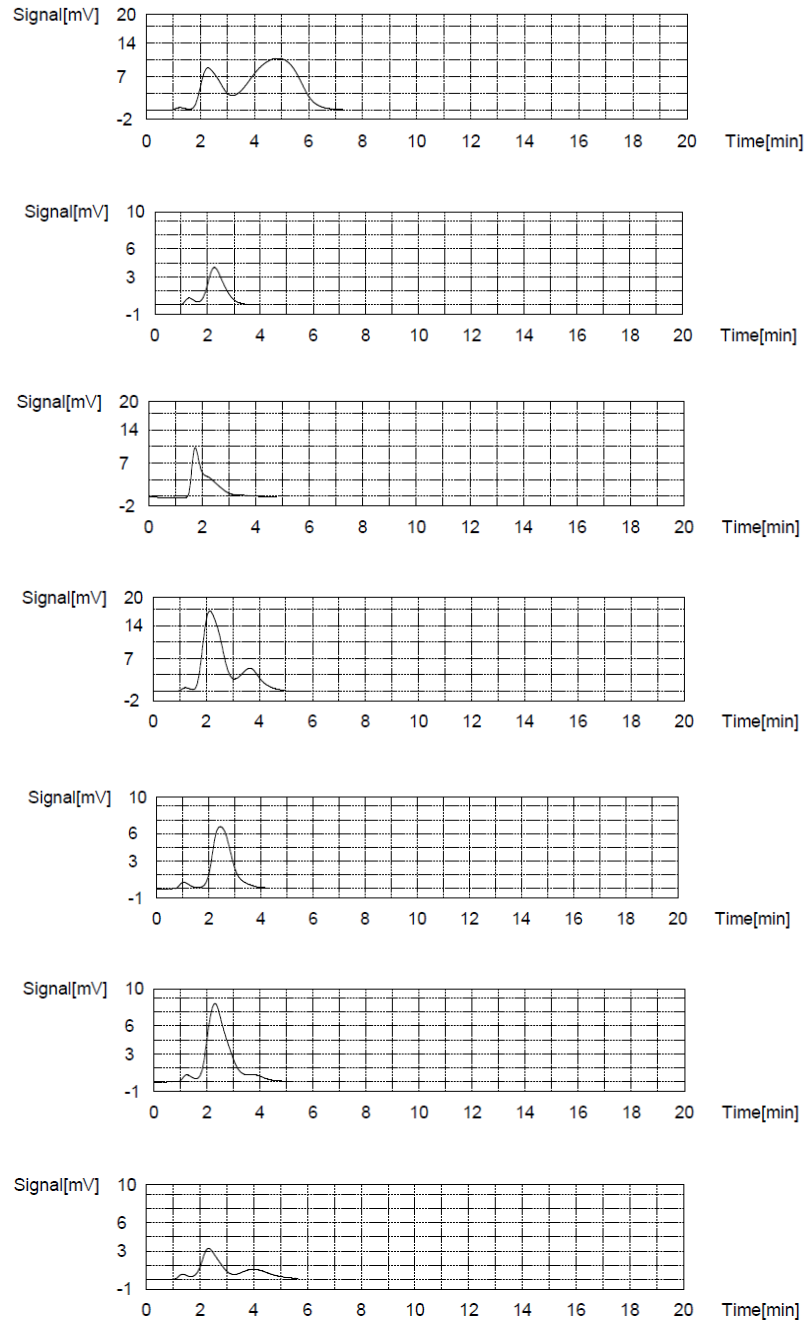


Figure 5.2 (Cont.) Total Organic Carbon measurement results: SHP region.

From top to bottom: S(18) 15; S(19) 16; S(20) 17; S(21) 18; S(22) 19; S(23) 20; and S(25) 21 samples.

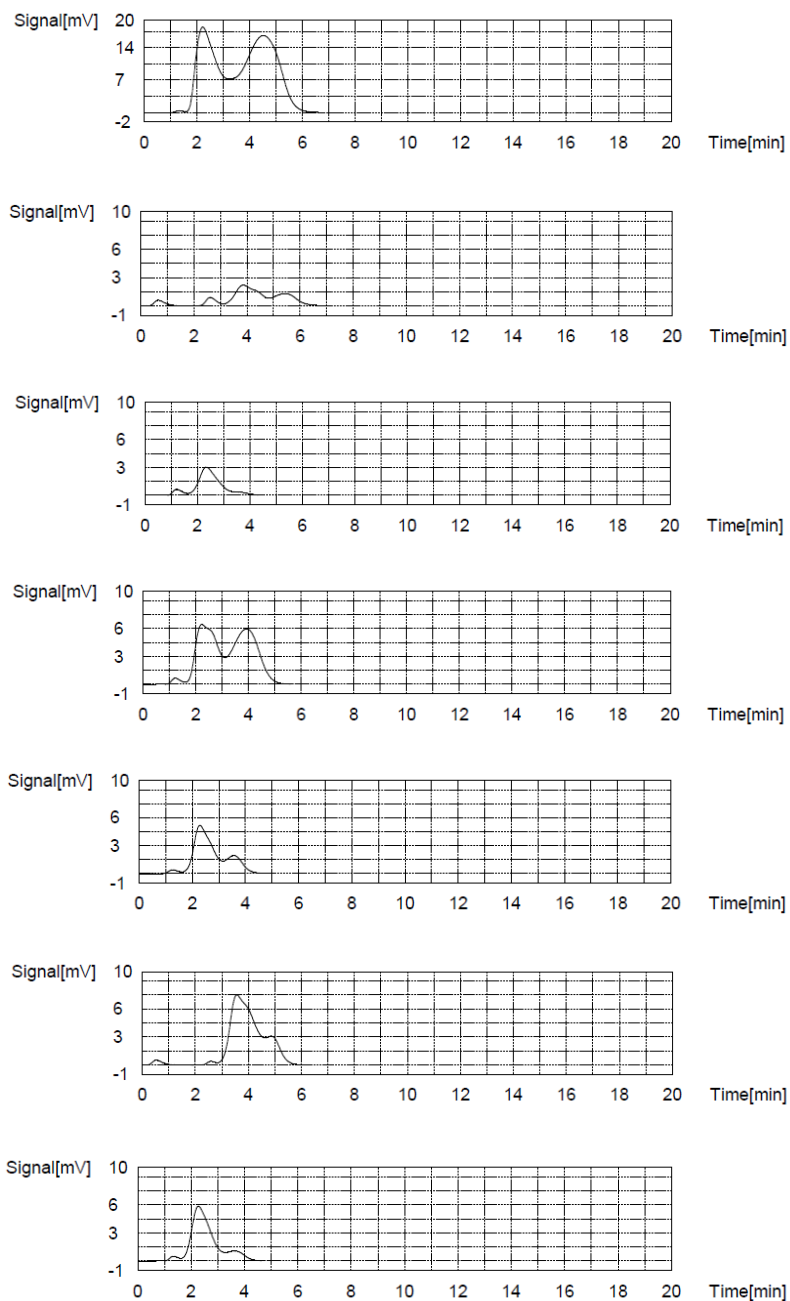


Figure 5.2 (Cont.) Total Organic Carbon measurement results: SHP region.

From top to bottom: S(26) 22; S(27) 23; S(28) 24; S(29) 25; S(30) 26; S(31) 27; and
 S(32) 28 samples.

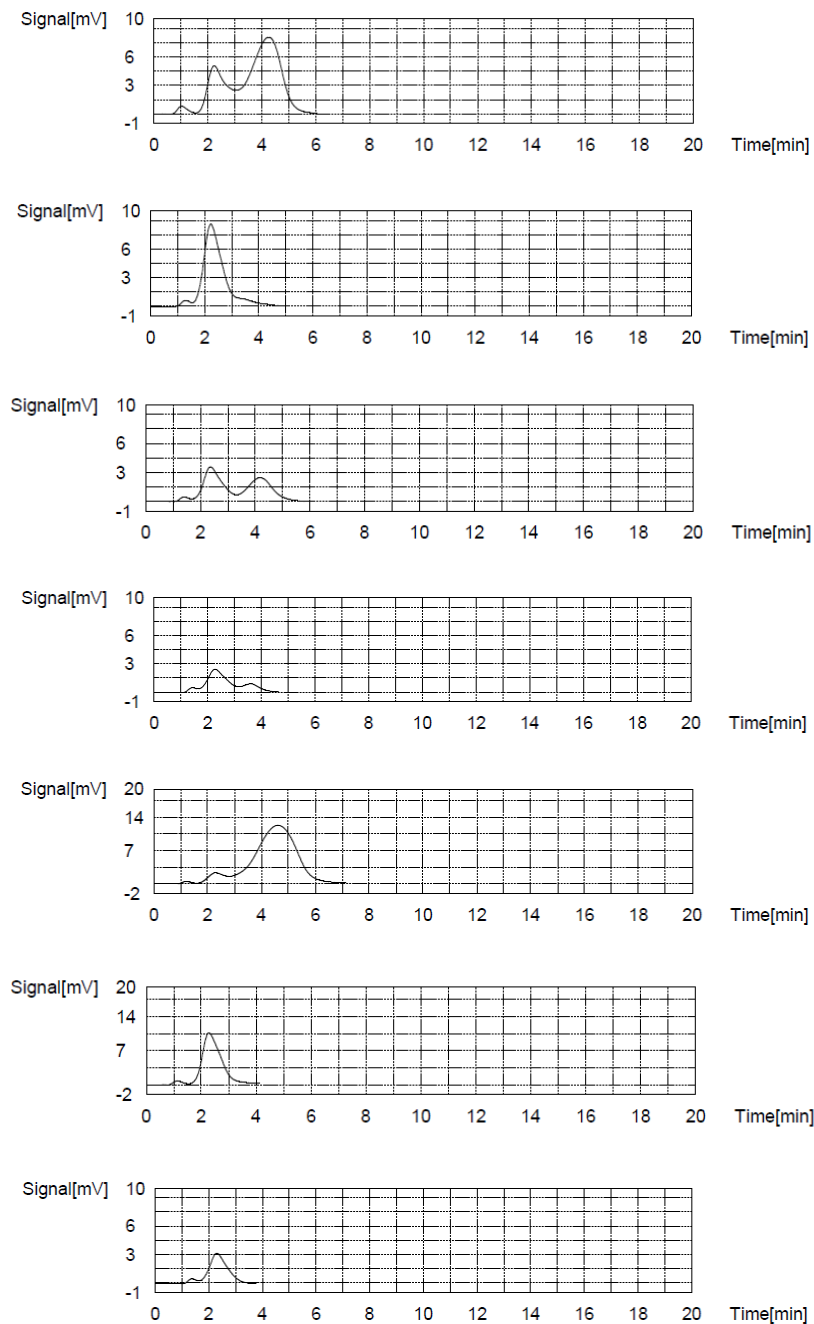


Figure 5.2 (Cont.) Total Organic Carbon measurement results: SHP region.

From top to bottom: S(33) 29; S(34) 67; S(35) 68; S(36) 69; S(37) 70; S(38) 71; and
S(39) 72 samples.

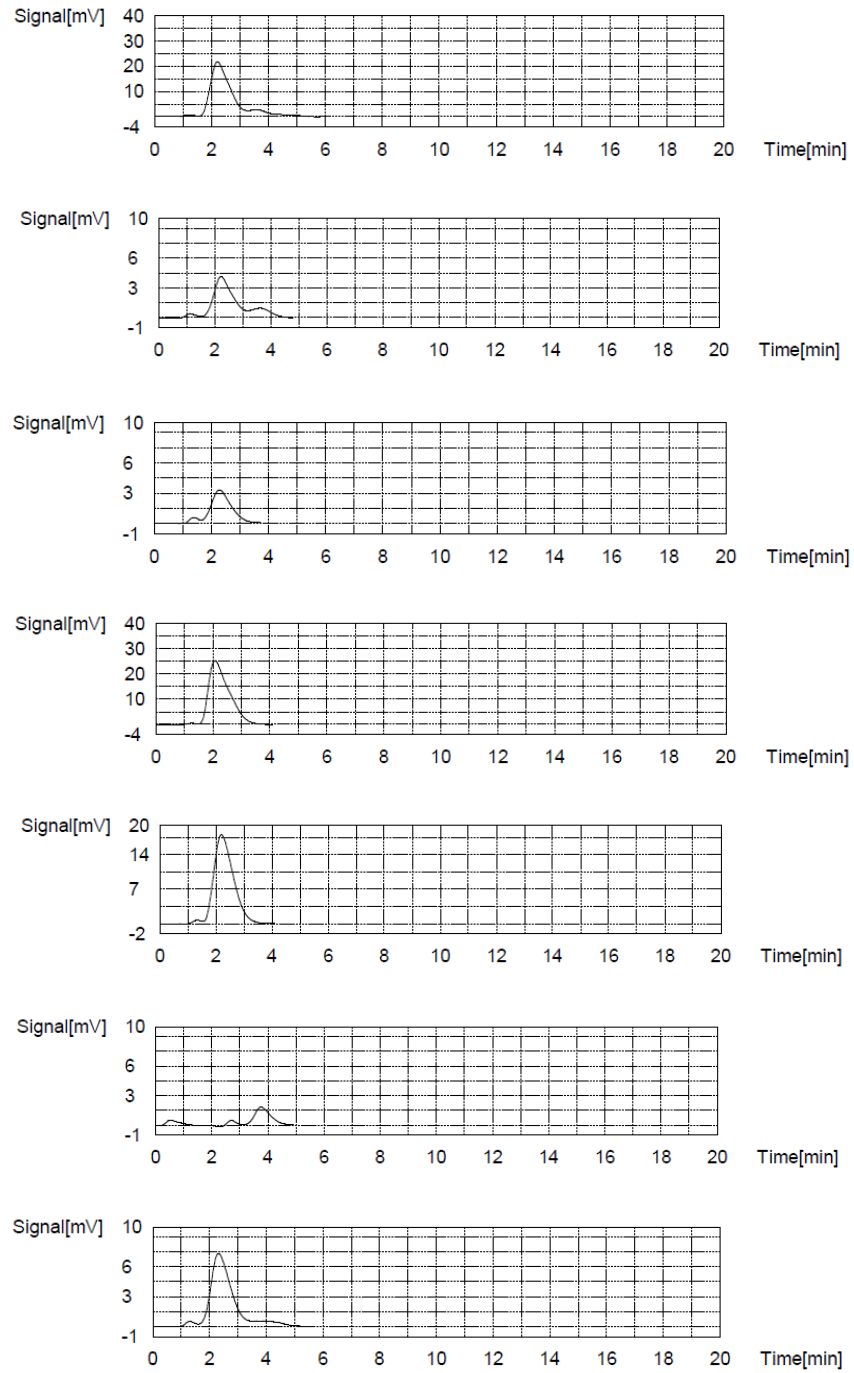


Figure 5.2 (Cont.) Total Organic Carbon measurement results: SHP region.

From top to bottom: S(41) 30; S(42) 31; S(43) 32; S(44) 33; S(45) 34; S(47) 35; and
S(48) 36 samples.

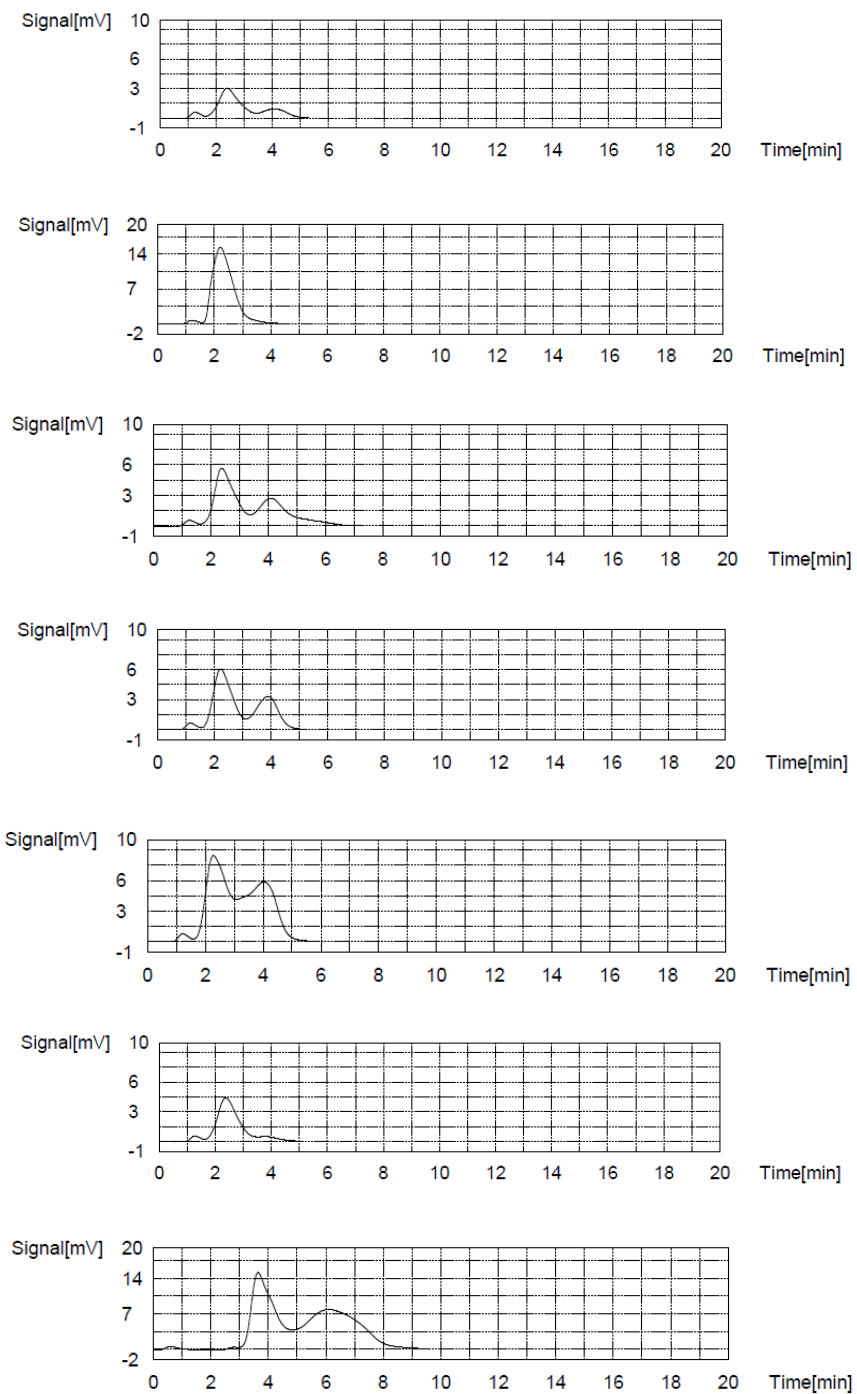


Figure 5.2 (Cont.) Total Organic Carbon measurement results: SHP region.

From top to bottom: S(49) 37; S(50) 38; S(51) 39; S(52) 40; S(53) 41; S(54) 42; and S(55) 43 samples.

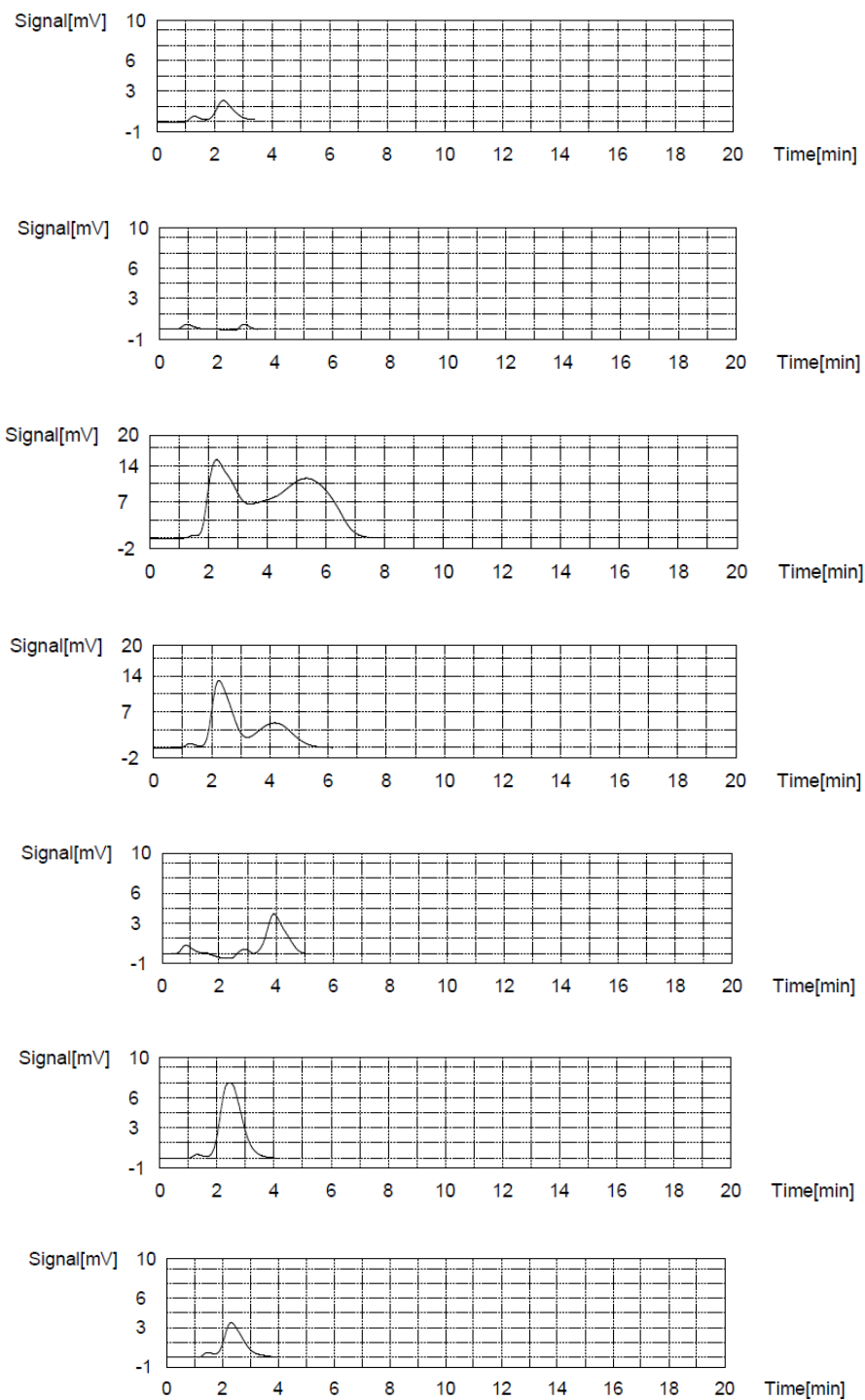


Figure 5.2 (Cont.) Total Organic Carbon measurement results: SHP region.

From top to bottom: S(56)44; S(57) 45; S(59) 46; S(61) 47; S(62) 48; S(63) 49; and S(64)

50 samples.

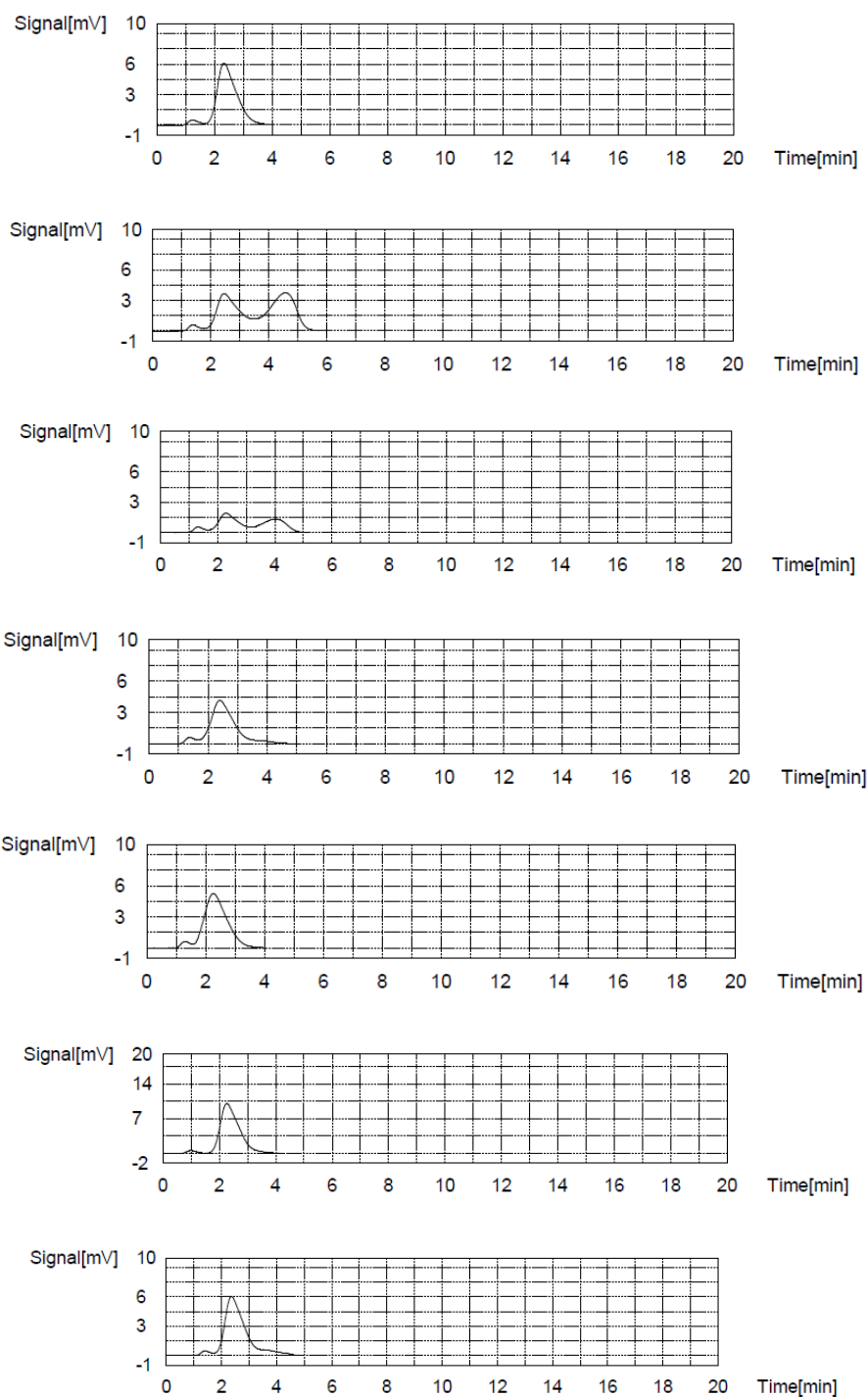


Figure 5.2 (Cont.) Total Organic Carbon measurement results: SHP region.

From top to bottom: S(65) 51; S(66) 52; S(67) 53; S(68) 54; S(71) 55; S(72)56; and S(73) 57 samples.

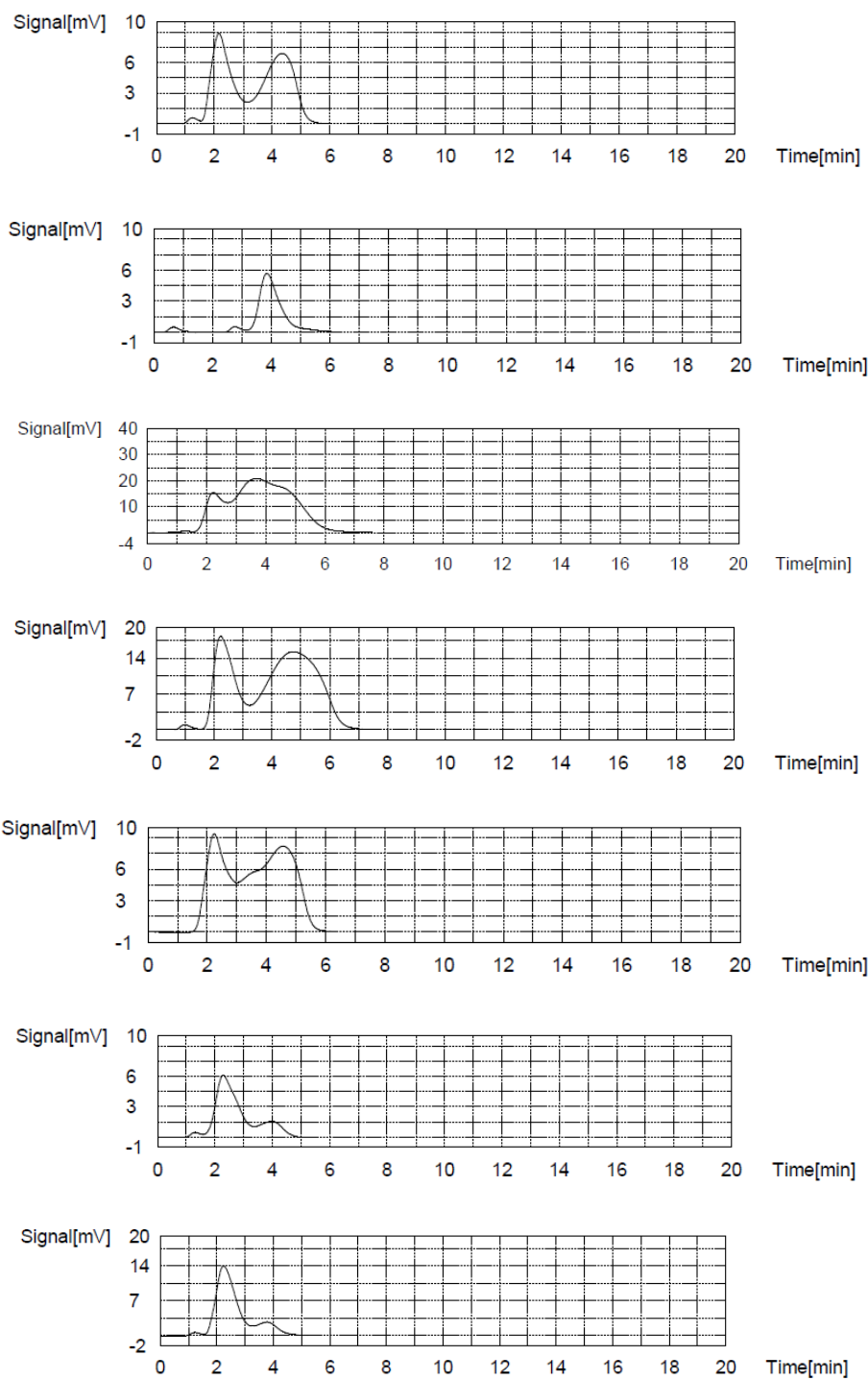


Figure 5.2 (Cont.) Total Organic Carbon measurement results: SHP region.

From top to bottom: S(74) 58; S(75) 59; S(76) 60; S(77) 61; S(78) 62; S(79) 63; and S(80) 64 samples.

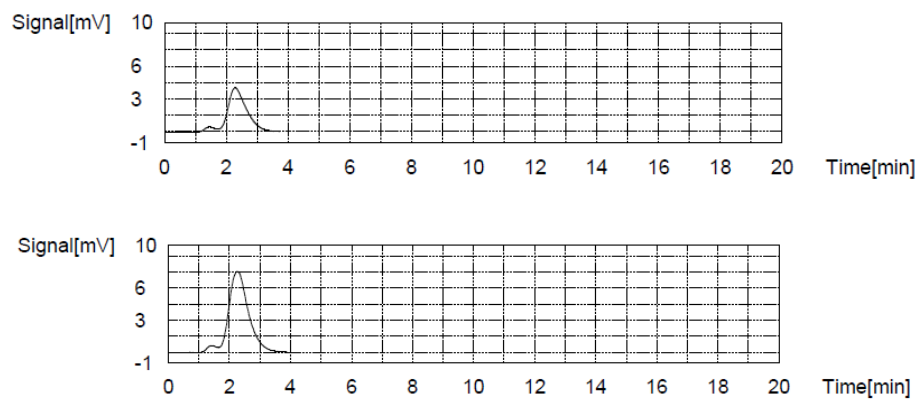


Figure 5.2 (Cont.) Total Organic Carbon measurement results: SHP region.

From top to bottom: S(81) 65; and S(82) 66 samples.

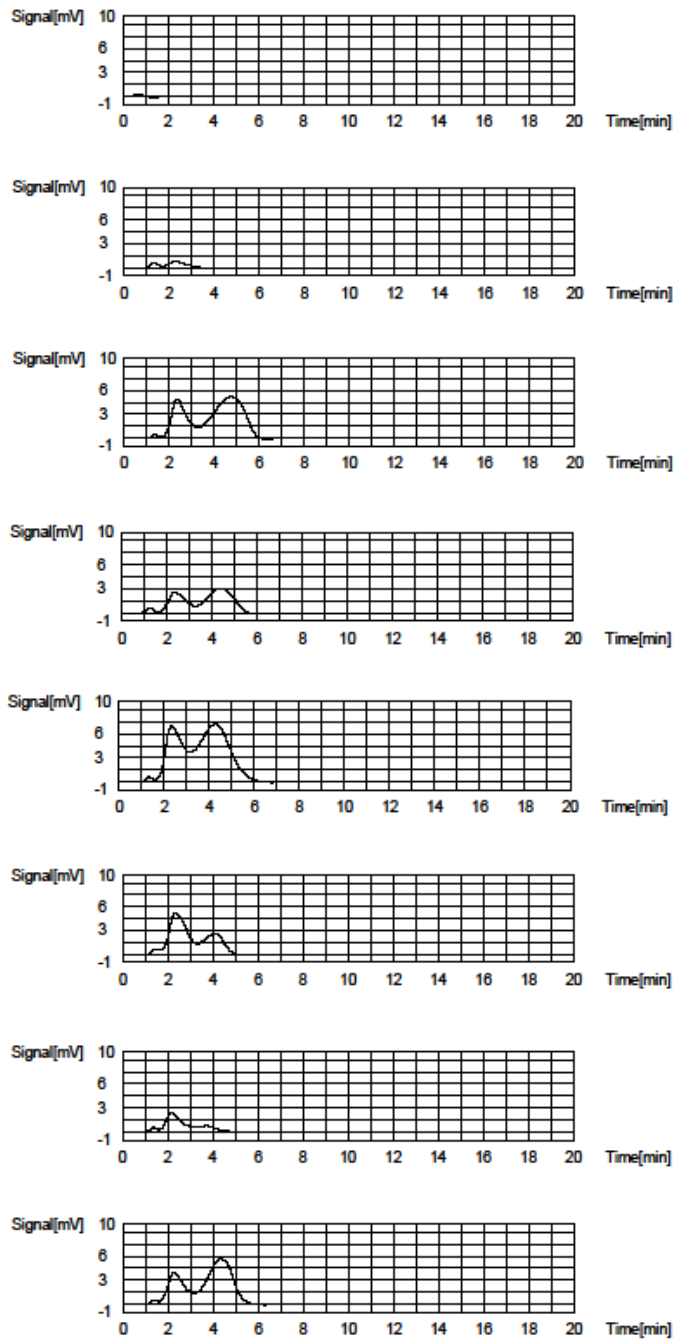


Figure 5.3 – Total Organic Carbon measurement results: CHD USA region.

From top to bottom: WS Dune; WS Interdune; Tula G; Well 9; Old Coe Lake; INBA; SPHA BOT; and McGregor samples.

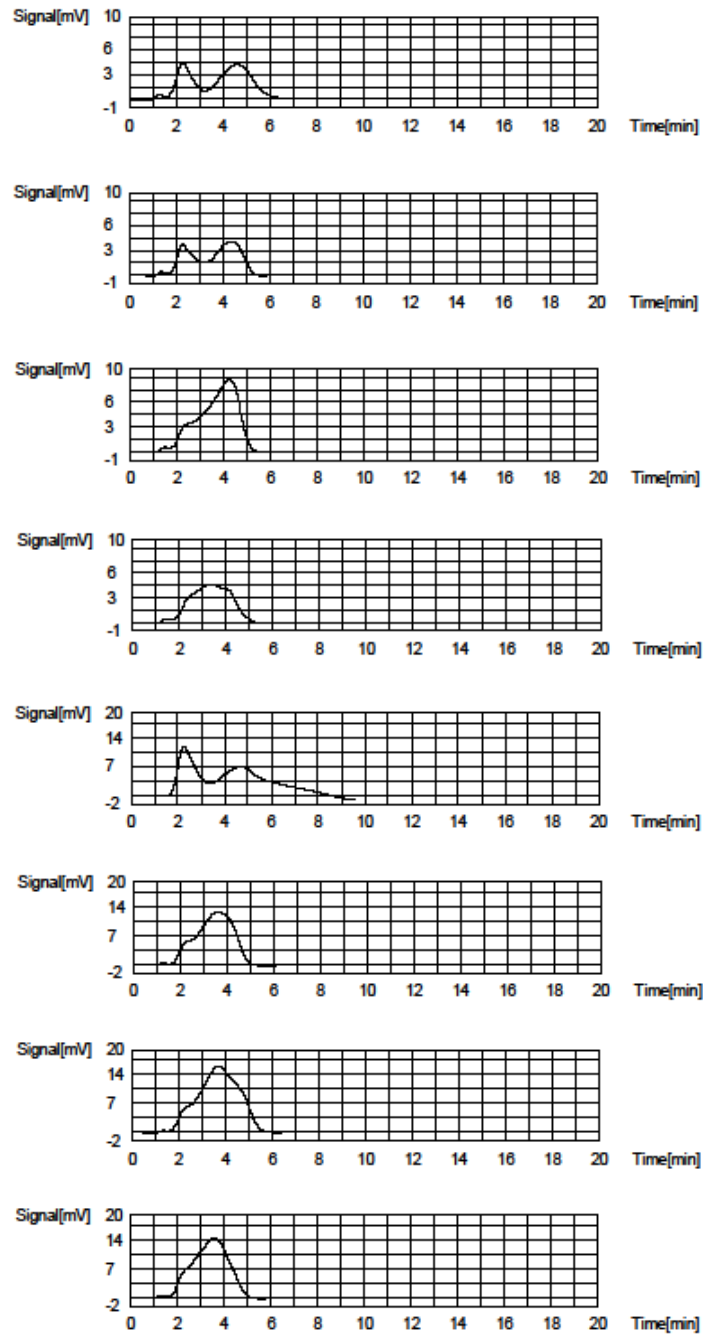


Figure 5.3 (Cont.) – Total Organic Carbon measurement results: CHD USA region.

From top to bottom: Doña Ana; Well 15; Hammock; Dune Surface; Coordinates; Salt Flat S36; Salt Flat S56; and Salt Flat S2 samples.

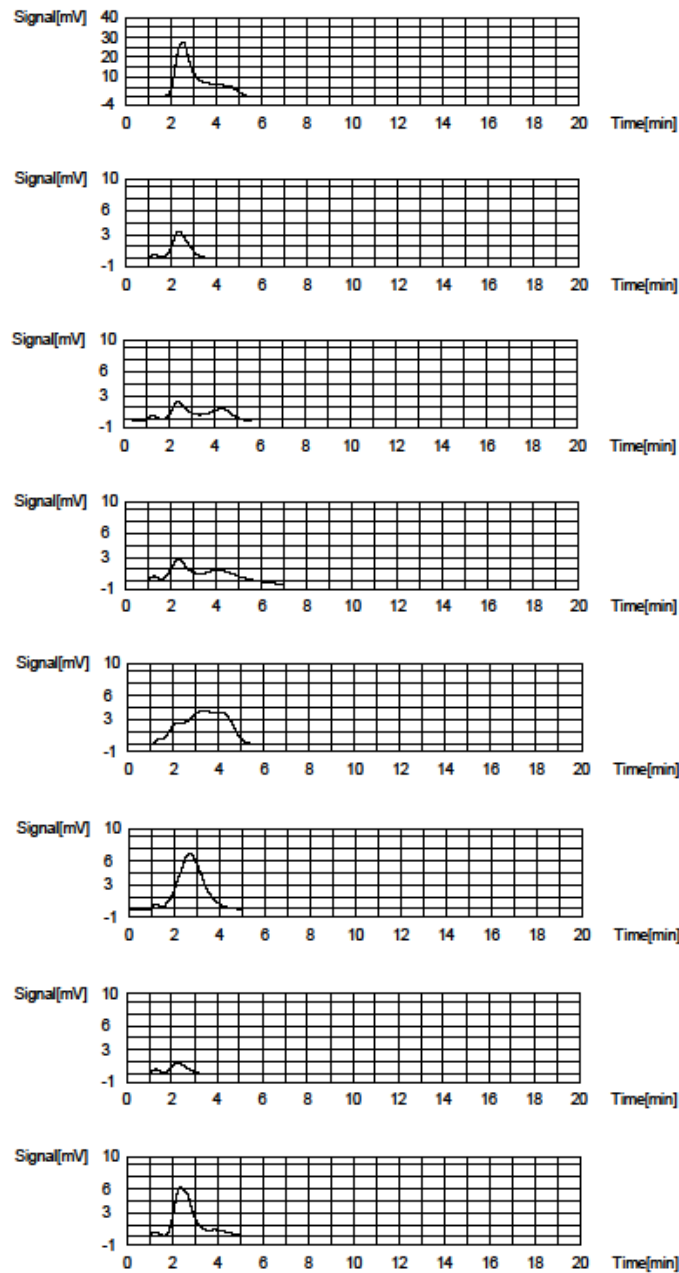


Figure 5.3 (Cont.) – Total Organic Carbon measurement results: CHD USA region.

From top to bottom: Blue House; RLMV-62A; RLMV-62B; WRJG001; WRJG006;
WRJG007; Du-1K-u; and Sh-1K-m-u samples.

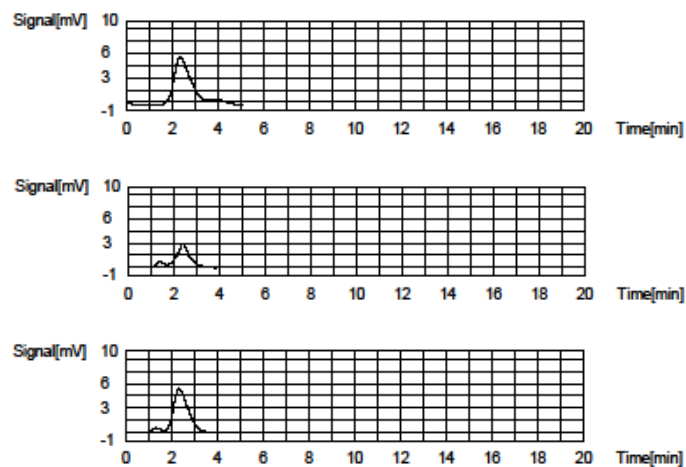


Figure 5.3 (Cont.) – Total Organic Carbon measurement results: CHD USA region.

From top to bottom: Sh-400m; Du-1.5K-m; and Jornada Scrap samples.

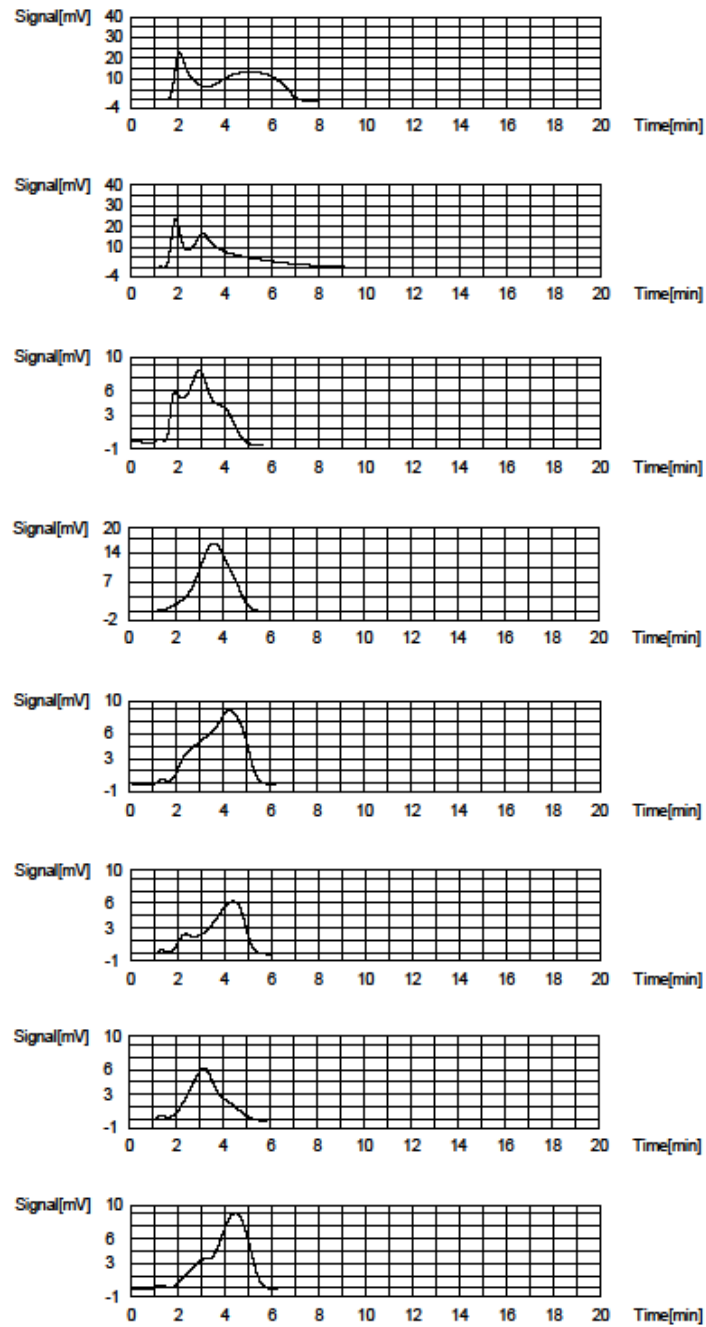


Figure 5.4 – Total Organic Carbon measurement results: CHD MEX region.

From top to bottom: ASC 001; ASC 003; ASC 003; CLP 001; CLP 002; COR 001; COR 002; and COR 004 samples.

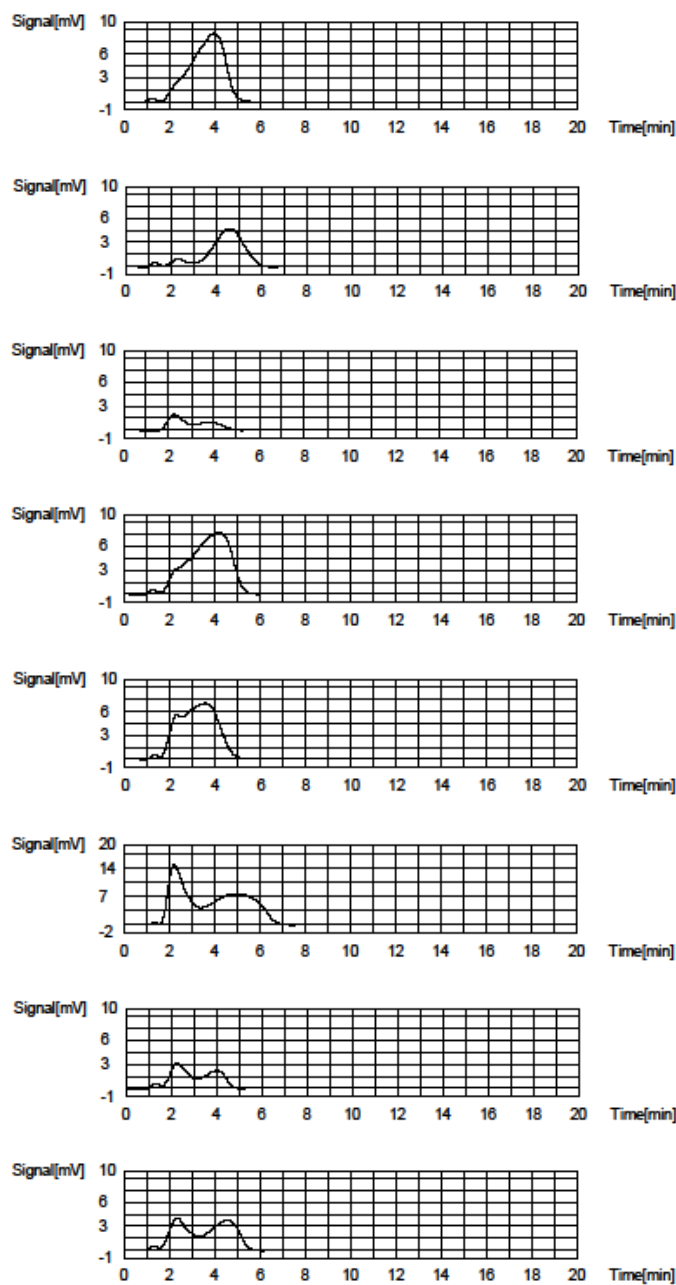


Figure 5.4 (Cont.) – Total Organic Carbon measurement results: CHD MEX region.

From top to bottom: COR 005; COR 008; COR 009; COR 010; DBM 002; GV 002;
HWY 45; and LDP 001 samples.

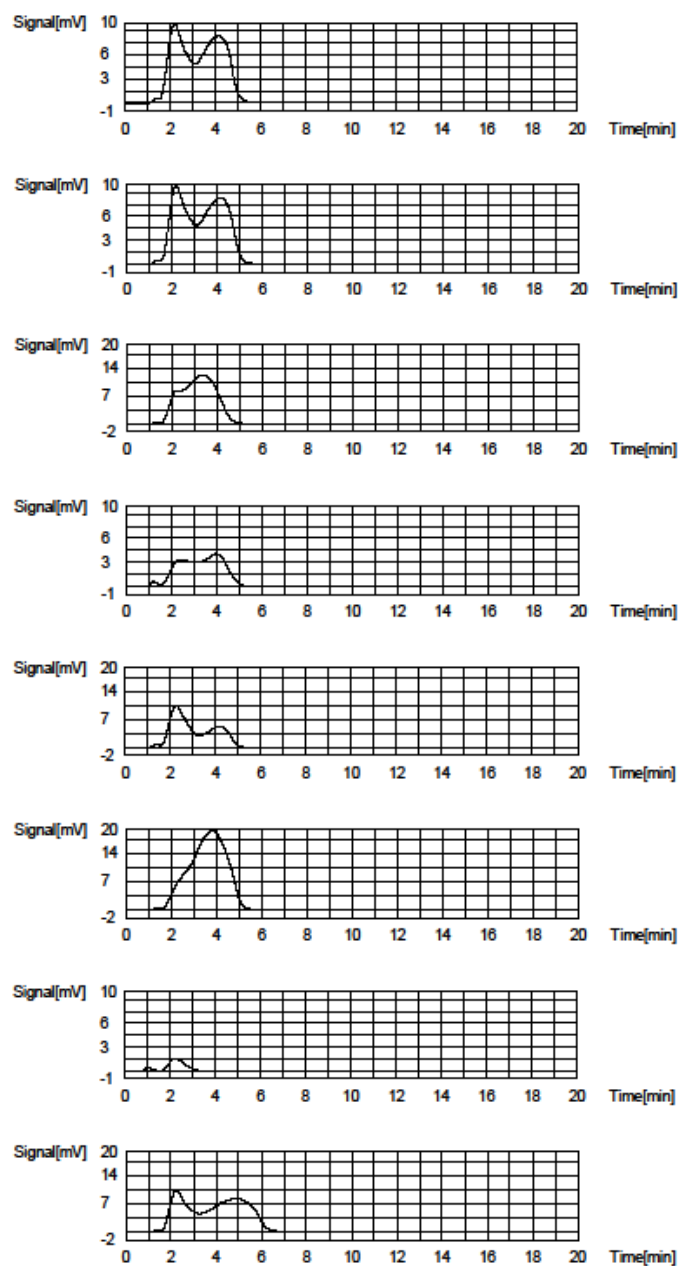


Figure 5.4 (Cont.) – Total Organic Carbon measurement results: CHD MEX region.

From top to bottom: LF 004 ; LG 004; LPAL 005; LSM 002; LSM 003; SELP 003; and
TLG 001 samples.

Chapter 6

Development of Land Use Classes and Geomorphic Surface Types

The study covered a specific aim of land use- and geomorphic surface-characterization of dust sources in the two regions: west Texas and eastern New Mexico (the Southern High Plains region), and northern Chihuahua, southern New Mexico and far west Texas (the Chihuahuan Desert region). Dust source areas (hotspots) on these regions were acknowledged during erosion occurrence days where dust plumes were perceptible on true color Moderate Resolution Imaging Spectroradiometer ([MODIS](#)) imagery from the Terra and Aqua satellites. From these images, soil samples from 125 individual sources of dust were obtained, and the associated land use/land cover was defined via field verification or, air photo interpretation for unreachable areas using the same procedure employed by ([Bullard et al. 2008](#)) and ([Lee et al. 2009, 2012](#)).

Land use and geomorphic surface classification were determined for a total of 125 physical soil samples previously detected from satellite-recognized dust sources in the Southern High Plains (west Texas and eastern New Mexico), (SHP), the Chihuahuan Desert USA region (southern New Mexico and far west Texas), (CHD USA), and the Chihuahuan Desert MEX region (northern Chihuahua), (CHD MEX). Furthermore, chemical characterization of 72-, 27-, as well as 26-physical soil samples coming from mineral dust producing zones of the SHP (which original database data are included on Tables 6.1 and 6.2), the CHD USA, and the CHD MEX regions (which original data are included on Table 6.3), in that order, would show chemical linkage between these three regions by performing descriptive statistics (multivariate techniques).

A geographical analysis was fulfilled to provide spatial representations of political boundaries, land use/land cover- as well as soil name-classifications. In addition, latitude and

longitude coordinates were obtained by the use of a global positioning system (GPS) instrument. Table 6.1 summarizes the Geographic Information System (GIS) data used for mapping mineral aerosol sources using the ESRI ArcGIS ArcMap version 10.1. The UTM Zone 13, NAD 83 projection was used to create an overlay of maps to select soil texture, soil name, and land class types not only for the SHP region, but also for both the CHD USA and the CHD MEX regions. Dust source sites with their geomorphic surface types, as well as land classes and their description were included to discover possible associations among soil texture types, and soil name classification. The location, soil texture- and land class-types, geomorphic surfaces, along with the soil name and a brief description for every single site are condensed in Table 6.4.

6.1 Developing Land Use Categories

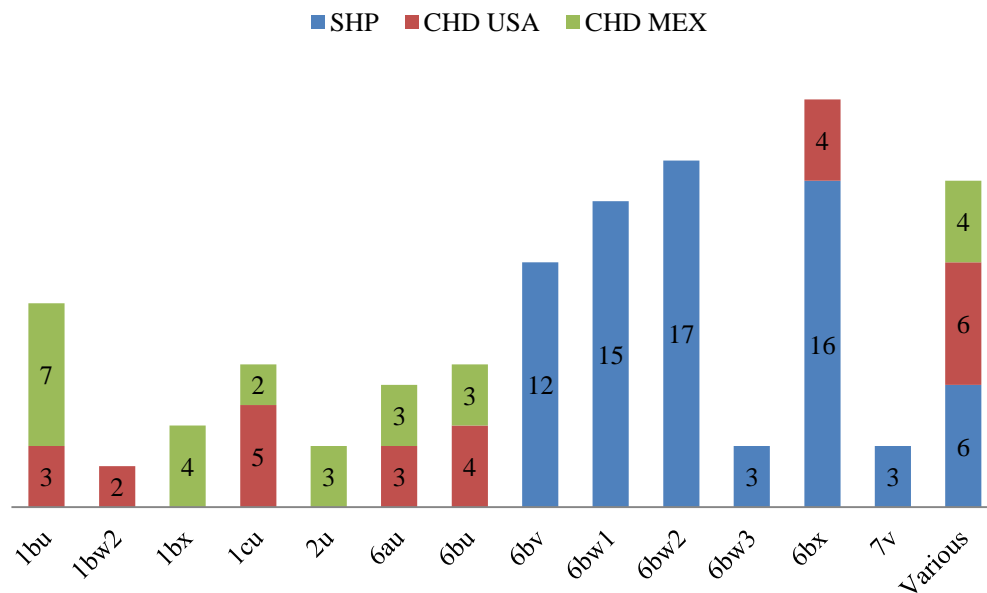
Land use categories were developed by examining the geomorphic classification in addition to the geomorphic modifier codes. Brief description and land use classification of the source locations were also taken in consideration for the land use categories phase development. The methodology used is listed below:

1. Historical imagery of a date closest to the date of the dust event observed was obtained by using Google Earth (version 5.0).
2. Latitude (N) and longitude (W) values of dust events were included into the “Fly To” window in Google Earth allowing the software to complete the zoom-in process. This command execution attained imagery fairly centered on the coordinates.
3. The location of dust events were zoomed at a scale of 750 meters. A perfect zoom scale was achieved by manipulating Google Earth software until the scale could read as “750m” \pm 1 meter; causing to represent an approximate 1:10,000 scale and 4 square miles (or 4 sections).

4. Geomorphology of the scaled locations was then identified by using the geomorphic classification and modifier codes in accordance with the ([Bullard et al. 2008](#)) and ([Lee et al. 2009, 2012](#)) studies (Table 6.5).
5. Noticeable landscape features and/or structures (draws, dairies, etc.) were included to better describe the area.
6. Land use classes were then generated by using both the classification and modification codes described above, and after combining these two codes among the landscape description.

Ultimately, a series of 44 unique land use classes were then obtained by following the methodology described above. Of these, 28 classes were characterized in more than a single soil sample: 1bu, 1bw2, 1bx, 1cu, 1cx, 2u, 2x, 5cu, 5cv, 5cw3, 5cx, 5cz, 5du, 5dx, 6au, 6ax, 6bu, 6bv, 6bw1, 6bw2, 6bw3, 6bx, 6bz, 7u, 7v, 7w2, 7w3, and 7x. It is important to note that the remaining 16 soil samples that resulted also with distinguished land use codes from the three regions being studied in this project, a total of 6-, 6-, and 4-soil samples originated in the SHP (5cv, 5cw3, 5cx, 5dx, 6ax, and 7w3 land use codes related to Ector, Glendale, Bigetty, Arno, Midessa, and Pullman soil names)-, the CHD USA (2x, 5cu, 5cz, 5du, 6bw1, and 6bz land use codes associated with Holloman, Pintura, Mimbres, Stellar, Glendale, and Turney soil names)-, and the CHD MEX (1cx, 7u, 7w2, and 7x land use codes linked to Xerosol L, Xerosol Sg, Xerosol Xh, and Xerosol Zo soil names)-regions, which are shown in that particular order. (See Fig. 6.4). In addition, Table 6.6, Table 6.7, and Table 6.8 summarize the land use classes listed above which were developed for the three regions under study after observing the classification and the modification codes developed by ([Bullard et al. 2008](#)) and ([Lee et al. 2009, 2012](#)) studies

previously discussed above along with field verification and aerial photo interpretation, when necessary.



Codes	Description
1bu	Playa ephemeral. Unknown use
1bw2	Playa ephemeral. Non irrigated farmland
1bx	Playa ephemeral. Rangeland
1cu	Playa dry (consolidated). Unknown use
2u	Duricrust (caliche). Unknown use
6au	Aeolian sand. Dune. Unknown use
6bu	Aeolian sand. Sheet. Unknown use
6bv	Aeolian sand. Sheet. Mixed use
6bw1	Aeolian sand. Irrigated farmland.
6bw2	Aeolian sand. Non irrigated farmland
6bw3	Aeolian sand. Irrigated/Non irrigated farmland
6bx	Aeolian sand. Sheet. Rangeland
7v	Loess. Mixed used

Figure 6.1 – Land Use Classification.

The main land uses: range, farm (N Irr), farm (Irr), and mixed, proceeded from aeolian sand and ephemeral playa areas. Land codes matching these land use categories are: 6bx, 6bw2, 6bw1, 6bv, and 1bu, correspondingly.

6.2 Dust Sources Characterization

Point sources were characterized with respect to land use categories and geomorphic surfaces.

6.2.1 Land Use Categories

Land use affected dust production. Figure 6.2 shows the various land use categories. Defining that every sample was considered a dust producer source, then rangeland category, comprising thirty-one dust sources, resulted in the highest percentage (24.8%) of all the land use categories. Non-irrigated farm category embraced twenty soil sources and brought about 16% of dust emission sites. A value of 13.6% of dust emission sites were obtained to both irrigated farm- and mixed-land categories involving nineteen dust sources each. Lastly, four soil sources emanated from irrigated/non-irrigated farm category totaling 3.2 percent. However, it must be noted that farmland as a whole (including irrigated and non-irrigated) comprised 32.8%, a larger number of dust sources than rangeland.

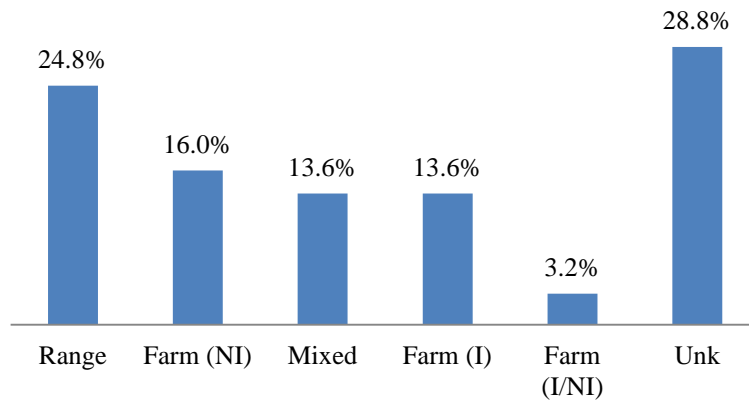


Figure 6.2 – Land use of dust sources

Land use categories dust source percentage. Number above bars is the dust emission sites percentage, number of dust source sites proceeding from a particular land category divided by the total of sites.

Subsequently, thirty-one of the sources were on range land, which was commonly found within the three regions studied in this project, where the Southern High Plains, (west Texas and eastern New Mexico), provided the highest number of dust sources localized on range land. Twenty samples were on non-irrigated farmland, seventeen sources were on irrigated farm land, and four samples were collected on irrigated/non-irrigated farm land. The three classes of farmlands mentioned above were located mostly in the Southern High Plains region (west Texas and eastern New Mexico) also. Dust plumes originates from mixed land, (from which farm- as well as range-land categories and rural development were perceived in these dust sources over an area of several hundred of meters around these point sources and no consistency was seen it) were labeled as “unknown”, and counted for about seventeen. For these unknown samples, the Southern High Plains was the region that originated a widely held quantity. However, land use classification as “unknown” were characterized also for thirty-six dust plume sites within playa basins (commonly named ephemeral or barren land) generally found across the entire

Chihuahuan Desert region (northern Chihuahua, southern New Mexico, and far west Texas regions), caused mainly by the lack of a suitable land use assessment process. Here, explainable reasons discussed pointed out that the dust sources detected from eastern New Mexico proceeded mostly from military restricted areas limiting the ability to characterize the details of these sites, besides the mainst samples taken from the Chihuahuan Desert Mexican region on playa basins, commonly located on uninterrupted land areas with no anthropogenic activities presented causing no anthropogenically disturbed soil, commonly defined as “dry land cover” category to be precise, defining this region that embraced more natural areas (See Figure 6.3).

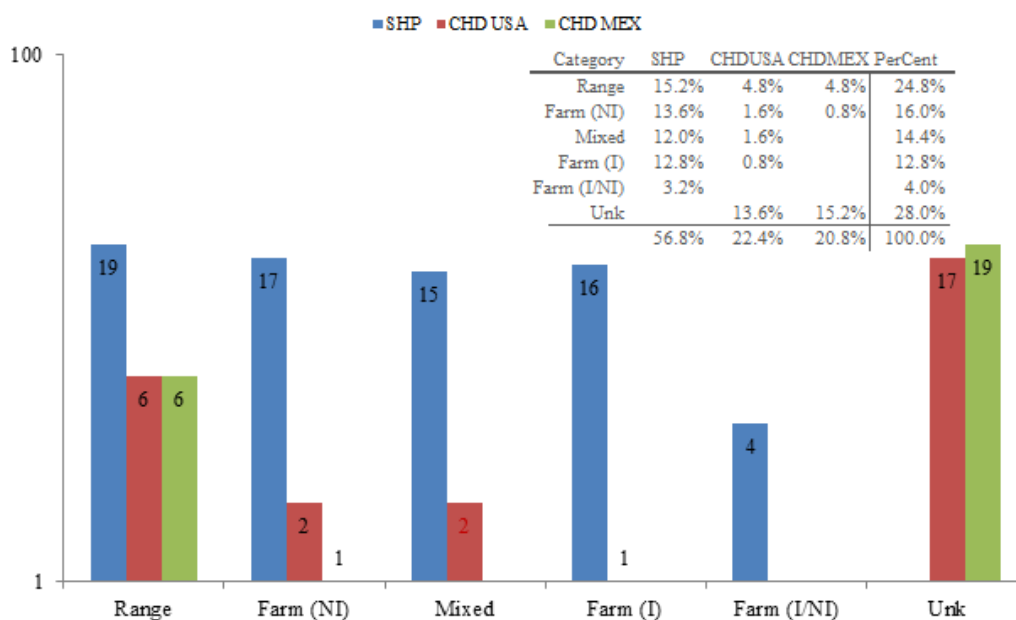


Figure 6.3 – Land use categories for dust source samples

Range and non-irrigated farm lands delivered the majority of dust sites, covering almost 25% of the dust sources studied in this project. Additionally, range was the only land use category that included sites in all the three regions under investigation.

Unequivocally, it can be seen from Figure 6.3 that range land covered roughly 24.8% of all the dust emission sites from all the regions under investigation. Non-irrigated farm land covered 16% of the entire dust sites from which a vast number of samples were collected in the west Texas and eastern New Mexico region. In addition, mixed- and irrigated farm-land categories comprised 14.4% and 12.8% percent value of dust source sites mostly originating in the Southern High Plains region. Lastly, irrigated/non-irrigated farm land category resulted in lowest dust source site percent value of 4. As mentioned before, unknown land category was labeled for dust sources when both, farm- and range-lands, in addition to rural development were observed at the sites of the dust origin, or the sources were located on military land and remained unidentified.

6.2.2 Geomorphic Surfaces Classification

Geomorphic surface impacted dust production. Figure 6.4 displays the various geomorphic surfaces. Outlining that every single location included in this project was considered as a dust source, then aeolian sand, from which a higher number of dust sources (eighty-four) was observed, resulted with the uppermost percentage (67.2%) of all the geomorphic surfaces. Twenty-three samples that were originating in playa, resulted with a percentage that counted for 18.4%. Similarly, seven dust samples from Alluvial-, as well as seven soil sources from loess-, to lastly four soil sources observed from caliche-geomorphic surface gave percentages for about 5.6%, 5.6%, and 3.2% in that particular order.

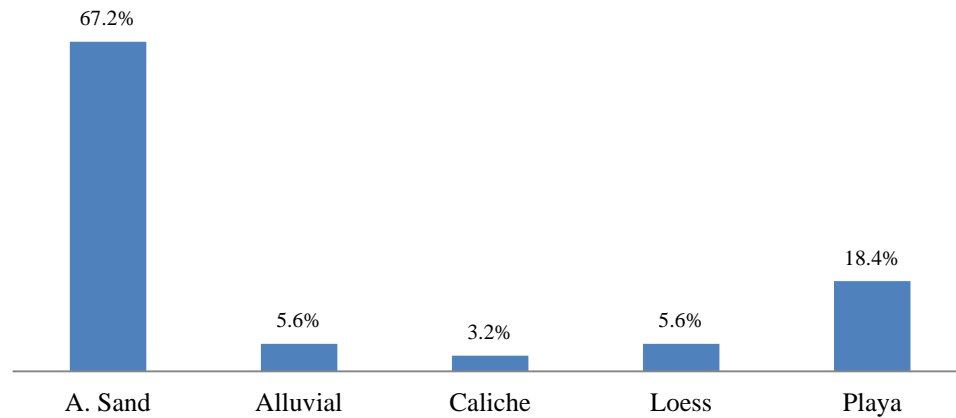


Figure 6.4 – Geomorphic surfaces percentage

Number above bars is the number of dust sources proceeding from a particular geomorphic surface divided by the total of dust sources.

Consequently, geomorphic classification was established in regards to categories that were observed in the dust sources after performing land use examination (based in analysis in surface geology and soil maps and satellite imagery, along with field observations). As previously mentioned above, the geomorphic categories resulted were aeolian sand, alluvial, caliche, loess, and playa. At this point for geomorphic classification, eighty-four of the sources were on aeolian sand surface, mostly on the Southern High Plains (west Texas and eastern New Mexico) region. Twenty-three were on playa surface, from across the entire Chihuahuan Desert region, that is, northern Chihuahua, southern New Mexico, and far west Texas regions. Seven samples were found on alluvial-, the same size of samples found on Loess-geomorphic surface, from which the Southern High Plains as well as the Chihuahuan Desert regions provided these samples. To end with, four of the dust plumes originated on caliche surface within the Chihuahuan Desert region, mostly in the northern Chihuahua region (See Figure 6.5).

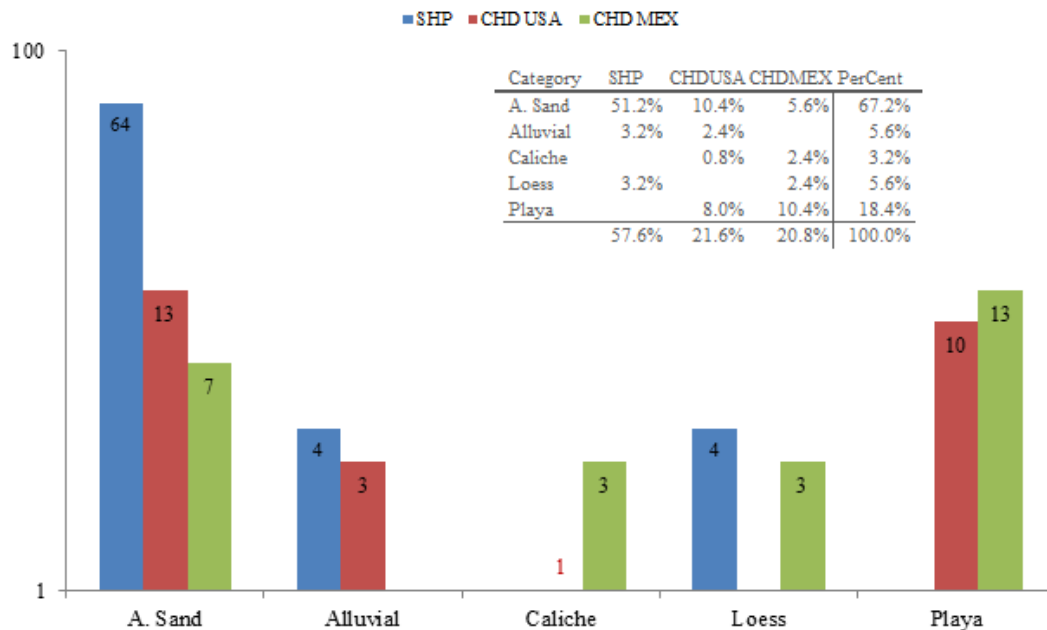


Figure 6.5 – Geomorphic surfaces dust source samples.

Aeolian sand surface provided the highest number of samples for both the Southern High Plains and the Chihuahuan Desert USA regions, covering roughly 50% of the sources included in this project. Playa surface sources are found the most in the northern Chihuahua.

In greater detail, it can be seen from Figure 6.5 that aeolian sand surface covered roughly 50% of all the sources studied in this project (67.2% of dust emission sources), more specific in the southern New Mexico and far west Texas (the Chihuahuan Desert USA) region, in addition to west Texas and eastern New Mexico (the Southern High Plains) region. Playa surface covered also 50% of all the sources taken from the northern Chihuahua (the Chihuahuan Desert Mexico) region. What is more, the origin of dust sources located from across the entire Chihuahuan

Desert region proceeded from playa surface totaling 43.4 percent. Caliche surface provided 3.2%, suggesting lower emissivities to these regions in the Chihuahuan Desert, but it can be argued these dust samples had their origin on playas, the most potent active dust emitter.

No single land category and geomorphic surface dominated the production of blowing dust within the three regions, the Southern High Plains (west Texas and eastern New Mexico), the Chihuahuan Desert USA (southern New Mexico and far west Texas), and the northern Chihuahua (the Chihuahuan Desert Mexico) regions. As with land use, neither single land category nor single geomorphic surface nor soil texture dominated dust production in the regions under examination. However, it is implied that both aeolian sand and playa surfaces formed in proportion more dust plumes than other surface types.

Aeolian sand surface dominated the west Texas and eastern New Mexico, that is, the Southern High Plains region. Of seventy-two samples, sixty-four were originated on aeolian sand-, and eight (four each) on alluvial-, besides loess-geomorphic surface.

Playa, aeolian sand and caliche geomorphic surfaces comprised most of the dust samples in northern Chihuahua, southern New Mexico and far west Texas (the Chihuahuan Desert region). Of fifty-three sample sites, twenty-three were collected on playa-, twenty on aeolian sand-, four on caliche-, and six (three each) on, alluvial- and loess-geomorphic surface (see Figure 6.6).

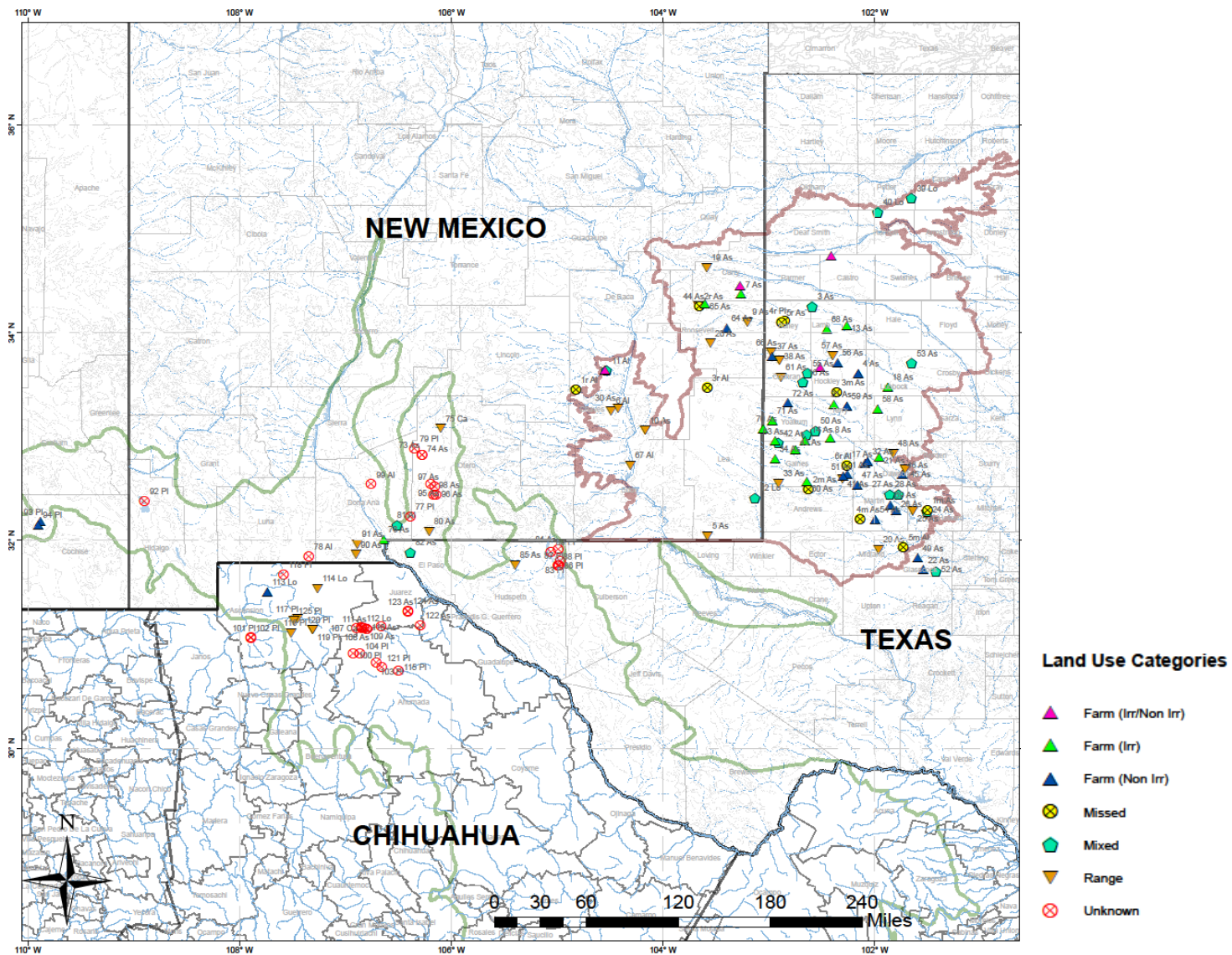


Figure 6.6 – Geomorphic surfaces dust source samples map.

The Chihuahuan Desert sites are west of 104 °W and the Southern High Plains sites are east of that line.

Table 6.1 – SHP dust sources sites original database Part 1

FID	Lat	Long	State	County	Soil Serie	Soil name	Classification	Texture	Sand	Silt	Clay	Land	Notes
0	32.632	-102.261	TX	Gaines	Bs	Patricia	Fine-loamy, mixed, thermic aridic paleustalfs	Fine Sand	92.7	1.3	6.0	6bw2	Playas present; dryland only
1	33.662	-102.519	TX	Hockley	AfA	Amarillo	Fine-loamy, mixed, thermic aridic paleustalfs	Fine Sandy Loam	66.1	19.9	14.0	6bw3	Oil, playas, farmhouses present
2	34.250	-102.592	TX	Lamb	PmA	Portales	Fine-loamy, mixed, thermic Aridic calcicustolls	Loam	42.1	37.9	20.0	6bv	Center pivots, farmhouses present
3	33.607	-102.158	TX	Hockley	AcA	Acuff	Fine-loamy, mixed, thermic aridic paleustols	Loam	47.1	33.3	19.6	6bu	Black-and-white image; unclear
4	32.047	-103.581	NM	LEA	MN/SR	Midessa	Fine-loamy, mixed, thermic aridic ustochrepts	Fine Sandy Loam	68.0	16.5	16.0	6ax	x only
5	33.452	-104.824	NM	Chavez	BQB	Blakeney	Loamy, mixed, thermic shallow Ustochreptic paleorthids	Fine Sandy Loam	70.5	16.5	13.0	5cx	
6	33.248	-104.491	NM	Chavez	RFB	Bigetty	Fine-silty, mixed, thermic Cumulic Haplustolls	Silt Loam	11.3	67.7	21.0	5cx	
7	34.369	-103.264	NM	Curry	AnB	Amarillo	Fine-loamy, mixed, superactive, thermic aridic paleustalfs	Loamy Fine Sand	82.2	9.2	8.5	6bw1	Town, playas, CAFO present
8	32.291	-101.505	TX	Howard	AfA	Amarillo	Fine-loamy, mixed, thermic aridic paleustalfs	Fine Sandy Loam	66.1	19.9	14.0	6bv	Town present
9	32.982	-102.422	TX	Terry	PAB	Patricia	Fine-loamy, mixed, superactive, thermic aridic paleustalfs	Loamy Fine Sand	85.9	6.6	7.5	6bw1	
10	34.105	-103.202	NM	Roosevelt	Ca	Church	Fine, mixed, mesic aquic camborthids	Clay Loam	33.3	31.7	35.0	6bx	dryland farms, farmhouses, draw present
11	34.250	-103.660	NM	Roosevelt	Ab	Amarillo	Fine-loamy, mixed, thermic aridic paleustalfs	Fine Sandy Loam	69.6	16.4	14.0	6bx	dryland farms, farmhouses present
12	33.059	-104.170	NM	Chaves	So	Setim	Fine-loamy, mixed, thermic typic calcicorthids	Fine Sandy Loam	70.1	16.4	13.5	x	Oil present
13	33.636	-104.534	NM	Chaves	EaC	Ector	Loamy-skeletal, carbonatic, thermic lithic calcicustolls	Cobbly Loam	39.2	37.3	23.5	5cv	Draw system; dryland farms, center pivots present
14	34.208	-103.134	NM	Lea	PU	Maljama	Fine-loamy, mixed, thermic arenic haplargids	Fine Sand	91.3	1.2	7.5	z	Oil patch; range present; dryland farms present
15	34.068	-102.265	TX	Lamb	Sg	Springer	Coarse-loamy, mixed, thermic udic paleustalfs	Fine Sandy Loam	65.4	19.6	15.5	6bw1	Playa, Range and dryland farms present
16	33.472	-103.584	NM	Lea	Av	Arch	Fine-loamy, mixed, thermic ustochreptic calcicorthids	Loam	42.1	37.9	20.0	x	Oil present
17	33.016	-102.644	TX	Yoakum	Bs	Patricia	Fine-loamy, mixed, thermic aridic paleustalfs	Fine Sand	92.7	1.3	6.0	6bv	Oil, dryland/irrigated mix present
18	33.642	-104.550	NM	Chaves	Gba	Glendale	Fine-silty, mixed (calcareous), thermic typic torrifluvents	Silt Loam	6.9	68.1	25.0	5cw3	Floodplain farm; farmhouses, center pivot, irrigated non-center pivot present
19	33.520	-102.679	TX	Cochran	AfB	Amarillo	Fine-loamy, mixed, superactive, thermic aridic paleustalfs	Fine Sandy Loam	66.1	19.9	14.0		Range, oil, center pivot, non-saline playa present
20	32.737	-102.094	TX	Dawson	AfB	Amarillo	Fine-loamy, mixed, superactive, thermic aridic paleustalfs	Fine Sandy Loam	66.1	19.9	14.0	6bw2	Range, non-saline playas present
21	33.475	-101.878	TX	Lubbock	l	Acuff	Fine-loamy, mixed, superactive, thermic aridic paleustolls	Loam	41.4	37.1	21.5	6bw1	Outskirts of Lubbock; z, non-saline playas, dryland farms, stockyard, landfill present
22	34.627	-103.586	NM	Curry	SnC	Spantara	Coarse-loamy, mixed, superactive, thermic aridic haplustalfs	Fine Sand	94.4	0.6	5.0	6bx	dryland farms present
23	33.899	-103.552	NM	Roosevelt	Cf	Clovias	Fine-loamy, mixed, mesic ustollic haplargids	Loam	42.1	37.9	20.0	6bx	Ranch houses, non-saline playas present
24	32.489	-102.630	TX	Andrews	TwB	Triomas	Fine-loamy, thermic ustollic haplargids	Fine Sand	91.7	1.3	7.0	6bv	Oil patch, w1, w2, and range
25	32.799	-101.960	TX	Dawson	AfB	Amarillo	Fine-loamy, mixed, thermic aridic paleustalfs	Fine Sandy Loam	66.1	19.9	14.0	6bw1	Non-saline playas, farmhouses present
26	31.716	-101.542	TX	Glasscock	ReA	Reagan	Fine-silty, mixed, superactive, thermic ustic haplocalcids	Silty Clay Loam	6.9	62.1	31.0	6bw2	Range, z, non-saline playas present
27	32.248	-101.514	TX	Howard	Ps/PfB	Potter	Loamy-skeletal, carbonatic, thermic, shallow ustic haplocalcids	Loam	37.9	35.6	26.5	x	w (dryland), y (Big Spring), reservoir, creek present
28	32.276	-101.506	TX	Howard	AmB	Amarillo	Fine-loamy, mixed, thermic aridic paleustalfs	Fine Sandy Loam	66.1	19.9	14.0	6bv	w (dryland), y (Big Spring), range present
29	32.283	-101.643	TX	Howard	SpA	Springer	Coarse-loamy, mixed, active, thermic typic paleustalfs	Fine Sandy Loam	65.4	19.6	15.0	x	Oil, w (dryland) present
30	32.286	-101.797	TX	Martin	PoA	portales	Fine-loamy, mixed, superactive, thermic aridic calcicustolls	Loam	42.1	37.9	20.0	6bw2	Range, non-saline playa present
31	32.443	-101.780	TX	Martin	MA	Amarillo	Fine-loamy, mixed, thermic aridic paleustalfs	Loamy Fine Sand	83.5	6.5	10.0		Non-saline playas, farmhouses present
32	32.443	-101.859	TX	Martin	AfA	Amarillo	Fine-loamy, mixed, thermic aridic paleustalfs	Fine Sandy Loam	66.1	19.9	14.0	6bv	Range, canyon, non-saline playas present
33	31.913	-101.965	TX	Midland	RvA	Reeves	Fine-loamy, gypsic, thermic calcic gypsiorthids	Loam	39.8	37.7	22.5	6bx	Draw, dryland farms, non-saline playas, z present
34	33.275	-104.423	NM	Chaves	ReB	Reagan	Info not available						Info not available
35	33.307	-102.387	TX	Terry	AfB/AfA	Amarillo	Info not available						Info not available
36	-102.068	32.762	TX	Dawson	AfA	Amarillo	Fine-loamy, mixed, thermic aridic paleustalfs	Fine Sandy Loam	66.1	19.9	14.0	6bw2	non-saline playas present
37	-102.909	32.548	TX	Gaines	Be	Berda	Fine-loamy, mixed, thermic Aridic Ustochrepts	Loam	38.0	36.0	25.0	6bx	Dryland farm present; CAFO present; draw present
38	-102.944	32.783	TX	Gaines	Sa	Simona	Loamy, mixed, thermic shallow typic paleorthids	Fine Sandy Loam	63.1	19.4	17.5	6bw1	z present (oil and gas facility)
39	-102.658	32.955	TX	Gaines	Br	Brownfield	Loamy, mixed, thermic arenic aridic paleustalfs	Fine Sand	92.2	1.3	6.5	6bw1	non-saline playas present
40	34.115	-102.854	TX	Bailey	DrE/PfA	Drake	Fine-loamy, mixed, superactive calcareous, thermic typic ustorthents	Loam	37.9	35.6	26.5	1bx	Salt lake; w2 present
41	34.742	-102.412	TX	Castro	PuA	Pullman	Fine, mixed, superactive, thermic torretic paleustolls	Clay Loam	34.2	32.3	35.5	7w3	x, farmhouses present
42	33.768	-102.970	TX	Cochran	AfA	Amarillo	Fine-loamy, mixed, thermic aridic paleustalfs	Fine Sandy Loam	66.1	19.9	14.0	6bw2	w1, x, z (rural community) present
43	33.731	-102.901	TX	Cochran	AmB	Amarillo	Fine-loamy, mixed, thermic aridic paleustalfs	Loamy Fine Sand	83.5	6.5	10.0	6bv	w1, w2, x, and farmhouses
44	35.292	-101.655	TX	Potter	PuB/PuA	Pullman	Fine, mixed, superactive, thermic torretic paleustolls	Silty Clay Loam	18.7	47.8	33.5	7v	w1, w2, x, z (rural residential), lake, non-saline playa
45	35.157	-101.973	TX	Randall	PxA	Pantex	Fine, mixed, superactive, thermic torretic paleustolls	Silty Clay Loam	12.3	53.8	33.9	7v	w1, w2, x
46	34.099	-102.882	TX	Bailey	DrE(H20)	Drake	Fine-loamy, mixed, superactive calcareous, thermic typic ustorthents	Loam	37.9	35.6	26.5	6bx	Salt lake present (~40% of viewscreen)
47	32.590	-102.305	TX	Gaines	Br	Brownfield	Loamy, mixed, thermic arenic aridic paleustalfs	Fine Sand	92.2	1.3	6.5	6bx	w2 present
48	32.936	-102.911	TX	Gaines	Br	Brownfield	Loamy, mixed, thermic arenic aridic paleustalfs	Fine Sand	92.2	1.3	6.5	6bv	mix of w1, x, and z (oil)
49	32.874	-102.750	TX	Gaines	Bs	Patricia	Fine-loamy, mixed, thermic aridic paleustalfs	Fine Sand	92.7	1.3	6.0	6bw1	w1, x, z (oil) present
50	34.254	-103.666	NM	Roosevelt	Ad	Amarillo	Fine-loamy, mixed, thermic aridic paleustalfs	Loam	41.4	37.1	21.5	6bx	x only

Samples red outlined were only geospatial analyzed.

Table 6.1 (Cont.) – SHP dust sources sites original database Part 1

FID	Lat	Long	State	County	Soil Serie	Soil name	Classification	Texture	Sand	Silt	Clay	Notes
51	32.684	-101.714	TX	Dawson	PaB	Pep	Fine-loamy, mixed, superactive, thermic aridic calcistolls	Loam	44.5	35.5	20.0	6bx Edge of Caprock; w1, w2, z (oil) present
52	32.631	-101.742	TX	Dawson	AfB	Amarillo	Fine-loamy, mixed, thermic aridic paleustalfs	Fine Sandy Loam	66.1	19.9	14.0	6bw2 terraced w2, x, z (oil), non-saline playas, farmhouses present
53	32.531	-102.167	TX	Dawson	GoA	Gomez	Coarse-loamy, mixed, active, thermic aridic calcisteps	Loamy Fine Sand	85.3	6.7	8.0	
54	32.838	-101.825	TX	Dawson	LhA	Hindman	Coarse-loamy, mixed, superactive, thermic torrifluventic haplustepts	Fine Sandy Loam	64.0	19.3	16.7	
55	31.830	-101.595	TX	Glasscock	ReA	Reagan	Fine-silty, mixed, superactive, thermic ustic haploscalcids	Silty Clay Loam	6.9	62.1	31.0	
56	33.053	-102.562	TX	Terry	PAB	Amarillo	Fine-loamy, mixed, thermic aridic paleustalfs	Loamy Fine Sand	85.9	6.6	7.5	
57	32.616	-102.299	TX	Gaines	Bs	Patricia	Fine-loamy, mixed, thermic aridic paleustalfs	Fine Sand	92.7	1.3	6.0	6bw2 x present
58	32.722	-102.265	TX	Gaines	Bs	Patricia	Fine-loamy, mixed, thermic aridic paleustalfs	Fine Sand	92.7	1.3	6.0	5cx w2 also present
59	31.699	-101.423	TX	Glasscock	ReA	Reagan	Fine-silty, mixed, superactive, thermic ustic haploscalcids	Silty Clay Loam	6.9	62.1	31.0	6bv x, w2; looks like some fields were w2 but are turning into x
60	33.425	-102.361	TX	Hockley	AcA/AfB	Abilene	Fine, mixed, superactive, thermic pachic argistolls	Clay Loam	35.3	33.2	31.5	6bx extensive z (oil pumpjacks)
61	33.706	-101.654	TX	Lubbock	33	portales	Fine-loamy, mixed, superactive, thermic aridic calcistolls	Loam	42.1	37.9	20.0	6bv w1, w2, x, playas present
62	32.203	-101.997	TX	Martin	AfA/AfB	Amarillo	Fine-loamy, mixed, thermic aridic paleustalfs	Fine Sandy Loam	66.1	19.9	14.0	6bw2 oil pumpjacks (z); playas; x present
63	33.609	-102.638	TX	Cochran	AmB	Amarillo	Fine-loamy, mixed, thermic aridic paleustalfs	Loamy Fine Sand	83.5	6.5	10.0	6bv x, w1, w2, z (rural res. And oil); non-saline playas present
64	33.710	-102.353	TX	Hockley	AfA	Amarillo	Fine-loamy, mixed, thermic aridic paleustalfs	Fine Sandy Loam	66.1	19.9	14.0	6bw2 w2, x, non-saline playa present
65	33.778	-102.397	TX	Hockley	AvA/AfA	Arvana	Fine-loamy, mixed, superactive, thermic petrocalcic paleustalfs	Fine Sandy Loam	66.1	19.9	14.0	6bx w1, w2, non-saline playas present
66	33.265	-101.974	TX	Lynn	AcA	Abilene	Fine, mixed, superactive, thermic pachic argistolls	Clay Loam	35.3	33.2	31.5	6bw3 x, non-saline playa, draw present
67	33.294	-102.265	TX	Terry	AfB	Amarillo	Fine-loamy, mixed, thermic aridic paleustalfs	Fine Sandy Loam	66.1	19.9	14.0	6bw2 w1, x, non-saline playas present
68	32.564	-102.641	TX	Gaines	Sm	Arvana	Loamy, siliceous, thermic, shallow petrocalcic ustollic paleargids	Loamy Fine Sand	85.9	6.6	7.5	
69	32.206	-102.142	TX	Martin	MdA/AfB	Midessa	Fine-loamy, mixed, superactive, thermic aridic calcisteps	Fine Sandy Loam	65.4	19.6	15.0	6bx w1, w2, z (oil) present
70	31.937	-101.732	TX	Glasscock	MfA	Midessa	Fine-loamy, mixed, thermic aridic ustochrepts	Fine Sandy Loam	65.4	19.6	15.0	v w1, x, and z (rural res.); draw and stock pond present
71	33.570	-102.887	TX	Cochran	AfA	Amarillo	Fine-loamy, mixed, thermic aridic paleustalfs	Fine Sandy Loam	66.1	19.9	14.0	6bx w2, z (oil) present
72	34.451	-103.275	NM	Curry	AcA	Abilene	Fine, mixed, superactive, thermic pachic argistolls	Clay Loam	35.3	33.2	31.5	6bw3 x, z (rural res.), non-saline playa present
73	32.956	-102.944	TX	Gaines	Bs	Patricia	Fine-loamy, mixed, thermic aridic paleustalfs	Fine Sand	92.7	1.3	6.0	6bw1 w2, x, z (rural res.) present
74	34.040	-103.400	NM	Roosevelt	Aa	Amarillo	Fine-loamy, mixed, thermic aridic paleustalfs	Loamy Fine Sand	80.8	9.2	10.0	6bw2 ~40% x
75	34.276	-103.604	NM	Roosevelt	Aa	Amarillo	Fine-loamy, mixed, thermic aridic paleustalfs	Loamy Fine Sand	80.8	9.2	10.0	6bw1 w2, x, z (rural res.) present
76	33.811	-102.982	TX	Cochran	Ao	Arch	Fine-loamy, carbonatic, thermic aridic ustochrepts	Loam	42.1	37.9	20.0	6bx w1 present
77	32.725	-104.309	NM	Eddy	AH	Arno	Fine, mixed, calcareous, thermic vertic torrifluvents	Silty Clay Loam	18.5	44.0	37.5	5dx Pecos River; x only
78	34.035	-102.454	TX	Lamb	Olton	Fine-loamy, mixed, superactive, thermic aridic paleustolls	Loam	36.7	34.8	28.5	6bw1 w1, x, z (CAFO and rural res.), non-saline playas present	
79	32.341	-101.855	TX	Martin	AfA	Amarillo	Fine-loamy, mixed, thermic aridic paleustalfs	Fine Sandy Loam	66.1	19.9	14.0	6bw2 w2 only
80	33.076	-103.057	TX	Yoakum	PmA	portales	Fine-loamy, mixed, superactive, thermic aridic calcistolls	Loam	42.1	37.9	20.0	6bw1 w2, x, z (rural res.) present
81	33.153	-102.969	TX	Yoakum	Br	Brownfield	Loamy, mixed, thermic arenic aridic paleustalfs	Fine Sand	92.2	1.3	6.5	6bw1 w2, x, z (rural res.) present
82	33.322	-102.823	TX	Yoakum	Bs	Patricia	Fine-loamy, mixed, thermic aridic paleustalfs	Fine Sand	92.7	1.3	6.0	6bw2 w1, x (~40%) present

Samples red outlined were only geospatial analyzed.

Table 6.2 – SHP dust sources sites original database Part 2

FID	Lat	Long	State	County	Soil Serie	Soil name	Geomorphology
0	32.632	-102.261	TX	Gaines	Bs	Patricia	Found on plains;the parent material consist of sandy aeolian deposits from the blackwater Draw formation of Pleistocene age
1	33.662	-102.519	TX	Hockley	AfA	Amarillo	Found on plains on plateaus. The parent material consist of sandy/loamy aeolian deposits from the Blackwater Draw formation of Pleistocene age
2	34.250	-102.592	TX	Lamb	PmA	Portales	Found on interdunes on plateaus, plains on plateaus, playa steps on plateaus. The parent material consists of calcareous, loamy lacustrine deposits of Quaternary age
3	33.607	-102.158	TX	Hockley	AcA	Acuff	Found on plains on plateaus. The parent material consist of loamy aeolian deposits from the Blackwater Draw formation of Pleistocene age
4	32.047	-103.581	NM	LEA	MN/SR	Midessa	Found on plains, uplands. The parent material consists of calcareous alluvium and/or calcareous eolian deposits derived from sedimentary rock
5	33.452	-104.824	NM	Chavez	BQB	Blakeney	Found on plateaus, plains. The parent material consists of alluvial and eolian deposits
6	33.248	-104.491	NM	Chavez	RFB	Bigetty	Found on hillslopes, plains, terraces. The parent material consists of calcareous alluvium derived from limestone
7	34.369	-103.264	NM	Curry	AnB	Amarillo	This component is on Playa slopes, plains, tablelands. The parent material consists of loamy eolian deposits
8	32.291	-101.505	TX	Howard	AfA	Amarillo	Found on plains on plateaus. The parent material consist of sandy/loamy aeolian deposits from the Blackwater Draw formation of Pleistocene age
9	32.982	-102.422	TX	Terry	PAB	Patricia	This component is on plains on plateaus. The parent material consists of sandy eolian deposits from the Blackwater Draw Formation of pleistocene age
10	34.105	-103.202	NM	Roosevelt	Ca	Church	This component is on plateaus, playa floors. The parent material consists of calcareous loamy alluvium derived from sedimentary rock
11	34.250	-103.660	NM	Roosevelt	Ab	Amarillo	This component is on plains,plateaus. The parent material consists of loamy eolian deposits derived from sedimentary rock
12	33.059	-104.170	NM	Chaves	So	Sotim	This component is on plains, plains. The parent material consists of mixed alluvium and/or eolian deposits derived from sedimentary rock
13	33.636	-104.534	NM	Chaves	EaC	Ector	The component is on ridges, plains. The parent material consists of residuum weathered from limestone
14	32.408	-103.134	NM	Lea	PU	Maljama	This component is on uplands, plains. The parent material consists of sandy aeolian deposits derived from sedimentary rock
15	34.068	-102.265	TX	Lamb	Sg	Springer	The component is on hummocks on sand sheets on plateaus. The parent material consists of sandy aeolian deposits of the blackwater Draw Formation of pleistocene age
16	33.472	-103.584	NM	Lea	Av	Arch	The component is on playa steps, tablelands, playa slopes. The parent material consists of calcareous alluvium derived from sedimentary rock
17	33.016	-102.644	TX	Yoakum	Bs	Patricia	Found on plains;the parent material consist of sandy aeolian deposits from the blackwater Draw formation of Pleistocene age
18	33.642	-104.550	NM	Chaves	GbA	Glendale	The component is on flood plains, river valleys. The parent material consists of calcareous alluvium
19	33.520	-102.679	TX	Cochran	AfB	Amarillo	The component is on plains on plateaus. The parent material consists of loamy eolian deposits from the Blackwater Draw Formation of Pleistocene age
20	32.737	-102.094	TX	Dawson	AfB	Amarillo	The component is on plains on plateaus. The parent material consists of loamy eolian deposits from the Blackwater Draw Formation of Pleistocene age
21	33.475	-101.878	TX	Lubbock	l	Acuff	The component is on plains on plateaus. The parent material consists of loamy eolian deposits from the Blackwater Draw Formation of Pleistocene age
22	34.627	-103.586	NM	Curry	SnC	Spantara	This component is on tablelands, plains, playa slopes. The parent material consists of coarse-loamy eolian deposits
23	33.899	-103.552	NM	Roosevelt	Cf	Clovis	The component is on plateaus, plains. The parent material consists of eolian deposits derived from sedimentary rock
24	32.489	-102.630	TX	Andrews	TwB	Triomas	This component is on plains on plateaus. The parent material consists of sandy eolian deposits from the Blackwater Draw Formation of pleistocene age
25	32.799	-101.960	TX	Dawson	AfB	Amarillo	The component is on playa slopes on plateaus, plains on plateaus. The parent material consists of loamy aeolian deposits from the Blackwater Draw Formation of Pleistocene age
26	31.716	-101.542	TX	Glasscock	ReA	Reagan	The component is on plains on plateaus. The parent material consists of alluvium derived from limestone
27	32.248	-101.514	TX	Howard	Ps/PfB	Potter	The component is on hillslopes on breaks, scarps on breaks. The parent material consists of calcareous, loamy alluvium in the Ogallala formation of miocene-pliocene age
28	32.276	-101.506	TX	Howard	AmB	Amarillo	The component is on playa slopes on plateaus, plains on plateaus. The parent material consists of loamy aeolian deposits from the Blackwater Draw Formation of Pleistocene age
29	32.283	-101.643	TX	Howard	SpA	Springer	The component is on sandheets on plateaus. The parent material consists of sandy aeolian deposits from the Blackwater draw Formation of Pleistocene age
30	32.286	-101.797	TX	Martin	PoA	portales	The component is on plains on plateaus, interdunes on plateaus, playa steps on plateaus. The parent material consists of calcareous,loamy lacustrine deposits of quaternary age
31	32.443	-101.780	TX	Martin	MIA	Amarillo	The component is on plains on plateaus. The parent material consists of loamy aeolian deposits from the Blackwater Draw Formation of Pleistocene age
32	32.443	-101.859	TX	Martin	AfA	Amarillo	The component is on plains on plateaus. The parent material consists of loamy aeolian deposits from the Blackwater Draw Formation of Pleistocene age
33	31.913	-101.965	TX	Midland	RvA	Reeves	The component is on basin floors on plateaus. The parent material consists of gypsum
34	33.275	-104.423	NM	Chaves	ReB	Reagan	Info not available
35	33.307	-102.387	TX	Terry	AfB/AfA	Amarillo	Info not available
36	-102.068	32.762	TX	Dawson	AfA	Amarillo	The component is on plains on plateaus. The parent material consists of loamy aeolian deposits from the Blackwater Draw Formation of Pleistocene age
37	-102.909	32.548	TX	Gaines	Be	Berda	Found on scarps on breaks, valley sides of breaks. The parent material consist of calcarious, loamy colluvium and slope alluvium derived from the Ogallala formation of Miocene-Pliocene age
38	-102.944	32.783	TX	Gaines	Sa	Simona	The component is on plains on plateaus. The parent material consist of calcarious, loamy alluvium in the Ogallala formation of Miocene-Pliocene age
39	-102.658	32.955	TX	Gaines	Br	Brownfield	The component is on sandheets on plateaus. The parent material consists of sandy aeolian deposits from the blackwater Draw formation of Pleistocene age
40	34.115	-102.854	TX	Bailey	DrE/PfA	Drake	This component is on playa dunes on plateaus. The parent material consists of calcareous, loamy aeolian deposits of quaternary age
41	34.742	-102.412	TX	Castro	PuA	Pullman	The component is on plains on plateaus. The parent material consists of clayey aeolian deposits from the Blackwater Draw Formation of Pleistocene age
42	33.768	-102.970	TX	Cochran	AfA	Amarillo	The component is on plains on plateaus. The parent material consists of loamy aeolian deposits from the Blackwater Draw Formation of Pleistocene age
43	33.731	-102.901	TX	Cochran	AmB	Amarillo	The component is on plains on plateaus. The parent material consists of loamy aeolian deposits from the Blackwater Draw Formation of Pleistocene age
44	35.292	-101.655	TX	Potter	PuB/PuA	Pullman	The component is on playa slopes on plateaus, plains on plateaus. The parent material consists of clayey aeolian deposits from the Blackwater Draw Formation of Pleistocene age
45	35.157	-101.973	TX	Randall	PxA	Pantex	The component is on playa slopes on plateaus, plains on plateaus. The parent material consists of clayey aeolian deposits from the Blackwater Draw Formation of Pleistocene age
46	34.099	-102.882	TX	Bailey	DrE(H20)	Drake	This component is on playa dunes on plateaus. The parent material consists of calcareous, loamy aeolian deposits of quaternary age
47	32.590	-102.305	TX	Gaines	Br	Brownfield	The component is on sandheets on plateaus. The parent material consists of sandy aeolian deposits from the blackwater Draw formation of Pleistocene age
48	32.936	-102.911	TX	Gaines	Br	Brownfield	The component is on sandheets on plateaus. The parent material consists of sandy aeolian deposits from the blackwater Draw formation of Pleistocene age
49	32.874	-102.750	TX	Gaines	Bs	Patricia	The component is on plains on plateaus. The parent material consists of sandy aeolian deposits from Blackwater draw Formation of pleistocene age
50	34.254	-103.666	NM	Roosevelt	Ad	Amarillo	The component is on plains on plateaus. The parent material consists of loamy aeolian deposits derived from sedimentary rock

Samples red outlined were only geospatial analyzed.

Table 6.2 (Cont.) – SHP dust sources sites original database Part 2

FID	Lat	Long	State	County	Soil Serie	Soil name	Geomorphology
51	32.684	-101.714	TX	Dawson	PeB	Pep	This component is on playa slopes on plateaus, plains on plateaus. The parent material consists of calcareous, loamy eolian deposits from the Blackwater Draw Formation of Pleistocene age
52	32.631	-101.742	TX	Dawson	AfB	Amarillo	The component is on playa slopes on plateaus, plains on plateaus. The parent material consists of loamy eolian deposits from the Blackwater Draw Formation of Pleistocene age
53	32.531	-102.167	TX	Dawson	GoA	Gomez	The component is on plains on plateaus. The parent material consists of calcareous, sandy eolian deposits from Blackwater draw Formation of pleistocene age
54	32.838	-101.825	TX	Dawson	LhA	Hindman	The component is on paleoterraces on plateaus, valley flats on plateaus. The parent material consists of calcareous loamy eolian deposits over sandy alluvium derived from the Tahoka Formation of pleistocene age
55	31.830	-101.595	TX	Glasscock	ReA	Reagan	The component is on plains on plateaus. The parent material consists of alluvium derived from limestone
56	33.053	-102.562	TX	Terry	PAB	Amarillo	The component is on plains on plateaus. The parent material consists of sandy eolian deposits from Blackwater draw Formation of pleistocene age
57	32.616	-102.299	TX	Gaines	Bs	Patricia	The component is on plains on plateaus. The parent material consists of sandy eolian deposits from Blackwater draw Formation of pleistocene age
58	32.722	-102.265	TX	Gaines	Bs	Patricia	The component is on plains on plateaus. The parent material consists of sandy eolian deposits from Blackwater draw Formation of pleistocene age
59	31.699	-101.423	TX	Glasscock	ReA	Reagan	The component is on plains on plateaus. The parent material consists of alluvium derived from limestone
60	33.425	-102.361	TX	Hockley	AcA/AfB	Abilene	The component is on alluvial plain remnants. The parent material consists of calcareous loamy alluvium and/or calcareous loamy alluvium
61	33.706	-101.654	TX	Lubbock	33	portales	The component is on plains on plateaus, interdunes on plateaus, playa steps on plateaus. The parent material consists of calcareous, loamy lacustrine deposits of quaternary age
62	32.203	-101.997	TX	Martin	AfA/AfB	Amarillo	The component is on plains on plateaus. The parent material consists of loamy eolian deposits from the Blackwater Draw Formation of Pleistocene age
63	33.609	-102.638	TX	Cochran	AmB	Amarillo	The component is plains on plateaus. The parent material consists of loamy eolian deposits from the blackwater draw formation of pleistocene age
64	33.710	-102.353	TX	Hockley	AfA	Amarillo	The component is on plains on plateaus. The parent material consists of loamy eolian deposits from the Blackwater Draw Formation of Pleistocene age
65	33.778	-102.397	TX	Hockley	AvA/AfA	Arvana	The component is on plains on plateaus. The parent material consists of loamy eolian deposits from the Blackwater Draw Formation of Pleistocene age
66	33.265	-101.974	TX	Lynn	AcA	Abilene	The component is on alluvial plain remnants. The parent material consists of calcareous loamy alluvium and/or calcareous loamy alluvium
67	33.294	-102.265	TX	Terry	AfB	Amarillo	The component is on playa slopes on plateaus, plains on plateaus. The parent material consists of loamy eolian deposits from the Blackwater Draw Formation of Pleistocene age
68	32.564	-102.641	TX	Gaines	Sm	Arvana	This component is on plains on plateaus. The parent material consists of loamy eolian deposits from the blackwater draw formation of pleistocene age
69	32.206	-102.142	TX	Martin	MdA/AfB	Midessa	This component is on plains on plateaus. The parent material consists of calcareous, loamy eolian and lacustrine deposits derived from the Tahoka and Blackwater draw formation of pleistocene age
70	31.937	-101.732	TX	Glasscock	MfA	Midessa	This component is on plains on plateaus. The parent material consists of calcareous, loamy eolian and lacustrine deposits derived from the Tahoka and Blackwater draw formation of pleistocene age
71	33.570	-102.887	TX	Cochran	AfA	Amarillo	The component is on playa slopes on plateaus, plains on plateaus. The parent material consists of loamy eolian deposits from the Blackwater Draw Formation of Pleistocene age
72	34.451	-103.275	NM	Curry	AcA	Abilene	The component is on alluvial plain remnants. The parent material consists of calcareous loamy alluvium and/or calcareous loamy alluvium
73	32.956	-102.944	TX	Gaines	Bs	Patricia	The component is on plains on plateaus. The parent material consists of sandy eolian deposits from Blackwater draw Formation of pleistocene age
74	34.040	-103.400	NM	Roosevelt	Aa	Amarillo	The component is on plains on plateaus. The parent material consists of loamy eolian deposits derived from sedimentary rock
75	34.276	-103.604	NM	Roosevelt	Aa	Amarillo	The component is on plains on plateaus. The parent material consists of loamy eolian deposits derived from sedimentary rock
76	33.811	-102.982	TX	Cochran	Ao	Arch	This component is on interdunes on plateaus, playa steps on plateaus. The parent material consists of calcareous, loamy eolian and lacustrine deposits derived from the Tahoka and Blackwater draw formation
77	32.725	-104.309	NM	Eddy	AH	Arno	The component is on alluvial fans, alluvial plains. The parent material consists of alluvium
78	34.035	-102.454	TX	Lamb	OrA	Olton	The component is on plains on plateaus. The parent material consists of clayey eolian deposits from blackwater formation
79	32.341	-101.855	TX	Martin	AfA	Amarillo	The component is on playa slopes on plateaus, plains on plateaus. The parent material consists of loamy eolian deposits from the Blackwater Draw Formation of Pleistocene age
80	33.076	-103.057	TX	Yoakum	PmA	portales	The component is on plains on plateaus, interdunes on plateaus, playa steps on plateaus. The parent material consists of calcareous, loamy lacustrine deposits of quaternary age
81	33.153	-102.969	TX	Yoakum	Br	Brownfield	The component is on sand sheets on plateaus. The parent material consists of sandy eolian deposits from the blackwater Draw formation of Pleistocene age
82	33.322	-102.823	TX	Yoakum	Bs	Patricia	The component is on plains on plateaus. The parent material consists of sandy eolian deposits from Blackwater draw Formation of pleistocene age

Samples red outlined were only geospatial analyzed.

Table 6.3 – Chihuahuan Desert dust sources sites original database

FID	Sample	Lat	Long	State	County	Soil Serie	Soil name	Classification	Texture	Sand	Silt	Clay	Land	Notes
0	WS DUNE	32.825	-106.277	NM	Otero		Holloman		Sand	99.6	0.1	0.0	6au	Aeolian sand (dune)
1	WS INTD	32.825	-106.277	NM	Otero		Holloman		Sand	99.4	0.1	0.0	6au	Aeolian sand (dune)
2	TULA G	33.077	-106.098	NM	Otero		Holloman		Silt Loam	31.6	57.5	9.9	2x	Duricrust (caliche). Grassland, CRP, and Randall clay playas
3	WELL 9	32.009	-106.637	NM	Doña Ana		Glendale		Silt Loam	21.9	63.2	14.6	6bw1	>75% of farmland coverage
4	OC LAKE	32.235	-106.387	NM	Doña Ana		Stellar		Silt Loam	31.1	67.6	1.3	1bu	Playa ephemeral
5	INBA	31.846	-107.346	NM	Luna		Pintura		Sandy Loam	66.8	26.7	6.4	5cu	Alluvial unarmoured, incised
6	SPHA	32.883	-106.348	NM	Otero		Holloman		Loamy Sand	78.0	17.0	0.4	1cu	Playa dry (consolidated)
7	McGREG	32.090	-106.207	NM	Otero		Huaco		Sample n/a				6bx	Grassland, CRP, and Randall clay playas
8	DOÑA A	32.147	-106.514	NM	Doña Ana		Mimbres		Sand	94.4	4.0	0.8	5cz	Alluvial unarmoured, incised. Development outside of main city/town
9	WELL 15	31.885	-106.388	TX	El Paso		Turney		Sand	92.9	5.1	1.6	6bv	Aeolian sand sheet. Development outside of main city/town
10	HAMM	31.800	-104.970	TX	Hudspeth		Holloman		Sandy Loam	57.1	36.0	5.8	1bu	Playa ephemeral
11	DUNE 8	31.920	-104.990	TX	Hudspeth		Holloman		Loamy Sand	77.7	18.7	3.6	6au	Aeolian sand (dune)
12	COORD	31.766	-105.397	TX	Hudspeth		Reakon		Loam	51.4	40.0	7.3	6bx	Aeolian sand sheet. Grassland, CRP, and Randall clay playas
13	SALT S36	31.760	-104.983	TX	Hudspeth		Holloman		Sandy Loam	51.3	42.3	2.9	1cu	Playa dry (consolidated)
14	SALT S56	31.764	-104.988	TX	Hudspeth		Holloman		Silt Loam	38.2	54.8	6.4	1cu	Playa dry (consolidated)
15	SALT S2	31.754	-104.993	TX	Hudspeth		Holloman		Silt Loam	21.8	71.8	6.4	1cu	Playa dry (consolidated)
16	B HOUSE	31.890	-105.060	TX	Hudspeth		Holloman		Silt Loam	15.9	74.2	9.4	1cu	Playa dry (consolidated)
17	RLMV62A	31.866	-106.901	NM	Doña Ana		Simona		Sand	94.6	4.0	1.3	6bx	Aeolian sand sheet. Grassland, CRP, and Randall clay playas
18	RLMV62B	31.965	-106.889	NM	Doña Ana		Simona		Sand	84.0	0.0	0.0	6bx	Aeolian sand sheet. Grassland, CRP, and Randall clay playas
19	WRJG001	32.377	-108.899	NM	Hidalgo		Hondale		Sand	93.3	4.6	1.8	1bu	Playa ephemeral
20	MRJG006	32.180	-109.880	AZ	Cochise		Hondale		Loamy Sand	82.3	10.5	6.8	1bw2	Playa ephemeral
21	WRJG007	32.148	-109.901	AZ	Cochise		Hondale		Loam	44.6	36.4	19.0	1bw2	Playa ephemeral
22	DuIK-u	32.542	-106.195	NM	Otero		Pintura		Sand	99.5	0.5	0.0	6bu	Aeolian sand sheet
23	Sh 1K-m-u	32.435	-106.145	NM	Otero		Pintura		Loamy Sand	69.8	19.3	2.1	6bu	Aeolian sand sheet
24	Sh 400m	32.519	-106.157	NM	Otero		Pintura		Loamy Sand	84.4	12.7	2.8	6bu	Aeolian sand sheet
25	Du 1.5K-m	32.438	-106.169	NM	Otero		Pintura		Sand	96.9	2.8	0.3	6bu	Aeolian sand sheet
26	JornScrap	32.539	-106.758	NM	Doña Ana		Stellar		Sand	92.5	6.5	1.0	5du	Alluvial unarmoured, unincised
27	ASC 001	30.913	-106.927	CHIH	Ahumada		Xerosol Sg		Silt Loam	16.3	65.5	17.4	1bu	Playa ephemeral. Small Playa. Fairly unvegetated
28	ASC 002	31.067	-107.893	CHIH	Ascension		Xerosol Zo		Sandy Loam	63.6	28.3	8.1	1bu	Playa ephemeral. Semi-large body of standing water. No vegetation present
29	ASC 003	31.058	-107.893	CHIH	Ascension		Xerosol Zo		Silty Clay Loam	8.0	58.7	33.2	1bu	Playa ephemeral. Semi-large body of standing water. No vegetation present
30	CLP 001	30.824	-106.710	CHIH	Ahumada		Xerosol Sg		Silt Loam	8.9	63.2	27.9	1bu	Playa ephemeral. None
31	CLP 002	30.913	-106.863	CHIH	Ahumada		Xerosol Sg		Silt Loam	12.5	61.2	26.3	1bu	Playa ephemeral. Northern area of the southwestern arm of Lake Palomas
32	COR 001	31.172	-106.661	CHIH	Juarez		Regosol Sg		Sandy Loam	70.3	25.0	4.7	2u	Duricrust (caliche). Interdune or bare soil area, surrounded by small grass dunes
33	COR 002	31.161	-106.842	CHIH	Juarez		Regosol Rc		Silt Loam	31.3	54.5	14.2	2u	Duricrust (caliche). Super soft thin crust. Fine gravel size. Extremely loose sediment
34	COR 004	31.161	-106.842	CHIH	Juarez		Regosol Rc		Sand	91.9	5.5	2.6	2u	Duricrust (caliche). Loose sand. Sandy shore 3 meters higher than playa base shore
35	COR 005	31.154	-106.894	CHIH	Ahumada		Xerosol Sg		Clay Loam	24.7	43.9	31.5	6bu	Aeolian sand sheet. Regular playa sediments, hard crust
36	COR 008	31.155	-106.822	CHIH	Ahumada		Xerosol Rc		Sand	100.0	0.0	0.0	6au	Aeolian sand dune. Dune field east of LP shore line, sample from transverse dune
37	COR 009	31.151	-106.799	CHIH	Ahumada		Xerosol Rc		Sand	100.0	0.0	0.0	6bu	Aeolian sand sheet. Loose sand in thin sand sheet coppice dunes anchored by grass
38	COR 010	31.151	-106.799	CHIH	Ahumada		Xerosol Rc		Loam	44.9	42.1	12.1	6bu	Aeolian sand sheet. Bare soil interdune area
39	DBM 002	31.161	-106.850	CHIH	Ahumada		Xerosol Sg		Silty Clay	6.2	41.6	52.2	7u	Loess. Regular playa sample, medium to thick fine crust. Heavily eroded
40	GV 002	31.506	-107.735	CHIH	Ascension		Xerosol Xh		Silt Loam	30.0	50.8	15.4	7w2	Loess. Undisturbed soil. Heavily vegetated (creosote and mesquite)
41	HWY 45	31.539	-107.262	CHIH	Ascension		Xerosol Zo		Silt Loam	22.5	61.1	16.4	7x	Cattle observed (<15%). Area is minimal disturbed. Little grass observed
42	LDP 001	30.746	-106.499	CHIH	Ahumada		Xerosol Zo		Clay	0.8	33.8	65.3	1cu	Playa dry (consolidated). Medium to thick fine crust, on small mudcracks, un-deflated
43	LF 004	31.111	-107.515	CHIH	Ascension		Xerosol Zt		Silty Clay	8.5	43.5	48.0	1bx	Playa ephemeral. Regulas sample. Some coarse clasts
44	LG 004	31.246	-107.452	CHIH	Ascension		Xerosol Vc		Silty Clay Loam	2.0	60.2	37.7	1bx	Playa ephemeral. Fine crust and flakes on top of mudcrack uneroded
45	LPAL 005	31.674	-107.585	CHIH	Ascension		Xerosol Xk		Sandy Loam	73.4	16.1	10.5	1cu	Playa dry (consolidated). Loose sediments from a channel depression; gravelly surface
46	LSM 002	31.139	-107.310	CHIH	Ascension		Xerosol Zg		Sandy Loam	70.4	22.5	4.0	1bx	Playa ephemeral. Abundant grasses in salty crust gravelly areas surrounding lake
47	LSM 003	31.139	-107.310	CHIH	Ascension		Xerosol Zg		Silt Loam	18.1	54.8	27.1	1bx	Playa ephemeral. Abundant grasses in salty crust gravelly areas surrounding lake
48	SELP 003	30.779	-106.658	CHIH	Ahumada		Xerosol Sg		Silty Clay Loam	10.2	56.5	33.1	1bu	Playa ephemeral. No farming observed, but minor cattle activity present
49	SMD 002	31.187	-106.294	CHIH	Juarez		Regosol Rc		Sand	100.0	0.0	0.0	6au	Aeolian sand dune
50	SMD 003	31.317	-106.409	CHIH	Juarez		Regosol Rc		Sand	100.0	0.0	0.0	6au	Aeolian sand dune
51	SMD 026	31.319	-106.409	CHIH	Juarez		Regosol Rc		Sand	100.0	0.0	0.0	6au	Aeolian sand dune
52	TLG 001	31.230	-107.487	CHIH	Ascension		Xerosol L		Silt Loam	29.7	51.1	18.0	1cx	Play dry (consolidated). Sample next to road. Abundant dried vegetation

Table 6.4 – Dust sources sites characterized complete matrix

Site	State	Latitude	Longitude	Soil Texture	Soil Name	Land Class	Land Description	Geomor	Sample	Site Description
1 As	TX	32.6318	-102.2610	Sand	Patricia	6bw2	Farm (N Irr)	AS	S(0) 1	Playas present; dryland only
2 As	TX	33.6623	-102.5190	Loamy Sand	Amarillo	6bw3	Farm (Irr/N Irr)	AS	S(1) 2	Oil, playas, farmhouses present
3 As	TX	34.2500	-102.5920	Sandy Loam	Portales	6bv	Mixed	AS	S(2) 3	Center pivots, farmhouse present
4 As	TX	33.6070	-102.1580	Sandy Loam	Acuff	6bw2	Farm (N Irr)	AS	S(3) 4	Black-and-white image; unclear
5 As	NM	32.0467	-103.5810	Sand	Midessa	6ax	Range	AS	S(4) 5	x only
1r A1	NM	33.4520	-104.8240	F. Sandy Loam	Blakeney	5cx	Range	AL	S(5)	No description available in Lubbock Soil Attribute List file
6 A1	NM	33.2477	-104.4910	Loam	Bigetty	5cx	Range	AL	S(6) 6	None
7 As	NM	34.3690	-103.2640	Loamy Sand	Amarillo	6bw1	Farm (Irr)	AS	S(7) 7	Town, playas, CAFO present
1m As	TX	32.2910	-101.5050	F. Sandy Loam	Amarillo	6bv	Mixed	AS	S(8)	Town present
8 As	TX	32.9821	-102.4220	Sand	Patricia	6bw1	Farm (Irr)	AS	S(9) 8	None
9 As	NM	34.1047	-103.2020	Loamy Sand	Church	6bx	Range	AS	S(10) 9	Dryland farms, farmhouses, draw present
2r As	NM	34.2500	-103.6600	F. Sandy Loam	Amarillo	6bx	Range	AS	S(11)	Dryland farms, farmhouses present
10 As	NM	33.0586	-104.1700	Sandy Loam	Sotim	6bx	Range	AS	S(12) 10	Oil present
11 A1	NM	33.6363	-104.5340	Sandy Loam	Ector	5cv	Mixed	AL	S(13) 11	Draw system; dryland farms, center pivots present
12 Lo	NM	32.4080	-103.1340	Sand	Maljama	7v	Mixed	LO	S(14) 12	Oil patch; range present; dryland farms present
13 As	TX	34.0683	-102.2650	Sand	Springer	6bw1	Farm (Irr)	AS	S(15) 13	Playa, Range and dryland farms present
3r A1	NM	33.4720	-103.5840	Loam	Arch	x	Range	AL	S(16)	Oil present
14 As	TX	33.0165	-102.6440	Sand	Patricia	6bv	Mixed	AS	S(17) 14	Oil, dryland/irrigated mix present
15 A1	NM	33.6419	-104.5500	Silt Loam	Glendale	5cw3	Farm (Irr/N Irr)	AL	S(18) 15	Floodplain farm; farmhouses, center pivot, irrigated non-center pivot present
16 As	TX	33.5200	-102.6790	Sand	Amarillo	6bv	Mixed	AS	S(19) 16	Range, oil, center pivot, non-saline playa present
17 As	TX	32.7372	-102.0940	Sand	Amarillo	6bw2	Farm (N Irr)	AS	S(20) 17	Range, non-saline playas present
18 As	TX	33.4750	-101.8780	Sandy Loam	Acuff	6bw1	Farm (Irr)	AS	S(21) 18	Outskirts of Lubbock; z, non-saline playas, dryland farms, stockyard, landfill present
19 As	NM	34.6266	-103.5860	Loamy Sand	Spantara	6bx	Range	AS	S(22) 19	Dryland farms present
20 As	NM	33.8994	-103.5520	Loamy Sand	Clovis	6bx	Range	AS	S(23) 20	Ranch houses, non-saline playas present
21 As	TX	32.7990	-101.9600	Sand	Amarillo	6bw1	Farm (Irr)	AS	S(25) 21	Non-saline playas, farmhouses present
2m As	TX	32.4890	-102.6300	Fine Sand	Triomas	6bv	Mixed	AS	S(24)	Oil patch, w1, w2, and range
22 As	TX	31.7164	-101.5420	Silt Loam	Reagan	6bw2	Farm (N Irr)	AS	S(26) 22	Range, z, non-saline playas present
23 As	TX	32.2482	-101.5140	Sand	Potter	6bx	Range	AS	S(27) 23	w (dryland), y (Big Spring), reservoir, creek present
24 As	TX	32.2756	-101.5060	Sand	Amarillo	6bv	Mixed	AS	S(28) 24	w (dryland), y (Big Spring), range present
25 As	TX	32.2827	-101.6430	Sandy Loam	Springer	6bx	Range	AS	S(29) 25	Oil, w (dryland) present
26 As	TX	32.2863	-101.7970	Loamy Sand	Portales	6bw2	Farm (N Irr)	AS	S(30) 26	Range, non-saline playa present
27 As	TX	32.4430	-101.7800	Sand	Amarillo	6bv	Mixed	AS	S(31) 27	Non-saline playas, farmhouses present
28 As	TX	32.4433	-101.8590	Sand	Amarillo	6bv	Mixed	AS	S(32) 28	Range, canyon, non-saline playas present
29 As	TX	31.9127	-101.9650	Loamy Sand	Reeves	6bx	Range	AS	S(33) 29	Draw, dryland farms, non-saline playas, z present
30 As	NM	33.2751	-104.4230	Loamy Sand	Reagan	6bx	Range	AS	S(34) 67	No description was available
31 As	TX	33.3068	-102.3870	Sand	Amarillo	6bw1	Farm (Irr)	AS	S(35) 68	No description was available
32 As	TX	32.7620	-102.0680	Sand	Amarillo	6bw2	Farm (N Irr)	AS	S(36) 69	Non-saline playas present
33 As	TX	32.5479	-102.9090	Sand	Berda	6bx	Range	AS	S(37) 70	Dryland farm present; CAFO present; draw present
34 As	TX	32.7834	-102.9440	Loamy Sand	Simona	6bw1	Farm (Irr)	AS	S(38) 71	z present (oil and gas facility)
35 As	TX	32.9547	-102.6580	Sand	Brownfield	6bw1	Farm (Irr)	AS	S(39) 72	non-saline playas present
4r P1	TX	34.1150	-102.8540	Loam	Drake	1bx	Range	PL	S(40)	Salt lake; w2 present
36 Lo	TX	34.7415	-102.4120	Silt Loam	Pullman	7w3	Farm (Irr/N Irr)	LO	S(41) 30	x, farmhouses present
37 As	TX	33.7683	-102.9700	Sand	Amarillo	6bw2	Farm (N Irr)	AS	S(42) 31	w1, x, z (rural community) present
38 As	TX	33.7314	-102.9010	Sand	Amarillo	6bv	Range	AS	S(43) 32	w1, w2, x, and farmhouses
39 Lo	TX	35.2920	-101.6550	Silt Loam	Pullman	7v	Mixed	LO	S(44) 33	w1, w2, x, z, (rural residential), lake, non-saline playa
40 Lo	TX	35.1567	-101.9730	Silt Loam	Pantex	7v	Mixed	LO	S(45) 34	w1, w2, x
5r As	TX	34.0990	-102.8820	Loam	Drake	6bx	Range	AS	S(46)	Salt lake present (~40% of viewscreen)
41 As	TX	32.5900	-102.3050	Sand	Brownfield	6bx	Range	AS	S(47) 35	w2 present
42 As	TX	32.9360	-102.9110	Sand	Brownfield	6bv	Mixed	AS	S(48) 36	mix of w1, x, and z (oil)
43 As	TX	32.8743	-102.7500	Sand	Patricia	6bw1	Farm (Irr)	AS	S(49) 37	w1, x, z (oil) present
44 As	NM	34.2544	-103.6660	Sand	Amarillo	6bx	Range	AS	S(50) 38	x only

Table 6.4 (Cont.) – Dust sources sites characterized complete matrix

45 As	TX	32.6843	-101.7140	Sand	Pep	6bx	Range	AS	S(51) 39	Edge of Caprock; w1, w2, z (oil) present
46 As	TX	32.6311	-101.7420	Loamy Sand	Amarillo	6bw2	Farm (N Irr)	AS	S(52) 40	Terraced w2, x, z (oil), non-saline playas, farmhouses present
47 As	TX	32.5310	-102.1670	Loamy Sand	Gomes	6bw2	Farm (N Irr)	AS	S(53) 41	No description was available
48 As	TX	32.8380	-101.8250	Sand	Hindman	6bx	Range	AS	S(54) 42	No description was available
49 As	TX	31.8300	-101.5950	Silt Loam	Reagan	6bw2	Farm (N Irr)	AS	S(55) 43	No description was available
50 As	TX	33.0530	-102.5620	Sand	Amarillo	6bv	Mixed	AS	S(56) 44	No description was available
51 As	TX	32.6161	-102.2990	Sand	Patricia	6bw2	Farm (N Irr)	AS	S(57) 45	x present
6r Al	TX	32.7220	-102.2650	Fine Sand	Patricia	5cx	Range	AL	S(58)	w2 also present
52 As	TX	31.6988	-101.4230	Silty Clay Loam	Reagan	6bv	Mixed	AS	S(59) 46	x, w2; looks like some fields were w2 but are turning into x
3m As	TX	33.4250	-102.3610	Clay Loam	Abilene	6bx	Mixed	AS	S(60)	extensive z (oil pumpjacks)
53 As	TX	33.7059	-101.6540	Loam	Portales	6bv	Mixed	AS	S(61) 47	w1, w2, x, playas present
54 As	TX	32.2033	-101.9970	Loamy Sand	Amarillo	6bw2	Farm (N Irr)	AS	S(62) 48	Oil pumpjacks (z); playas; x present
55 As	TX	33.6091	-102.6380	Sand	Amarillo	6bv	Mixed	AS	S(63) 49	x, w1, w2, z (rural res. And oil); non-saline playas present
56 As	TX	33.7102	-102.3530	Sand	Amarillo	6bw2	Farm (N Irr)	AS	S(64) 50	w2, x, non-saline playa present
57 As	TX	33.7780	-102.3970	Sand	Arvana	6bx	Range	AS	S(65) 51	w1, w2, non-saline playas present
58 As	TX	33.2652	-101.9740	Sand	Abilene	6bw3	Farm (Irr)	AS	S(66) 52	x, non-saline playa, draw present
59 As	TX	33.2938	-102.2650	Sand	Amarillo	6bw2	Farm (N Irr)	AS	S(67) 53	w1, x, non-saline playas present
60 As	TX	32.5640	-102.6410	Sand	Arvana	6bw1	Farm (Irr)	AS	S(68) 54	No description was available
4m As	TX	32.2060	-102.1420	F. Sandy Loam	Midessa	6bx	Mixed	AS	S(69)	w1, w2, z (oil) present
5m Al	TX	31.9370	-101.7320	F. Sandy Loam	Midessa	v	Mixed	AL	S(70)	w1, x, and z (rural res.); draw and stock pond present
61 As	TX	33.5702	-102.8870	Loamy Sand	Amarillo	6bx	Range	AS	S(71) 55	w2, z (oil) present
62 As	NM	34.4506	-103.2750	Sandy Loam	Abilene	6bw3	Farm (Irr/N Irr)	AS	S(72) 56	x, z (rural res.), non-saline playa present
63 As	TX	32.9563	-102.9440	Sand	Patricia	6bw1	Farm (Irr)	AS	S(73) 57	w2, x, z (rural res.) present
64 As	NM	34.0401	-103.4000	Loamy Sand	Amarillo	6bw2	Farm (N Irr)	AS	S(74) 58	~40% x
65 As	NM	34.2757	-103.6040	Sand	Amarillo	6bw1	Farm (Irr)	AS	S(75) 59	w2, x, z (rural res.) present
66 As	TX	33.8110	-102.9820	Clay Loam	Arch	6bx	Range	AS	S(76) 60	w1 present
67 Al	NM	32.7248	-104.3090	Silt Loam	Arno	5dx	Range	AL	S(77) 61	Pecos River; x only
68 As	TX	34.0347	-102.4540	Loamy Sand	Olton	6bw1	Farm (Irr)	AS	S(78) 62	w1, x, z (CAFO and rural res.), non-saline playas present
69 As	TX	32.3405	-101.8550	Loamy Sand	Amarillo	6bw2	Farm (N Irr)	AS	S(79) 63	w2 only
70 As	TX	33.0758	-103.0570	Loamy Sand	Portales	6bw1	Farm (Irr)	AS	S(80) 64	w2, x, z (rural res.) present
71 As	TX	33.1531	-102.9690	Sand	Brownfield	6bw1	Farm (Irr)	AS	S(81) 65	w2, x, z (rural res.) present
72 As	TX	33.3220	-102.8230	Sand	Patricia	6bw2	Farm (N Irr)	AS	S(82) 66	w1, x (~40%) present
73 As	NM	32.8251	-106.2772	Sand	Holloman	6au	Unk	AS	WS DUN	Aeolian sand (dune)
74 As	NM	32.8251	-106.2766	Sand	Holloman	6au	Unk	AS	WS INTI	Aeolian sand (dune)
75 Ca	NM	33.0770	-106.0980	Silt Loam	Holloman	2x	Range	CA	TULA G	Duricrust (caliche). Grassland, CRP, and Randall clay playas
76 As	NM	32.0086	-106.6369	Silt Loam	Glendale	6bw1	Farm (Irr)	AS	WELL 9	>75% of farmland coverage
77 Pl	NM	32.2350	-106.3870	Silt Loam	Stellar	1bu	Unk	PL	OC LAKI	Playa ephemeral
78 Al	NM	31.8460	-107.3460	Sandy Loam	Pintura	5cu	Unk	AL	INBA	Alluvial unarmoured, incised
79 Pl	NM	32.8830	-106.3480	Loamy Sand	Holloman	1cu	Unk	PL	SPHA	Playa dry (consolidated)
80 As	NM	32.0900	-106.2070	N/A	Hueco	6bx	Range	AS	McGREG	Grassland, CRP, and Randall clay playas
81 Al	NM	32.1470	-106.5140	Sand	Mimbres	5cz	Mixed	AL	DOÑA A	Alluvial unarmoured, incised. Development outside of main city/town
82 As	TX	31.8850	-106.3880	Sand	Turney	6bv	Mixed	AS	WELL 1:	Aeolian sand sheet. Development outside of main city/town
83 Pl	TX	31.8000	-104.9700	Sandy Loam	Holloman	1bu	Unk	PL	HAMM	Playa ephemeral
84 As	TX	31.9200	-104.9900	Loamy Sand	Holloman	6au	Unk	AS	DUNE S	Aeolian sand (dune)
85 As	TX	31.7658	-105.3970	Loam	Reakon	6bx	Range	AS	COORD	Aeolian sand sheet. Grassland, CRP, and Randall clay playas
86 Pl	TX	31.7600	-104.9833	Sandy Loam	Holloman	1cu	Unk	PL	SALT S3:	Playa dry (consolidated)
87 Pl	TX	31.7640	-104.9882	Silt Loam	Holloman	1cu	Unk	PL	SALT S5:	Playa dry (consolidated)
88 Pl	TX	31.7542	-104.9925	Silt Loam	Holloman	1cu	Unk	PL	SALT S2	Playa dry (consolidated)
89 Pl	TX	31.8900	-105.0600	Silt Loam	Holloman	1cu	Unk	PL	B HOUSE	Playa dry (consolidated)
90 As	NM	31.8661	-106.9014	Sand	Simona	6bx	Range	AS	RLMV62.	Aeolian sand sheet. Grassland, CRP, and Randall clay playas

Table 6.4 (Cont.) – Dust sources sites characterized complete matrix

91 As	NM	31.9653	-106.8886	Sand	Simona	6bx	Range	AS	RLMV62: Aeolian sand sheet. Grassland, CRP, and Randall clay playas
92 Pl	NM	32.3773	-108.8988	Sand	Hondale	1bu	Unk	PL	WRJG001 Playa ephemeral
93 Pl	AZ	32.1797	-109.8801	Loamy Sand	Hondale	1bw2	Farm (N Irr)	PL	MRJG006 Playa ephemeral
94 Pl	AZ	32.1484	-109.9013	Loam	Hondale	1bw2	Farm (N Irr)	PL	WRVG00 Playa ephemeral
95 As	NM	32.5423	-106.1949	Sand	Pintura	6bu	Unk	AS	Du1K-u Aeolian sand sheet
96 As	NM	32.4349	-106.1446	Loamy Sand	Pintura	6bu	Unk	AS	Sh 1K-m Aeolian sand sheet
97 As	NM	32.5193	-106.1567	Loamy Sand	Pintura	6bu	Unk	AS	Sh 400m Aeolian sand sheet
98 As	NM	32.4375	-106.1687	Sand	Pintura	6bu	Unk	AS	Du 1.5K- Aeolian sand sheet
99 Al	NM	32.5390	-106.7583	Sand	Stellar	5du	Unk	AL	JornScrap Alluvial unarmoured, unincised
100 Pl	CHIH	30.9127	-106.9268	Silt Loam	Xerosol Sg	1bu	Unk	PL	ASC 001 Playa ephemeral. Small Playa. Fairly unvegetated
101 Pl	CHIH	31.0668	-107.8928	Sandy Loam	Xerosol Zo	1bu	Unk	PL	ASC 002 Playa ephemeral. Semi-large body of standing water. No vegetation present
102 Pl	CHIH	31.0577	-107.8928	Silty Clay Loam	Xerosol Zo	1bu	Unk	PL	ASC 003 Playa ephemeral. Semi-large body of standing water. No vegetation present
103 Pl	CHIH	30.8240	-106.7098	Silt Loam	Xerosol Sg	1bu	Unk	PL	CLP 001 Playa ephemeral. None
104 Pl	CHIH	30.9127	-106.8628	Silt Loam	Xerosol Sg	1bu	Unk	PL	CLP 002 Playa ephemeral. Northern area of the southwestern arm of Lake Palomas
105 Ca	CHIH	31.1722	-106.6611	Sandy Loam	Regosol Sg	2u	Unk	CA	COR 001 Duricrust (caliche). Interdune or bare soil area, surrounded by small grass dunes
106 Ca	CHIH	31.1608	-106.8422	Silt Loam	Regosol Rc	2u	Unk	CA	COR 002 Duricrust (caliche). Super soft thin crust. Fine gravel size. Extremely loose sediment
107 Ca	CHIH	31.1608	-106.8422	Sand	Regosol Rc	2u	Unk	CA	COR 004 Duricrust (caliche). Loose sand. Sandy shore 3 meters higher than playa base shore
108 As	CHIH	31.1539	-106.8942	Clay Loam	Xerosol Sg	6bu	Unk	AS	COR 005 Aeolian sand sheet. Regular playa sediments, hard crust
109 As	CHIH	31.1547	-106.8217	Sand	Xerosol Rc	6au	Unk	AS	COR 008 Aeolian sand dune. Dune field east of LP shore line, sample from transverse dune
110 As	CHIH	31.1515	-106.7992	Sand	Xerosol Rc	6bu	Unk	AS	COR 009 Aeolian sand sheet. Loose sand in thin sand sheet coppice dunes anchored by grass
111 As	CHIH	31.1515	-106.7992	Loam	Xerosol Rc	6bu	Unk	AS	COR 010 Aeolian sand sheet. Bare soil interdune area
112 Lo	CHIH	31.1612	-106.8499	Silty Clay	Xerosol Sg	7u	Unk	LO	DBM 002 Loess. Regular playa sample, medium to thick fine crust. Heavily eroded
113 Lo	CHIH	31.5064	-107.7353	Silt Loam	Xerosol Xh	7w2	Farm (N Irr)	LO	GV 002 Loess. Undisturbed soil. Heavily vegetated (creosote and mesquite)
114 Lo	CHIH	31.5390	-107.2624	Silt Loam	Xerosol Zo	7x	Range	LO	HWY 45 Cattle observed (<15%). Area is minimal disturbed. Little grass observed
115 Pl	CHIH	30.7460	-106.4987	Clay	Xerosol Zo	1cu	Unk	PL	LDP 001 Playa dry (consolidated). Medium to thick fine crust, on small mudcracks, un-deflated
116 Pl	CHIH	31.1110	-107.5150	Silty Clay	Xerosol Zt	1bx	Range	PL	LF 004 Playa ephemeral. Regulas sample. Some coarse clasts
117 Pl	CHIH	31.2464	-107.4519	Silty Clay Loam	Xerosol Vc	1bx	Range	PL	LG 004 Playa ephemeral. Fine crust and flakes on top of mudcrack uneroded
118 Pl	CHIH	31.6744	-107.5848	Sandy Loam	Xerosol Xk	1cu	Unk	PL	LPAL 00 Playa dry (consolidated). Loose sediments from a channel depression; gravelly surface
119 Pl	CHIH	31.1387	-107.3100	Sandy Loam	Xerosol Zg	1bx	Range	PL	LSM 002 Playa ephemeral. Abundant grasses in salty crust gravelly areas surrounding lake
120 Pl	CHIH	31.1387	-107.3100	Silt Loam	Xerosol Zg	1bx	Range	PL	LSM 003 Playa ephemeral. Abundant grasses in salty crust gravelly areas surrounding lake
121 Pl	CHIH	30.7786	-106.6584	Silty Clay Loam	Xerosol Sg	1bu	Unk	PL	SELP 001 Playa ephemeral. No farming observed, but minor cattle activity present
122 As	CHIH	31.1874	-106.2939	Sand	Regosol Rc	6au	Unk	AS	SMD 002 Aeolian sand dune
123 As	CHIH	31.3173	-106.4088	Sand	Regosol Rc	6au	Unk	AS	SMD 003 Aeolian sand dune
124 As	CHIH	31.3193	-106.4088	Sand	Regosol Rc	6au	Unk	AS	SMD 026 Aeolian sand dune
125 Pl	CHIH	31.2300	-107.4865	Silt Loam	Xerosol L	1cx	Range	PL	TLG 001 Play dry (consolidated). Sample next to road. Abundant dried vegetation. Cows observed

Table 6.5 – Geomorphic classification and modifier codes observed for land use characterization.

Geomorphic Classification	Geomorphic Modifier	Description
1 Playa	b Ephemeral	Not Randall clay playas, salt lakes
	c Dry (Consolidated)	
	d Dry (Non-consolidated)	
	e Dry (no lacustrine material exposed)	
2 Duricrust (Caliche)		
5 Alluvial	c Unarmoured, incised	e.g., arroyos and draws
	d Unarmoured, unincised	e.g., Pecos River
6 Aeolian Sand	a Dune	Visible on imagery or known
	b Sheet	Not fine or very fine textures
7 Loess		

Land-use Classification	Land-use Modifier	Description
u Unknown Use		Indeterminate land-use
v Mixed Use		No more than 50% w, x, y, or z
w Farmland (> 50%)	1 Irrigated	> 75% of w coverage
	2 Non-irrigated	> 75% of w coverage
	3 Mixed Irrigated / Non-irrigated	No more than 75% of 1 or 2
x Rangeland (> 50%)		Grassland, CRP, and Randall clay Playas
y Urban (> 50%)		Commercial, residential, industrial in city
z Rural Developed (> 50%)		Development outside of main city/town

This classification is based on [Bullard et al. \(2011\)](#).

Table 6.6 – Geomorphic categories for the Southern High Plains region

Class	Geomorphic Classification	Geomorphic Modifier	Description	Land-use Classification	Land-use Modifier	Description
1bx	Playa	Ephemeral	Not Randall clay playas; salt lakes	Rangeland (>50%)		Grassland, CRP, and Randall clay playas
5cv	Alluvial	Unarmoured, incised	e.g., arroyos and draws	Mixed use		
5cw3	Alluvial	Unarmoured, incised	e.g., arroyos and draws	Farmland (> 50%)	Mixed Irrigated/Non irrigated	No more than 75% of irrigated/non irrigated
5cx	Alluvial	Unarmoured, incised	e.g., arroyos and draws	Rangeland (>50%)		Grassland, CRP, and Randall clay playas
5dx	Alluvial	Unarmoured, unincised	e.g., Pecos River	Rangeland (>50%)		Grassland, CRP, and Randall clay playas
6ax	Aeolian Sand	Dune	Visible on imagery or known	Rangeland (>50%)		Grassland, CRP, and Randall clay playas
6bu	Aeolian Sand	Sheet	Not fine or very fine textures	Unknown use		Indeterminate land-use
6bv	Aeolian Sand	Sheet	Not fine or very fine textures	Mixed use		No more than 50% of farmland, rangeland, urban, or rural development
6bw1	Aeolian Sand	Sheet	Not fine or very fine textures	Farmland (>50%)	Irrigated	>75% of farmland coverage
6bw2	Aeolian Sand	Sheet	Not fine or very fine textures	Farmland (>50%)	Non-irrigated	>75% of farmland coverage
6bw3	Aeolian Sand	Sheet	Not fine or very fine textures	Farmland (>50%)	Mixed Irrigated/Non irrigated	No more than 75% of irrigated/non irrigated
6bx	Aeolian Sand	Sheet	Not fine or very fine textures	Rangeland (>50%)		Grassland, CRP, and Randall clay playas
7v	Loess			Mixed use		No more than 50% of farmland, rangeland, urban, or rural development
7w3	Loess			Farmland (>50%)	Mixed Irrigated/Non irrigated	No more than 75% of irrigated/non irrigated
v	Mixed used					No more than 50% w, x, y, or z
x				Rangeland (>50%)		Grassland, CRP, and Randall clay playas
z				Rural developed (>50%)		Development outside of main city/town
Unk						

A total of 18 geomorphic categories for the Southern High Plains, SHP (west Texas and eastern New Mexico) were developed on surface geology and soil maps, satellite imagery analysis, and field observations. These categories are based on [Bullard et al. \(2011\)](#).

Table 6.7 – Geomorphic categories for the Chihuahuan Desert USA region

Class	Geomorphic Classification	Geomorphic Modifier	Description	Land-use Classification	Land-use Modifier	Description
1bu	Playa	Ephemeral	Not Randall clay playas; salt lakes	Unknown use		Indeterminable land use
1bw2	Playa	Ephemeral	Not Randall clay playas; salt lakes	Farmland (> 50%)	Non-irrigated	>75% of farmland coverage
1cu	Playa	Dry (consolidated)		Unknown use		Indeterminable land use
2x	Duricrust (caliche)			Rangeland (>50%)		Grassland, CRP, and Randall clay playas
5cu	Alluvial	Unarmoured, incised	e.g., arroyos and draws	Unknown use		Indeterminable land use
5cz	Alluvial	Unarmoured, incised	e.g., arroyos and draws	Rural developed (>50%)		Development outside of main city/town
5du	Alluvial	Unarmoured, unincised	e.g., Pecos River	Unknown use		Indeterminate land-use
6au	Aeolian Sand	Dune	Visible on imagery or known	Unknown use		Indeterminable land use
6bu	Aeolian Sand	Sheet	Not fine or very fine textures	Unknown use		Indeterminable land use
6bw1	Aeolian Sand	Sheet	Not fine or very fine textures	Farmland (>50%)	Irrigated	>75% of farmland coverage
6bx	Aeolian Sand	Sheet	Not fine or very fine textures	Rangeland (>50%)		Grassland, CRP, and Randall clay playas
6bz	Aeolian Sand	Sheet	Not fine or very fine textures	Rural development (>50%)		Development outside of main city/town
Unk						

A total of 13 geomorphic categories established for the Chihuahuan Desert USA region (southern New Mexico and far west Texas), created on surface geology and soil maps, satellite imagery analysis, and field observations. These categories are based on [Bullard et al. \(2011\)](#) classification scheme.

Table 6.8 – Geomorphic categories for the Chihuahuan Desert MEX region

Class	Geomorphic Classification	Geomorphic Modifier	Description	Land-use Classification	Land-use Modifier	Description
1bu	Playa	Ephemeral	Not Randall clay playas; salt lakes	Unknown use		Indeterminable land use
1bx	Playa	Ephemeral	Nor Randall clay playas; salt lakes	Rangeland (> 50%)		Grassland, CRP, and Randall clay playas
1cu	Playa	Dry (consolidated)		Unknown use		Indeterminable land use
1cx	Playa	Dry (consolidated)		Rangeland (>50%)		Grassland, CRP, and Randall clay playas
2u	Duricrust (caliche)			Unknown use		Indeterminable land use
6au	Aeolian Sand	Dune	Visible on imagery or known	Unknown use		Indeterminable land use
6bu	Aeolian Sand	Sheet	Not fine or very fine textures	Unknown use		Indeterminable land use
7u	Loess			Unknown use		Indeterminable land use
7w2	Loess			Farmland (>50%)	Non-irrigated	>75% of farmland coverage
7x	Loess			Rangeland (>50%)		Grassland, CRP, and Randall clay playas

A total of 10 geomorphic categories established for the Chihuahuan Desert MEX region, (northern Chihuahua), made on surface geology and soil maps, satellite imagery analysis, and field observations. These categories are based on [Bullard et al. \(2011\)](#) classification scheme.

Chapter 7

X-Ray Diffraction

Phase identification and quantitative analysis of the resultant soil examination patterns, along with precise lattice parameters were obtained when performing search-match coupled with Powder Diffraction Files (PDFTM-2), the most complete and most often-used powder diffraction database that is maintained and updated by the International Centre for Diffraction Data (ICDD). This computer searchable crystallographic database (that contains either or both the experimentally measured and calculated digitized powder patterns for hundreds of thousands of compounds, including minerals, metals and alloys, inorganic materials, organic compounds and pharmaceuticals that preserves a classic text-based format that allows to search-match using positions and intensities of several strong Bragg peaks in addition to searching a limited number of other fields) found substantial use in both simple identification of compounds (qualitative analysis) and in quantitative determination of the amounts of crystalline phases presented in a mixture (quantitative analysis). The results were employed to establish and/or clarify relationship between mineral composition and properties of the soil.

7.1 Preliminary Data Processing

Satisfactory powder diffraction patterns (raw powder diffraction data converted into the list of observed Bragg angles and intensities) resulted from soil samples, but these powder diffraction data needed not only the positions but also the intensities of Bragg peaks being determined in order to continue with phase identification. After suppressing statistical noise presented in the patterns due to random intensity measurement errors by completing the numerical conditioning procedure called smoothing, the visual appearance of the powder diffractions were improved producing highly accurate observed peak positions and integrated

intensities. Smoothing approach was based on the fast Fourier transformation algorithm (the higher-order Fourier coefficient represented the higher-frequency signals.)

For that, automated Peak – Search procedure was executed in the patterns to eliminate the background and the $K\alpha_2$ component of the peaks. Patterns were fitted with a background curve (pseudo-Voigt function as a realistic analytical peak shape algorithm) to strip $K\alpha_2$ (a second set of reflections from every reciprocal lattice point that decreases resolution and increases overlapping of peaks causing to distort the intensities of Bragg peaks). Automatic peak search analysis in the $K\alpha_2$ stripped patterns was carried out to obtain computed areas and reduced patterns suitable with effective identification of phases were produced when coupled them with the PDF™ database search-match algorithm.

Peak localization was necessary in order to bring about both qualitative and quantitative scrutiny as well as database search for matching patterns. The second derivative method analysis achieved background subtraction, $K\alpha_2$ stripping, and smoothing when needed. This extremely-sensitive- to- noise method calculated the first, and then the second derivatives of $Y(2\theta)$ with respect to 2θ , and utilized them in the definition of peak positions. The derivatives were computed numerically as:

$$\frac{\partial Y_i}{\partial 2\theta_i} = \frac{Y_{i+1} - Y_i}{s} \text{ and } \frac{\partial^2 Y_i}{(\partial 2\theta_i)^2} = \frac{Y_{i+2} - 2Y_{i+1} + Y_i}{s^2} \quad (7.1)$$

where Y_i , Y_{i+1} and Y_{i+2} referred the intensities of three consecutive data points and s stated the data collection step.

Patterns based on crystal structure and Bragg's law were located by accessing the Powder Diffraction File™ (PDF) maintained and distributed by the International Centre for Diffraction Data (ICDD) database and a computer algorithm with a 4th-order polynomial based on the

Savitzky-Golay 2nd derivatives interpolating the background noise and accounting for it in a more flexible manner, achieving that experimental data were not exposed to an irreversible modification. Here, the data processing algorithm was automatic, meaning that the background points were chosen based on certain criteria and then these points were employed to approximate the background by means of certain smooth analytical function.

Smoothing was reached by using a 4th – order polynomial algorithm fitted in the vicinity of every data point with the point in question located in the middle of a sequence. The first-, second-, third- and fourth-order derivatives were calculated analytically once the coefficients of the polynomial were determined. That is, for a fourth – order polynomial

$$y = ax^4 + bx^3 + cx^2 + dx + e \quad (7.2)$$

The first, second, and third derivatives, respectively, are

$$\begin{aligned} y' &= 4ax^3 + 3bx^2 + cx + d \\ \text{and} \\ y'' &= 12ax^2 + 6bx + c \\ \text{and} \\ y''' &= 24ax + 6b \end{aligned} \quad (7.3)$$

where x is the Bragg angle.

Overlaying Elected Powder Diffraction Files (PDFTM-2) with their d-spacings included, a set of colored vertical line markers appeared on the 2θ axis at points where X-ray diffraction (XRD) peaks were expected to occur and with heights that corresponded to the expected peak intensities. Whole pattern fitting and Rietveld refinement were performed next to obtain phase identification with major, minor, trace, and residual phases, as well as precise lattice constant determination through quantitative analysis (Rietveld refinement is broadly used for quantitative phase and chemical analyses). In refinement involving multiple phases, the refined scale factors

were related directly to the weight fractions of individual phases. This was because the scale factors were applied to the integrated intensities (i.e. peak areas) rather than to the peak heights of fitted profiles. The calculated intensities of a structure phase were then normalized to its density internally making the scale factors directly proportional to the weight fractions of structure phases.

Eventually, phase identification was accomplished after matching the list of Bragg angles and intensities of diffraction patterns and following the guidance that even though all automatically found patterns are ranked according to certain matching criteria, visual analysis of at least several solutions (better yet, all that appear reasonable) is always recommended.

7.2 Mineral analyses

Mineral composition was accomplished by RIGAKU MiniFlex II X-ray diffractometer (RIGAKU Americas Corp., The Woodlands, TX) with a CuK α radiation source operated at 35kV and 15 mA, performing the XRD analysis by attaching the samples as powder specimens for XRD examination, prepared as previously described.

7.2.1 Preliminary Results

Raw powder diffraction data from soil sample analysis was converted into a digitized pattern by background subtraction, K α 2 stripping and smoothing, followed by automatic peak detection in overlaid patterns. No relative rigid restrictions were imposed on the chemical composition and search parameters were quite relaxed: the window was 0.03° of 2 θ and only 3 Bragg reflections were required to coincide within the tolerance established by the window.

Several matching patterns were found and several strong peaks present in the PDFTM-2 database record matched in the measured patterns, but others did not match in the experimental pattern which is common when performing X-ray diffractometry in soil examination. Soil could

be categorized as a specimen with a mixture of several phases where having a successful qualitative analysis became more challenging due to the complexity of its powder diffraction pattern (sample bearing multiple phases). Yet, soil mineralogy composition was helpful in identifying the phases in a multiple-phase material as it imposed much-needed constraints, and limited the number of viable solutions when visual analysis was required.

Concentration of various phases presented in soil examination after the characteristics of every phase was recognized was defined by quantitative phase analysis. The Rietveld method was used for quantitative analysis performance because of its reliability in quantifying phase contents. By using this method, the intensities calculated from crystallographic data previously normalized to the content of a single unit cell of each phase, were scaled to match the corresponding detected intensities in the same diffraction pattern via common scale factor. Therefore, the scale factors of the individual phases represented the total number of the unit cells of each phase presented in the irradiated volume of the sample.

Individual digitized pattern process was performed on 83 soil samples from three different regions: the Southern High Plains, the Chihuahuan Desert USA, and the Chihuahuan Desert MEX regions. Qualitative and quantitative results were obtained after performing the PDFTM-2 records searching to find alike matching patterns suitable for experimental scans obtained from soil examination. Several strong peaks of the experimental patterns matched with the PDFTM-2 database records. After performing automated searching followed by manual searching (visual selection analysis) from which the right solution was acquired from a considerable number of matches, the mineral composition from the X-ray diffractometry study resulted in about 14 matching patterns that covered the majority of strong reflections resulting from soil investigation: Calcite, syn (Calcium Carbonate) [CaCO_3 PDFTM-2 card No. 5-0586],

Sodium Plagioclase Ordered (Sodium Aluminum Silicate) [$\text{NaAlSi}_3\text{O}_8$ PDFTM-2 card No. 9-0466], Gypsum, syn (Calcium Sulfate Hydrate) [$\text{CaSO}_4 \cdot 2\text{H}_2\text{O}$ PDFTM-2 card No. 33-0311], Dolomite (Calcium Magnesium Carbonate) [$\text{CaMg}(\text{CO}_3)_2$ PDFTM-2 card No. 36-0426], Calcite, magnesian (Calcium Magnesium Carbonate) [$(\text{Ca}, \text{Mg})\text{CO}_3$ PDFTM-2 card No. 43-0697], Quartz, syn (Silicon Oxide) [SiO_2 PDFTM-2 card No. 46-1045], Calcite (Calcium Carbonate) [CaCO_3 PDFTM-2 card No. 47-1743], Calcium Plagioclase (Anorthite, sodian, ordered) [$(\text{Ca}, \text{Na})(\text{Al}, \text{Si})_2\text{Si}_2\text{O}_8$ PDFTM-2 card No. 9-0465], Sodium Plagioclase (Albite, disordered) [$\text{Na}(\text{Si}_3\text{Al})\text{O}_8$ PDFTM-2 card No. 10-0393], Calcium Plagioclase (Anorthite, sodian, ordered) [$(\text{Ca}, \text{Na})(\text{Al}, \text{Si})_2\text{Si}_2\text{O}_8$ PDFTM-2 card No. 20-0528], Muscovite 2M_2 (Potassium Sodium Aluminum Silicate Hydroxide) [$(\text{K}, \text{Na})_2\text{Al}(\text{Si}, \text{Al})_4\text{O}_{10}(\text{OH})_2$ PDFTM-2 card No. 34-0175], Muscovite (Muscovite, vanadian barian) [$(\text{K}, \text{Ba}, \text{Na})_{0.75}(\text{Al}, \text{Mg}, \text{Cr}, \text{V})_2(\text{Si}, \text{AlV})_4\text{O}_{10}(\text{OH}, \text{O})_2$ PDFTM card No. 46-1409], Halite, syn (Sodium Chloride) [NaCl PDFTM card No. 5-0628], and Orthoclase, barian (Potassium Barium Aluminum Silicate) [$(\text{K}, \text{Ba}, \text{Na})(\text{Si}, \text{Al})_4\text{O}_8$ PDFTM card No. 19-002].

One of these trusted records, Quartz [SiO_2 PDFTM-2 card No. 46-1045], was by far the best match that coincided with the majority of the experimental patterns much better among all others, including peak positions and their intensities. Strong Bragg reflections accorded nearly (within a few tenths of a degree). The remaining Bragg peaks fitted several PDFTM-2 records between minor and trace or lower concentrations. Few weak reflections remained unidentified due to either impurity of phase, low quality of data, or high peaks presented with very low intensity.

Table 7.1 lists the mineralogy from the Southern High Plains soil sampling. “Quartz” at 100% abundance denoted the only mineral in soil characterizations that were suitable to comprise all strong Bragg peaks as a single match. “Quartz + Calcite” as well as “Quartz + Gypsum” conformed the 2-PDF™ multiple phase scans group. Finally, 3-PDF™ multiple phase patterns included the “Quartz + Calcite + Dolomite” and the “Quartz + Calcite + Calcium Plagioclase” completing the effective phase identification in multiple phase sample scans.

Table 7.2 displays the soil mineralogy of the Chihuahuan Desert USA region with a more diverse mineralogy compared to the SHP region. Here, not only “Gypsum”, but also “Quartz” were the minerals found at 100% abundance in single matches. In addition multiple phase samples in both the 2-PDF™ (“Quartz + Calcite”, “Quartz + Sodium Plagioclase”, “Quartz + Gypsum”, and Quartz + Calcium Plagioclase patterns groups) and the 3-PDF™ (“Quartz + Sodium Plagioclase + Calcite”, “Quartz + Calcite + Muscovite”, and “Quartz + Gypsum + Dolomite” scans groups) strengthened the mineral diversity within the region.

Table 7.3 exhibits the soil characterization for the Chihuahuan Desert MEX region. As expected, this large geological region resulted with broader mineralogy coming from the fewer samples for soil diffractometry analysis. Multiple phase sample identification gave rise to augmenting the 2-PDF™ and the 3-PDF™ groups. Quartz was the mineral found at 100% abundance in single matches. “Quartz + Calcite”, Quartz + Sodium Plagioclase”, “Halite + Orthoclase”, and “Quartz + Halite” comprised the 2-PDF™ multiple phase scan group, whereas “Quartz + Calcite + Sodium Plagioclase”, “Quartz + Calcite + Halite”, and “Quartz + Calcite + Dolomite” conformed the 3-PDF™ multiple phase patterns.

Table 7.1 – Concentration in percent on SHP soil sources.

Sample	Quartz	Calcite	Gypsum	Dolomite	Calcium Plagioclase
S(1) 2	100%				
S(4) 5	100%				
S(10) 9	100%				
S(12) 10	100%				
S(14) 12	100%				
S(22) 19	100%				
S(23) 20	100%				
S(27) 23	100%				
S(38) 71	100%				
S(44) 33	100%				
S(45) 34	100%				
S(49) 37	100%				
S(51) 39	100%				
S(54) 42	100%				
S(65) 51	100%				
S(72) 56	100%				
S(81) 65	100%				
S(2) 3	77%	23%			
S(13) 11	79%	21%			
S(18) 15	70%	30%			
S(21) 18	96%	4%			
S(26) 22	57%	43%			
S(37) 70	76%	24%			
S(53) 41	94%	6%			
S(59) 46	44%	56%			
S(78) 62	88%	12%			
S(29) 25	58%		42%		
S(33) 29	84%		16%		
S(76) 60	28%	57%		15%	
S(77) 61	48%	41%		11%	
S(6) 6	81%	3%			17%

Quartz (PDF™ card No. 46-1045), Calcite (PDF™ card No. 47-1743), Gypsum (PDF™ card No. 33-0311), Dolomite (PDF™ card No. 36-0426), and Calcium Plagioclase (PDF™ card No. 9-0465) records comprised the soil mineralogy of the SHP region.

Table 7.2 – Concentration in percent on Chihuahuan Desert USA soil sources.

Sample	Quartz	Gypsum	Calcite	Sodium Plagioclase	Muscovite	Dolomite	Calcium Plagioclase
D 1K U	100%						
DU 1.5 K M	100%						
RL-MV-60B	100%						
RL-MV-62A	100%						
Sh 1K M U	100%						
Sh 400 M	100%						
Dune Surface		100%					
Hammock		100%					
Salt Flat S2		100%					
Salt Flat S36		100%					
Salt Flat S56		100%					
SPHA BOT		100%					
WS Dune		100%					
WS Interdune		100%					
Coordinates	87%		13%				
McGregor	91%		9%				
Old Coe Lake	64%		36%				
Well 9	95%		5%				
Doña Ana	63%		1%	36%			
WRJG 006	76%		13%	10%			
WRJG 001	44%			56%			
Jornada Scrap	79%			21%			
WRJG 007	21%		22%		58%		
Well 15	81%		6%		13%		
Tula G	16%	84%					
Blue House	4%	56%				40%	
INBA	63%						37%

Quartz (PDF™ card No. 46-1045), Gypsum (PDF™ card No. 33-0311), Calcite (PDF™ card No. 5-0586), Sodium Plagioclase (PDF™ card No. 10-0393), Muscovite 2M2 (PDF™ card No. 34-0175), Dolomite (PDF™ card No. 36-0426), and Calcium Plagioclase (PDF™ card No. 20-0528) records contained the soil mineralogy of the CHD USA region.

Table 7.3 – Concentration as fraction of Chihuahuan Desert MEX soil sources.

Sample	Quartz	Calcite	Sodium Plagioclase	Orthoclase	Halite	Dolomite
COR 009	100%					
SMD 002	100%					
SMD 003	100%					
SMD 026	100%					
ASC 001	33%	67%				
COR 001	74%	26%				
COR 010	66%	34%				
DBM 001	59%	42%				
GV 002	52%	48%				
LPAL 005	37%	63%				
LF 004	54%	46%				
COR 004	66%		35%			
COR 008	89%		11%			
HWY 45	62%		39%			
TLG 001	33%		67%			
LSM 002	75%	12%	13%			
LSM 003	73%	11%	16%			
SELP 003	29%	55%	16%			
LG 004	17%	44%	40%			
COR 005	35%	28%	37%			
LDP 001	55%	6%	39%			
CLP 001	21%	66%			14%	
COR 002	69%	16%			16%	
ASC 002				20%	80%	
ASC 003	66%				34%	
CLP 002	49%	42%				9%

Quartz (PDF™ card No. 46-1045), Calcite (PDF™ card No. 5-0586), Sodium Plagioclase (PDF™ card No. 9-0466) - (PDF™ card No. 10-0393), Halite (PDF™ card No. 5-0628), and Dolomite (PDF™ card No. 36-0426) records denoted the soil mineralogy of the CHD MEX region.

7.2.2 Overlaying scan analysis

Overlaying multiple phase raw powder diffraction scans reached both pattern comparison and peak comparison after applying uniform offsets to all the overlays and scaling the overlay intensity to the primary pattern (defined as the alluded pattern) to tabulate their peak for numerical comparison.

Detailed surveillance of the mineralogy of the 83 soil samples after completion of X-ray diffraction analysis resulted in performing a multiple phase search-match PDFTM examination immediately afterwards overlaying alike raw scans with identical mineralogy characterization from the three regions under investigation: The Southern High Plains, the Chihuahuan Desert USA and the Chihuahuan Desert MEX regions. This multiple phase analyzed into similar overlaid raw scans led to finding two single PDFTM-2 match groups (“Quartz” and “Gypsum”), two 2-PDFTM-2 match groups (“Quartz + Calcite” as well as “Quartz + Gypsum”), and finally two 3-PDFTM-2 matching groups (“Quartz + Calcite + Dolomite” and “Quartz + Calcite + Sodium Plagioclase”). Discussion of these groups is presented next.

7.2.2.1 Quartz overlaid specimens

Quartz at 100% abundance resulted from single match of patterns with Bragg reflections obtained after diffraction completion of samples with d-spacing ranging from 10° to 65° values in multiple phase examination performance, i.e., qualitative analysis. A total of 26 soil samples from the three regions being studied in this project fitted into this match: 17, 6, and 3 specimens from the Southern High Plains, Chihuahuan Desert USA and Chihuahuan Desert MEX regions, in that order. Bragg reflections from primary pattern coincided with 13 Bragg reflections of Quartz PDFTM-2 record, (card No. 46-1045) (see Figure 7.1). It can be suggested that Quartz was

by far the best match that coincided with the majority of the experimental overlaid patterns including peak positions and their intensities (localized between 10° and 65° 2θ related range) from which strong Bragg reflections accorded only nearly (within a few tenths of a degree). Detailed explanation of Quartz overlaid specimens are discussed next.

PDF#00-046-1045: QM=Star(S); d=Diffraction; I=Diffraction Quartz, syn (Silicon Oxide) SiO ₂ Radiation=CuKα1 Calibration=Internal(Si) Ref: Kern, A., Eysel, W., Mineralogisch-Petrograph. Inst., Univ. Heidelberg, Germany. ICDD Grant-in-Aid (1993) Hexagonal - Powder Diffraction, P3221 (154) CELL: 4.91344 x 4.91344 x 5.40524 <90.0 x 90.0 x 120.0> Density(c)=2.650 Ref: Z. Kristallogr., v198 p177 (1992) Strong Lines: 3.34/X 4.25/2 1.82/1 1.54/1 2.46/1 2.28/1 1.37/1 2.13/1 NOTE: Pattern taken at 23(1) C. Low temperature quartz. 58 reflections in pattern.											
2-Theta	I(f)	(h k l)	2-Theta	I(f)	(h k l)	2-Theta	I(f)	(h k l)	2-Theta	I(f)	(h k l)
19.779			67.744	6	(2 1 2)	94.650	1	(1 0 5)	118.312	<1	(2 1 5)
20.857	16	(1 0 0)	68.144	7	(2 0 3)	95.118	<1	(4 0 1)	120.123	1	(3 1 4)
26.625	100	(1 0 1)	68.318	5	(3 0 1)	96.237	1	(2 1 4)	121.852	<1	(1 0 6)
27.401			73.467	2	(1 0 4)	98.750	1	(2 2 3)	122.604	<1	(4 1 2)
28.176			75.659	3	(3 0 2)	102.230	<1	(1 1 5)	127.250	<1	(3 0 5)
34.988			77.675	1	(2 2 0)	102.566	<1	(3 1 3)	131.202	<1	(1 1 6)
36.525	9	(1 1 0)	79.884	2	(2 1 3)	103.876	<1	(3 0 4)	132.755	<1	(5 0 1)
39.455	8	(1 0 2)	80.046	<1	(2 2 1)	104.202	<1	(3 2 0)	134.292	<1	(4 0 4)
40.270	4	(1 1 1)	81.173	2	(1 1 4)	106.592	<1	(3 2 1)	136.422	1	(2 0 6)
42.430	6	(2 0 0)	81.491	2	(3 1 0)	112.113	<1	(4 1 0)	137.893	2	(4 1 3)
45.763	4	(2 0 1)	83.840	1	(3 1 1)	114.060	<1	(3 2 2)	140.316	<1	(3 3 0)
49.029			84.957	<1	(2 0 4)	114.466	2	(4 0 3)	143.249	3	(5 0 2)
50.111	13	(1 1 2)	87.439	<1	(3 0 3)	114.638	2	(4 1 1)	144.117	<1	(3 3 1)
50.713	1	(0 0 3)	90.831	2	(3 1 2)	115.884	<1	(2 2 4)			
54.849	4	(2 0 2)	92.788	<1	(4 0 0)	117.536	<1	(0 0 6)			
55.271	2	(1 0 3)									
59.924	9	(2 1 1)									
61.568											
64.003	2	(1 1 3)									
Total Quartz											
26 Samples											
17 SHP											
6 CHD USA											
3 CHD MEX											
S(1) 2 primary pattern											
00-046-1045											
19 reflections in pattern											
13 fitted by Quartz											
6 empty											

Figure 7.1 – Quartz indexed (card No. 46-1045) compared to experimental patterns

Quartz indexed (card No. 46-1045) extracted from ICDD powder diffraction file with all observed reflections identified by their Bragg angles and relative intensities normalized to 100 as well as the Miller indices plus overlaid digitized experimental patterns that relied upon in positive phase identification within this mineral (red outlined box) after multiple match analysis.

S(1) 2 sample represented the primary pattern from overlaid patterns displaying 13 reflections that coincided with those reflections of the Quartz PDFTM-2 record.

Overlaid patterns research with d-spacing and its established range from 10° to 65° in 0.03° increments, was then performed when manipulating the PDFTM-2 powder diffraction database into the Jade 9 software package loaded from the RIGAKU MiniFlex II X-ray diffractometer of the UTEP Material Science and Engineering lab. Quartz mineralogical characterization from overlaid scans was obtained by using the powder diffraction methodology: that is, assertive preliminary data processing and profile fitting, in addition to satisfactory phase identification that reached indexing besides precise refinement of lattice parameters followed by suitable pattern simulation confident enough to reach completion and Rietveld refinement.

After multiple phase analysis completion, the single match group Quartz at 100% abundance was acquired from overlaying scans that proceeded from the regions under investigation. Experimental patterns (from which individual digitized pattern examination, previously performed, found solely quartz after mineralogical characterization completion) from soil specimens of the Southern High Plains included in the overlaid patterns analysis were: S(1) 2, S(4) 5, S(10) 9, S(12) 10, S(14) 12, S(22) 19, S(23) 20, S(27) 23, S(38) 71, S(54) 42, S(65) 51, S(72) 56, S(81) 65, S(44) 33, S(45) 34, S(49) 37, and S(51) 39 (Table 7.1). Moreover, not only Du-1.5k-m, RL-MV-60B, RL-MV-62A, Sh-1k-m-u, and Sh 400m (Table 7.2), but also the SMD-002, SMD-003, and the SMD-026 (Table 7.3), were the selected experimental scans proceeding from both the Chihuahuan Desert USA and the Chihuahuan Desert MEX regions, which likeness was observed quite similar when comparing to those of the Southern High Plains region causing acquisition of a smooth fit acceptable enough to perform powder diffraction practice after overlaying all of these experimental scans. Individual digitized pattern S(1) 2

became the primary pattern comparing the peaks of all the overlaid scans when executing the “find peaks” command in overlaid patterns. The peaks were sorted on their 2-Theta (2θ) positions, and peak intensity percent (I%) values for the overlay diffractograms were scaled to the 100% peak of the primary pattern. As a result, the sample’s primary pattern produced an acceptable diffraction scan similitude with that of the quartz PDFTM-2 record. After performing automated search-match procedure in the primary pattern (previously processed to eliminate both the background and the $K\alpha_2$ component of the peaks), the positions and intensities of Bragg peaks were resolved. Phase identification was achieved with suitability of the obtained Bragg reflections when compared with those of the Powder Diffraction FileTM database. Bragg reflection completely indexed (that is, obtaining Miller indexes) in primary pattern for sample S(1) 2 generated 13 Bragg reflections that nicely fitted the equal reflection values when associating them to those of the PDFTM ICDD Quartz record (Fig. 7.1). A brief description of the 5 top highest intensities (I) Bragg reflections is written next. Quartz (card No. 46-1045) was obvious by its d-spacing value in Angstrom $d(\text{\AA})$ of 3.3435, 2-Theta value in degrees (2θ) of 26.625° and with Miller indexes of (101) the higher diffraction peak in the experimental primary pattern. More precisely, quartz was identified from the highest peak at $d(\text{\AA})$ value of 3.3435 with 2θ equal to 26.625° at (101); a second order peak with $d(\text{\AA})$ equal to 4.2550 with 2θ value of 20.857° at (100); and others at $d(\text{\AA})$ of 1.8180 with a 2θ value of 50.111° at (112), and the peak with a $d(\text{\AA})$ value of 2.4569 and 2θ equivalent value of 36.525° at (110) which peak intensity (I) was similar to the peak marked at $d(\text{\AA})$ equal to 1.5415 and 2θ value of 59.924° at (211) (See Figure 7.2). Few weak reflections remained unidentified due to either impurity of phase, low quality of data, or high peaks presented with very low intensity.

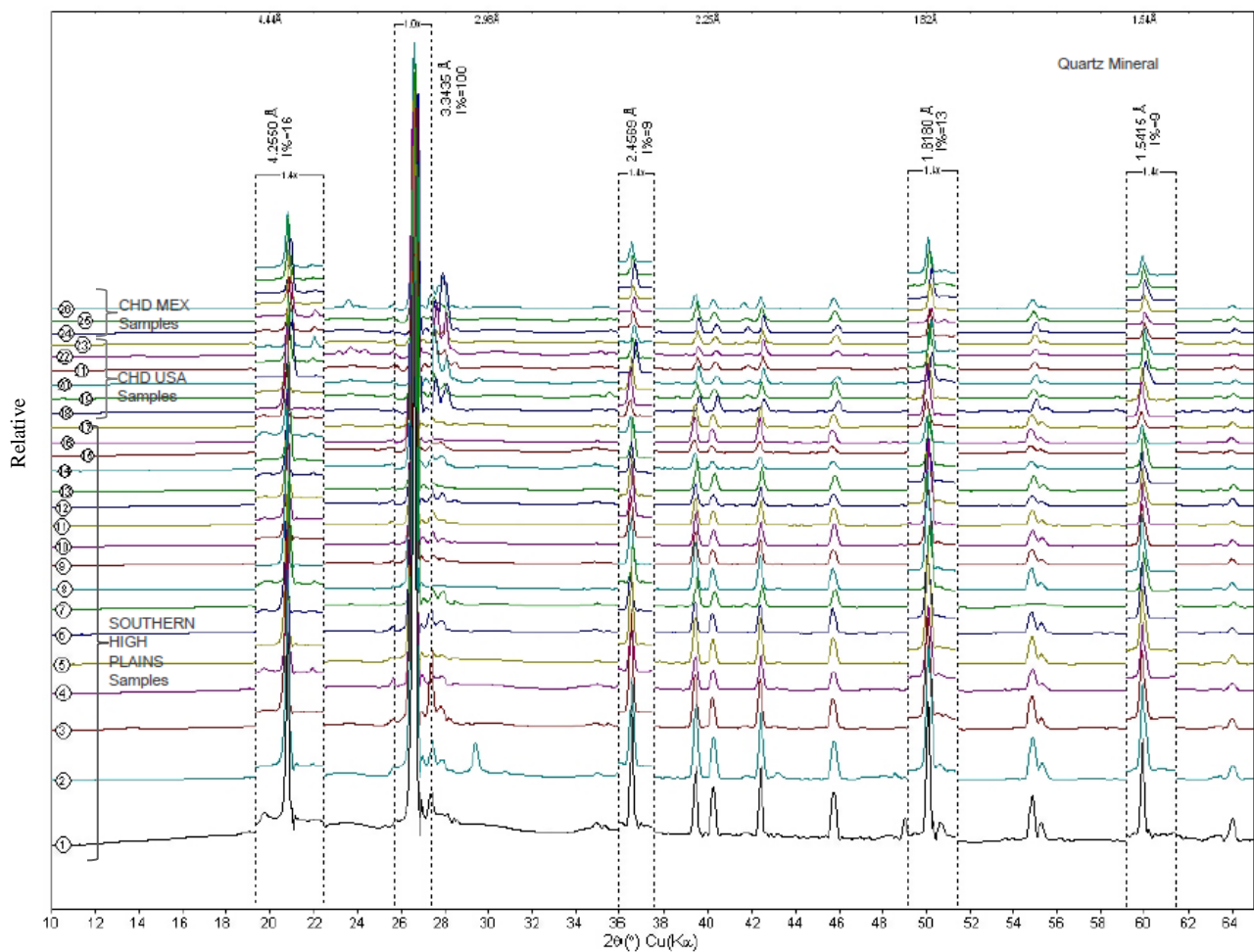


Figure 7.2 – Quartz overlaid powder diffraction patterns.

26 Overlaid powder diffraction patterns collected from the three different regions investigated in this study on a RIGAKU MiniFlex II X-ray diffractometer using Cu-K α radiation at 30 Kv and 15 mA with a Kb filter. S(1) 2 established as primary pattern noted with number 1, representing a soil sample with excellent crystallinity: narrow and sharp Bragg reflections with K α_1 / K α_2 doublets becoming partially resolved at $2\theta \cong 21^\circ$, low and nearly linear background.

7.2.2.2 Quartz 2θ peak matching chart

A 2θ peak matching chart was created by scatter plotting the difference between the 2θ peaks from those of the overlaid patterns peak-values. A total of 564 peak values generated from the overlaid diffractograms after peak search completion, were statistically analyzed finding excellent match between these experimental patterns, including peak positions and their intensities, that is, strong Bragg reflections accorded only nearly amongst each other (within a few tenths of a degree), specifically, differed values were fitted mostly onto the $-0.4^{\circ} < 0.0^{\circ} < +0.2^{\circ}$ degree range suggesting that the overlaid scans produced no significant discrepancies when comparing their stepsize among each others. (Figure 7.3).

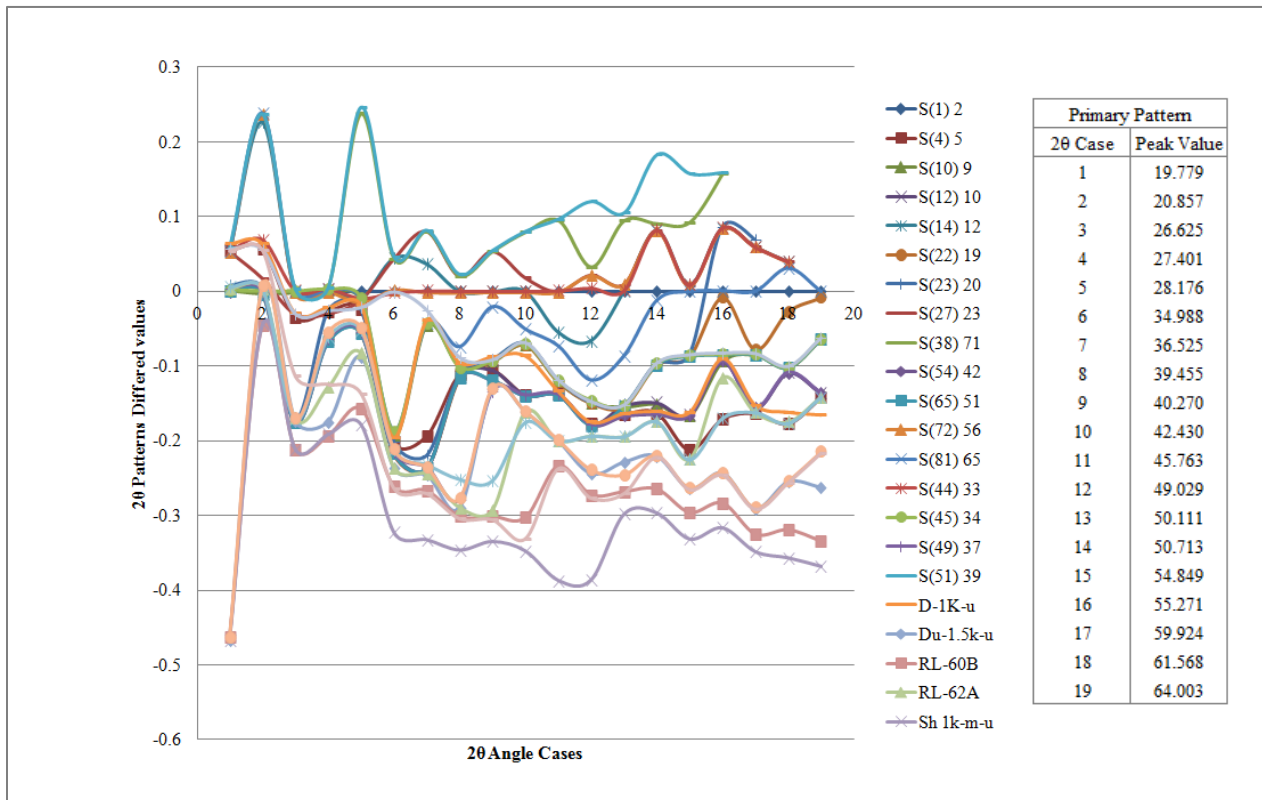


Figure 7.3 – Quartz 2θ peak matching in overlaid patterns.

Peak search 2θ different values comparison in quartz pattern overlays. 19 Bragg reflections from the primary pattern S(1) 2 sample producing great matching in overlaid scans.

7.2.2.3 Pattern Overlays 3D view for quartz

3D view of scan (pattern) overlays was useful in comparing and presenting these quite similar XRD patterns acquired from samples of the three different regions being studied and experimental conditions such as chemical composition. Subsequently, detailed 2θ values localized from peaks with d-spacing enough to produce significant intensity values in the Peak ID Report of the primary pattern and its scan (overlays) patterns (Appendix A.1) were noted in the 3D view of the 26 soil samples with similar chemical composition (quartz at 100%). A total of 13 peaks with sufficient intensity resulted in being observed into the 3D chart (Figure 7.4).

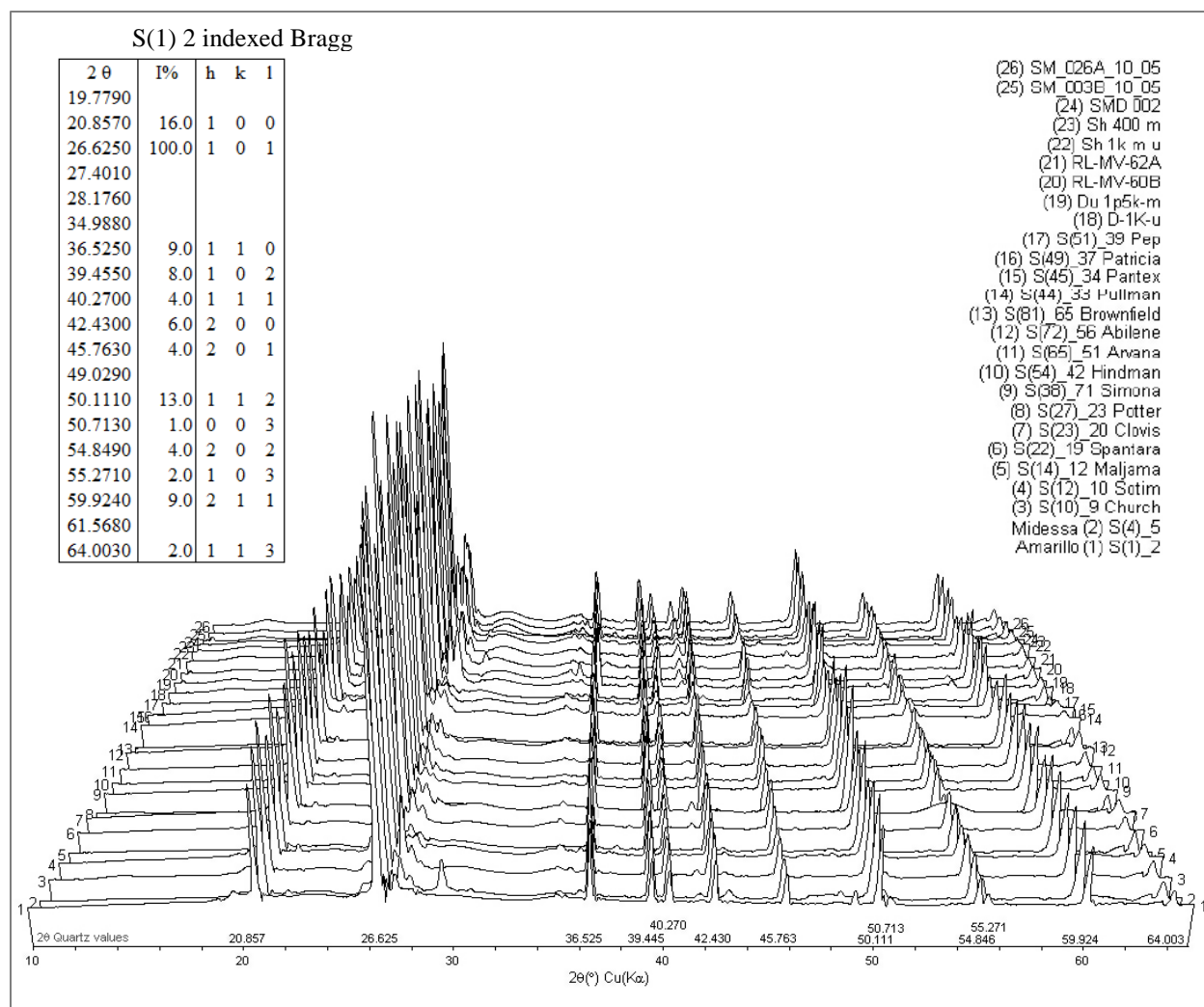


Figure 7.4 – 3D view of quartz XRD patterns with major high peaks illustrated.

7.2.2.4 2D contour plots for quartz

Similarly, 2D contour plots with a based square-root intensity at the Y axis scale $\text{SQR}(I)$, boosted visibility of weak peaks and confirmed stepsize likeness of 3D overlays by observing their coloring peak intensities. From observing the 2D contour plot, quite similar stepsize of the quartz 3D overlaid patterns was confirmed due to great uniformity among peak intensity color lines. (Figure 7.5).

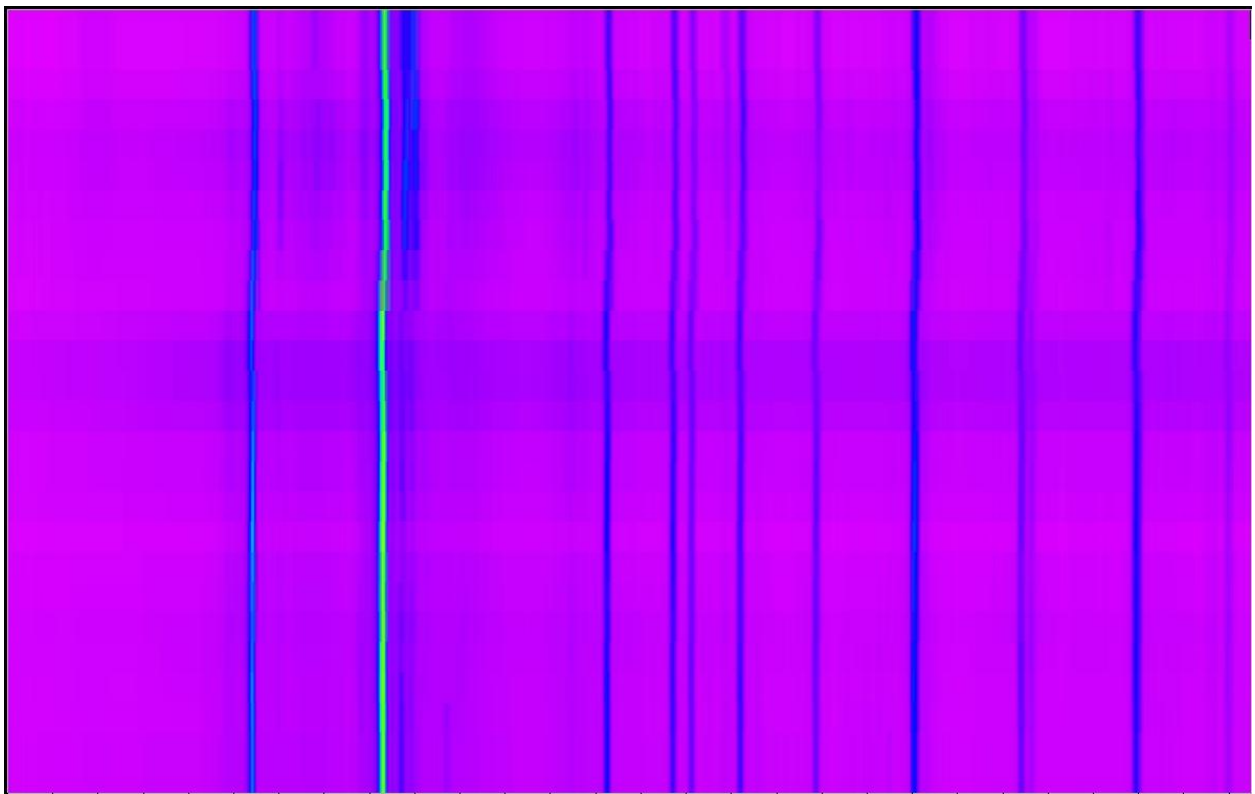


Figure 7.5 – 2D contour plot of 3D quartz overlaid scans.

7.2.2.5 Gypsum overlaid specimens

Deposits of gypsum in the Chihuahuan Desert USA region were formed when an ancient sea covered parts of both present day Texas and New Mexico (USA states): once marine waters receded this mineral was left behind in brines and formed as evaporite deposits.

Soil examination conveying Gypsum at 100% abundance came from samples of the Chihuahuan Desert USA region only. A total of 8 samples after multiple phase examination fitted peak positions and their intensities with those of the experimental primary pattern (that is, the Dune Surface sample) when associating among each other. Bragg reflections from primary pattern matched with 26 Bragg Intensities of Gypsum PDFTM-2 record, (card No. 33-0311) (See Figure 7.6). Same as quartz, gypsum was occasioned from single match of scans refraction analysis.

PDF#00-033-0311: QM=Star(S); d=Diffraction; I=Diffraction Gypsum, syn (Calcium Sulfate Hydrate) CaSO ₄ ·2H ₂ O Colorless Radiation=CuKα1 Lambda=1 Filter= Calibration=Internal(Si) 2T=11.588 I/Ic(RIR)=1.83 Ref. Natl. Bur. Stand. (U.S.) Monogr. 25, v17 p16 (1980) Monoclinic - (U) Z=4 Density(m)=2.320 CELL: 6.2845 x P.S=mC48 (?) Mwt=172.17 Density(c)=2.308 Vol=495.37 Ref. Ibid. F(30)=51.2(.0120,49/0) Strong Lines: 4.28/X 7.63/X 3.07/8 2.87/5 2.69/4 2.69/4 2.09/3 3.80/2 NOTE: Sample prepared by adding H ₂ S O ₄ to a Ca (N O ₃) ₂ solution; the precipitate was filtered out, washed in water and bottled while moist; the crystals were dried immediately before use with care taken to prevent dehydration. Pattern taken at 25 C. To replace 6-46 and validated by calculated pattern 36-432. Preferred orientation enhances 0k0 reflections. 73 reflections in pattern.											
2-Theta	I(f)	(h k l)	2-Theta	I(f)	(h k l)	2-Theta	I(f)	(h k l)	2-Theta	I(f)	(h k l)
11.588	100	(0 2 0)	44.554	<1	(1 7 0)	62.042	<1	(-2 6 3)	77.482	2	(-4 2 4)
20.722	100	(0 2 1)	45.498	4	(-1 7 1)	63.731	3	(0,10,1)			
23.397	17	(1 3 0)	46.209	3	(-2 6 1)	63.731	3	(-3 7 2)			
23.397	17	(0 4 0)	47.840	16	(0 8 0)	64.718	5	(-4 4 1)			
28.109	4	(1 1 1)	47.840	16	(2 6 0)	64.911	3	(3 7 0)			
29.111	75	(0 4 1)	48.390	12	(2 4 1)	65.299	2	(0 6 3)			
31.104	45	(-2 2 1)	48.790	3	(-1 1 3)	65.299	2	(2 8 1)			
32.066	10	(-1 1 2)	50.321	13	(0 6 2)	65.818	3	(-2 0 4)			
32.754	2	(1 3 1)	50.689	6	(-2 2 3)	66.682	2	(-4 2 3)			
33.344	35	(2 2 0)	51.149	9	(0 8 1)	68.670	5	(2 6 2)			
33.344	35	(1 5 0)	51.331	12	(-2 6 2)	68.670	5	(-2,10,1)			
34.508	6	(-1 5 1)	53.571	1	(1 5 2)	69.938	1	(2,10,0)			
35.394	2	(0 6 0)	54.420	3	(0 2 3)	69.938	1	(1,11,0)			
35.966	11	(-2 0 2)	55.151	6	(-2 4 3)	70.638	2	(-1,11,1)			
36.252	1	(-1 3 2)	55.821	4	(2 6 1)	71.018	4	(-2 8 3)			
36.619	6	(0 2 2)	56.748	9	(1 9 0)	71.191	4	(-4 6 2)			
37.345	4	(-2 4 1)	56.748	9	(-2 8 1)	74.098	1	(0 8 3)			
39.294	<1	(2 4 0)	57.539	1	(-1 9 1)	74.527	<1	(1,11,1)			
40.624	15	(1 5 1)	58.171	4	(2 8 0)	74.858	<1	(0,12,0)			
42.153	2	(0 4 2)	60.341	2	(0 8 2)	76.22	3	(-4 0 4)			
43.341	25	(-2 4 2)	60.858	1	(0,10,0)	76.22	3	(4 6 0)			
43.605	15	(-1 5 2)	60.858	1	(-4 2 2)	76.509	2	(2,10,1)			
43.605	15	(-3 1 1)	61.259	1	(-2 8 2)	77.281	3	(2 8 2)			
44.187	6	(1 1 2)	61.881	<1	(1 9 1)	77.482	2	(0,12,1)			
2-Theta	I(f)	(h k l)	2-Theta	I(f)	(h k l)	2-Theta	I(f)	(h k l)	2-Theta	I(f)	(h k l)
10.536											
11.654	100	0 2 0									
12.124											
20.736	100	0 2 1									
23.405	34	0 4 0									
23.831											
28.118	4	1 1 1									
29.109	75	0 4 1									
31.090	45	-2 2 1									
31.689											
32.081	10	-1 1 2									
33.342	70	1 5 0									
34.508	6	-1 5 1									
35.380	2	0 6 0									
35.978	11	-2 0 2									
36.579	6	0 2 2									
37.329	4	-2 4 1									
40.601	15	1 5 1									
40.990											
43.331	25	-2 4 2									
44.173	6	1 1 2									
44.739	1	1 7 0									
45.431	4	-1 7 1									
46.419	3	-2 6 1									
47.828	32	0 8 0									
48.339	12	2 4 1									
55.242	6	-2 4 3									
55.809	4	2 6 1									
56.739	18	-2 8 1									
58.205	4	2 8 0									
58.546											
63.730	6	-3 7 2									
Total Gypsum 8 Samples 8 CHD USA Dune S primary pattern 00-033-0311 32 reflections in pattern 26 fitted by Gypsum 6 empty											

Figure 7.6 – Gypsum indexed (card No. 33-0311) compared to experimental patterns.

Gypsum indexed (card No. 33-0311) taken from ICDD powder diffraction file with its Bragg angles and relative intensities normalized to 100 proceeding from its observed reflections along with the Miller Indices values. Overlaid digitized experimental scans counted on positive phase identification within this mineral (red outlined box) after multiple match examination.

Dune Surface sample was assigned the primary pattern from overlaid patterns revealing 26 reflections that accorded with those of the Gypsum PDFTM-2 record.

Gypsum at 100% richness was obtained after mineralogical characterization completion by using Jade 9 powder diffraction database loaded from the RIGAKU MiniFlex II X-ray diffractometer in the UTEP Material Science and Engineering lab. Multiple phase analysis was completed on a set of overlapped experimental individual digitized scans from specimens in the Chihuahuan Desert USA region whose diffractograms showed only gypsum. The soil samples comprised in the overlapped analysis were: Dune Surface, Hammock, Salt Flat S2, Salt Flat S36, Salt Flat S56, WS Dune, and WS Interdune (Table 7.2). Individual digitized pattern for the Dune Surface sample came to be the primary pattern to associate the peaks of all the overlapped scans after completing the “find peaks” command in overlapped scans. After eliminating both background and $K\alpha_2$ component of the peaks, the positions and intensities of Bragg peaks were acquired. Indexed Bragg reflections in the primary pattern of the Dune Surface sample produced 26 Bragg reflections that fitted equal reflection values when comparing to those of the PDFTM ICDD Gypsum record (Figure 7.6).

The 5 top highest intensities (I) Bragg reflections are noted next. Gypsum (card No. 33-0311) had its highest diffraction peak in a d-spacing value in Angstrom $d(\text{\AA})$ of 7.6300, 2-Theta value in degrees (2θ) of 11.654° and with Miller indexes of (020); a second order peak with $d(\text{\AA})$ equal to 4.2830 with 2θ value of 20.736° at (021); a third order peak with $d(\text{\AA})$ of 3.0650 with a 2θ value of 29.109° at (041); a fourth order peak with a $d(\text{\AA})$ value equal to 2.6850 and 2θ equivalent value of 33.342° at (150); and the fifth order peak localized in a $d(\text{\AA})$ equals to 2.8730 and 2θ value of 31.090° at (-221) (Figure 7.7). Unidentified weak reflections were attributed to either low quality data, impure phase, or high peaks with low intensity.

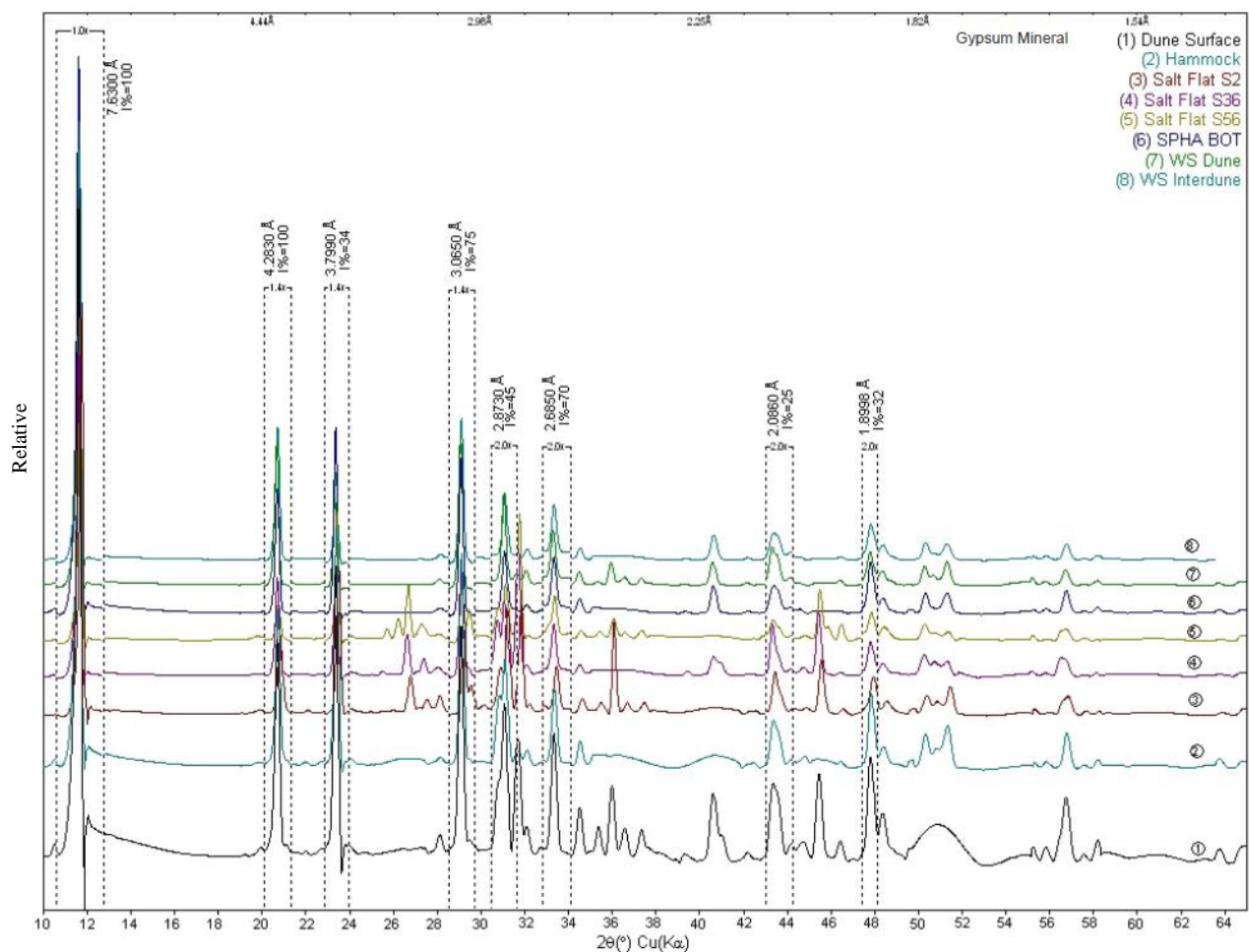


Figure 7.7 – Gypsum overlaid powder diffraction patterns.

Overlapped powder diffraction scans collected from the Chihuahuan Desert USA region on a RIGAKU MiniFlex II X-ray diffractometer using Cu-K α radiation at 30Kv and 15mA with a Kb filter. Dune Surface recognized as primary pattern marked with number 1, depicting a soil sample with good crystallinity: narrow and sharp Bragg reflections with $K\alpha_1/K\alpha_2$ doublets in part resolved at $2\theta \cong 11^\circ$, low and linear background.

7.2.2.6 Gypsum 2θ peak matching chart

2θ peak matching chart was formed by scatter plotting the difference between the 2θ peaks- from those of the overlaid pattern peak-values. A total of 257 peaks observed from the overlapped scans after peak search investigation, were statistically examined to obtaining close match between these experimental scans resulting that strong Bragg reflections rendered close values amongst each other (within a few tenths of a degree). Differed values were comprised mostly into the $-0.2^{\circ} < 0.0^{\circ} < 0.3^{\circ}$ degree range meaning that the overlapped scans have no meaningful divergences when associating their stepsize between them (Figure 7.8).

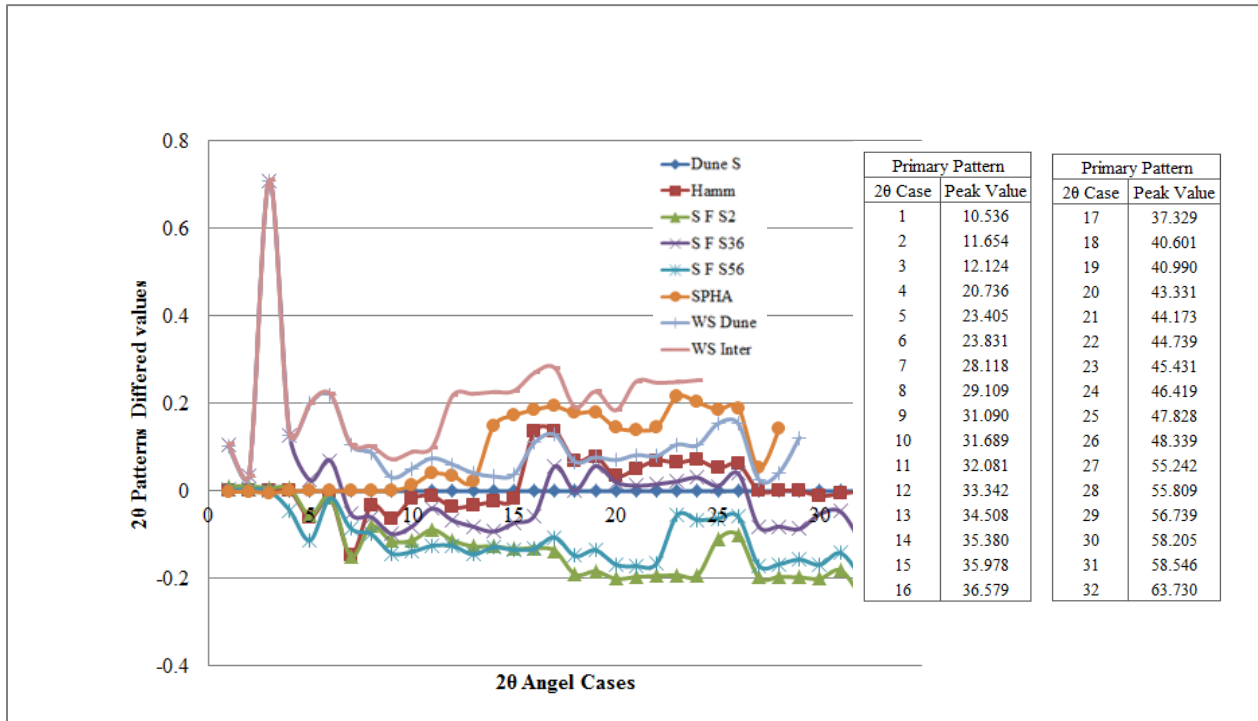


Figure 7.8 – Gypsum 2θ peak matching in overlaid patterns.

Peak search 2θ different values comparison in gypsum overlap scans. 32 Bragg reflections from the primary pattern Dune Surface sample generating good matching in overlapped scans.

7.2.2.7 Pattern overlays 3D view for gypsum

3D views of scan overlaps helped associate and present the 100% gypsum diffractograms from soil samples coming from the Chihuahuan Desert USA region. Successively, detailed 2θ values located onto prominent intensity peaks noted in the Peak ID Report of the primary pattern and its scan patterns (Appendix A.2) appeared in the 3D view of the 8 soil specimens with likely chemical composition (gypsum at 100%). A total of 26 peaks with enough intensity were observed on the 3D chart (Figure 7.9).

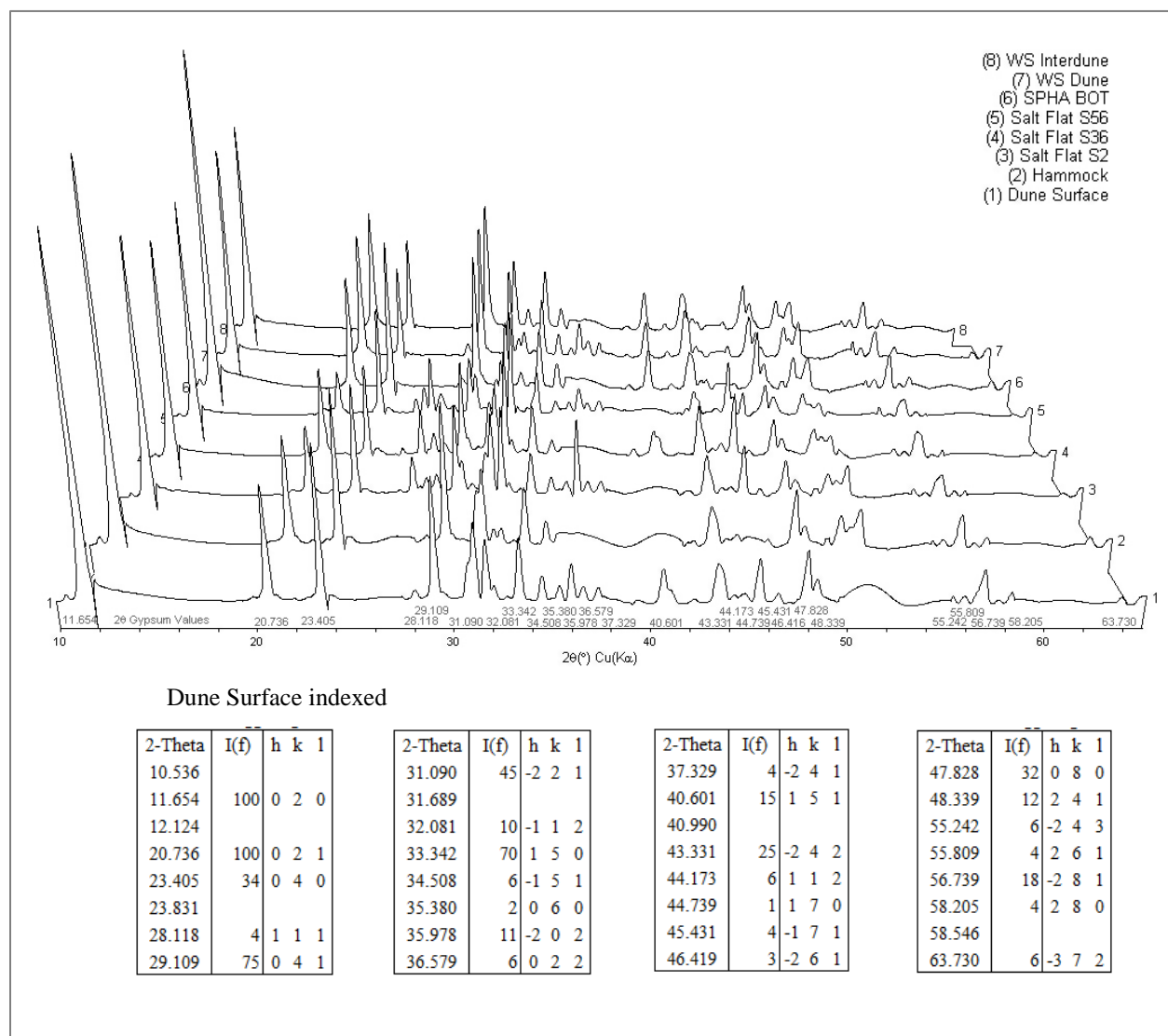


Figure 7.9 – 3D view of gypsum XRD patterns with major high peaks illustrated.

7.2.2.8 2D contour plots for gypsum

Likewise, 2D contour plots with a based square-root intensity at the Y axis scale $\text{SQR}(I)$, boosted visibility of weak peaks and confirmed stepsize likeness of 3D overlaps by observing their coloring peak intensities. From noticing the 2D contour plot, quite similar stepsize of the gypsum 3D overlapped scans was confirmed due to good consistency between peak intensity color lines. (Figure 7.10).

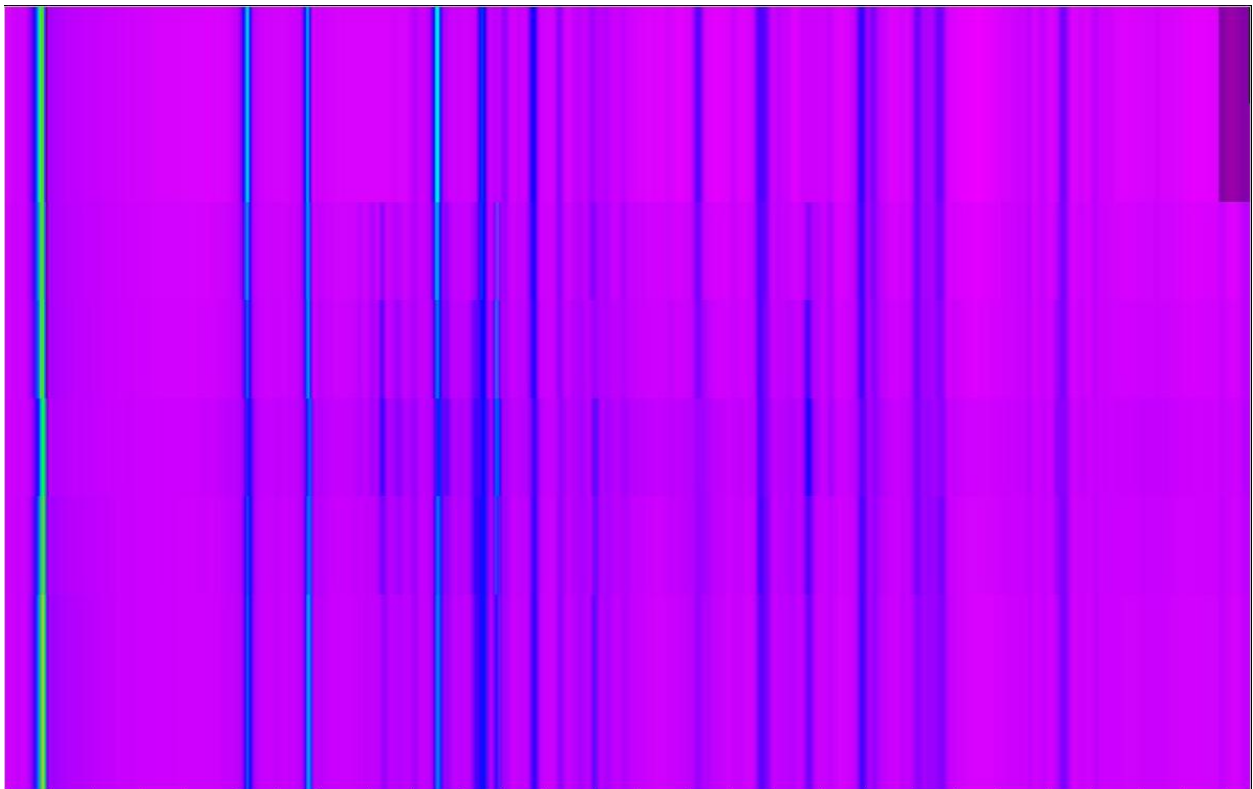


Figure 7.10 – 2D contour plot of 3D gypsum overlaid scans.

7.2.2.9 Quartz + Calcite overlaid specimens

Quartz + Calcite at different abundances resulted after multiple search-match phase analysis and qualitative analysis completion. Mineralogical characterization from X-ray diffraction study of 83 soil samples coming from the three regions under investigation previously described in this document from which quartz + calcite comprised their mineral composition were not only overlaid but also multiple phase analyzed leading to find the PDFTM-2 quartz and the PDFTM-2 calcite matching groups. To be exact, several strong Bragg reflections of the experimental overlapped patterns matched with the PDFTM-2 database record of these two minerals. Therefore, 9 specimens originating in the Southern High Plains region and 8 samples from the Chihuahuan Desert region (from the USA as well as the MEX areas in similar quantity) were mineralogically only characterized by quartz and calcite. Here, Bragg reflections from the primary pattern S(2) 3, coincided with 12 and 8 Bragg reflections of Quartz PDFTM-2 (card No. 46-1045) (Fig. 7.11) and Calcite PDFTM-2 (card No. 5-0586) (Fig.7.12), correspondingly.

PDF#00-046-1045: QM=Star(S); d=Diffraction; I=Diffraction Quartz, syn (Silicon Oxide) SiO ₂ Radiation=CuKα1 Calibration=Internal(Si) Ref. Kern, A., Eysel, W., Mineralogisch-Petrograph. Inst., Univ. Heidelberg, Germany. ICDD Grant-in-Aid (1993) Hexagonal - Powder Diffraction, P3221 (154) CELL: 4.91344 x 4.91344 x 5.40524 <90.0 x 90.0 x 120.0> Density(c)=2.650 Ref. Z. Kristallogr., v198 p177 (1992) Strong Lines: 3.34/X 4.25/2 1.82/1 1.54/1 2.46/1 2.28/1 1.37/1 2.13/1 NOTE: Pattern taken at 23(1) C. Low temperature quartz. 58 reflections in pattern.											
2-Theta	I(f)	(h k l)	2-Theta	I(f)	(h k l)	2-Theta	I(f)	(h k l)	2-Theta	I(f)	(h k l)
19.718			67.744	6	(2 1 2)	94.650	1	(1 0 5)	118.312	<1	(2 1 5)
20.771	16	(1 0 0)	68.144	7	(2 0 3)	95.118	<1	(4 0 1)	120.123	1	(3 1 4)
25.511			68.318	5	(3 0 1)	96.237	1	(2 1 4)	121.852	<1	(1 0 6)
26.558	100	(1 0 1)	73.467	2	(1 0 4)	98.750	1	(2 2 3)	122.604	<1	(4 1 2)
27.369			75.659	3	(3 0 2)	102.230	<1	(1 1 5)	127.250	<1	(3 0 5)
27.731			77.675	1	(2 2 0)	102.566	<1	(3 1 3)	131.202	<1	(1 1 6)
29.377	100	(1 0 4)	79.884	2	(2 1 3)	103.876	<1	(3 0 4)	132.755	<1	(5 0 1)
30.701			80.046	<1	(2 2 1)	104.202	<1	(3 2 0)	134.292	<1	(4 0 4)
34.839			81.173	2	(1 1 4)	106.592	<1	(3 2 1)	136.422	1	(2 0 6)
35.921	14	(1 1 0)	81.491	2	(3 1 0)	112.113	<1	(4 1 0)	137.893	2	(4 1 3)
36.402	9	(1 1 0)	83.840	1	(3 1 1)	114.060	<1	(3 2 2)	140.316	<1	(3 3 0)
39.339	18	(1 1 3)	84.957	<1	(2 0 4)	114.466	2	(4 0 3)	143.249	3	(5 0 2)
40.122	4	(1 1 1)	87.439	<1	(3 0 3)	114.638	2	(4 1 1)	144.117	<1	(3 3 1)
40.899			90.831	2	(3 1 2)	115.884	<1	(2 2 4)			
42.309	6	(2 0 0)	92.788	<1	(4 0 0)	117.536	<1	(0 0 6)			
43.122	18	(2 0 2)									
44.682											
45.668	4	(2 0 1)									
47.108	5	(0 2 4)									
47.470	17	(0 1 8)									
48.521	17	(1 1 6)									
50.019	13	(1 1 2)									
50.531	1	(0 0 3)									
54.702	4	(2 0 2)									
55.208	2	(1 0 3)									
59.802	9	(2 1 1)									
60.759	5	(2 1 4)									
63.880	2	(1 1 3)									
Total Quartz + Calcite											

17 Samples	S(2) 3 primary pattern	28 reflections in pattern
9 SHP	00-046-1045	12 fitted by Quartz
4 CHD USA	00-005-0586	8 fitted by Calcite
4 CHD MEX		8 empty

Figure 7.11 – Quartz indexed (card No. 46-1045) compared to experimental patterns.

Quartz indexed (card No. 46-1045) obtained from ICDD powder diffraction file with its observed reflections recognized by the Bragg angles and relative intensities normalized to 100 in addition to the Miller indices. S(2) 3 sample representing the primary pattern of overlapped patterns that relied upon in positive phase identification within this mineral (blue colored numbers enclosed in red outlined box) after multiple search match exploration comprising 12 Bragg reflections that coincided with those of the Quartz PDF™-2 record.

numbers enclosed in red outlined box) after multiple search match analysis including 8 Bragg reflections that coincided with those of the Calcite PDFTM-2 record.

Utilizing RIGAKU MiniFlex II X-ray diffractometer in the UTEP Material Science and Engineering lab, quartz and calcite characterized soil samples were overlapped by using Jade 9 powder diffraction database software package. After executing automated search match followed by visual selection investigation, several strong peaks acquired in the primary pattern accorded with those of the quartz [SiO_2 PDFTM-2 card No. 46-1045] and calcite [CaCO_3 PDFTM-2 card No. 5-0586] records. Selected experimental overlapped patterns of soil specimens from which the diffractograms characterized only these two minerals within different abundance concentrations after concluding their individual X-ray diffraction analysis were: S(2) 3, S(13) 11, S(18) 15, S(21) 18, S(26) 22, S(37) 70, S(51) 39, S(59) 46, and S(78) 62 from the Southern High Plains region (Table 7.1). Also Coordinates, McGregor, Old Coe Lake and Well 9 (Table 7.2) in addition to ASC 001, COR 001, COR 010, and GV 002 (Table 7.3) were the soil specimens originating in the Chihuahuan Desert from both USA and MEX areas, in that order. Powder diffraction practice after overlapping process then was achieved acquiring a fit smoothly shaped enough to obtaining a good match between these experimental patterns, including peak positions and their intensities where Bragg reflections rendered a slight difference within a few tenths of a degree among each other.

Once the Bragg reflections proceeding from the primary pattern S(2) 3 were indexed completely, a confirmed identification of quartz and calcite was then attained by comparing the experimental Bragg reflections with those of the Powder Diffraction FilesTM database. Primary pattern generated 12 Bragg reflections that fitted equal reflections values after comparing with those of the PDFTM ICDD Quartz record (Fig. 7.11). Still, 8 Bragg reflections of this

experimental pattern fitted similar reflections values when associating them to those of the PDFTM ICDD Calcite record (Fig. 7.12). A description of the 5 top highest intensities (I) Bragg reflections values is given next. Quartz (card No. 46-1045) was by its d-spacing value in Angstrom $d(\text{\AA})$ of 3.3435, 2-Theta value in degrees (2θ) of 26.558° and with Miller indexes of (101) the higher peak in the experimental primary pattern. In more detail, highest peak of quartz mineral was identified with a $d(\text{\AA})$ value of 3.3435 with 2θ value of 26.558° at (101); a second order peak with $d(\text{\AA})$ equal to 4.2550 with 2θ value of 20.771° at (100); and others at $d(\text{\AA})$ of 1.8180 with 2θ value of 50.019° at (112), and the peak with a $d(\text{\AA})$ value of 2.4569 and 2θ equivalent value of 36.402° at (110) which peak intensity (I) was similar to the peak marked at $d(\text{\AA})$ equal to 1.5415 and 2θ value of 59.802° at (211) (Fig. 7.13). Similarly, Calcite (card No. 5-0586) was by its d-spacing value in Angstrom $d(\text{\AA})$ of 3.0350, 2-Theta value in degrees (2θ) of 29.377° and with Miller indexes of (104) the highest peak in the experimental primary pattern. More concisely, calcite was identified from the highest peak at $d(\text{\AA})$ value of 3.0350 with 2θ equal to 29.377° at (104); a second order peak with $d(\text{\AA})$ equal to 2.2850 with 2θ value of 39.339° at (113); and others at $d(\text{\AA})$ of 1.9130 with 2θ value of 47.470° at (018) which peak intensity (I) was similar to the peak marked at $d(\text{\AA})$ equal to 1.8750 and 2θ value of 48.521° at (116); lastly the peak with a $d(\text{\AA})$ value of 2.4950 and 2θ equivalent value of 35.921° at (110) (Figure 7.13). Unidentified reflections may be caused due to either higher peaks with low intensities, impure phases, or low quality of data.

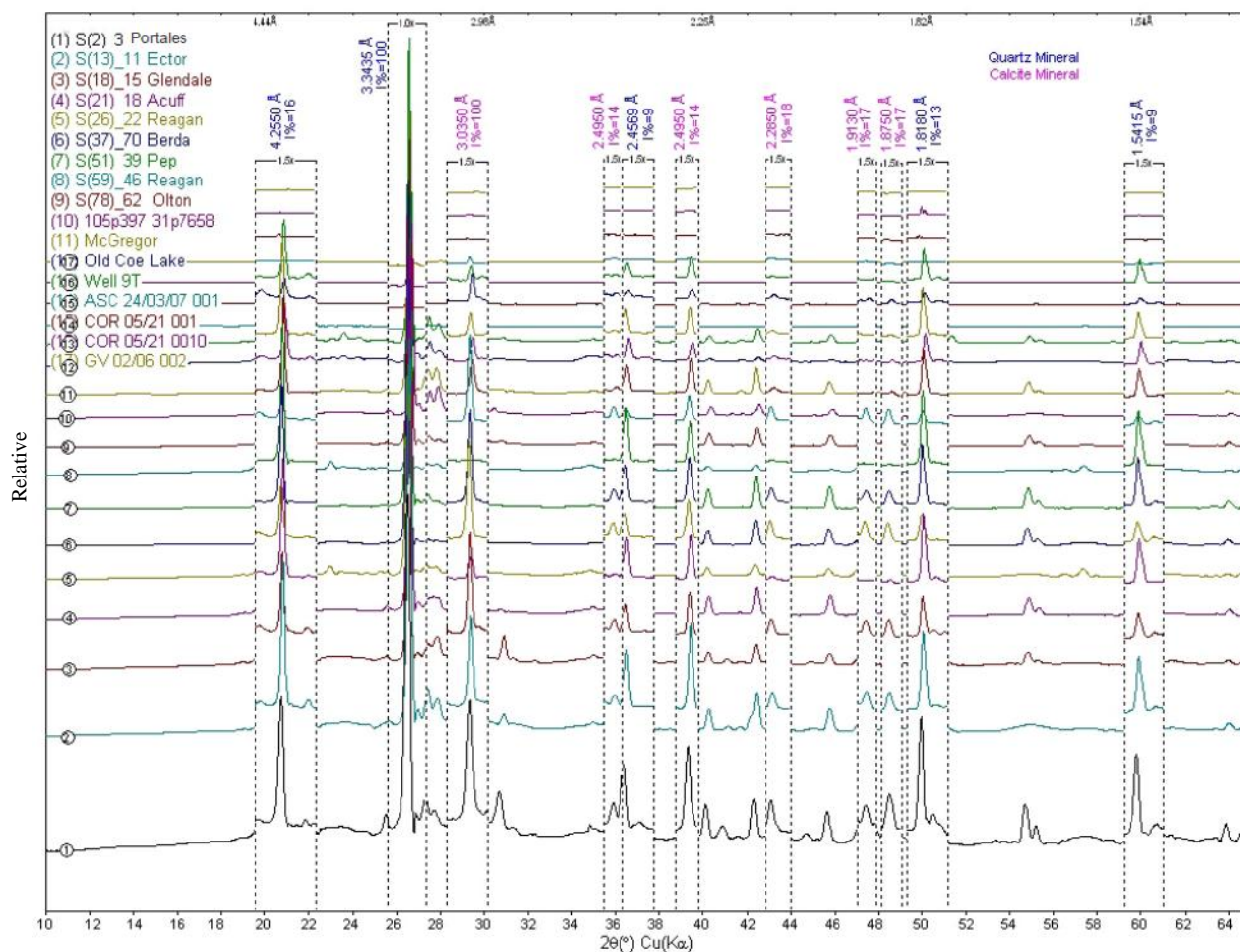


Figure 7.13 – Quartz + Calcite overlaid powder diffraction patterns.

A total of 17 overlapped soil powder diffraction patterns collected from the three different regions examined in this study on a RIGAKU MiniFlex II X-ray diffractometer using $\text{Cu-K}\alpha$ radiation at 30 Kv and 15mA with a K β filter. S(2) 3 defined as primary pattern enlisted with number 1, representing a soil specimen with abundant crystallinity: narrow and sharp Bragg reflections with $K\alpha_1/K\alpha_2$ doublets becoming partially resolved at $2\theta \cong 21^\circ$ and $2\theta \cong 29^\circ$ for quartz and calcite, correspondingly.

7.2.2.10 Quartz + Calcite 2θ peak matching chart

2θ peak matching chart was developed by scatter plotting the difference between the 2θ peaks- from those of the overlapped patterns peak-values. A total of 405 peaks included in the overlapped patterns after peak search completion, were statistically examined to find trusted matches among these experimental diffractograms, containing peak positions and their intensities. Still, strong Bragg reflections conferred nearly among each other (within a few tenths of a degree), explicitly, differed values were fitted mostly onto the $-0.2^{\circ} < 0.0^{\circ} < 0.3^{\circ}$ degree range suggesting that the overlapped patterns had no meaningful discrepancies with comparing stepsize among them (Figure 7.14).

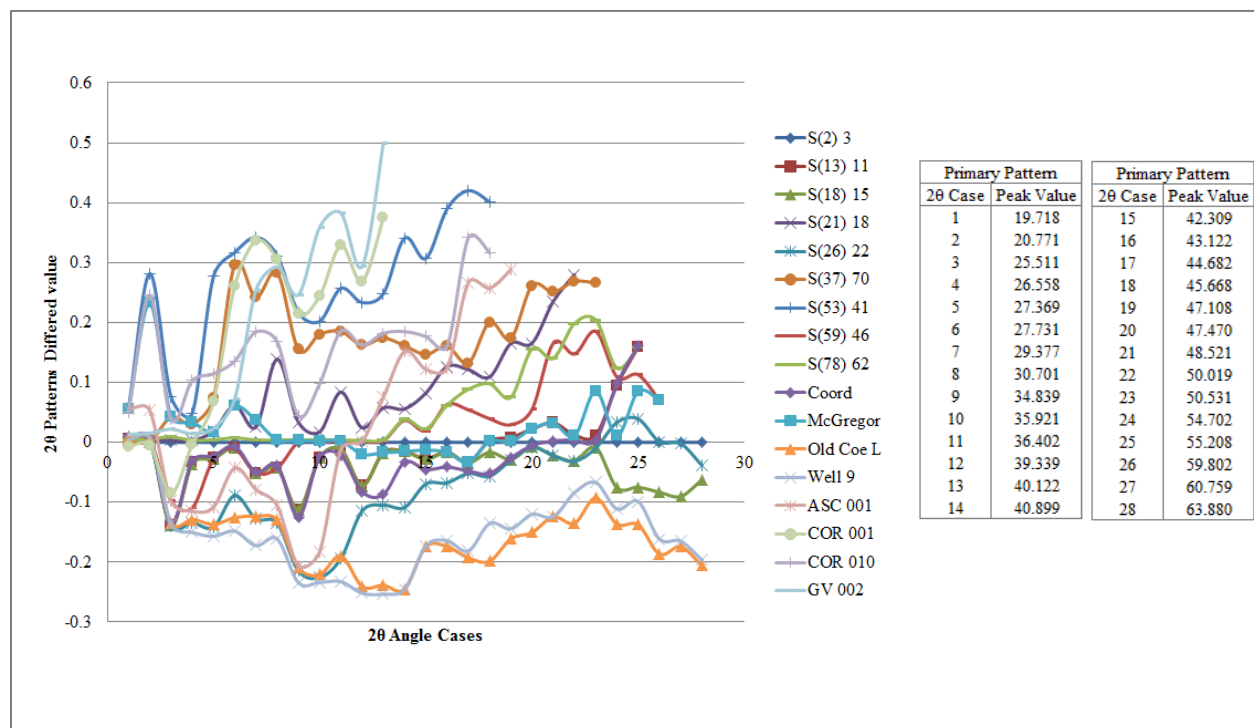


Figure 7.14 – Quartz + Calcite 2θ peak matching in overlaid patterns.

Peak search 2θ difference values comparison in quartz + calcite overlapped patterns. 28 Bragg reflections from the primary pattern S(2) 3 sample generating fair matching in overlapped patterns.

7.2.2.11 Pattern overlays 3D view for quartz + calcite

3D views of overlapped patterns were associated with only quartz + calcite scans from soil samples coming from the three different regions studied in this project. Featured 2 θ values from intensity peaks included in the Peak ID Report of the primary pattern and its scan patterns (Appendix A.3) appeared in the 3D view of 17 soil specimens with quartz + calcite chemical composition at different abundance concentrations. A total of 12 plus 8 peaks with enough intensity were classified in the 3D chart for quartz and calcite, respectively (Figure 7.15).

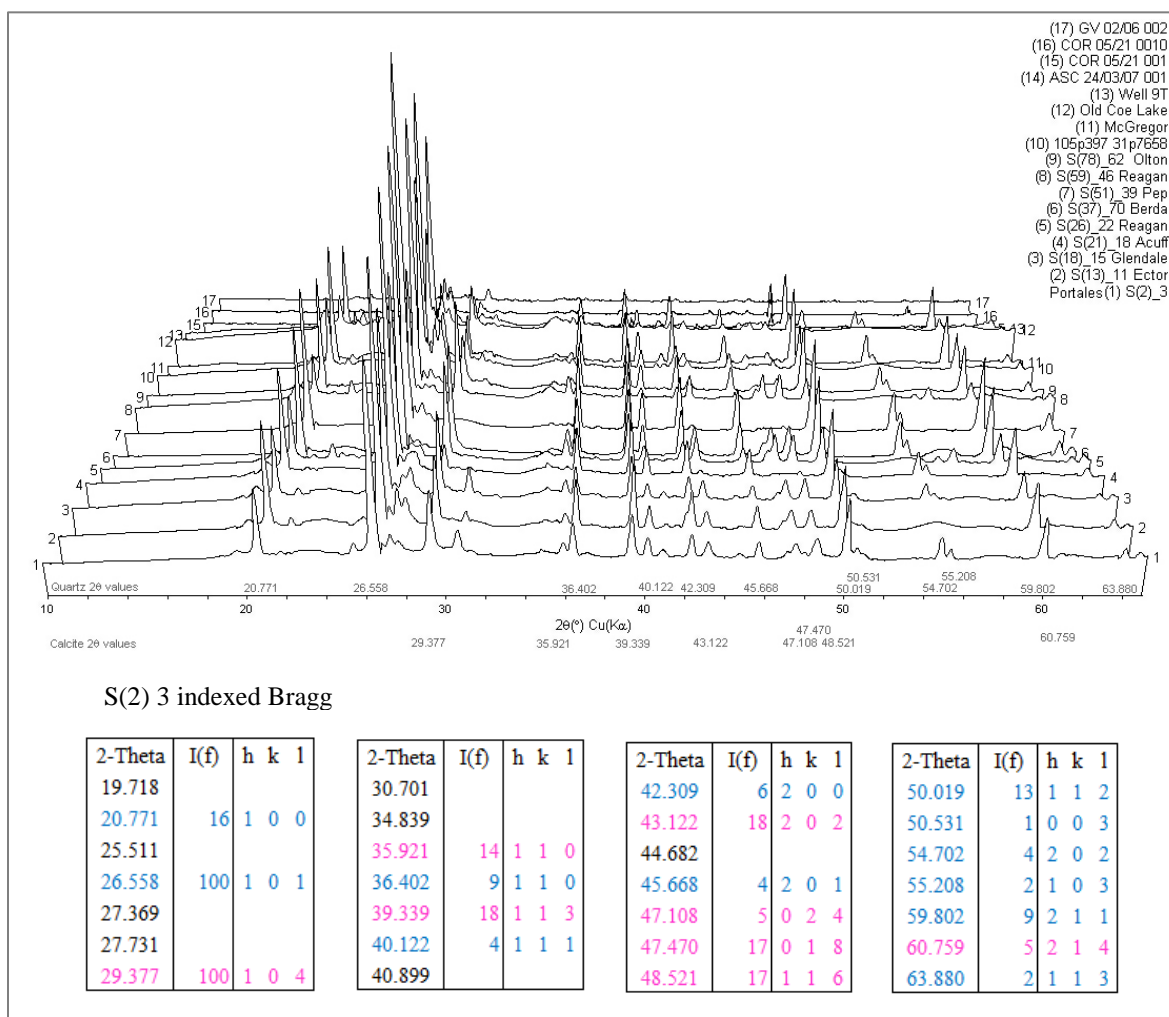


Figure 7.15 – 3D view of quartz + calcite XRD patterns with major high peaks illustrated.

7.2.2.12 2D contour plots for quartz + calcite

2D contour plots with a based square-root intensity at Y axis scale $\text{SQR}(I)$, increased visibility of small peaks and confirmed stepsize likeness of 3D overlaps by examining their coloring peak intensities. From observing the 2D contour plot, alike stepsize of the quartz + calcite overlapped patterns was obtained due to fair consistency between peaks intensity color lines (Figure 7.16).

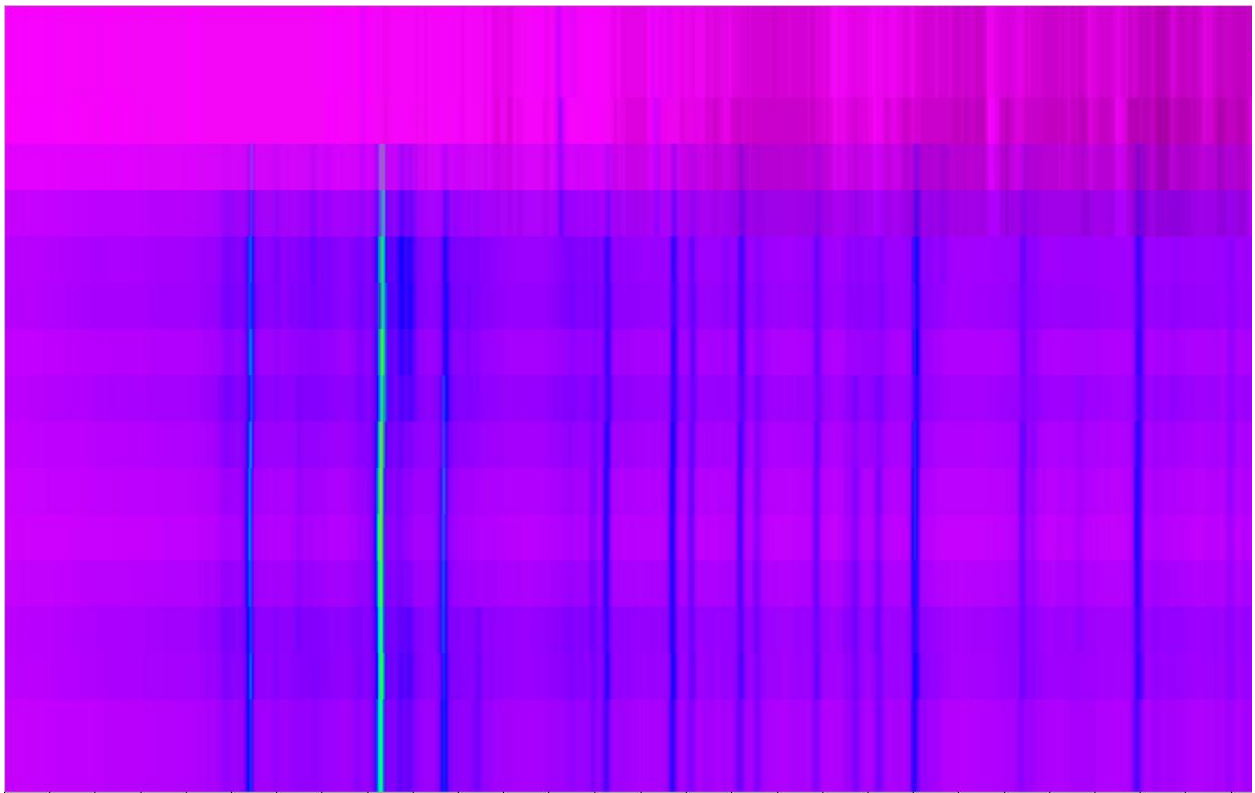


Figure 7.16 – 2D contour plot of 3D quartz + calcite overlaid scans.

7.2.2.13 Quartz + Gypsum overlaid specimens

Soil samples which mineral composition resulted in only quartz + gypsum at dissimilar concentrations after completing the X-ray diffraction enquiry of the 83 specimens that came from the regions under study, were overlaid and multiple phase analyzed to find the PDFTM-2 quartz and the PDFTM-2 gypsum ICDD matching records. Strong Bragg reflections produced by the designated primary pattern (that is, S(29) 25), accorded to the PDFTM-2 database group of these two minerals. Hence, quartz and gypsum mineralogical characterized scans proceeding from three specimens (two soil samples from the Southern High Plains and one sample coming from the Chihuahuan Desert USA regions) were overlaid to perform search match analysis resulting that 28 strong Bragg reflections of the primary pattern matched with 17 in addition 9 Bragg reflections of the Quartz PDFTM-2 record (card No. 46-1045) (Fig. 7.17) and Gypsum PDFTM-2 record (card No. 33-0311) (Fig 7.18), respectively.

PDF#00-046-1045: QM=Star(S); d=Diffractometer; I=Diffractometer												2-Theta	I(f)	h	k	l
Quartz, syn (Silicon Oxide)												11.588	100	0	2	0
SiO2												19.748				
Radiation=CuKa1												20.682	100	0	2	1
Calibration=Internal(Si)												23.320	34	0	4	0
Ref. Kern, A., Eysel, W., Mineralogisch-Petrograph. Inst., Univ. Heidelberg, Germany.												26.587	100	1	0	1
ICDD Grant-in-Aid (1993)												27.881	4	1	1	1
Hexagonal - Powder Diffraction, P3221 (154)												29.049	75	0	4	1
CELL: 4.91344 x 4.91344 x 5.40524 <90.0 x 90.0 x 120.0>												29.379				
Density(c)=2.650												31.030	45	-2	2	1
Ref. Z. Kristallogr., v198 p177 (1992)												31.993	10	-1	1	2
												33.281	70	1	5	0
Strong Lines: 3.34/X 4.25/2 1.82/1 1.54/1 2.46/1 2.28/1 1.37/1 2.13/1												34.449	6	-1	5	1
NOTE: Pattern taken at 23(1) C.												35.918	11	-2	0	2
Low temperature quartz.												36.489	9	1	1	0
58 reflections in pattern.												37.277	4	-2	4	1
2-Theta	I(f)	(h k l)	2-Theta	I(f)	(h k l)	2-Theta	I(f)	(h k l)	2-Theta	I(f)	(h k l)	39.398	8	1	0	2
20.860	16	(1 0 0)	67.744	6	(2 1 2)	94.650	1	(1 0 5)	118.312	<1	(2 1 5)	40.214	4	1	1	1
26.640	100	(1 0 1)	68.144	7	(2 0 3)	95.118	<1	(4 0 1)	120.123	1	(3 1 4)	40.541	15	1	5	1
36.544	9	(1 1 0)	68.318	5	(3 0 1)	96.237	1	(2 1 4)	121.852	<1	(1 0 6)	42.372	6	2	0	0
39.465	8	(1 0 2)	73.467	2	(1 0 4)	98.750	1	(2 2 3)	122.604	<1	(4 1 2)	43.270	25	-2	4	2
40.300	4	(1 1 1)	75.659	3	(3 0 2)	102.230	<1	(1 1 5)	127.250	<1	(3 0 5)	44.109	6	1	1	2
42.450	6	(2 0 0)	77.675	1	(2 2 0)	102.566	<1	(3 1 3)	131.202	<1	(1 1 6)	45.283	4	-1	7	1
45.793	4	(2 0 1)	79.884	2	(2 1 3)	103.876	<1	(3 0 4)	132.755	<1	(5 0 1)	48.492	12	2	4	1
50.139	13	(1 1 2)	80.046	<1	(2 2 1)	104.202	<1	(3 2 0)	134.292	<1	(4 0 4)	50.079	13	1	1	2
50.622	<1	(0 0 3)	81.173	2	(1 1 4)	106.592	<1	(3 2 1)	136.422	1	(2 0 6)	50.561	1	0	0	3
54.875	4	(2 0 2)	81.491	2	(3 1 0)	112.113	<1	(4 1 0)	137.893	2	(4 1 3)	51.249	12	-2	6	2
55.325	2	(1 0 3)	83.840	1	(3 1 1)	114.060	<1	(3 2 2)	140.316	<1	(3 3 0)	59.863	9	2	1	1
57.235	<1	(2 1 0)	84.957	<1	(2 0 4)	114.466	2	(4 0 3)	143.249	3	(5 0 2)	63.941	2	1	1	3
59.960	9	(2 1 1)	87.439	<1	(3 0 3)	114.638	2	(4 1 1)	144.117	<1	(3 3 1)					
64.035	2	(1 1 3)	90.831	2	(3 1 2)	115.884	<1	(2 2 4)				Total Quartz + Gypsum				
65.786	<1	(3 0 0)	92.788	<1	(4 0 0)	117.536	<1	(0 0 6)								

3 Samples	S(29) 25 primary pattern	28 reflections in pattern
2 SHP	00-046-1045	9 fitted by Quartz
1 CHD USA	00-033-0311	17 fitted by Gypsum
		2 empty

Figure 7.17 – Quartz indexed (card No. 46-1045) compared to experimental patterns.

Quartz index (card No. 46-1045) extracted from the ICDD powder diffraction file with its resulted reflections identified by their Bragg angles and relative intensities normalized to 100 along with the Miller indices. S(29) 25 specimen was the primary pattern of overlaid scans that relied upon in positive phase identification within this mineral (blue colored data enclosed in red outlined box) after multiple search match examination matching 9 Bragg reflections with great similitude when comparing to those of the Quartz PDF™-2 record.

red outlined box) after multiple search match analysis matching 17 Bragg reflections with great similarity when comparing to those of the Gypsum PDFTM-2 record.

Jade 9 powder diffraction database software package installed in the RIGAKU MiniFlex II X-ray diffractometer in the UTEP Material Science and Engineering lab, was used to perform both automated and visual selection search match exploration after compiling quartz and gypsum characterized soil specimens. Strong Bragg reflections developed in the primary pattern accorded with those of the quartz [SiO_2 PDFTM-2 card No. 46-1045] and gypsum [$\text{CaSO}_4 \cdot 2\text{H}_2\text{O}$ PDFTM-2 card No. 33-0311] records. Overlaid scans proceeding from selected samples from which the quartz and gypsum minerals existed with different concentrations after X-ray diffraction analysis completion were: S(29) 25 and S(33) 29 from the Southern High Plains (Table 7.1) and Tula G from the Chihuahuan Desert USA regions (Table 7.2), respectively. Powder diffraction practice produced a smoothed fit assuring great matching among these experimental scans, including peak positions and their intensities from which Bragg reflections rendered a negligible difference within a few tenths of a degree between each other.

Indexed process performed in Bragg reflections resulted from X-ray diffractometry of the primary pattern S(29) 25, a corresponding identification of the quartz and gypsum minerals was achieved by comparing the resulted experimental Bragg reflections among those of the ICDD Powder Diffraction FilesTM database. From angle comparison process 17 Bragg reflections of the primary pattern matched equal number of reflections values from those of the PDFTM ICDD quartz record (Fig. 7.17). Yet, 9 Bragg reflections contained in the primary pattern fitted similar reflection angle values when linking them to those of the PDFTM ICDD gypsum record (Fig. 7.18).

A brief description of the highest intensities values for quartz and gypsum is described next. Quartz (card No. 46-1045) was by its d-spacing value in Angstrom $d(\text{\AA})$ of 3.3435, 2-Theta value in degrees (2θ) of 26.587° and with Miller indexes of (101) the higher peak in the experimental primary pattern. More precisely, highest peak of quartz was recognized with a $d(\text{\AA})$ value of 3.3435 with 2θ value of 26.587° at (101); a second order peak with $d(\text{\AA})$ equal to 1.8180 with 2θ value of 50.079° at (112); and others at $d(\text{\AA})$ of 2.4569 with 2θ value of 36.489° at (110) which peak intensity (I) was similar to the peak marked at $d(\text{\AA})$ equal to 1.5415 and 2θ value of 59.863° at (211); and the peak with a $d(\text{\AA})$ value of 2.2815 and 2θ equivalent value of 39.398° at (102) (Figure 7.19). Likewise, Gypsum (card No. 33-0311) was by its d-spacing value in Angstrom $d(\text{\AA})$ of 7.6300, 2-Theta value in degrees (2θ) of 11.588° and with Miller indexes of (020) the higher peak in the experimental primary pattern. Gypsum was identified from the highest peak at $d(\text{\AA})$ equal to 7.6300 with 2θ equal to 11.588° at (020) which peak intensity (I) was similar to the peak marked at $d(\text{\AA})$ equal to 4.2830 and 2θ value of 20.682° at (021); a second order peak with $d(\text{\AA})$ equal to 3.0650 with 2θ value of 29.049° at (041); and others at $d(\text{\AA})$ of 2.6850 with 2θ value of 33.281° at (150); the peak at $d(\text{\AA})$ equal to 2.8730 with 2θ equal to 31.030° at (-221); and the peak with a $d(\text{\AA})$ value of 2.0860 and 2θ equivalent value of 43.270° at (-242) (Figure 7.19). Higher peaks with low intensities, low quality of data, or impure phase may negatively affect the appropriate reflections identity.

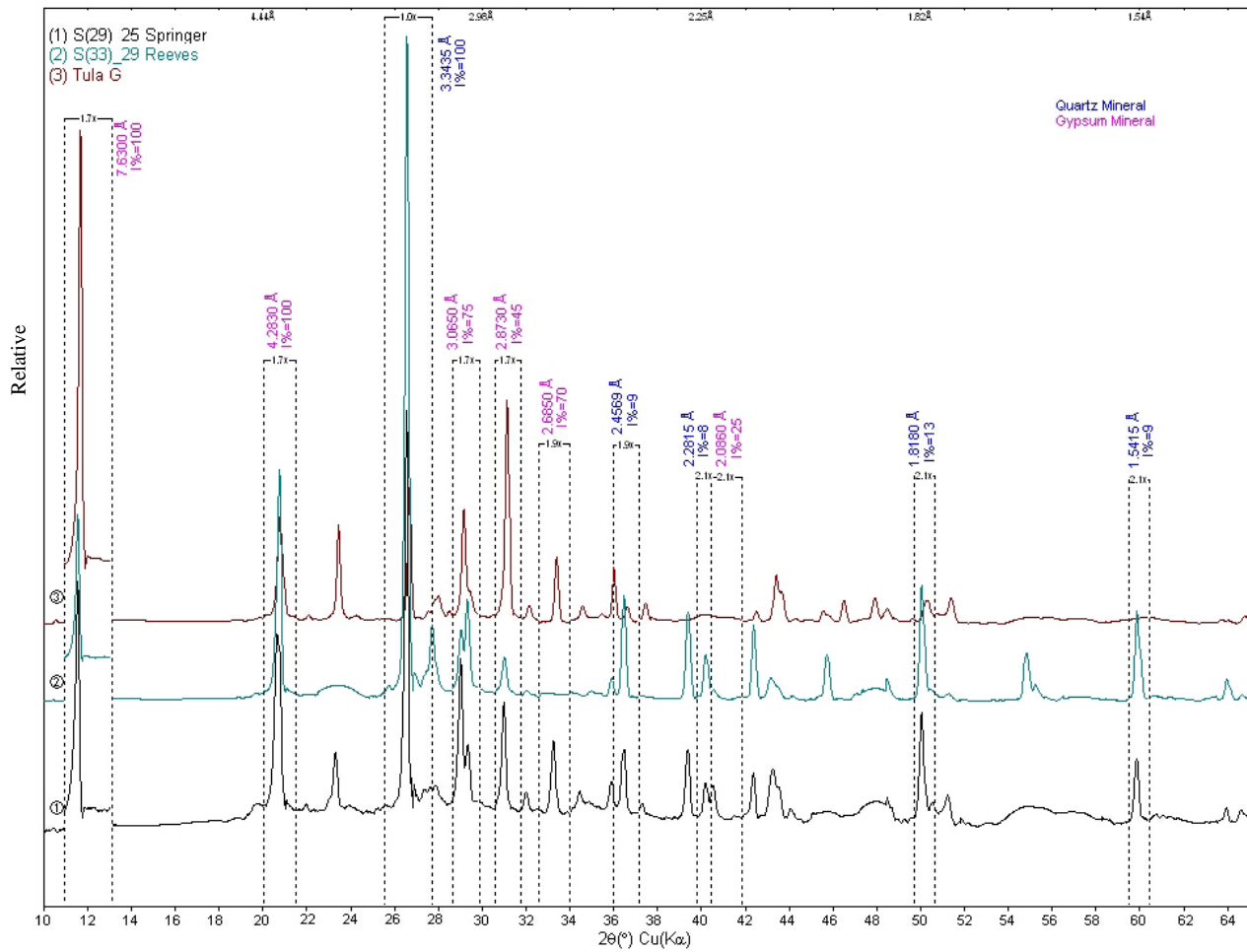


Figure 7.19 – Quartz + Gypsum overlaid powder diffraction patterns.

A total of 3 overlaid powder diffraction scan patterns collected from both the Southern High Plains and the Chihuahuan Desert USA regions on a RIGAKU MiniFlex II X-ray diffractometer using Cu-K α radiation at 30 Kv and 15 mA with a Kb filter. S(29) 25 selected as primary pattern shown with number 1, signifying a soil sample with plentiful crystallinity: narrow and sharp Bragg reflections with K α_1 / K α_2 doublets being partly resolved at $2\theta \cong 11^\circ$ and $2\theta \cong 27^\circ$ for gypsum and quartz, respectively.

7.2.2.14 Quartz + Gypsum 2θ peak matching chart

2θ peak matching chart was created by scatter plotting the difference among the 2θ peaks- from those of the overlaid patterns peak-values. Peak search analysis provided a total of 86 peaks. The peaks were statistically observed to obtain match affinity between these experimental scan patterns. As result, strong Bragg reflections were kept slightly between each other (within a few tenths of a degree), concisely, differed values comprised commonly onto the $-0.4^{\circ} < 0.0^{\circ} < 0.1^{\circ}$ degree range suggestive of quite significant divergences in the stepsize of the scan patterns when associating them against each other (Figure 7.20).

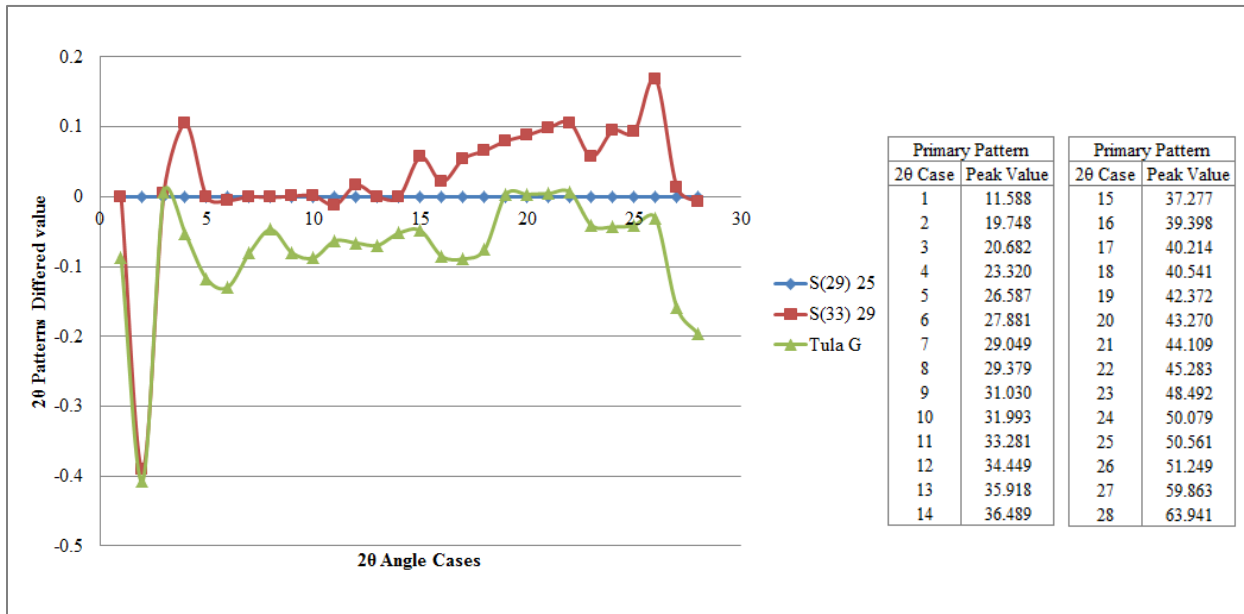


Figure 7.20 – Quartz + Gypsum 2θ peak matching in overlaid patterns.

Peak search 2θ difference values comparison in quartz + gypsum overlaid scan patterns. 28 Bragg reflections from the primary pattern S(29) 25 sample generating somewhat uneven matching in overlaid scans.

7.2.2.15 Pattern overlays 3D view for quartz + gypsum

3D views of overlaid patterns showed the quartz + gypsum experimental scans from soil samples coming from both the Southern High Plains and the Chihuahuan Desert USA regions. 2 θ angle values with high intensities enough to be considered in the Peak ID Report of the primary pattern and its scan patterns (Appendix A.4) were also noted in the 3D view of the three soil samples with quartz + gypsum mineral composition at diverse richness concentrations. A total of 9 as well as 17 peaks with high intensity values were derived in the 3D chart for quartz and gypsum, in that order (Figure 7.21).

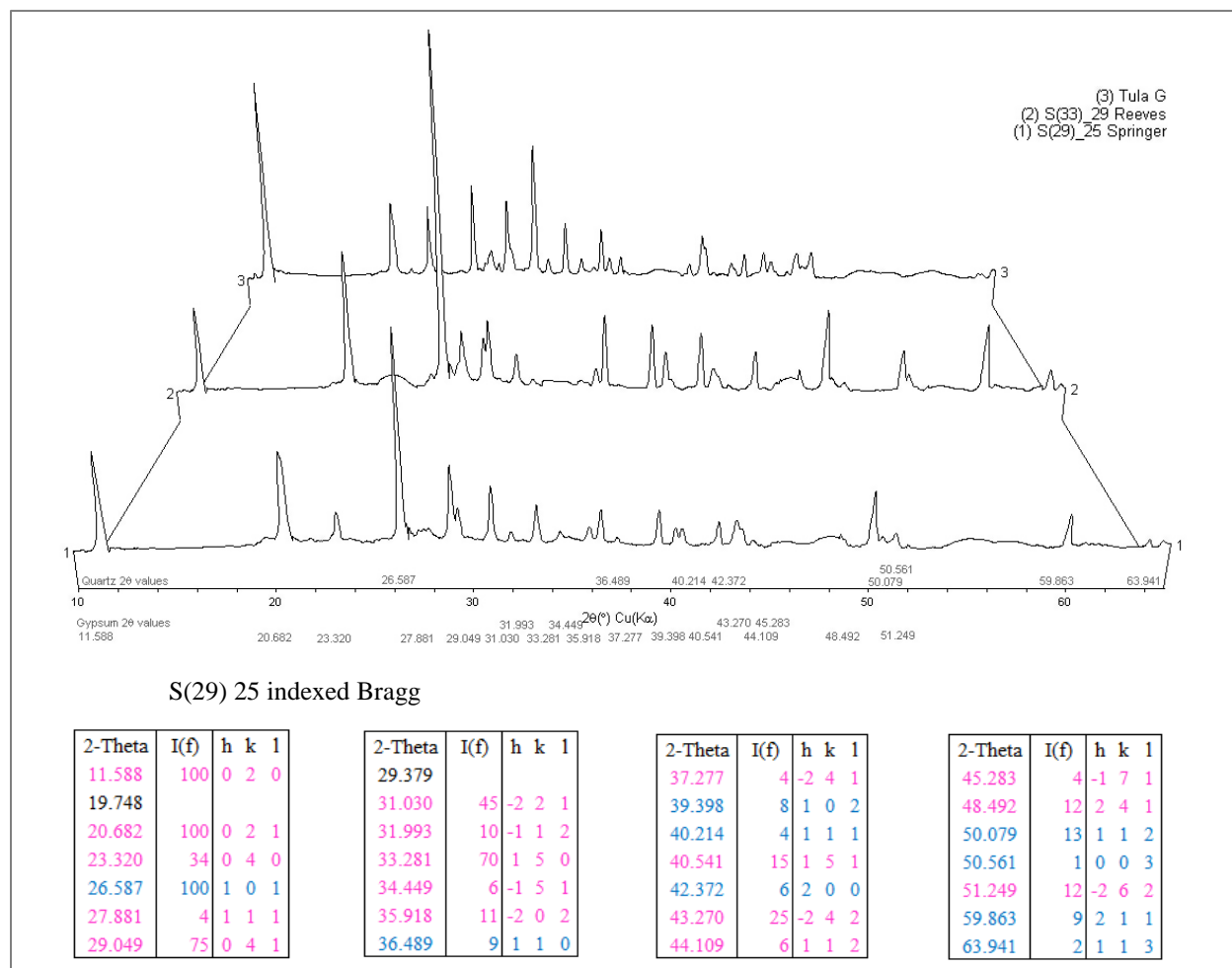


Figure 7.21 – 3D view of quartz + calcite XRD patterns with major high peaks illustrated.

7.2.2.16 2D contour plots for quartz + gypsum

2D contour plots with a based square-root intensity at Y axis scale $\text{SQR}(I)$, boosted visibility of weak peaks and confirmed stepsize similarity of 3D overlaps by observing their coloring peak intensities. After analyzing the 2D contour plot, uneven stepsize of the quartz + calcite overlaid patterns resulted with untrusted consistency among peak intensity color lines (Figure 7.22).

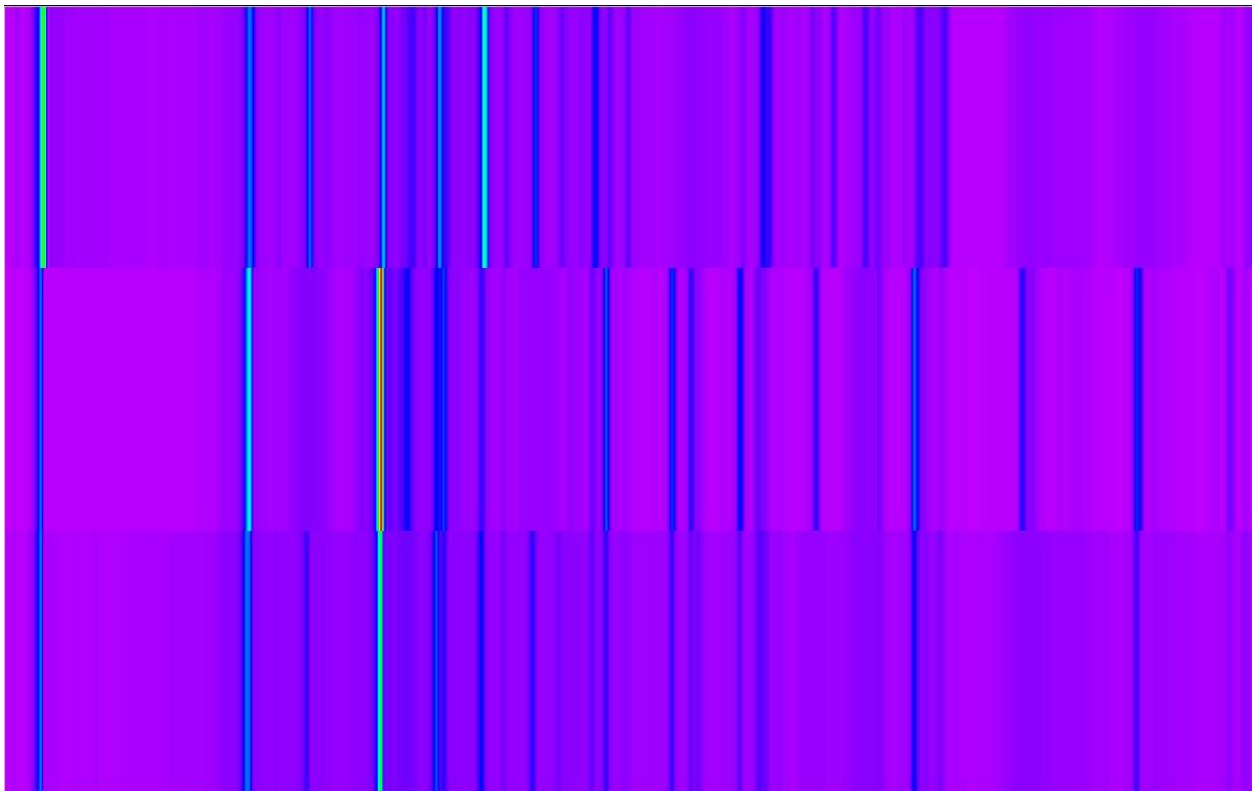


Figure 7.22 – 2D contour plot of 3D quartz + gypsum overlaid scans.

7.2.2.17 Quartz + Calcite Magnesian + Dolomite overlaid specimens

Mineral composition of quartz + calcite magnesian + dolomite at different abundance concentrations were obtained from soil samples collected from the three regions under examination after X-ray diffractometry of 83 specimens previously listed (Table 7.1, Table 7.2, and Table 7.3). Multiple phase search match PDT™ was performed immediately after overlapping similar scans that resulted with this mineralogy, leading to find PDF™-2-3-records matching group, that is, quartz + calcite magnesian + dolomite. Strong intensities obtained from the selected primary pattern (namely, S(76) 60), matched the PDF™-2 database record of these three minerals. Therefore, quartz, calcite magnesian, and dolomite mineral XRD patterns coming from three samples (two soil samples from the Southern High Plains and one sample coming from the Chihuahuan Desert MEX region) were overlapped for search match analysis performance resulting that 27 Bragg reflections of the primary pattern coincided with 8, in addition to 5 as well as 6 reflections of the Quartz PDF™-2 record (card No. 46-1045) (Fig. 7.23), Calcite Magnesian PDF™-2 record (card No. 43-0697) (Fig. 7.24), and Dolomite PDF™-2 record (card No. 36-0426) (Fig. 7.25), in that order.

PDF#00-043-0697: QM=Star(S); d=Diffraction; I=Diffraction										2-Theta	I(f)	h	k	l															
Calcite, magnesian (Calcium Magnesium Carbonate)										19.748																			
(Ca,Mg)CO3										20.830	16	1	0	0															
Radiation=CuKa1 Lambda=1 Filter=Graph										23.079	5	0	1	2															
Calibration=Internal(Si) 2T=23.264 I/Ic(RIR)=										23.952	4	0	1	2															
Ref: Blanchard, F., Dept. of Geology, University of Florida, Gainesville, Florida, USA.										26.615	100	1	0	1															
ICDD Grant-in-Aid (1991)										27.789																			
Rhombohedral - Z=6 Density(m)=2.38A										29.440	100	1	0	4															
CELL: 4.9426 x P.S=hR10 (?) Mwt=97.88										30.850	100	1	0	4															
Density(c)=2.735 Vol=356.53										34.810																			
Ref: Ibid. F(28)=69.5(.0122,33/0)										36.011	12	1	1	0															
										36.488	9	1	1	0															
Strong Lines: 3.00/X 1.89/3 2.26/2 1.86/2 2.07/1 2.47/1 1.43/1 1.59/1										39.431	8	1	0	2															
NOTE: Specimen of calcite, magnesian from a recent echinoid fossil, Clypeaster rosaceus										40.239	4	1	1	1															
(Linnaeus), from Cedar Key, Levy County, Florida, USA.										41.020	19	1	1	3															
ICP analysis yields a composition of Ca0.861 Mg0.136 Sr0.002 C O3.										42.400	6	2	0	0															
28 reflections in pattern.										43.210																			
2-Theta	I(f)	(h k l)	2-Theta	I(f)	(h k l)	2-Theta	I(f)	(h k l)	2-Theta	I(f)	(h k l)																		
23.264	5	(0 1 2)	61.737	3	(2 0 8)	85.852	2	(2 2 6)				44.832	10	2	0	2													
29.714	100	(1 0 4)	62.158	3	(1 1 9)	87.609	<1	(1,2,11)				47.200																	
31.846	3	(0 0 6)	63.755	2	(1 2 5)							47.559	7	0	2	4													
36.310	12	(1 1 0)	65.363	9	(3 0 0)							48.579																	
39.810	22	(1 1 3)	66.542	3	(0,0,12)							50.106	13	1	1	2													
43.601	13	(2 0 2)	69.998	2	(2 1 7)							50.924	13	1	1	6													
47.619	7	(0 2 4)	71.138	2	(0,2,10)							56.648																	
48.127	28	(0 1 8)	73.806	2	(1 2 8)							57.461	1	2	1	0													
49.063	21	(1 1 6)	74.528	<1	(3 0 6)							59.889	4	1	2	2													
57.171	3	(2 1 1)	77.137	1	(2 2 0)							60.730																	
58.009	9	(1 2 2)	78.244	3	(1,1,12)							61.511	6	2	1	4													
58.837	1	(1,0,10)	82.617	2	(2,1,10)							Total																	
61.348	6	(2 1 4)	84.757	4	(1 3 4)							Quartz + Calcite +																	
														Dolomite															
3 Samples										S(76) 60 primary pattern										27 reflections in pattern									
2 SHP										00-046-1045										8 fitted by Quartz									
1 CHD MEX										00-043-0697										5 fitted by Calcite Magnesian									
										00-036-0426										6 fitted by Dolomite									
																				8 empty									

Figure 7.24 – Calcite Magnesian indexed (card No. 43-0697) compared to experimental patterns.

Calcite magnesian extracted from the ICDD powder diffraction file with its resulted reflections identified by their Bragg angles and relative intensities normalized to 100 along the Miller indices. S(76) 60 sample was assigned the primary pattern of overlapped patterns that relied upon in positive phase identification within this mineral (magenta colored data enclosed in red outlined box) once multiple search match completed obtaining 5 Bragg reflections with good similarity when compared to those of the Calcite magnesian PDF™-2 record.

PDF#00-036-0426: QM=Star(S); d=Diffractionmeter; I=Diffractionmeter											2-Theta	I(f)	h	k	l
Dolomite (Calcium Magnesium Carbonate)											19.748				
CaMg(CO3)2 Light yellowish brown											20.830	16	1	0	0
Radiation=CuKα Lambda=1 Filter=Graph											23.079	5	0	1	2
Calibration=Internal(Si) 2T=22.022 I/Ic(RIR)=											23.952	4	0	1	2
Ref. Keller, L., McCarthy, G., North Dakota State Univ., Fargo, ND, USA.											26.615	100	1	0	1
ICDD Grant-in-Aid (1985)											27.789				
Rhombohedral - Z=3 Density(m)=2.860											29.440	100	1	0	4
CELL: 4.8092 x P.S=hR10 (?) Mwt=184.40											30.850	100	1	0	4
Density(c)=2.869 Vol=320.88											34.810				
Ref. Ibid. F(30)=148.1(.0063,32/0)											36.011	12	1	1	0
											36.488	9	1	1	0
Strong Lines: 2.89/X 2.19/2 1.79/1 1.80/1 2.02/1 2.40/1											39.431	8	1	0	2
NOTE: Specimen from Baxter Springs, AR, USA.											40.239	4	1	1	1
Chemical analysis by EDX at University of North Dakota, ND, USA, (wt.%): CaO 30.18,											41.020	19	1	1	3
MgO 21.10, FeO 0.44, MnO 0.11, C O2 47.18, Na2 O 0.17, Al2 O3 0.13, Si O2 0.47 (chiefly											42.400	6	2	0	0
from traces of quartz and plagioclase): Ca (Mg0.977 Fe0.011 Na0.005 Mn0.003 Ca0.004) (C O3)2.											43.210				
Optical data on specimen from Haley, Ross Township, Ontario, Canada.											44.832	10	2	0	2
To replace 11-78.											47.200				
41 reflections in pattern.											47.559	7	0	2	4
2-Theta	I(f)	(h k l)	2-Theta	I(f)	(h k l)	2-Theta	I(f)	(h k l)	2-Theta	I(f)	(h k l)	2-Theta	I(f)	(h k l)	
22.022	1	(1 0 1)	50.527	10	(0 1 8)	66.075	1	(1 2 5)	82.104	<1	(2 2 3)	50.106	13	1 1 2	
24.039	4	(0 1 2)	51.069	13	(1 1 6)	67.389	2	(3 0 0)	82.592	1	(1,1,12)	50.924	13	1 1 6	
30.939	100	(1 0 4)	51.284	2	(0 0 9)	69.962	<1	(3 0 3)	84.714	<1	(3 1 2)	56.648			
33.536	4	(0 0 6)	52.355	<1	(2 0 5)	70.480	1	(0,0,12)	86.636	1	(2,1,10)	57.461	1	2 1 0	
35.322	3	(0 1 5)	58.900	2	(2 1 1)	72.869	1	(2 1 7)	87.899	<1	(1 3 4)	59.889	4	1 2 2	
37.377	7	(1 1 0)	59.828	4	(1 2 2)	74.692	1	(0,2,10)	88.551	<1	(0,1,14)	60.730			
41.128	19	(1 1 3)	60.012	<1	(0 2 7)	76.999	1	(1 2 8)	89.277	1	(2 2 6)	61.511	6	2 1 4	
43.805	3	(0 2 1)	62.005	<1	(1,0,10)	77.414	<1	(3 0 6)	89.443	<1	(3 0 9)	Total Quartz + Calcite + Dolomite			
44.950	10	(2 0 2)	63.434	2	(2 1 4)	79.694	1	(2 2 0)							
45.163	1	(1 0 7)	64.502	2	(2 0 8)	80.393	<1	(2,0,11)							
49.289	3	(0 2 4)	65.145	1	(1 1 9)	81.363	<1	(1,0,13)							
3 Samples S(76) 60 primary pattern 27 reflections in pattern															
2 SHP 00-046-1045 8 fitted by Quartz															
1 CHD MEX 00-043-0697 5 fitted by Calcite Magnesian															
00-036-0426 6 fitted by Dolomite															
											8 empty				

Figure 7.25 – Dolomite indexed (card No. 36-0426) compared to experimental patterns.

Dolomite obtained from the ICDD powder diffraction file with its resulted reflections identified by their Bragg angles and relative intensities normalized to 100 as well as the Miller indices. S(76) 60 specimen was the primary pattern of overlapped scans that was relied upon in positive phase identification within this mineral (red colored data enclosed in red outlined box) after multiple search match inspection matching 6 Bragg reflections with great likeness when linked to those of the Dolomite PDFTM-2 record.

Automated- and visual selection-search match assessment (on quartz, calcite magnesium, and dolomite characterized soil samples), was performed the RIGAKU MiniFlex II X-ray diffractometer located in the UTEP Material Science and Engineering lab. By manipulating Jade 9 powder diffraction database software package, strong Bragg reflections included in the primary pattern coincided with those of the quartz [SiO_2 PDFTM-2 card No. 46-1045], calcite magnesiumian [$(\text{Ca}, \text{Mg})\text{CO}_3$ PDFTM-2 card No. 43-0697], and dolomite [$\text{CaMg}(\text{CO}_3)_2$ PDFTM-2 card No. 36-0426] records. Samples with quartz, calcite magnesiumian, and dolomite minerals with diverse abundance concentrations after X-ray diffraction examination that were considered in the overlapping scan process were S(76) 60, and S(77) 61 from the Southern High Plains (Table 7.1) along with CLP 002 from the Chihuahuan Desert MEX regions (Table 7.2), respectively. Unfit smoothly shaped obtained from powder diffraction practice causing little matching between the experimental scans, containing peak positions and their intensities from which Bragg reflections provided a significant difference within few tenths of a degree among each other. Related identification of the quartz, calcite, and dolomite minerals was attained by performing the indexed process of the primary pattern S(76) 60 which experimental Bragg reflections were compared among those of the ICDD Powder Diffraction FileTM database. A total of 8 Bragg reflections of the primary pattern linked same number of reflections values from those of the PDFTM ICDD quartz record (Figure 7.23). Still, 5 Bragg reflections enclosed in the primary pattern matched comparable reflection angle values when comparing them to those of the PDFTM ICDD calcite magnesiumian record (Fig. 7.24). Lastly, 6 Bragg reflections contained in the primary pattern resulted similar to those of the PDFTM ICDD dolomite record (Fig. 7.25).

A concise narrative of the top highest Bragg reflection values for quartz, calcite magnesian, and dolomite is provided next. Quartz (card No. 46-1045) was by its d-spacing value in Angstrom $d(\text{\AA})$ of 3.3435, 2-Theta value in degrees (2θ) of 26.615° and with Miller indexes of (101) the higher peak in the experimental pattern. Indeed, highest peak of quartz was found with a $d(\text{\AA})$ value of 3.3435 with 2θ value of 26.615° at (101); a second order peak with $d(\text{\AA})$ equal to 4.2550 with 2θ value of 20.830° at (100); and others at $d(\text{\AA})$ of 1.8180 with 2θ equivalent value of 50.106° at (112); along with the peak marked at $d(\text{\AA})$ equal to 2.4569 and 2θ value of 36.488° at (110); and the peak with a $d(\text{\AA})$ value of 2.2815 and 2θ equal to 39.431° at (102). The same, calcite magnesian (card No. 43-0697) was by its d-spacing value in Angstrom $d(\text{\AA})$ of 3.0042, 2-Theta value in degrees (2θ) of 29.440° and with Miller Indexes of (104) the higher peak in the experimental pattern. The top peak of calcite magnesian was obtained with a $d(\text{\AA})$ value of 3.0042 with 2θ equal to 29.440° at (104); a second order peak with $d(\text{\AA})$ equal to 2.4722 with 2θ value of 36.011° at (110); and others at $d(\text{\AA})$ 1.9081 with 2θ equal to 47.559° at (024); the peak at $d(\text{\AA})$ equal to 1.5099 with 2θ equals to 61.511° at (214); and the peak with a $d(\text{\AA})$ value of 3.8205 and 2θ equivalent value of 23.079° at (012). Dolomite (card No. 36-0426) was by its d-spacing value in Angstrom $d(\text{\AA})$ of 2.8880, 2-Theta value in degrees (2θ) of 30.850° and with Miller indexes of (104). The top peak of dolomite resulted from a $d(\text{\AA})$ value of 2.8880 with 2θ equal to 30.850° at (104); a second order peak with a $d(\text{\AA})$ equal to 2.1930 with 2θ value of 41.020° at (113); and others at $d(\text{\AA})$ 1.7870 with 2θ equal to 50.924° at (116), and the peak placed at $d(\text{\AA})$ value of 2.0150 with a 2θ equivalent value of 44.832° at (202) (Figure 7.26).

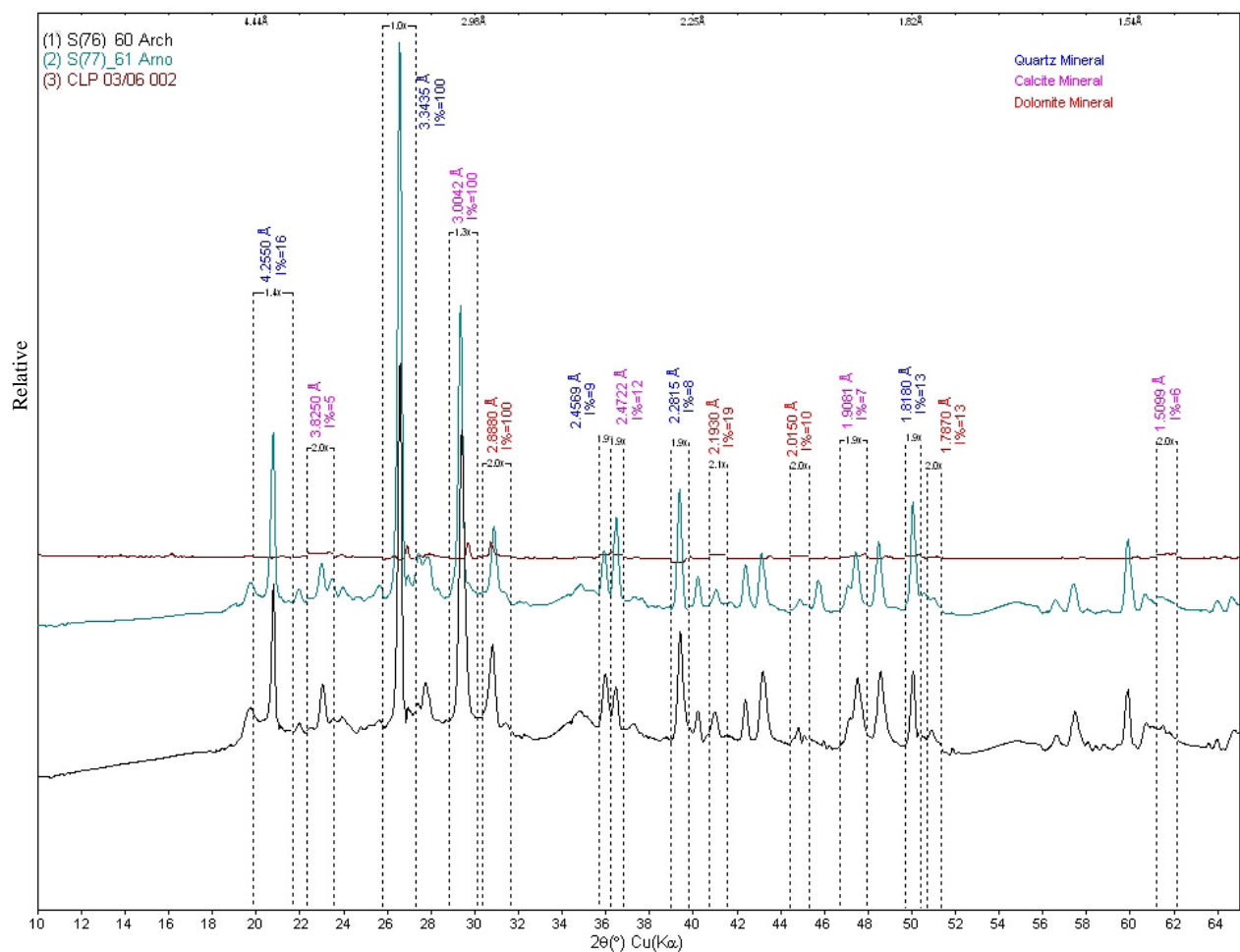


Figure 7.26 – Quartz + Calcite Magnesian + Dolomite overlaid powder diffraction patterns.

A total of 3 overlapped powder diffraction scans collected from both the Southern High Plains and the Chihuahuan Desert MEX regions on a RIGAKU MiniFlex II X-ray diffractometer using $\text{Cu-K}\alpha$ radiation at 30 Kv and 15 mA with a Kb filter. S(76) 60 designated as primary pattern located with number 1, meaning a soil sample with mixed crystallinity: few narrow and sharp Bragg reflections with $\text{K}\alpha_1/\text{K}\alpha_2$ doublets partly resolved at $2\theta \cong 27^\circ$, $2\theta \cong 29^\circ$, and $2\theta \cong 31^\circ$ for quartz, calcite magnesian and dolomite, in that order.

7.2.2.18 Quartz + Calcite Magnesian + Dolomite 2θ peak matching chart

2θ peak matching chart was created by scatter plotting the variance between the 2θ peaks- from those of the overlaid patterns peaks-values. Peak search analysis included a total of 79 peak values. The peaks were statistically examined to obtain match similarity among these experimental scan patterns. Bragg reflection comparison results were widely spaced among each other with a differed values degree range $-0.3^{\circ} < 0.0^{\circ} < 0.4^{\circ}$ suggesting significant differences in the stepsize of the scan patterns when correlating them against each other, but obtaining little divergences in the stepsize when observing separately the patterns coming from the 2 different soil regions (that is, $-0.2^{\circ} < 0.0^{\circ} < 0.0^{\circ}$ degree range for the Southern High Plain region) (Figure 7.27).

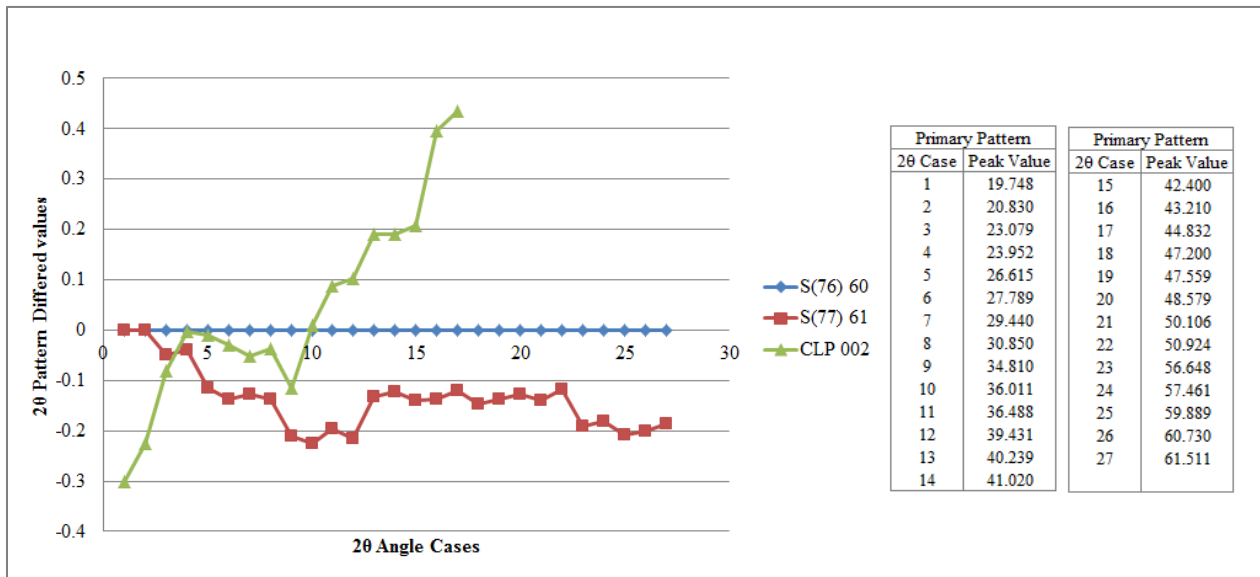


Figure 7.27 – Quartz + Calcite Magnesian + Dolomite 2θ peak matching in overlaid patterns.

Peak search 2θ difference values comparison in quartz + calcite magnesium + dolomite scans patterns. 27 Bragg reflections from the primary pattern S(29) 25 sample generated a certain extent irregular matching overlapped scans.

7.2.2.19 Pattern overlays 3D view for quartz + calcite magnesium + dolomite

3D views of overlapped scans displaying quartz + calcite magnesium + dolomite experimental patterns from soil specimens coming from both the Southern High Plains and the Chihuahuan Desert MEX regions. Bragg reflections that were considered in the Peak ID Report because of their high intensities (Appendix A.5) were also distinguished in the 3D view of the three soil samples with quartz + calcite magnesium + dolomite chemical composition at different concentrations. A total of 8, 5 as well as 6 peaks with high intensity values were observed in the 3D chart for quartz, calcite magnesium, and dolomite, respectively (Figure 7.28).

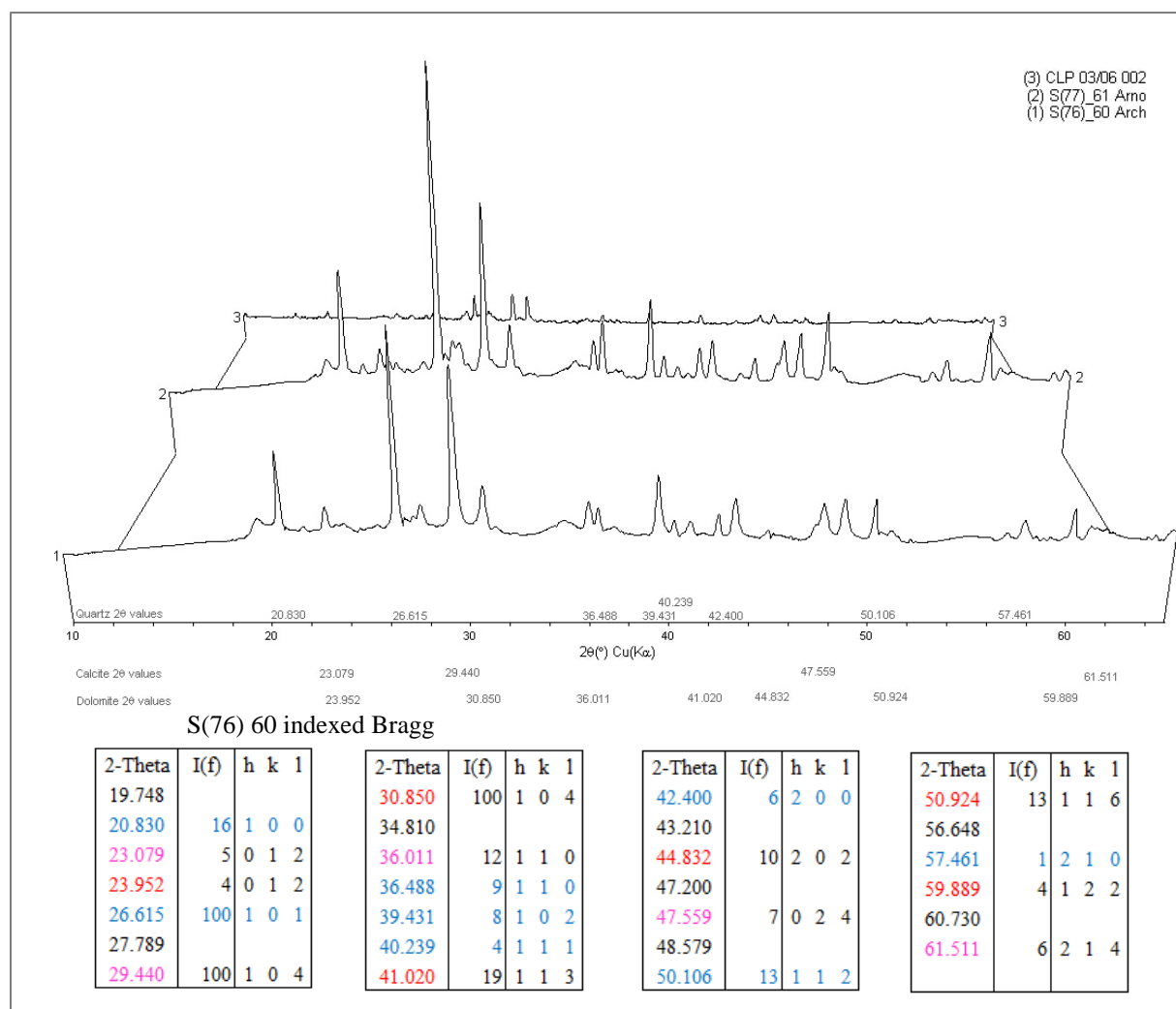


Figure 7.28 – 3D view of quartz + calcite m. + dolomite XRD patterns with major high peaks.

7.2.2.20 2D contour plots for quartz + calcite magnesian + gypsum

2D contour plots with a based square-root intensity at Y axis scale $\text{SQR}(I)$, increased visibility of weak peaks and completed stepsize similarity of 3D overlaps by examining their coloring peak intensities. After comparing the 2D contour plot, irregular stepsize of the quartz + calcite magnesian + dolomite scans resulted with poor evenness among peak intensity color lines (Figure 7.29).

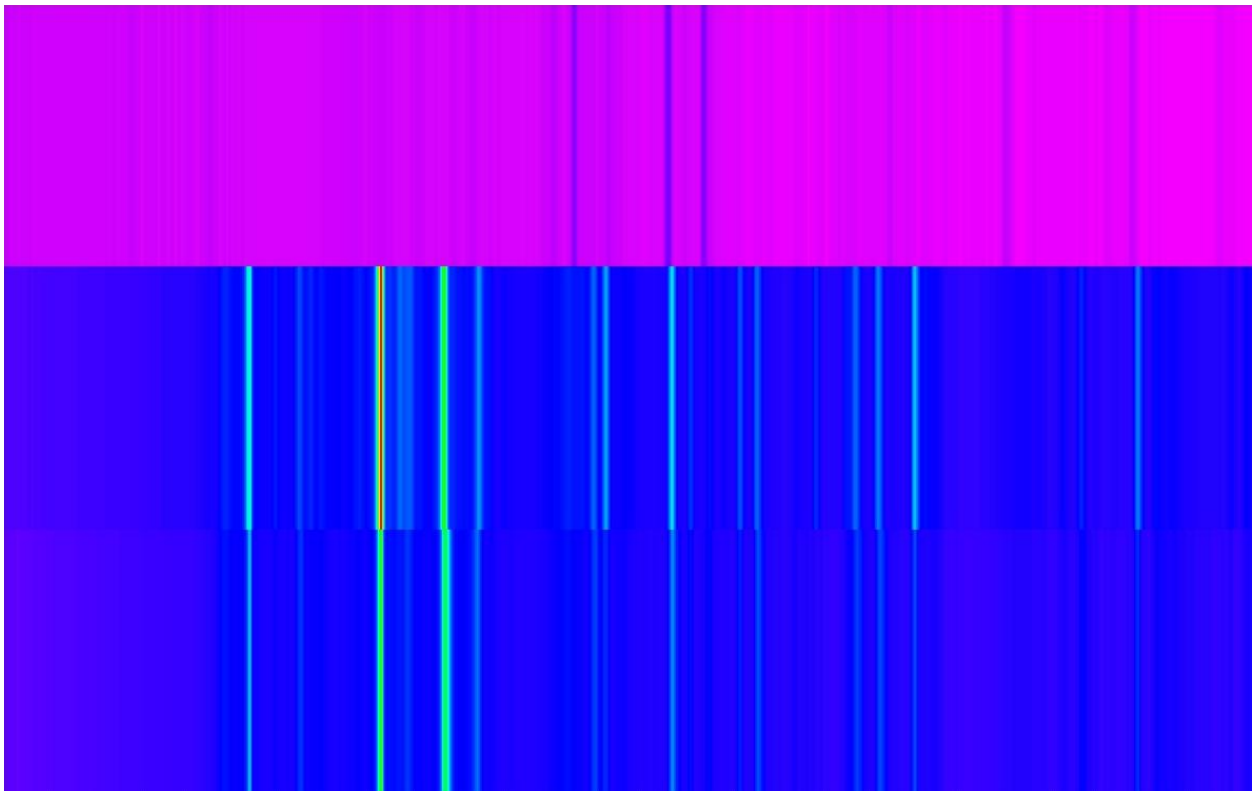


Figure 7.29 – 2D contour plot of 3D quartz + calcite magnesian + dolomite overlaid scans.

7.2.2.21 Quartz + Calcite + Sodium Plagioclase overlaid specimens

Only the Chihuahuan Desert MEX region provided samples with mineral composition comprised of quartz, calcite, and sodium plagioclase at diverse concentrations after X-ray diffractometry completion of the 83 samples listed earlier (Table 7.1, Table 7.2, and Table 7.3.). Multiple phase search match PDFTM was examined after overlaying alike patterns that consisted of this mineralogy, leading to discover PDFTM-2-3-records matching group, to be exact, quartz + calcite + sodium plagioclase. The primary pattern, sample LSM 002, resulted with several strong Bragg reflections that accorded the PDFTM-2 database record of these three minerals. Therefore, the three samples from the Chihuahuan Desert MEX region in which mineral XRD patterns involved quartz, calcite, and sodium plagioclase, were overlaid for searching matching analysis process occasioning that 11 strong intensities of the primary pattern coincided with 3, in addition to 2, and 3 reflections of Quartz PDFTM -2 record (card No. 43-0697) (Fig. 7.30), Calcite PDFTM-2 record (card No. 47-1743) (Fig. 7.31), and Sodium Plagioclase PDFTM-2 record (card No. 9-0465) (Fig. 7.32), correspondingly.

PDF#00-046-1045: QM=Star(S); d=Diffractometer; I=Diffractometer Quartz, syn (Silicon Oxide) SiO ₂ Radiation=CuKα1 Calibration=Internal(Si) Ref. Kern, A., Eysel, W., Mineralogisch-Petrograph. Inst., Univ. Heidelberg, Germany. ICDD Grant-in-Aid (1993) Hexagonal - Powder Diffraction, P3221 (154) CELL: 4.91344 x 4.91344 x 5.40524 <90.0 x 90.0 x 120.0> Density(c)=2.650 Ref. Z. Kristallogr., v198 p177 (1992) Strong Lines: 3.34/X 4.25/2 1.82/1 1.54/1 2.46/1 2.28/1 1.37/1 2.13/1 NOTE: Pattern taken at 23(1) C. Low temperature quartz. 58 reflections in pattern.											
2-Theta	I(f)	(h k l)	2-Theta	I(f)	(h k l)	2-Theta	I(f)	(h k l)	2-Theta	I(f)	(h k l)
20.860	16	(1 0 0)	67.744	6	(2 1 2)	94.650	1	(1 0 5)	118.312	<1	(2 1 5)
26.640	100	(1 0 1)	68.144	7	(2 0 3)	95.118	<1	(4 0 1)	120.123	1	(3 1 4)
36.544	9	(1 1 0)	68.318	5	(3 0 1)	96.237	1	(2 1 4)	121.852	<1	(1 0 6)
39.465	8	(1 0 2)	73.467	2	(1 0 4)	98.750	1	(2 2 3)	122.604	<1	(4 1 2)
40.300	4	(1 1 1)	75.659	3	(3 0 2)	102.230	<1	(1 1 5)	127.250	<1	(3 0 5)
42.450	6	(2 0 0)	77.675	1	(2 2 0)	102.566	<1	(3 1 3)	131.202	<1	(1 1 6)
45.793	4	(2 0 1)	79.884	2	(2 1 3)	103.876	<1	(3 0 4)	132.755	<1	(5 0 1)
50.139	13	(1 1 2)	80.046	<1	(2 2 1)	104.202	<1	(3 2 0)	134.292	<1	(4 0 4)
50.622	<1	(0 0 3)	81.173	2	(1 1 4)	106.592	<1	(3 2 1)	136.422	1	(2 0 6)
54.875	4	(2 0 2)	81.491	2	(3 1 0)	112.113	<1	(4 1 0)	137.893	2	(4 1 3)
55.325	2	(1 0 3)	83.840	1	(3 1 1)	114.060	<1	(3 2 2)	140.316	<1	(3 3 0)
57.235	<1	(2 1 0)	84.957	<1	(2 0 4)	114.466	2	(4 0 3)	143.249	3	(5 0 2)
59.960	9	(2 1 1)	87.439	<1	(3 0 3)	114.638	2	(4 1 1)	144.117	<1	(3 3 1)
64.035	2	(1 1 3)	90.831	2	(3 1 2)	115.884	<1	(2 2 4)			
65.786	<1	(3 0 0)	92.788	<1	(4 0 0)	117.536	<1	(0 0 6)			
<div> <div> 3 Samples 3 CHD MEX </div> <div> LSM 002 primary pattern 00-046-1045 00-047-1743 00-009-0466 </div> <div> 11 reflections in pattern 3 fitted by Quartz 2 fitted by Calcite 3 fitted by Sodium Plagioclase 3 empty </div> </div>											
<div> <div> 2-Theta 13.945 17.324 26.761 27.064 27.773 28.322 29.514 48.662 50.301 60.037 62.488 </div> <div> I(f) 20 100 100 100 100 10 100 23 13 9 </div> <div> h k l 0 0 1 1 0 1 1 0 1 0 0 2 -2 2 0 1 0 4 1 1 -6 1 1 2 2 1 1 </div> </div>											
Total Quartz + Calcite + Sodium Plagioclase											

Figure 7.30 – Quartz indexed (card No. 46-1045) compared to experimental patterns.

Quartz resulted from the ICDD powder diffraction file with its included reflections acknowledged by their Bragg angles and relative intensities normalized to 100 besides the Miller indices. LSM 002 sample was assigned the primary pattern of overlaid patterns that was dependent on upon a positive phase identification within this mineral (blue colored data enclosed in red outlined box) after multiple searching matching examination resulting with 3 Bragg reflections with good similarity when comparing to those of the Quartz PDF™-2 record.

PDF#00-047-1743: QM=Calculated(C); d=Calculated; I=Calculated Calcite (Calcium Carbonate) CaCO3 Radiation=CuK α ; Lambda=1.54056 Filter= Calibration= 2 θ =23.054-135.725 I/Ic(RIR)= Ref: Bernstein, L., Menlo Park, CA, USA. Private Communication (1994) Rhombohedral - Z=6 Density(m)=2.37A CELL: 4.9896 x P.S=hR10 (?) Mwt=100.09 Density(c)=2.711 Vol=367.85 Ref: Effenberger, H. et al. F(30)=999.9(.0003,33/0) Z. Kristallogr., v156 p233 (1981) Strong Lines: 3.04/X 1.88/2 1.91/2 2.28/2 2.09/2 2.49/1 1.60/1 3.85/1 NOTE: Pattern calculated using Lazy-Pulverix including anomalous dispersion corrections. Specimen from Iceland. R=0.022; Rw=0.023. Microprobe analysis (wt.%): Ca O 55.7, Mg O 0.2, Fe O 0.1 Data collected using MoK α GA-radiation, graphite monochromator.											2-Theta	I(f)	h	k	l	
60 reflections in pattern.											13.945	20	0	0	1	
											17.324					
											26.761	100	1	0	1	
											27.064					
											27.773	100	0	0	2	
											28.322	10	-2	2	0	
											29.514	100	1	0	4	
											48.662	23	1	1	-6	
											50.301	13	1	1	2	
											60.037	9	2	1	1	
											62.488					
											Total Quartz + Calcite + Sodium Plagioclase					
2-Theta	I(f)	(h k l)	2-Theta	I(f)	(h k l)	2-Theta	I(f)	(h k l)	2-Theta	I(f)						(h k l)
23.054	8.9	(0 1 2)	63.052	2.7	(2 1 -5)	93.055	1.4	(2,0,14)	109.552	4.2						(4 1 0)
29.400	100	(1 0 4)	64.659	8.4	(3 0 0)	94.711	4.9	(4 0 4)	110.472	1.9						(2,2,-12)
31.435	2.2	(0 0 6)	65.612	4.8	(0,0,12)	95.000	5.3	(1 3 -8)	114.037	0.6						(2 3 -7)
35.969	14.7	(1 1 0)	69.186	1.9	(1 2 -7)	96.158	2.5	(1,0,16)	117.936	1.9						(3 2 -8)
39.408	20.2	(1 1 -3)	70.240	3.1	(0,2,10)	96.200	0.8	(1,1,-15)	118.779	1.8						(4 1 -6)
43.158	16.1	(2 0 2)	72.891	3.7	(2 1 -8)	97.695	0.6	(1,2,-13)	119.248	2.2						(1,2,-16)
47.114	7	(0 2 4)	73.667	0.8	(0 3 6)	99.155	5.4	(3,0,12)	120.770	2.8						(1,1,-18)
47.506	21.7	(0 1 8)	76.271	1.5	(2 2 0)	102.218	0.7	(2 3 -1)	127.243	0.6						(5 0 2)
48.504	23.2	(1 1 -6)	77.159	2.8	(1,1,-12)	102.936	2.7	(3 2 -2)	127.970	3.2						(2,3,-10)
56.562	4.2	(1 2 -1)	80.940	0.8	(1 3 -2)	103.528	0.6	(3,1,-10)	128.545	0.6						(2,1,-17)
57.398	11.8	(1 2 2)	81.523	3.7	(1,2,-10)	104.121	2.4	(2,1,-14)	128.704	0.8						(1,3,-14)
58.079	1.2	(1,0,10)	82.105	0.5	(0,1,14)	105.83	1.8	(2 3 -4)	130.852	2.5						(0 5 4)
60.667	6.6	(1 2 -4)	83.768	6.8	(1 3 4)	106.13	4.4	(0 4 8)	133.975	3.1						(0,1,20)
60.997	3	(2 0 8)	84.804	3.5	(2 2 -6)	107.333	1	(0,2,16)	134.496	0.8						(3,2,-11)
61.374	3.6	(1 1 -9)	86.458	0.9	(2,1,-11)	108.028	0.6	(3 2 -5)	135.725	1.6						(3 3 0)
3 Samples LSM 002 primary pattern 11 reflections in pattern																
3 CHD MEX 00-046-1045 3 fitted by Quartz																
00-047-1743 2 fitted by Calcite																
00-009-0466 3 fitted by Sodium Plagioclase																
3 empty																

Figure 7.31 – Calcite indexed (card No. 47-1743) compared to experimental patterns.

Calcite obtained from the ICDD powder diffraction file with its resulted reflections classified by their Bragg angles and relative intensities normalized to 100 in addition to the Miller indices. LSM 002 soil specimen was the primary pattern of overlaid scans that was dependent upon positive phase identification within this mineral (magenta colored data enclosed

in red outlined box) after multiple search match analysis completion matching 2 Bragg reflections with fair similarity when associated with those of the Calcite PDFTM-2 record.

PDF#00-009-0465: QM=Blank(B); d=Other/Unknown(20.0mm); I=Film/Visual Anorthite, sodian, ordered (Sodium Calcium Aluminum Silicate) (Ca,Na)(Al,Si) ₂ Si ₂ O ₈ Radiation=CoK α ; Lambda=1 Filter=Fe Calibration= 2 θ =13.654 I/Ic(RIR)= Ref: Goodyear, Duffin. Mineral. Mag., v30 p306 (1954) Triclinic - Powd Z=4 Density(m)=2.705 CELL: 8.1648 x P.S=aP26 Mwt=278.21 Density(c)=2.685 Vol=333.82 Ref: Cole et al. F(19)=5.3(0.086,42/0) Acta Crystallogr., v4 p20 (1951) Strong Lines: 3.20/X 3.18/9 4.04/8 3.75/8 3.23/8 3.64/7 3.14/7 2.53/7 NOTE: Photograph calibrated with NaCl. Specimen occurs in anorthosite from Grand Marais, MN, USA. Chemical composition (wt.%): albite 32.7; anorthite 64.5; orthoclase 2.8. Probably of low-temperature origin. Indexed by analogy with labradorite with 55% anorthite with dimensions by Cole, Sorum, Taylor, Acta Crystallogr., 4 20-29 (1951). 19 reflections in pattern.											
2-Theta	I(f)	(h k l)	2-Theta	I(f)	(h k l)	2-Theta	I(f)	(h k l)	2-Theta	I(f)	(h k l)
13.654	40	(-1 1 0)	24.435	70	(-1-3 1)	27.594	80	(0 4 0)	30.273	70	(0-4 1)
18.947	40	(0-2 1)	25.652	50	(-1-1 2)	27.858	100	(-2 0 2)	33.666	60	(-3 1 1)
21.983	80	(-2 0 1)	25.956	30	(-2-2 1)	28.037	90	(0 0 2)	35.452	70	(-2-4 1)
22.842	50	(1-1 1)	26.426	60	(-1 1 2)	28.401	70	(2 2 0)	35.744	60	(1-1 2)
23.707	80	(-1 3 0)	27.335	50	(-2 2 0)	29.555	50	(1-3 1)			
Total Quartz + Calcite + Sodium Plagioclase											
3 Samples LSM 002 primary pattern 11 reflections in pattern 3 CHD MEX 00-046-1045 3 fitted by Quartz 00-047-1743 2 fitted by Calcite 00-009-0465 3 fitted by Sodium Plagioclase 3 empty											

Figure 7.32 – Sodium Plagioclase (card No. 47-1743) compared to experimental patterns.

Sodium Plagioclase extracted from the ICDD powder diffraction file with its resulted reflections recognized by their Bragg angles and relative intensities normalized to 100 along with the Miller indices. LSM 002 sample was assigned the primary pattern of overlaid scans that relied upon in positive phase identification within this mineral (red colored data enclosed in red outlined box) after multiple search match inspection matching 3 Bragg reflections with good likeness when linked them to those of the Sodium Plagioclase PDTTM-2 record.

Automated- and visual selection-search match appraisal on overlaid soil samples from the Chihuahuan Desert MEX region was completed by using the RIGAKU MiniFlex II X-ray diffractometer of the UTEP Material Science and Engineering lab. Jade 9 powder diffraction database software package allowed to establish a coinciding evaluation within strong Bragg reflections of the primary pattern with those of the quartz [SiO_2 PDFTM-2 card No. 46-1045], calcite [CaCO_3 PDFTM-2 card No. 47-1743], and Sodium Plagioclase [$(\text{Ca}, \text{Na})(\text{Al}, \text{Si})_2\text{Si}_2\text{O}_8$ PDFTM-2 card No. 9-0465] records. LSM 002, LSM 003, and SELP 003 soil samples from the Chihuahuan Desert MEX region were the experimental specimens that comprised quartz, calcite, and sodium plagioclase minerals at different concentrations. X-ray diffraction performance of these samples (previous overlay process completion) acquired an unfit smooth shape causing little match between the experimental patterns, including peak positions and their intensities from which Bragg reflections afforded a significant difference within few tenths of a degree between each other. Suitable identification of quartz, calcite, and sodium plagioclase was obtained by making the indexed procedure of the primary pattern LSM 002 from which experimental Bragg reflections were associated with those of the ICDD Powder Diffraction FileTM database. A total of 3 strong reflections of the primary pattern connected the same number of angle values from those of the PDFTM ICDD quartz record (Fig. 7.30). Yet, 2 Bragg reflections contained in the primary pattern linked same number of angle reflections from those of the PDFTM ICDD calcite record (Fig. 7.31). To sum up, 3 Bragg reflections enclosed in the primary pattern resulted similar those of the PDFTM ICDD sodium plagioclase after angle comparison (Fig. 7.32).

Brief description of the top highest Bragg reflection values for quartz, calcite and sodium plagioclase is indicated next. Quartz (card No. 46-1045) was by its d-spacing value in Angstrom $d(\text{\AA})$ of 3.345, 2-Theta value in degrees (2θ) of 26.761° and with Miller indexes of (101) the higher peak in the experimental pattern. Indeed, top peak of quartz was obtained with a $d(\text{\AA})$ value of 3.345 with 2θ equals to 26.761° at (101); a second order peak with $d(\text{\AA})$ equals to 1.8180 with 2θ value of 50.301° at (112); and the peak with a $d(\text{\AA})$ value of 1.5415 and 2θ equivalent value of 60.037° at (211). The same, Calcite (card No. 47-1743) was by its d-spacing value in Angstrom $d(\text{\AA})$ of 3.0355, 2-Theta value in degrees (2θ) of 29.514° and with Miller Indexes of (104) the higher peak in the experimental pattern. The top peak of calcite resulted from a $d(\text{\AA})$ value of 3.0355 with 2θ value of 29.514° at (104); and the peak placed at $d(\text{\AA})$ value of 1.8753 with a 2θ equals to 48.662° at (11-6). As well, Sodium Plagioclase (card No. 9-0465) was by its d-spacing value in Angstrom $d(\text{\AA})$ of 3.1960, 2-Theta value in degrees (2θ) of 27.773° and with Miller indexes of (002). The top peak of sodium plagioclase was found with a $d(\text{\AA})$ value of 3.1960 with 2θ equals to 27.773° at (002); a second order peak with $d(\text{\AA})$ equals to 6.3900 with a 2θ value of 13.945° at (001); and the peak with a $d(\text{\AA})$ value of 3.1510 and 2θ equals to 28.322° at (-220) (Fig 7.33).

Unidentified peaks could be caused by low quality of data, higher peaks with lower intensities or peaks with impure phases.

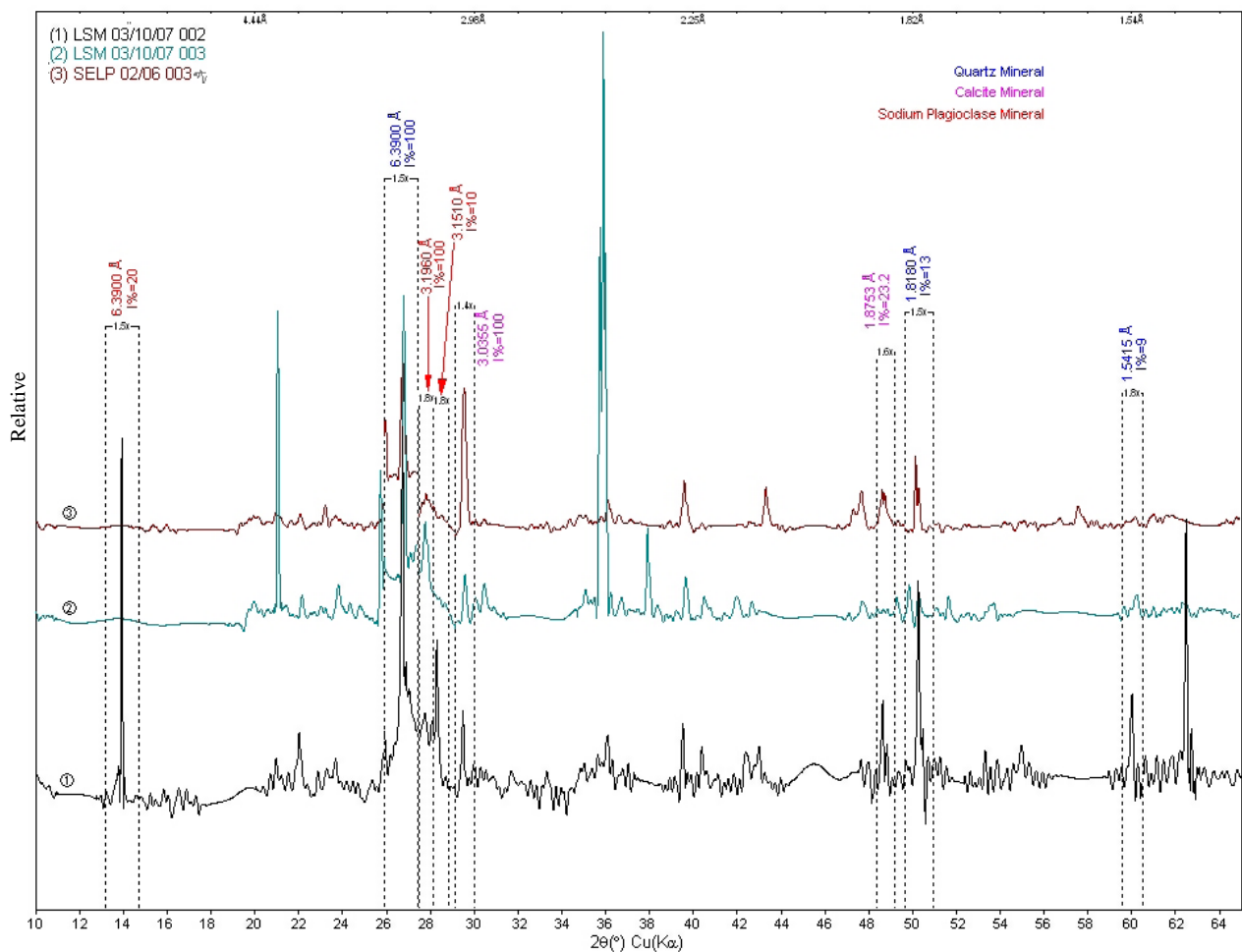


Figure 7.33 – Quartz + Calcite + Sodium Plagioclase overlaid powder diffraction patterns.

A total of 3 overlaid powder diffraction scans collected from the Chihuahuan Desert MEX region on a RIGAKU MiniFlex II X-ray diffractometer using $\text{Cu-K}\alpha$ radiation at 30 Kv and 15 mA with a Kb filter. LSM 002 selected as primary pattern noted with number 1, meaning a soil sample with mixed crystallinity: few narrow and sharp Bragg reflections with $\text{K}\alpha_1/\text{K}\alpha_2$ doublets partly resolved at $2\theta \cong 27^\circ$, $2\theta \cong 29^\circ$, and $2\theta \cong 13^\circ$ for quartz, calcite and sodium plagioclase, respectively.

7.2.2.22 Quartz + Calcite + Sodium Plagioclase 2θ peak matching chart

2θ peak matching chart was made by scattered plotting the difference between the 2θ peaks- from those of the overlaid patterns peaks-values. Peak search study comprised a total of 29 peaks. These peak values were statistically analyzed to obtain match affinity between them. Bragg reflection comparison results were extensively stand among each other with a fluctuated values degree range $-0.2^{\circ} < 0.0^{\circ} < 0.5^{\circ}$ signifying important differences in the stepsize of the scan patterns when comparing them against each other. Major discrepancies in the stepsize resulted from the patterns from the Chihuahuan Desert MEX region (Fig. 7.34).

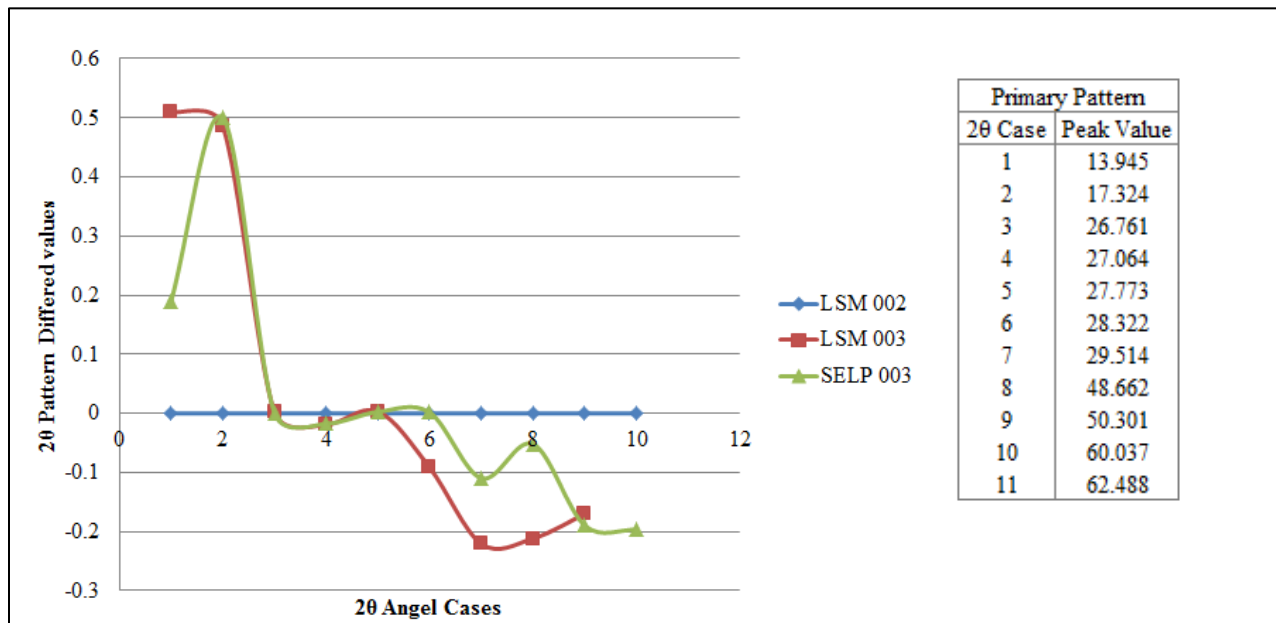


Figure 7.34 – Quartz + Calcite + Sodium Plagioclase 2θ peak matching in overlaid patterns.

Peak search 2θ difference values comparison for quartz + calcite + sodium plagioclase scan patterns. 11 Bragg reflections from the primary pattern LSM 002 specimen produced a certain unequal matching overlaid scans.

7.2.2.23 Pattern overlays 3D view for quartz + calcite + sodium plagioclase

3D views of overlaid patterns presented the quartz + calcite + sodium plagioclase scans of soil samples from the Chihuahuan Desert MEX region. Bragg reflections with high intensities that appeared in the Peak ID Report (Appendix A.6), were also noticeable in the 3D view of the three soil specimens with quartz + calcite + sodium plagioclase chemical composition at different richness concentrations. A total of 3, 2 as well as 3 high intensity peaks were indicated in the 3D chart for quartz, calcite and sodium plagioclase, in that order (Fig. 7.35).

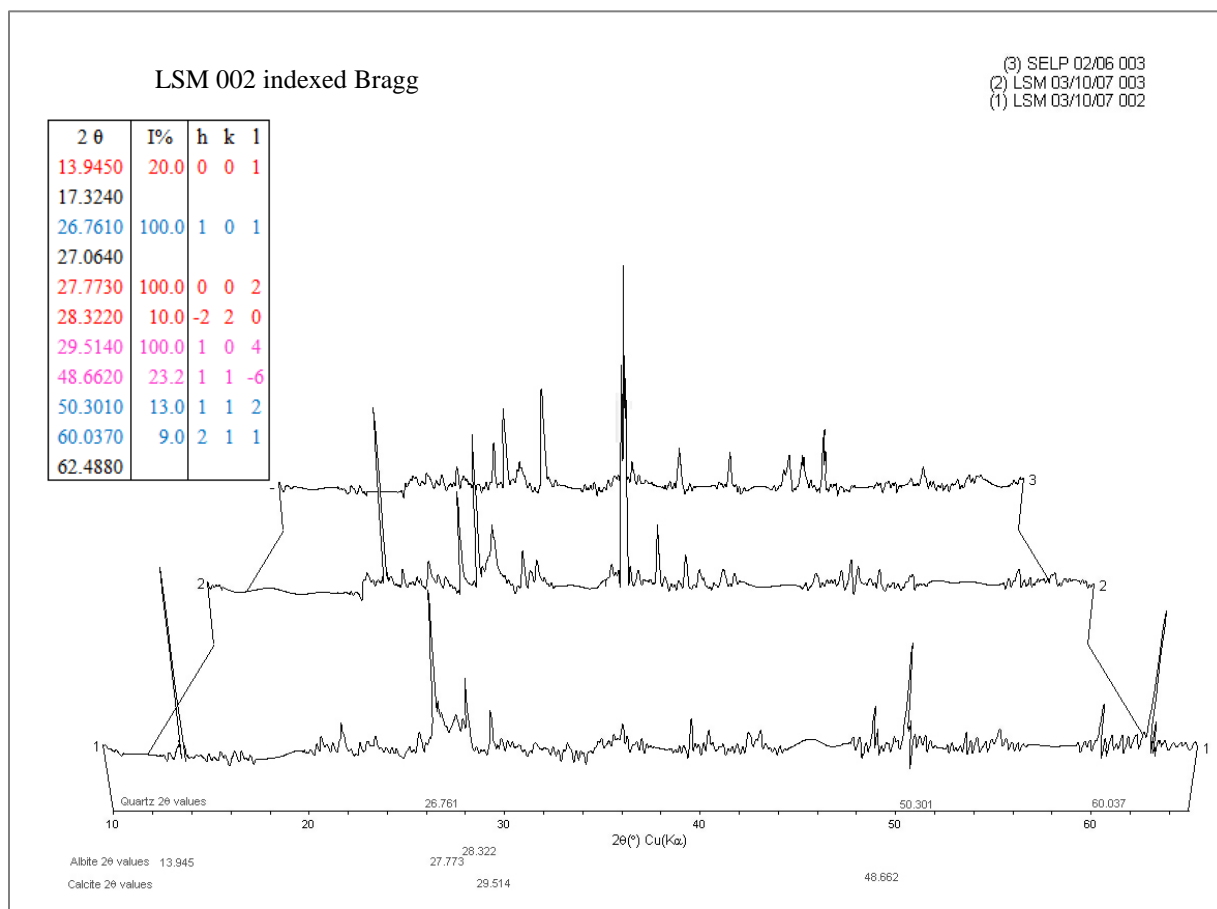


Figure 7.35 – 3D view of quartz + calcite m. + sodium plagioclase XRD patterns with major high peaks.

7.2.2.24 2D contour plots for quartz + calcite + sodium plagioclase

2D contour plots with a based square-root intensity at Y axis scale $\text{SQR}(I)$, amplified visibility of fragile peaks and completed stepsize affinity of 3D overlays by inspecting their coloring peak intensities. After inspecting the 2D contour plot, uneven stepsize of the quartz + calcite + sodium plagioclase patterns resulted with poor sameness between peak intensity color lines (Fig. 7.36).

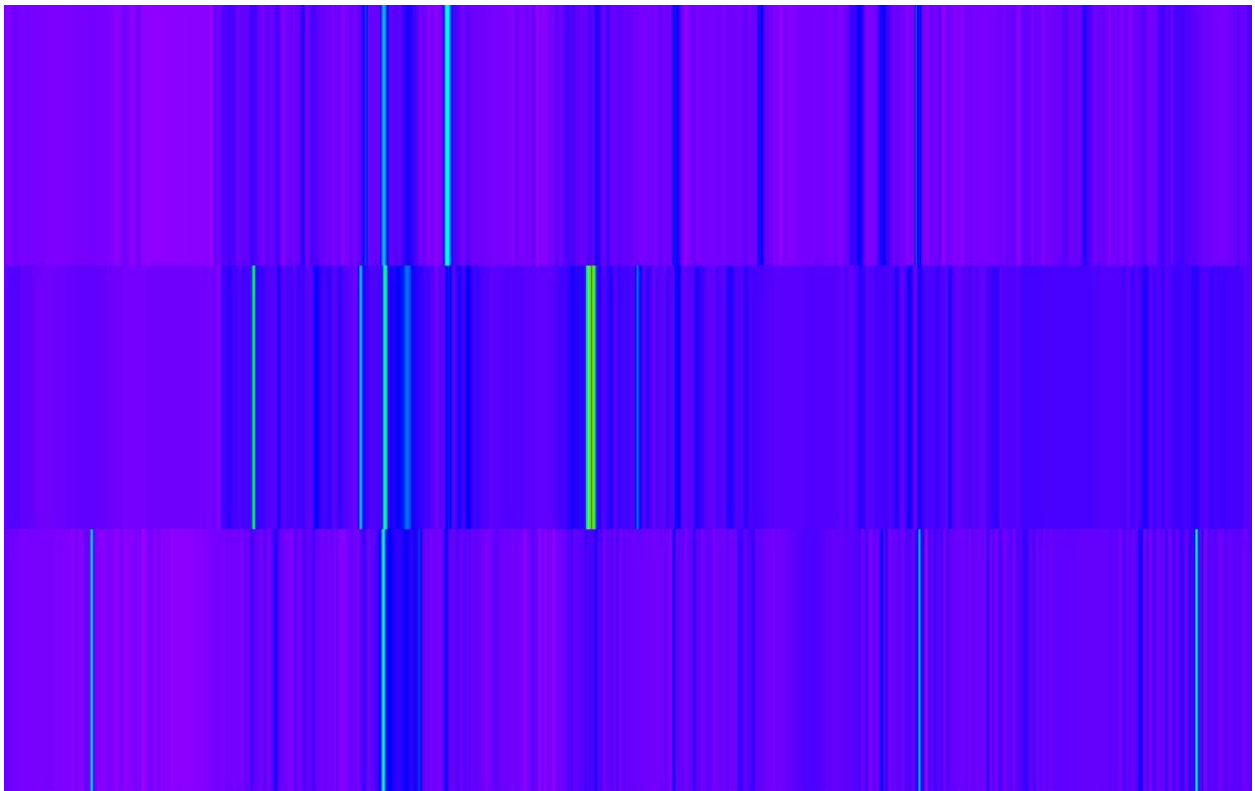


Figure 7.36 – 2D contour plot of 3D quartz + calcite + sodium plagioclase overlaid scans.

Chapter 8

Inductively Coupled Plasma Optical Emission Spectrometry (ICP-OES)

The study covers a specific purpose of chemical element characterization of fugitive dust sources in the two regions: west Texas and eastern New Mexico (the Southern High Plains region) (SHP), and northern Chihuahua, southern New Mexico and far west Texas (the Chihuahuan Desert region) (CHD). It is stated that the majority of the airborne particulate matter (PM) is classified firstly as inorganic in nature that arises for naturally occurring dust storms and secondly from anthropogenic origin. Therefore unprotected surfaces and materials including trace elements of anthropogenic origin are considered sources of particulate matter (PM) in both the SHP and the CHD regions.

Elemental characterization was initially performed from 72 bulk soil samples, from sites where dust storms originated and were detected from satellite in the Southern High Plains (west Texas and eastern New Mexico). Furthermore the specific goal of elemental analysis in potential dust sources could explain the linkage between these dust producing sites and those of the Chihuahuan Desert region when finishing descriptive statistical exploration (maximums and minimums, as well as multivariate analyses, that is, principal component- and cluster-analysis). A total of 20 elements with concentrations in parts per million [ppm] were detected with Inductively Coupled Plasma Optical Emission Spectrometry (ICP-OES) analysis completion, from which target metals Arsenic (As), Copper (Cu), and Lead (Pb) were included in order to assess anthropogenic perturbation of soil samples relative to dust sources.

A geographical analysis was fulfilled to propose spatial representations of political boundaries, land use-, and soil name-classifications for each soil site that was sampled. In

addition, latitude and longitude coordinates were obtained by the use of a global positioning system (GPS.) Table 8.6 summarizes the Geographic Information System (GIS) data used for mapping dust sources that were under ICP-OES analyses, mapped with ESRI ArcGIS ArcMap version 10.1. The UTM Zone 13, NAD83 projection was used to create an overlay of maps to select soil texture, soil name, and land class types associated with each site. Land class and its description was included for discovering possible associations between data and soil texture types as well as data and land class types. The location, soil texture-, and land class-types, as well as the soil name with a brief description to every single site are condensed in Table 8.6.

8.1 Metallic Characterization

A total of 39 elements with concentrations in ppm were found for the bulk of 56 selected dust source samples from the Southern High Plains (SHP) region (the Chihuahuan Desert region was not included in this chemical analysis). The detected elements that resulted after analyzing the samples via Inductively Coupled Plasma Optical Emission Spectrometry (ICP-OES) included Ag, Al, As, B, Ba, Be, Ca, Cd, Co, Cr, Cs, Cu, Fe, Ga, Ge, K, Li, Mg, Mn, Mo, Na, Nb, Ni, P, Pb, Rb, Re, S, Se, Si, Sr, Ta, Ti, Tl, U, V, W, Zn and Zr. Of these, Ag, B, Be, Cd, Co, Li, Mo, Na, Nb, Ni, Re, S, Se, Ta, Tl, U, V, W, and Zn were not considered in the database because of the lack of values above the detection limit. Likewise, both samples S(7) 7 and S(44) 33 were not included in statistics analyses due to their blank results from ICP-OES analysis. Table 8.7 includes the elemental concentrations resulting from ICP-OES analysis on the soils.

8.1.1 Relationships among standardized values of elemental concentrations and soil textures

Standardized value ranges were calculated for each element by applying the difference between the maximum and minimum standardized values through all sample soils belonging to the same soil texture class. As well, the range values for each element were linked amongst soil texture classes to obtain possible links between the elemental standardized concentrations and the soil texture classes. Specifically, high value for a specific texture class may indicate major impacts from anthropogenic or natural sources, whereas weak natural or anthropogenic effect may result from a continuous pattern of range values thru all texture classes.

Concentration values obtained from Inductively Coupled Plasma Optical Emission Spectrometry (ICP-OES) examination were standardized (Z) by calculating the mean (\bar{X}) and the standard deviation ($\sigma_{\bar{X}}$) for each variable- and metal-concentrations through all soil samples sites, by using the following formula:

$$Z = \frac{(X - \bar{X})}{\sigma_{\bar{X}}}$$

As simple, it is relevant to say that high Z values may denote the presence of a substantial source for the variables and/or element at that site.

Table 8.1 – Relationships among elemental concentrations and sites.

Element	Highest Z			Range of Z values for soil texture					
	Value	Site	Sample	Clay Loam	Loam	Loamy Sand	Sandy Loam	Silt Loam	Silty Clay Loam
Al	3.00	36	S(41) 30	0.61	1.98	0.22	0.01	1.78	2.85
As	2.28	25	S(29) 25	-0.37	0.22	0.27	1.00	0.29	-0.35
Ba	3.62	22	S(26) 22	1.98	1.47	0.16	0.13	2.02	1.91
Ca	3.89	66	S(76) 60	3.89	0.42	-0.13	0.57	1.27	2.88
Cr	3.38	36	S(41) 30	-0.64	0.54	0.10	0.05	1.25	1.01
Cs	3.60	22	S(26) 22	1.95	1.42	0.19	0.15	1.98	1.98
Cu	2.47	42	S(48) 36	0.55	0.21	0.21	1.13	0.78	0.42
Fe	2.88	36	S(41) 30	0.80	2.06	0.15	0.09	1.76	2.79
Ga	2.16	6	S(6) 6	0.14	-0.13	0.36	1.10	0.55	0.00
Ge	2.02	34	S(38) 71	-0.83	0.64	0.33	-0.59	-0.27	-0.43
K	2.83	52	S(59) 46	0.73	1.95	0.17	0.18	1.76	2.83
Mg	6.69	66	S(76) 60	6.69	0.55	-0.05	0.35	0.76	1.25
Mn	3.42	40	S(45) 34	0.93	1.76	0.03	0.07	2.05	2.53
P	3.33	36	S(41) 30	1.60	0.67	0.16	-0.04	2.01	3.16
Pb	2.09	3	S(2) 3	-0.84	-0.25	0.35	1.09	0.25	-0.40
Rb	3.24	36	S(41) 30	0.36	2.20	0.16	-0.44	1.43	1.87
Sr	4.23	66	S(76) 60	4.23	-0.10	0.01	0.58	0.02	0.17
Si	1.93	34	S(38) 71	-1.45	-0.10	0.27	-0.60	-0.49	-0.96
Ti	3.39	40	S(45) 34	0.14	1.70	0.24	0.01	1.93	2.13
Zr	2.76	40	S(45) 34	-1.05	0.47	0.19	-0.71	0.90	-0.02

The results included in the first 4 columns of Table 8.1 above show that: (1) Al, Cr, Fe, P, and Rb had their maximum value at site S(41) 30 with a geomorphic surface classified as loess and with the land use class categorized as farm (irrigated/non-irrigated) that covered more than 75% of the entire site area. (1) Laser diffraction analysis results for S(41) 30 dust source showed that silt loam was the corresponding soil texture at this particular site. However, highest standardized values for Aluminum (2.85, 1.98, and 1.78) and Iron (2.79, 2.06, and 1.76) were found on silty clay loam, loam, and silty loam soil textures correspondingly. Uppermost standardized values for Rubidium (2.20, 1.87, and 1.43) were observed on loam, silty clay loam, and silt loam soil textures. Phosphorous (3.16, and 2.01) top standardized values were perceived on silty clay loam and silt loam textures. Lastly, Chromium highest standardized value (1.25) was found at the silt loam soil class. Hence silty clay loam, silt loam and loam soil textures

comprised the soil texture types found on both irrigated/non-irrigated farm and mixed land use categories. Yet, Cr is known to be a hazardous air pollutant, suggesting that anthropogenic perturbations of soils within the region could be the cause that Cr appeared on regular basis in this loess area. (2) Peak values for Ca, Mg, and Sr occurred at site S(76) 60 located in a Aeolian Sand sheet with no fine or very fine texture geomorphic class, and this area was classified as rangeland mostly although irrigated farmland activity was observed. Consequently, these two anthropogenic land uses covered more than 50% the area. Nonetheless grassland and Randall clay playas were also observed where naturally occurring weathering physical processes may have intrinsically influenced the concentration values determined on these three metals. Particle size analysis results confirmed that clay loam texture was the soil class concentrated in this region. (3) The highest values for Mn, Ti, Zr arose at site S(45) 34 with a geomorphic classification defined as loess surface, prevailing a mixed land class region where farmland, rangeland, urban, and rural development, comprised this mixed land site that covered a total of 50% at most within the entire region. Here, particle size analysis stated that silty loam was the soil texture on this mixed area. Furthermore, Mn (2.53, 2.05, and 1.76) and Ti (2.13, 1.93, and 1.70) highest standardized values were found in silty clay loam, silt loam, and loam soil textures which origin came from rangeland-, farmland-, and urban/rural-activities whereas Zr (0.90) top standardized values was concentrated on the silt loam soil texture located in irrigated/non-irrigated farmland, rangeland, and rural development. Furthermore Mn is considered a hazardous air pollutant implying that soil could be anthropogenically perturbed in this region. (4) Ba and Cs showed their maximum value at site S(26) 22, a non-irrigated farmland activity that covered more than 75% of the site. In this area with a geomorphic surface defined as Aeolian Sand Sheet with not fine or very fine textures, rural development outside of main city/town as well as

rangeland and non-saline playas were observed. Silt loam texture was the soil class resulted from laser diffractometry for this area, with a maximum standardized values on both Barium (2.02) and Cesium (1.98), respectively. (5) Ge and Si highest concentration values resulted from site S(38) 71, an irrigated farmland with a 75% or more of activity coverage which surface was geomorphic classified as an Aeolian Sand Sheet with not fine or very fine textures. Rural development was observed where oil and gas facilities were present. Germanium highly standardized values were present on both loam (0.64) and loamy sand (0.33) soil textures while Silicon top standardized value (0.27) was found in loamy sand soil texture, the same texture resulted after particle laser diffractometry analysis completion. (6) Anthropogenic metals As (1.00), Cu (1.13), and Pb (1.09) high standardized values resulted from dust samples S(29) 25, S(48) 36, and S(2) 3 accordingly. Irrigated farmland areas with a 75% or more coverage of this land activity with a geomorphic surface of Aeolian Sand Sheet with not fine or very fine textures, suggested that these elements could result from an anthropogenic disturbance on the soil from these sites. Furthermore, the results from laser diffractometry analysis on these soil sources pointed out that both sandy loam and sandy soil textures may have been anthropogenically contaminated. As, Cu, and Pb uppermost standardized values originated in rangeland and mixed land classes, where farmland, rangeland, urban, and rural development comprised the mixed land site, covering around 50% at most the entire sites. It also was observed that the site where As was found, not only oil but also dry farmland were noticed. Cu related-site was comprised as a mix of irrigated farmland, rangeland, and rural development with apparent oil development. Pb high standardized concentration prevailed from sites showing the presence of farmhouses and center pivot irrigation. (7) K was highly valued (2.83) at site S(59) 46 in a geomorphic Aeolian Sand Sheet surface with not fine or very fine textures which mixed

activities (farmland, rangeland, urban, or rural development) were observed on 50% the entire site. Particle size analysis provided high values of K on the silty clay loam soil texture. Non-irrigated farmlands and rangeland as well as non-irrigated farmlands turning to rangeland, were observed within the site.

8.1.2 Discussions

Statistical analysis results of Table 8.1 may infer the following: (1) The range values of As, Cu, Ga, and Pb through all soil texture classes were inconsistent and reach their peak values in the sandy loam texture class inferring that anthropogenic interference may be the cause for at least three elements associated within this texture class: as mentioned before, As was found in a site where not only oil but also degraded farmland were observed and noticed; Cu was associated with a site that involved a mix of irrigated farmland, rangeland, and rural development with oil development residues; Pb was obtained from a site surrounded by farmhouses where center pivots were present. Ga on the contrary, may be an element whose presence originated due to naturally occurring processes instead of those caused by anthropogenic activities. However, the site where Ga high standardized concentration was obtained came from an irrigated farmland area suggesting that the absence of anthropogenic influences may not be classified as null for this element in particular. (2) Al, Fe, K, Mn, P and Ti obtained their high range standardized values that fitted the silty clay loam texture class. Al, Fe, and P site samplings came from rangeland with grass, Randall Clay playas, and farmhouses present. Mn and Ti site samplings were taken in both irrigated- and non-irrigated-farmland. Rangeland and non-irrigated farmland moving into rangeland was the area where K site sampling had the top standardized concentration value. However, natural geologic processes suggest the origin of these elements, through their presence

in clay minerals. (3) The highest concentration range values through all sample soils of the same texture class were obtained on Ca, Mg, and Sr in soils with the clay loam texture. This result supported the fact that weathering is highly active and constant within the region and forms calcareous soils. Moreover, notice that the particular site S(76) 60 embraced the peak standardized concentration values of these three elements in discussion. For this case in particular, irrigated farmland activity was observed in the area. (4) Ba, Cr, Cs, and Zr concentration values matched on the silt loam soil texture. Three different sites provided the top values of these elements: site S(26) 22 for Ba and Cs, site S(41) 30 for Cr, and site S(45) 34 for Zr. Three of these samples were taken in non-irrigated farmland, while the site S(41) 30 was in a mixed land, where farmland, rangeland, urban or rural development were all perceived at the site. As indicated before, Cr is classified as hazardous air pollutant. Then the presence of range, rural development and non-saline playas could represent natural and/or anthropogenic influences that impacted directly onto the element concentration values. (5) Ge and Rb highest values were found in the loam soil texture class. These two elements are considered as trace elements. Naturally occurring geological processes or anthropogenic intrusion either could cause their origin due to the small concentration value obtained after ICP-OES analysis completion. Correspondingly, the presence of rural development outside of main city/town along with rangeland with farmhouses observed on the sites where Ge and Rb highest concentrations values were found inferred that anthropogenic disturbance could be a source in impacting these elements in discussion. (6) Si top value fitted among the loamy sand soil texture. Top standardized concentration value of Si was the only result that fitted the loamy sand texture. Si origin came mostly from geologic naturally occurring materials characterized as the Blackwater Draw formation.

8.2 Relationship between standardized values of elemental concentrations and land use classes

Before determining relationships between elemental concentrations and land use classes, land use classification had to be created by following the methodology attached below:

1. Historical imagery of a date closest to the date of the dust event observed was obtained by using Google Earth (version 5.0).
2. Latitude (N) and longitude (W) values of dust events were included into the “Fly To” window in Google Earth allowing the software to complete the zoom-in process. This command execution attained imagery fairly centered on the coordinates.
3. The location of dust events were zoomed at a scale of 750 meters. A perfect zoom scale was achieved by manipulating Google Earth software until the scale could read as “750m” \pm 1 meter; causing to represent an approximate 1:10,000 scale and 4 square miles (or 4 sections.)
4. Geomorphology of the scaled location was then identified by using the geomorphic classification and modifier codes below (Table 8.2) in accordance with the B. L. Allen soils map.
5. Noticeable landscape features and/or structures (draws, dairies, etc.) were included to better describe the area.

6. Land use classes were then generated by using both the classification and modifier codes above, and after combining these two codes among the landscape descriptions. Hence, a series of unique land use classes were then established. Ultimately, 16 land use classes were defined by following this methodology, and they are named as 5cv, 5cw3, 5cx, 5dx, 6ax, 6bu, 6bv, 6bw1, 6bw2, 6bw3, 6bx, 7v, 7w3, x, z, and Unknown (Unk.) Table 8.3 describes the land use classes mentioned above which were considered to analyze the relationship between elemental concentrations and land uses classes.

Once the land use classifications were determined the analysis of the relationship between elemental and land use classes was accomplished.

8.2.1 Discussions

As with the soil texture categories procedure development, standardized value ranges were calculated for each element by calculating the difference between the maximum and minimum standardized values through all soil samples pertaining to the same land use class. Moreover, the standardized ranges of each element were associated amongst land use classes to acquire likely links between the elemental standardized concentrations and the land use classes. Clearly, a high range value for a specific land use class might refer major impacts from anthropogenic or natural sources, whereas small natural or anthropogenic effect may result from a variable pattern with small range values for all land use classes. From observing Table 8.4, highest standardized values were found in 4 out of 16 land uses classes: 6bv (mixed), 6bw1 (irrigated farmland), 6bw2 (non-irrigated farmland), and 6bx (rangeland.) The results of this analysis confirmed the logical assumptions regarding to anthropogenic interference. Precisely, it can be inferred that (1) Al, Cr, Fe, P, Rb, Mn, Ti and K were more prone to be highly present in

soil samples taken from sites which had a mixed activity classification (farmland, rangeland, urban, or rural development). (2) As, Cu, Ga, Ge, Pb, and Si top standardized concentration values were found on sites where irrigated farmland activity was developed. It is imperative to mention that the group of metals generated directly from anthropogenic disruption fitted this land class: As, Cu, and Pb. (3) Non-irrigated farmland land class comprised the uppermost standardized values for Ba, Cs, and Zr suggesting both natural and/or anthropogenic impacts. (4) Ca, Mg, and Sr maximum standardized concentration values were originated on sites proceeding from rangeland areas where not only grassland but also Randall clay playas shaped this land class. Natural geologic processes appeared to be the sources of these elements.

Quick reference between standardized elemental concentrations on both soil texture categories and land use classes with their top standardized values are shown in Table 8.5.

Table 8.2 – Geomorphology of Southern High Plains dust events soil samples.

Geomorphic Classification	Geomorphic Modifier	Description
1 Playa	b Ephemeral	Not Randall clay playas; salt lakes
	c Dry (Consolidated)	
	d Dry (Non-consolidated)	
	e Dry (no lacustrine material exposed)	
2 Duricrust (Caliche)		
5 Alluvial	c Unarmoured, incised	e.g., arroyos and draws
	d Unarmoured, unincised	e.g., Pecos River
6 Aeolian Sand	a Dune	Visible on imagery or known
	b Sheet	Not fine or very fine textures
7 Loess		

Land-use Classification	Land-use Modifier	Description
u Unknown Use		Indeterminate land-use
v Mixed Use		No more than 50% w, x, y, or z
w Farmland (> 50%)	1 Irrigated	> 75% of w coverage
	2 Non-irrigated	> 75% of w coverage
	3 Mixed Irrigated / Non-irrigated	No more than 75% of 1 or 2
x Rangeland (> 50%)		Grassland, CRP, and Randall clay Playas
y Urban (> 50%)		Commercial, residential, industrial in city
z Rural Developed (> 50%)		Development outside of main city/town

Table 8.3 – Land use classes for Southern High Plains dust events soil samples.

Class	Geomorphic Classification	Geomorphic Modifier	Description	Land-use Classification	Land-use Modifier	Description
1bx	Playa	Ephemeral	Salt lakes	Rangeland (>50%)		Grassland, CRP, and Randall clay playas
5cv	Alluvial	Unarmoured, incised	e.g., arroyos and draws	Mixed use		
5cw3	Alluvial	Unarmoured, incised	e.g., arroyos and draws	Farmland (> 50%)	Mixed Irrigated/Non irrigated	No more than 75% of irrigated/non irrigated
5cx	Alluvial	Unarmoured, incised	e.g., arroyos and draws	Rangeland (>50%)		Grassland, CRP, and Randall clay playas
5dx	Alluvial	Unarmoured, unincised	e.g., Pecos River	Rangeland (>50%)		Grassland, CRP, and Randall clay playas
6ax	Aeolian Sand	Dune	Visible on imagery or known	Rangeland (>50%)		Grassland, CRP, and Randall clay playas
6bu	Aeolian Sand	Sheet	Not fine or very fine textures	Unknown use		Indeterminate land-use
6bv	Aeolian Sand	Sheet	Not fine or very fine textures	Mixed use		Nor more than 50% of farmland, rangeland, urban, or rural development
6bw1	Aeolian Sand	Sheet	Not fine or very fine textures	Farmland (>50%)	Irrigated	>75% of farmland coverage
6bw2	Aeolian Sand	Sheet	Not fine or very fine textures	Farmland (>50%)	Non-irrigated	>75% of farmland coverage
6bw3	Aeolian Sand	Sheet	Not fine or very fine textures	Farmland (>50%)	Mixed Irrigated/Non irrigated	No more than 75% of irrigated/non irrigated
6bx	Aeolian Sand	Sheet	Not fine or very fine textures	Rangeland (>50%)		Grassland, CRP, and Randall clay playas
7v	Loess			Mixed use		Nor more than 50% of farmland, rangeland, urban, or rural development
7w3	Loess			Farmland (>50%)	Mixed Irrigated/Non irrigated	No more than 75% of irrigated/non irrigated
v	Mixed used					No more than 50% w, x, y, or z
x				Rangeland (>50%)		Grassland, CRP, and Randall clay playas
z				Rural developed (>50%)		Development outside of main city/town
Unk						

Table 8.4 – Relationships among elemental concentrations values and land use classes.

Element	Highest Z			Range of Z values for land use															
	Value	Site	Sample	5cv	5cw3	5cx	5dx	6ax	6bu	6bv	6bw1	6bw2	6bw3	6bx	7v	7w3	x	z	Unk
Al	3.00	36	S(41) 30	0.56	1.58	2.19	0.94	-0.93	-1.18	4.39	3.04	2.01	0.79	1.64	2.98	3.00	2.19	1.82	-1.09
As	2.28	25	S(29) 25	1.63	1.72	1.13	-1.22	1.88	-0.85	2.45	6.14	3.00	2.27	3.09	-0.06	-0.09	0.65	0.47	1.70
Ba	3.62	22	S(26) 22	0.62	1.52	1.53	0.54	-0.02	-1.40	3.90	2.93	4.71	0.62	3.12	2.43	2.15	3.04	2.19	-0.72
Ca	3.89	66	S(76) 60	1.17	1.82	-0.11	2.49	-0.08	-0.61	3.49	1.59	3.14	0.46	4.47	-0.45	-0.19	1.98	3.12	-0.46
Cr	3.38	36	S(41) 30	0.72	0.87	1.03	0.01	-0.03	-0.62	3.85	3.48	3.36	0.50	2.66	2.17	3.38	3.57	0.67	-0.30
Cs	3.60	22	S(26) 22	0.66	1.50	1.49	0.53	-0.01	-1.33	4.04	3.27	4.63	0.59	3.04	2.34	2.03	3.00	2.10	-0.70
Cu	2.47	42	S(48) 36	1.62	1.91	1.92	0.02	1.05	-0.67	3.66	4.67	2.86	1.85	2.51	0.72	0.10	1.27	1.02	1.07
Fe	2.88	36	S(41) 30	0.62	1.68	2.35	0.94	-1.12	-1.20	4.36	3.70	2.15	0.83	1.92	2.82	2.88	2.24	1.86	-1.03
Ga	2.16	6	S(6) 6	1.86	2.09	2.16	-0.38	1.68	-0.74	2.58	3.05	2.63	2.18	2.70	0.05	-0.01	0.45	0.36	1.50
Ge	2.02	34	S(38) 71	-0.32	-0.85	-0.78	-0.83	-0.73	-0.41	2.58	7.77	2.58	1.57	1.54	0.40	0.65	1.55	0.62	0.28
K	2.83	52	S(59) 46	0.77	1.82	2.48	0.99	-0.92	-1.30	4.49	3.68	2.35	0.85	1.73	2.77	2.70	2.18	1.86	-0.87
Mg	6.69	66	S(76) 60	0.42	1.41	0.64	1.42	-0.32	-0.62	2.38	2.03	1.57	0.10	7.26	0.36	0.58	1.32	1.83	-0.57
Mn	3.42	40	S(45) 34	0.55	2.01	2.96	1.61	-0.94	-1.02	3.62	2.00	1.73	0.92	1.80	3.42	2.86	2.37	1.38	-0.96
P	3.33	36	S(41) 30	0.26	1.79	2.81	2.77	-0.77	-0.75	4.17	2.44	2.05	0.45	2.40	1.74	3.33	2.07	1.10	-0.94
Pb	2.09	3	S(2) 3	1.76	1.60	1.89	-0.65	1.99	-0.84	2.90	3.56	2.54	2.08	2.92	-0.33	-0.20	0.41	0.28	1.84
Rb	3.24	36	S(41) 30	-0.15	0.45	1.11	0.47	-1.57	-0.98	4.10	2.26	1.44	1.36	1.74	2.86	3.24	2.59	1.76	-1.57
Sr	4.23	66	S(76) 60	-0.15	-0.08	-0.14	0.46	-0.25	-0.49	2.23	1.07	1.04	0.05	4.71	-0.21	-0.14	2.53	4.22	-0.43
Si	1.93	34	S(38) 71	-0.39	-0.98	-0.74	-1.37	-0.72	-1.01	2.92	5.68	5.49	1.67	2.41	0.43	0.35	4.87	1.32	0.11
Ti	3.39	40	S(45) 34	0.80	1.55	2.29	1.15	-1.10	-1.27	3.77	3.28	2.50	0.95	1.54	3.39	2.61	2.59	1.64	-0.93
Zr	2.76	40	S(45) 34	-0.69	-0.71	-0.31	0.03	-1.21	-1.32	3.02	3.12	3.44	0.59	2.08	2.76	1.57	2.82	0.60	-1.32

Table 8.5 – Complete relationship between elemental concentrations on both, soil texture types and land use classes.

Element	Highest Z			Range of Z values for soil texture						Range of Z values for land use			
	Value	Site	Sample	Clay Loam	Loam	Loamy Sand	Sandy Loam	Silt Loam	Silty Clay Loam	6bv	6bw1	6bw2	6bx
Al	3.00	36	S(41) 30	0.61	1.98	0.22	0.01	1.78	2.85	4.39	3.04	2.01	1.64
As	2.28	25	S(29) 25	-0.37	0.22	0.27	1.00	0.29	-0.35	2.45	6.14	3.00	3.09
Ba	3.62	22	S(26) 22	1.98	1.47	0.16	0.13	2.02	1.91	3.90	2.93	4.71	3.12
Ca	3.89	66	S(76) 60	3.89	0.42	-0.13	0.57	1.27	2.88	3.49	1.59	3.14	4.47
Cr	3.38	36	S(41) 30	-0.64	0.54	0.10	0.05	1.25	1.01	3.85	3.48	3.36	2.66
Cs	3.60	22	S(26) 22	1.95	1.42	0.19	0.15	1.98	1.98	4.04	3.27	4.63	3.04
Cu	2.47	42	S(48) 36	0.55	0.21	0.21	1.13	0.78	0.42	3.66	4.67	2.86	2.51
Fe	2.88	36	S(41) 30	0.80	2.06	0.15	0.09	1.76	2.79	4.36	3.70	2.15	1.92
Ga	2.16	6	S(6) 6	0.14	-0.13	0.36	1.10	0.55	0.00	2.58	3.05	2.63	2.70
Ge	2.02	34	S(38) 71	-0.83	0.64	0.33	-0.59	-0.27	-0.43	2.58	7.77	2.58	1.54
K	2.83	52	S(59) 46	0.73	1.95	0.17	0.18	1.76	2.83	4.49	3.68	2.35	1.73
Mg	6.69	66	S(76) 60	6.69	0.55	-0.05	0.35	0.76	1.25	2.38	2.03	1.57	7.26
Mn	3.42	40	S(45) 34	0.93	1.76	0.03	0.07	2.05	2.53	3.62	2.00	1.73	1.80
P	3.33	36	S(41) 30	1.60	0.67	0.16	-0.04	2.01	3.16	4.17	2.44	2.05	2.40
Pb	2.09	3	S(2) 3	-0.84	-0.25	0.35	1.09	0.25	-0.40	2.90	3.56	2.54	2.92
Rb	3.24	36	S(41) 30	0.36	2.20	0.16	-0.44	1.43	1.87	4.10	2.26	1.44	1.74
Sr	4.23	66	S(76) 60	4.23	-0.10	0.01	0.58	0.02	0.17	2.23	1.07	1.04	4.71
Si	1.93	34	S(38) 71	-1.45	-0.10	0.27	-0.60	-0.49	-0.96	2.92	5.68	5.49	2.41
Ti	3.39	40	S(45) 34	0.14	1.70	0.24	0.01	1.93	2.13	3.77	3.28	2.50	1.54
Zr	2.76	40	S(45) 34	-1.05	0.47	0.19	-0.71	0.90	-0.02	3.02	3.12	3.44	2.08

Table 8.6 – GIS overlay analysis and sampling site characteristics. The Southern High Plains region.

Site	State	Latitude	Longitude	Soil Texture	Soil Name	Land Class	Land Description	Geomor	Sample	Site Description
1 As	TX	32.6318	-102.2610	Sand	Patricia	6bw2	Farm (N Irr)	AS	S(0) 1	Playas present; dryland only
2 As	TX	33.6623	-102.5190	Loamy Sand	Amarillo	6bw3	Farm (Irr/N Irr)	AS	S(1) 2	Oil, playas, farmhouses present
3 As	TX	34.2500	-102.5920	Sandy Loam	Portales	6bv	Mixed	AS	S(2) 3	Center pivots, farmhouse present
4 As	TX	33.6070	-102.1580	Sandy Loam	Acuff	6bw2	Farm (N Irr)	AS	S(3) 4	Black-and-white image; unclear
5 As	NM	32.0467	-103.5810	Sand	Midessa	6ax	Range	AS	S(4) 5	x only
6 Al	NM	33.2477	-104.4910	Loam	Bigetty	5cx	Range	AL	S(6) 6	None
7 As	NM	34.3690	-103.2640	Loamy Sand	Amarillo	6bw1	Farm (Irr)	AS	S(7) 7	Town, playas, CAFO present
8 As	TX	32.9821	-102.4220	Sand	Patricia	6bw1	Farm (Irr)	AS	S(9) 8	None
9 As	NM	34.1047	-103.2020	Loamy Sand	Church	6bx	Range	AS	S(10) 9	Dryland farms, farmhouses, draw present
10 As	NM	33.0586	-104.1700	Sandy Loam	Sotim	6bx	Range	AS	S(12) 10	Oil present
11 Al	NM	33.6363	-104.5340	Sandy Loam	Ector	5cv	Mixed	AL	S(13) 11	Draw system; dryland farms, center pivots present
12 Lo	NM	33.6080	-103.1340	Sand	Maljama	7v	Mixed	LO	S(14) 12	Oil patch; range present; dryland farms present
13 As	TX	34.0683	-102.2650	Sand	Springer	6bw1	Farm (Irr)	AS	S(15) 13	Playa, Range and dryland farms present
14 As	TX	33.0165	-102.6440	Sand	Patricia	6bv	Mixed	AS	S(17) 14	Oil, dryland/irrigated mix present
15 Al	NM	33.6419	-104.5500	Silt Loam	Glendale	5cw3	Farm (Irr/N Irr)	AL	S(18) 15	Floodplain farm; farmhouses, center pivot, irrigated non-center pivot present
16 As	TX	33.5200	-102.6790	Sand	Amarillo	6bv	Mixed	AS	S(19) 16	Range, oil, center pivot, non-saline playa present
17 As	TX	32.7372	-102.0940	Sand	Amarillo	6bw2	Farm (N Irr)	AS	S(20) 17	Range, non-saline playas present
18 As	TX	33.4750	-101.8780	Sandy Loam	Acuff	6bw1	Farm (Irr)	AS	S(21) 18	Outskirts of Lubbock; z, non-saline playas, dryland farms, stockyard, landfill present
19 As	NM	34.6266	-103.5860	Loamy Sand	Spantara	6bx	Range	AS	S(22) 19	Dryland farms present
20 As	NM	33.8994	-103.5520	Loamy Sand	Clovis	6bx	Range	AS	S(23) 20	Ranch houses, non-saline playas present
21 As	TX	32.7990	-101.9600	Sand	Amarillo	6bw1	Farm (Irr)	AS	S(25) 21	Non-saline playas, farmhouses present
22 As	TX	31.7164	-101.5420	Silt Loam	Reagan	6bw2	Farm (N Irr)	AS	S(26) 22	Range, z, non-saline playas present
23 As	TX	32.2482	-101.5140	Sand	Potter	6bx	Range	AS	S(27) 23	w (dryland), y (Big Spring), reservoir, creek present
24 As	TX	32.2756	-101.5060	Sand	Amarillo	6bv	Mixed	AS	S(28) 24	w (dryland), y (Big Spring), range present
25 As	TX	32.2827	-101.6430	Sandy Loam	Springer	6bx	Range	AS	S(29) 25	Oil, w (dryland) present
26 As	TX	32.2863	-101.7970	Loamy Sand	Portales	6bw2	Farm (N Irr)	AS	S(30) 26	Range, non-saline playa present
27 As	TX	32.4430	-101.7800	Sand	Amarillo	6bv	Mixed	AS	S(31) 27	Non-saline playas, farmhouses present
28 As	TX	32.4433	-101.8590	Sand	Amarillo	6bv	Mixed	AS	S(32) 28	Range, canyon, non-saline playas present
29 As	TX	31.9127	-101.9650	Loamy Sand	Reeves	6bx	Range	AS	S(33) 29	Draw, dryland farms, non-saline playas, z present
30 As	NM	33.2751	-104.4230	Loamy Sand	Reagan	6bx	Range	AS	S(34) 67	No description was available
31 As	TX	33.3068	-102.3870	Sand	Amarillo	6bw1	Farm (Irr)	AS	S(35) 68	No description was available
32 As	TX	32.7620	-102.0680	Sand	Amarillo	6bw2	Farm (N Irr)	AS	S(36) 69	Non-saline playas present
33 As	TX	32.5479	-102.9090	Sand	Berda	6bx	Range	AS	S(37) 70	Dryland farm present; CAFO present; draw present
34 As	TX	32.7834	-102.9440	Loamy Sand	Simona	6bw1	Farm (Irr)	AS	S(38) 71	z present (oil and gas facility)
35 As	TX	32.9547	-102.6580	Sand	Brownfield	6bw1	Farm (Irr)	AS	S(39) 72	non-saline playas present
36 Lo	TX	34.7415	-102.4120	Silt Loam	Pullman	7w3	Farm (Irr/N Irr)	LO	S(41) 30	x, farmhouses present
37 As	TX	33.7683	-102.9700	Sand	Amarillo	6bw2	Farm (N Irr)	AS	S(42) 31	w1, x, z (rural community) present
38 As	TX	33.7314	-102.9010	Sand	Amarillo	6bv	Range	AS	S(43) 32	w1, w2, x, and farmhouses
39 Lo	TX	35.2920	-101.6550	Silt Loam	Pullman	7v	Mixed	LO	S(44) 33	w1, w2, x, z, (rural residential), lake, non-saline playa
40 Lo	TX	35.1567	-101.9730	Silt Loam	Pantex	7v	Mixed	LO	S(45) 34	w1, w2, x
41 As	TX	32.5900	-102.3050	Sand	Brownfield	6bx	Range	AS	S(47) 35	w2 present
42 As	TX	32.9360	-102.9110	Sand	Brownfield	6bv	Mixed	AS	S(48) 36	mix of w1, x, and z (oil)
43 As	TX	32.8743	-102.7500	Sand	Patricia	6bw1	Farm (Irr)	AS	S(49) 37	w1, x, z (oil) present
44 As	NM	34.2544	-103.6660	Sand	Amarillo	6bx	Range	AS	S(50) 38	x only

Table 8.6 (Cont.) – GIS overlay analysis and sampling site characteristics. The Southern High Plains region.

Site	State	Latitude	Longitude	Soil Texture	Soil Name	Land Class	Land Description	Geomor	Sample	Site Description
45 As	TX	32.6843	-101.7140	Sand	Pep	6bx	Range	AS	S(51) 39	Edge of Caprock; w1, w2, z (oil) present
46 As	TX	32.6311	-101.7420	Loamy Sand	Amarillo	6bw2	Farm (N Irr)	AS	S(52) 40	Terraced w2, x, z (oil), non-saline playas, farmhouses present
47 As	TX	32.5310	-102.1670	Loamy Sand	Gomes	6bw2	Farm (N Irr)	AS	S(53) 41	No description was available
48 As	TX	32.8380	-101.8250	Sand	Hindman	6bx	Range	AS	S(54) 42	No description was available
49 As	TX	31.8300	-101.5950	Silt Loam	Reagan	6bw2	Farm (N Irr)	AS	S(55) 43	No description was available
50 As	TX	33.0530	-102.5620	Sand	Amarillo	6bv	Mixed	AS	S(56) 44	No description was available
51 As	TX	32.6161	-102.2990	Sand	Patricia	6bw2	Farm (N Irr)	AS	S(57) 45	x present
52 As	TX	31.6988	-101.4230	Silty Clay Loam	Reagan	6bv	Mixed	AS	S(59) 46	x, w2; looks like some fields were w2 but are turning into x
53 As	TX	33.7059	-101.6540	Loam	Portales	6bv	Mixed	AS	S(61) 47	w1, w2, x, playas present
54 As	TX	32.2033	-101.9970	Loamy Sand	Amarillo	6bw2	Farm (N Irr)	AS	S(62) 48	Oil pumpjacks (z); playas; x present
55 As	TX	33.6091	-102.6380	Sand	Amarillo	6bv	Mixed	AS	S(63) 49	x, w1, w2, z (rural res. And oil); non-saline playas present
56 As	TX	33.7102	-102.3530	Sand	Amarillo	6bw2	Farm (N Irr)	AS	S(64) 50	w2, x, non-saline playa present
57 As	TX	33.7780	-102.3970	Sand	Arvana	6bx	Range	AS	S(65) 51	w1, w2, non-saline playas present
58 As	TX	33.2652	-101.9740	Sand	Abilene	6bw3	Farm (Irr)	AS	S(66) 52	x, non-saline playa, draw present
59 As	TX	33.2938	-102.2650	Sand	Amarillo	6bw2	Farm (N Irr)	AS	S(67) 53	w1, x, non-saline playas present
60 As	TX	32.5640	-102.6410	Sand	Arvana	6bw1	Farm (Irr)	AS	S(68) 54	No description was available
61 As	TX	33.5702	-102.8870	Loamy Sand	Amarillo	6bx	Range	AS	S(71) 55	w2, z (oil) present
62 As	NM	34.4506	-103.2750	Sandy Loam	Abilene	6bw3	Farm (Irr/N Irr)	AS	S(72) 56	x, z (rural res.), non-saline playa present
63 As	TX	32.9563	-102.9440	Sand	Patricia	6bw1	Farm (Irr)	AS	S(73) 57	w2, x, z (rural res.) present
64 As	NM	34.0401	-103.4000	Loamy Sand	Amarillo	6bw2	Farm (N Irr)	AS	S(74) 58	~40% x
65 As	NM	34.2757	-103.6040	Sand	Amarillo	6bw1	Farm (Irr)	AS	S(75) 59	w2, x, z (rural res.) present
66 As	TX	33.8110	-102.9820	Clay Loam	Arch	6bx	Range	AS	S(76) 60	w1 present
67 Al	NM	32.7248	-104.3090	Silt Loam	Arno	5dx	Range	AL	S(77) 61	Pecos River; x only
68 As	TX	34.0347	-102.4540	Loamy Sand	Olton	6bw1	Farm (Irr)	AS	S(78) 62	w1, x, z (CAFO and rural res.), non-saline playas present
69 As	TX	32.3405	-101.8550	Loamy Sand	Amarillo	6bw2	Farm (N Irr)	AS	S(79) 63	w2 only
70 As	TX	33.0758	-103.0570	Loamy Sand	Portales	6bw1	Farm (Irr)	AS	S(80) 64	w2, x, z (rural res.) present
71 As	TX	33.1531	-102.9690	Sand	Brownfield	6bw1	Farm (Irr)	AS	S(81) 65	w2, x, z (rural res.) present
72 As	TX	33.3220	-102.8230	Sand	Patricia	6bw2	Farm (N Irr)	AS	S(82) 66	w1, x (~40%) present

Table 8.7 – Metallic concentrations (ppm) on Southern High Plains dust sources. ICP-OES analysis results

Site	Al	As	Ba	Ca	Cr	Cs	Cu	Fe	Ga	Ge	K	Mg	Mn	P	Pb	Rb	Sr	Si	Ti	Zr
S(0)1	37838.08	14.23	364.28	47434.23	39.54	38.07	42.31	14667.01	12.96	75.33	11519.23	10229.74	204.74	419.71	10.08	56.96	410.88	269889.35	2129.24	276.24
S(1)2	24909.00	20.29	211.98	4986.92	25.29	22.60	57.33	10758.65	18.78	61.24	9272.05	2841.90	115.36	338.73	20.51	52.47	57.15	173746.07	1599.23	239.30
S(2)3	20697.05	21.35	314.16	74436.97	31.64	32.13	62.61	7255.74	19.13	59.59	6412.03	14242.16	77.28	402.01	24.37	51.83	846.17	168011.31	1191.25	200.22
S(3)4	11616.76	12.92	77.08	331.25	20.98	10.96	31.74	4275.89	11.93	68.63	2430.97	944.34	10.46	237.52	7.23	53.04	6.87	183852.48	721.87	130.47
S(4)5	15037.75	22.92	257.87	17794.23	28.57	27.25	57.12	4769.65	19.02	65.39	4257.06	2662.53	20.30	234.44	23.74	51.38	97.93	203292.06	848.23	138.37
S(6)6	57871.20	20.17	461.52	16868.16	42.12	45.79	69.97	25104.00	20.41	64.79	20768.57	8165.37	533.53	862.80	23.21	58.89	138.87	201960.80	3401.01	203.66
S(9)8	25143.82	14.06	174.23	1174.86	30.18	20.16	34.99	10200.77	12.53	69.67	7778.73	2204.54	68.37	320.49	8.84	54.11	28.92	243925.80	1487.33	250.27
S(10)9	23530.93	22.43	245.91	5306.34	26.22	25.97	60.49	8354.38	19.20	70.59	1712.90	2881.52	87.27	297.88	24.31	53.19	64.46	258167.15	1402.15	175.99
S(12)10	31277.63	22.67	342.75	13311.88	29.68	34.74	72.92	12968.23	19.45	71.99	10860.53	4441.37	181.23	373.16	22.58	54.80	82.26	256848.96	1702.18	127.63
S(13)11	35530.42	22.00	342.19	59142.19	38.15	35.57	65.45	15006.07	19.56	69.57	12492.15	6900.04	216.22	416.03	22.41	55.37	135.05	225492.76	2278.01	176.28
S(14)12	12862.93	22.25	166.79	5381.04	25.16	18.77	57.44	5292.64	18.51	75.75	4505.31	1233.69	18.15	204.81	22.90	51.38	29.25	258541.81	978.63	130.81
S(15)13	27041.25	12.72	217.38	1773.24	27.63	24.06	34.07	9800.06	12.63	82.42	7150.42	2517.02	111.51	304.44	9.49	56.53	36.24	318818.89	1583.86	257.92
S(17)14	14290.32	12.38	110.37	1659.11	12.90	13.73	31.39	6540.11	11.57	64.63	5354.08	1334.30	38.02	223.31	7.46	50.45	17.76	219984.99	1162.00	291.12
S(18)15	49584.63	22.33	460.55	80672.99	40.09	45.95	69.85	21176.64	20.24	64.13	17578.70	12547.29	408.69	683.81	21.48	57.04	159.01	185528.10	2846.55	174.40
S(19)16	25761.18	14.78	163.95	970.47	51.72	19.42	28.13	9472.94	12.73	83.64	6856.92	1940.53	70.37	261.65	9.29	56.47	22.92	326022.43	1344.84	193.09
S(20)17	15523.65	12.77	130.30	2100.79	15.57	15.84	32.57	5783.85	11.78	67.35	3962.27	1708.91	59.15	257.31	7.33	53.61	22.15	243627.53	997.40	183.60
S(21)18	42093.95	22.53	361.15	18008.35	44.58	36.83	69.03	21703.44	19.41	69.62	17832.38	4447.91	263.05	457.85	23.78	56.75	99.12	248209.39	2520.90	216.37
S(22)19	28394.46	20.36	279.13	3438.33	27.16	29.14	60.50	11402.03	19.32	69.75	9685.02	2039.43	123.95	307.74	22.82	53.87	44.09	237724.43	1845.41	211.56
S(23)20	34052.93	22.29	316.71	4727.05	36.63	32.40	63.70	14344.33	19.87	76.70	11931.02	2588.74	163.62	331.08	22.51	55.47	52.45	273190.97	2160.01	222.34
S(25)21	237.24			4697.08					10.49	13.60		181.98		218.07	3.02	58.11		148.35	49.45	46.16
S(26)22	40368.64	23.79	736.05	104608.26	36.43	71.92	67.38	17291.37	19.49	64.78	14364.09	6140.80	255.98	582.48	22.14	55.94	207.13	187562.01	2666.32	229.47
S(27)23	6243.60	23.96	55.29	4784.86	21.06	8.74	57.79	2073.96	18.44	71.42	1833.52	1497.44		179.75	21.02	49.87	60.89	236178.64	463.24	84.10
S(28)24	6672.84	16.57		430.04	0.70	1.87	23.89	2140.32	11.77	65.47	696.67	640.78		296.08	7.66	53.82		138438.63	440.31	131.11
S(29)25	22743.98	24.38	242.91	107932.81	23.62	25.93	68.51	9179.43	19.49	65.59	7453.29	11955.03	133.52	306.48	20.96	53.68	1664.65	168164.94	1325.83	99.53
S(30)26	27134.76	15.73	244.48	7055.38	27.00	26.11	29.99	10667.53	12.97	80.36	7724.89	3021.39	121.25	291.26	9.98	57.26	55.87	333978.70	1738.44	264.64
S(31)27	25535.17	13.78	251.01	15859.08	27.36	26.63	29.47	9605.83	12.82	77.52	6803.97	4475.99	119.06	325.50	8.39	57.85	973.32	313489.98	1712.47	296.42
S(32)28	33309.66	15.17	268.81	5437.06	34.16	28.35	29.73	12133.26	12.93	81.86	8948.70	3081.01	96.30	298.28	9.79	58.53	56.85	329088.93	1719.10	293.63
S(33)29	14605.41	21.17	227.46	67355.11	14.24	24.47	63.52	4810.45	18.37	74.59	3901.09	3198.61	39.32	255.48	21.51	52.63	1556.34	265316.81	1000.21	146.11
S(34)67	27849.32	14.20	246.82	3039.21	22.85	26.00	30.79	12014.49	12.68	74.72	9016.63	2536.52	138.22	340.80	8.25	56.69	46.38	279373.65	1920.57	336.55
S(35)68	21101.00	13.69	177.36	9976.00	17.72	20.21	25.45	8650.89	11.91	78.64	6274.78	2290.24	61.44	271.72	9.88	55.45	37.07	326193.77	1366.85	276.02
S(36)69	12708.18	14.24	119.07	2535.82	7.63	14.65	25.13	4705.14	12.41	75.56	2961.63	1461.22	27.99	221.33	10.13	54.21	27.37	291020.47	780.20	168.70
S(37)70	26670.35	13.77	253.93	15948.94	27.82	27.66	30.52	9688.57	12.40	80.19	7020.70	4523.96	121.17	312.63	8.94	57.30	977.78	315363.45	1728.50	297.27
S(38)71	33656.22	15.69	274.70	4925.20	34.70	29.97	37.14	14015.32	13.28	93.69	10591.05	3657.53	126.69	646.98	11.19	58.32	58.12	380575.59	1954.24	272.79
S(39)72	20567.98	14.93	133.28	721.31	28.89	16.11	26.62	8376.39	12.59	85.63	5834.62	1885.65	39.69	276.96	9.36	55.77	23.16	343752.76	1221.16	206.90
S(41)30	69017.80	15.70	542.46	14213.80	72.33	52.48	43.14	28248.34	14.08	79.62	21826.80	7828.77	520.35	955.49	10.97	64.89	136.98	274807.87	3646.87	340.02
S(42)31	27927.16	15.90	235.68	6379.76	35.82	25.09	30.86	12722.38	12.78	91.35	9438.30	2433.33	131.96	304.52	11.07	57.35	32.22	367572.98	2107.00	417.93
S(43)32	24549.62	13.54	165.49	1537.44	50.01	18.79	25.37	11760.78	12.08	79.91	8664.76	2070.50	94.92	243.00	9.82	55.99	24.76	318871.49	1918.76	350.00
S(45)34	68782.82	15.79	579.83	5661.21	56.79	56.33	52.26	27875.53	14.25	76.96	22162.36	6548.85	594.16	675.50	10.25	63.82	111.76	280028.94	4235.11	426.75
S(47)35	16700.36	14.37	110.62	1116.43	35.84	13.87	26.67	6048.96	11.97	79.88	4020.67	1218.01	29.74	228.98	8.13	54.44	11.89	308168.64	1020.13	221.05
S(48)36	23595.52	13.56	207.85	3534.34	40.04	22.85	78.01	9064.89	12.60	86.22	6520.12	1816.95	77.78	191.57	11.60	56.71	29.67	334164.26	1539.76	275.63
S(49)37	15781.61	12.90	129.85	5866.39	9.76	15.91	33.73	6524.35	11.96	72.82	4404.97	2146.04	25.26	283.48	9.13	54.19	32.96	287707.46	955.54	179.61
S(50)38	29129.73	11.08	244.92	3356.81	43.04	26.11	35.46	10610.49	12.06	71.36	8582.04	2373.98	136.43	358.28	8.83	54.25	39.39	266681.27	1543.81	210.55
S(51)39	19794.35	14.20	204.31	10577.31	8.92	22.62	34.82	7872.29	12.38	75.02	5605.21	2048.07	92.47	282.63	8.30	54.90	38.47	253163.98	1312.40	279.04
S(52)40	28747.42	15.10	269.62	13238.41	47.21	28.81	37.29	10493.48	12.97	82.75	7664.43	2853.93	116.30	323.51	9.25	56.66	56.79	296763.48	1647.62	243.81
S(53)41	20073.09	14.21	254.06	32005.12	11.53	26.85	37.62	7169.97	12.39	77.23	6052.90	8855.84	79.84	389.93	10.29	52.69	519.49	278641.81	1502.03	277.17
S(54)42	16482.20	12.78	149.02	2332.09	5.93	17.82	33.64	6355.68	11.92	70.49	4307.34	1535.70	59.70	238.91	10.37	54.60	18.63	251932.42	998.60	181.80
S(55)43	45068.85	13.35	500.88	66284.33	35.24	50.56	44.18	18455.72	13.17	70.86	14063.21	7530.08	343.74	588.66	8.43	59.97	199.29	222044.35	2873.87	349.83
S(56)44	18521.64	14.33	102.16	1267.28	18.84	13.47	33.58	8095.03	11.89	67.61	8095.03	1737.51	42.41	225.13	7.96	52.73	12.86	219304.67	1088.49	159.76
S(57)45	16776.35	13.47	135.16	1114.23	22.75	16.10	30.84	6559.79	11.99	68.95	4572.95	1294.21	38.69	235.27	8.73	53.62	15.86	246102.22	1184.79	195.46
S(59)46	67065.26	14.73	511.09	115783.43	41.86	51.84	47.79	27696.17	14.10	68.43	22461.54	11619.60	476.29	925.13	9.80	61.03	255.50	187088.22	3283.55	224.93
S(61)47	55087.23	16.84	452.93	34451.39	35.86	44.88	44.70	23448.30	13.72	79.50	18192.49	7634.20	376.01	487.93	10.68	61.95	151.28	244312.86	2957.39	260.01

Table 8.7 (Cont.) – Metallic concentrations (ppm) on Southern High Plains dust sources. ICP-OES analysis results

Site	Al	As	Ba	Ca	Cr	Cs	Cu	Fe	Ga	Ge	K	Mg	Mn	P	Pb	Rb	Sr	Si	Ti	Zr
S(62) 48	30752.16	14.75	299.43	3854.99	50.66	31.09	31.65	10514.80	12.45	75.81	7782.56	2681.08	114.59	317.16	9.58	57.59	45.81	192068.71	1899.88	270.54
S(63) 49	22983.54	12.81	163.32	1276.75	24.46	18.64	30.28	9189.48	12.15	73.67	6949.81	1817.17	75.55	289.47	9.75	54.74	21.63	231661.61	1356.37	209.25
S(64) 50	23066.91	13.68	211.89	1847.08	29.15	23.03	33.59	9724.96	12.36	72.53	7279.08	1813.62	109.55	260.29	9.04	55.00	27.23		1846.86	316.95
S(65) 51	26053.11	14.80	250.93	2218.98	14.32	26.92	36.08	9380.30	13.21	76.58	7678.56	2365.23	96.35	308.22	9.87	53.44	39.64	272308.46	1518.16	236.06
S(66) 52	20541.69	13.78	182.47	17271.17	22.23	20.98	30.04	7880.70	12.47	77.37	5552.49	2261.27	70.28	262.86	8.37	55.31	59.47	285718.21	1361.72	228.86
S(67) 53	25431.19	15.36	198.83	6473.13	23.39	21.95	29.27	10416.22	12.14	76.83	7815.88	2625.41	89.96	250.36	9.87	56.16	38.44	278122.95	1566.67	265.57
S(68) 54	14972.26	12.41	133.70	1063.38	12.66	15.97	30.39	5331.05	11.84	68.49	3488.04	1312.65	32.37	275.74	8.36	53.63	21.09		919.48	145.08
S(71) 55	37182.58	13.76	257.47	1440.06	35.92	27.84	35.49	14717.82	13.06	73.40	11131.16	2925.96	162.96	299.17	7.97	57.52	43.56	269098.71	1996.76	227.89
S(72) 56	31367.92	11.98	264.32	2228.90	18.89	28.23	37.67	12776.31	12.41	62.59	9659.11	2631.89	190.84	342.63	8.41	56.30	42.13	225769.55	2078.42	271.47
S(73) 57	28119.44	14.35	223.74	2387.96	32.62	24.53	29.84	10752.61	12.08	59.90	8023.37	2680.61	89.35	382.55	7.75	55.75	47.23	107264.70	1503.68	169.52
S(74) 58	34132.77	14.38	253.32	31826.72	31.15	26.86	30.83	13960.40	12.92	75.10	10447.82	3782.05	124.01	412.68	9.94	57.64	55.41	247213.35	1588.33	188.05
S(75) 59	23273.47	15.71	181.22	2937.33	31.55	20.52	30.11	9629.87	12.54	67.28	7309.58	2457.60	61.88	359.49	7.96	54.52	31.42	132412.69	1336.95	142.65
S(76) 60	36215.47	14.66	520.22	148989.41	20.79	51.46	49.71	16049.85	14.53	64.28	12298.08	42663.77	266.17	650.56	7.25	56.79	1799.73	154091.17	1783.83	150.37
S(77) 61	40665.50	11.56	331.79	102942.60	29.13	33.91	41.86	16861.38	13.00	64.33	13543.81	12621.49	356.46	855.92	8.37	57.10	367.28	159322.50	2545.20	228.20
S(78) 62	36327.95	13.36	384.22	53190.82	17.21	40.39	43.86	13706.54	13.13	81.99	10167.20	11736.12	149.85	472.36	9.51	59.59	404.77	285642.70	1922.38	237.85
S(79) 63	31106.87	14.15	270.81	8552.54	25.21	29.38	35.85	12319.43	12.43	76.81	9246.06	3780.86	164.78	348.23	9.58	56.80	63.22	258090.50	2058.96	304.36
S(80) 64	34228.19	17.17	292.12	13968.58	40.14	30.90	33.28	13227.17	13.30	86.63	10024.02	4435.17	157.08	527.56	10.78	58.80	71.04	347453.93	1919.28	254.07
S(81) 65	14808.90	11.45	104.82	587.78	23.45	13.70	33.61	6363.49	11.81	70.11	4426.88	1272.42	28.80	279.05	8.27	53.23	13.67	253154.15	974.67	198.71
S(82) 66	18955.19	16.84	184.11	859.21	26.29	20.87	28.91	6487.33	12.22	84.25	4455.74	1577.57	36.57	274.39	10.04	56.03	21.78	345613.78	1235.06	248.02

Chapter 9

Statistical Analysis

9.1 Cluster Analysis

Cluster analysis was used as a common technique for data analysis; an explorative data mining process which assigns a set of objects into groups (clusters), thus, the values in the same cluster were quite alike. Interactive multi-objective optimization that involved trial and error represented the key for this ordination analysis to enhance the best iterative process, i.e., achieving the desired objective properties by adjusting preprocessing and parameters.

Connectivity base clustering (hierarchical clustering) analysis was used applying Ward's minimum variances method criterion to obtain elemental values being more related to nearby values than those farther away. Ward's criterion minimized the total within-cluster variance by calculating the initial cluster distances which are defined to be the squared Euclidean distance between points: $d_{ij} = d(\{x_i\}, \{x_j\}) = \|x_i - x_j\|^2$. Dendrograms were then developed by taking the Euclidean distance that every single cluster required to connect its values. Euclidean distance represents the geometric distance in the multidimensional space and is the most commonly chosen type of distance, which was computed by using the formula:

$$\text{distance}(x, y) = \left\{ \sum_i (x_i - y_i)^2 \right\}^{1/2}$$

The joining of tree clustering was then computed to obtain the most straightforward way of totaling distances between objects and/or observations in a multi-dimensional space. Eventually, extensive hierarchy of cluster that merged within each other at certain distances was obtained after statistical analysis completion. The resulting clusters exhibited high internal (within-cluster) homogeneity and high external (between-cluster) heterogeneity.

9.1.1 Elemental Concentrations

Using Ward's minimum variances method, a cluster analysis was implemented for the soil elemental concentration values of the Southern High Plains dust sources with Euclidean distances as the criterion in forming the hierarchical clustering connectivity. Here, a total of two particle size data variables (clay, silt), one naturally occurring soil-property variable (total organic carbon, TOC), 20 chemical element concentrations in parts per million [ppm], (Al, As, Ba, Ca, Cr, Cs, Cu, Fe, Ga, Ge, K, Mg, Mn, P, Pb, Rb, Si, Sr, Ti, and Zr), and 30 soil name categories (Abilene, Acuff, Amarillo, Arch, Arno, Arvana, Berda, Bigetty, Brownfield, Church, Clovis, Ector, Glendale, Gomes, Hindman, Maljama, Midessa, Olton, Pantex, Patricia, Pep, Portales, Potter, Pullman, Reagan, Reeves, Simona, Sotim, Spantara, and Springer) that in association with the 13 land use classes (5cv, 5cw3, 5cx, 5dx, 6ax, 6bv, 6bw1, 6bw2, 6bw3, 6bx, 7v, 7w3, and x), as well as the 4 geomorphic/land-use types (Aeolian Sand, Range, Loess, and Alluvial), and the land use categories (Irrigated-, no irrigated-, irrigated/no irrigated-farmland types, as well as Rural, Mixed and Range land use categories) observed in the region, were included in the cluster analysis examination. The results of the different analyses mentioned above comprised a database to explore statistically their relation between each other resulting in linkages to both, the potential-wind erosion of fine grained soils during dust storm events, and natural weathering, soil formation, and geochemical processes.

Henceforward, linked clusters (formed from particle size-, elemental concentration-, soil name-, and source dust site-variables after analysis completion) with appropriate similar (short and large Euclidean) distances were observed by analyzing variance approach convening with Ward's criterion. Figure 9.1 exhibits 5 hierarchical clusters that resulted after using this approach: (1) K-Fe-Al-Ti-Mn-Cs-Ba-P-Silt-Rb-Cr-Mixed-Rural; (2) Pep-Hindman-Berda-

Reeves-Clovis-Spantara-Church-Arch; (3) Olton-Simona-Spring-F(NI)-Brownfield-Arvana-Si-Ge-Zr-Abilene; (4) Pantex-Pullman-Maljama-Potter-Sotim-Portales-F(I)-Reagan-Gomes; and (5) Pb-Ga-As-Cu-Patricia-Acuff-Range-TOC-Ca-Mg-Clay-Sr-Amarillo. Hence, 53 out of 58 variables were fitted successfully into hierarchical clustering connectivity on closer and farther correlation characteristics after explorative data mining process completion. Yet, five variables remained containing the poorest elemental concentration values, which presented no hierarchical clustering relativeness after statistical analysis examination. These were the Midessa, Arno, Bigetty, Glendale, and Ector soils.

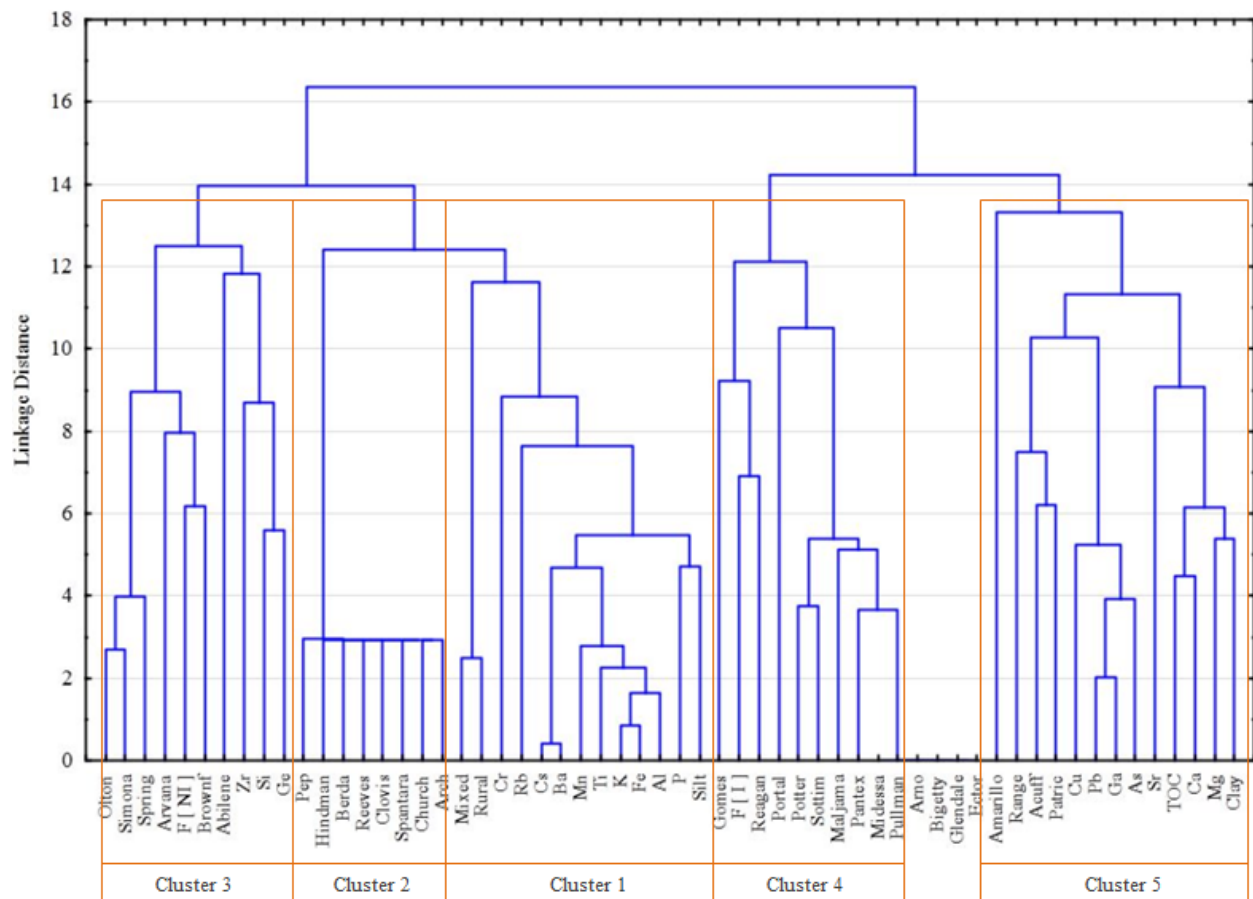


Figure 9.1 – Tree diagram of 58 variables with complete linkage and geometric distance.

Tree Diagram for 58 variables with complete linkage covering, with geometric distance in the multidimensional space. Hierarchical clustering with complete dendograms connectivity divided in 5 Clusters for detailed discussion purposes.

9.1.1.1 Discussions

It was observed that the minimum variances criterion of Cluster 1, the first group which was comprised of K, Fe, Al, Ti, and Mn, exposed perhaps a common source implication for this cluster. After applying Ward's minimum variances analysis, it was perceived also that a second group including Cs, Ba, P, Rb and Cr values maintained an unfairly related linkage resulting from their large Euclidean distances. Cluster 1, however, suggested Rural- besides Mixed-land use activities positioned on silty soils embracing the most likely affinity to the elements mentioned previously.

Ward's analysis of Cluster 5 suggested the existence of a probable affinity among the anthropogenic-related metals Pb, Ga, As, and Cu as well as the naturally occurring elements from calcareous soils Ca and Mg which shaped a strong link between both total organic carbon, TOC, and Clay variables. Furthermore, Range land use class from Cluster 5 (located on Patricia, Acuff, and Amarillo soils), was the principal land use class involving anthropogenic activities that may have been associated with the source of the anthropogenic related metals mentioned above. Furthermore, a like affinity between the concentrations of the elements that formed Cluster 5 could not only probably be related to clay and silt textured soils, which would be prone to aeolian travel across the region (compared to those that comprised the rest of the element concentrations under statistical examination), being carried away in the fine particles fraction emitted from fugitive dust storm sites. Therefore, the elemental concentration from this cluster could have been suspended in the atmosphere long enough to be transported long distances.

Explorative data mining process on Cluster 2 revealed a minimal affinity between Pep, Hindman, Berda, Reeves, Clovis, Spantara, Church, and Arch soils from those of concentration and land use categories enclosed in Cluster 1.

It was noted also from Cluster 4 that Irrigated farmlands F(I), situated on Gomes, Reagan, Portales, Potter, Sotim, Maljama, Pantex, and Pullman soils showed linkage to those of Patricia, Acuff, and Amarillo soils encountered in Cluster 1. However, soils comprising Cluster 4 may be associated within the origin of anthropogenic metals derived from Rangeland as well as Irrigated farmland land use categories.

Also, Non-irrigated farmlands sited on Brownfield, Arvana, Olton, Simona, Springer, and Abilene soils resulted in a weak connectivity base clustering between Zr, Si, and Ge. Yet, soils and elements contained in Cluster 3 resulted with the weakest affinity to those soils and elements contained within Cluster 1.

It was observed, finally, that the hierarchical clustering of group 1 linked with clusters 2, and 3 at higher level implying perhaps a common source for these cluster groups. Similarly, cluster 5 suggested relativeness among group 4 at farther Euclidean distances.

9.1.2 Dust Source Sites

Minimum variances method performed in cluster analysis connectivity was also implemented on the Southern High Plains dust source site soil data using Euclidean distances as the standard in establishing the hierarchical clustering connectivity.

As with elemental concentration analysis, a database was created including the results of the different analyses mentioned in the previous section to search the linkage relative to the potential wind-erosion of soils during dust storm events, in addition to natural weathering, soil formation, and geochemical processes, respectively. Henceforth, linked groups (shaped from particle size-, elemental concentration-, soil name-, and source dust site-variables after analysis finishing points) with like (short and large Euclidean) distances were perceived by variance approach examination agreeing with Ward's criterion. Six hierarchical clusters resulted after performing this methodology: **(1)** S(67) 53 – S(79) 63 – S(74) 58 – S(62) 48 – S(52) 40 – S(42) 31 – S(36) 69 – S(20) 17 – S(64) 50 – S(19) 16 – S(32) 28 – S(31) 27 – S(43) 32 – S(72) 56 – S(66) 52; **(2)** S(82) 66 – S(57) 45 – S(53) 41 – S(30) 26 – S(3) 4 – S(0) 1 – S(48) 36 – S(17) 14 – S(2) 3; **(3)** S(81) 65 – S(39) 72 – S(35) 68 – S(15) 13 – S(73) 57 – S(9) 8 – S(75) 59 – S(49) 37 – S(68) 54 – S(38) 71 – S(80) 64 – S(78) 62 – S(21) 18; **(4)** S(50) 38 – S(71) 55 – S(34) 67 – S(54) 42 – S(51) 39 – S(47) 35 – S(65) 51 – S(22) 19 – S(10) 9 – S(23) 20 – S(33) 29; **(5)** S(56) 44 – S(63) 49 – S(28) 24 – S(27) 23 – S(4) 5 – S(14) 12 – S(1) 2 – S(12) 10 – S(13) 11 – S(29) 25 – S(25) 21; **(6)** S(18) 15 – S(6) 6 – S(77) 61 – S(41) 30 – S(45) 34 – S(26) 22 – S(55) 43 – S(61) 47 – S(59) 46 – S(76) 60. Hence, 70 cases proceeding from Southern High Plains dust source sites fitted into hierarchical clustering connectivity into closer and farther correlation characteristics after an explorative data mining process.

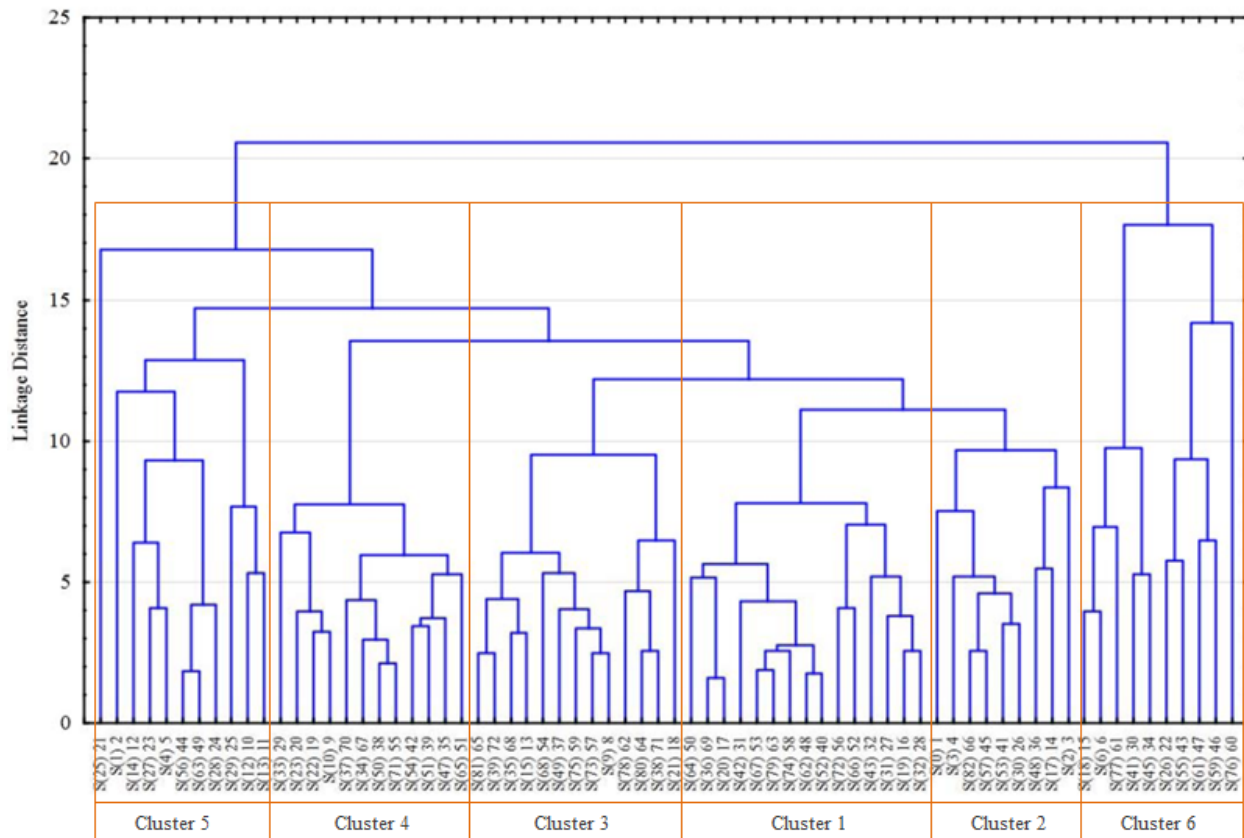


Figure 9.2 – Tree diagram of 70 cases with complete linkage and geometric distance.

Tree Diagram for 70 cases (dust source sites) with complete linkage covering, with geometric distance in the multidimensional space. Hierarchical clustering with complete dendograms connectivity divided in 6 clusters for detailed discussion purposes.

9.1.2.1 Discussions

It was observed from dust source sites statistical analysis, that Cluster 1 comprised 15 dust source sites from which the main characteristic (contained on 10 sites), was Sand soil texture category previously observed from laser diffraction examination results. Likewise, other soil textures pertained to this cluster (including 5 source sites), with Loamy Sand and Sandy Loam soil textures categories that were obtained from Particle Size Distribution analysis. Consequently, 66.7% (10/15), 26.7% (4/15), and 6.6% (1/15) were the percentages calculated for Sand, Loamy Sand, and Sandy Loam soil texture categories, in that particular order. Corresponding soil names were attained by following the U. S. General Soil Map Data criteria. Based on that, Amarillo and Abilene were the soil names that were given to 13, and 2 dust sites of the Southern High Plains region under examination and from which hierarchical clustering connectivity formed Cluster 1. Subsequently, 86.7% (13/15), and 13.3% (2/15) were the percentages totaled for Amarillo and Abilene soil names, respectively. Non-Irrigated farmland activity was the typical land use class enclosed into this group. Mixed, Irrigated-, Irrigated/non-Irrigated-farmland and Rangeland appeared to be the uncharacteristic land use classes included in Cluster 1, however. Therefore, 60% (9/10), 20% (3/15), and 20% (3/15) totaled the percentages for Non-Irrigated, Mixed, as well as Irrigated-, Irrigated/Non Irrigated-farmland, and Range (with 6.66% totaled percentage each) land use classes, correspondingly.

After mapping dust sources sites contained in Cluster 1 using the ESRI ArcGIS ArcMap version 10.1, the majority of the sites shown in this group occurred in the southeast of the Southern High Plains region. Decreasing number of sites occurred from Central to Northeast areas of the region on the map. As expected, Aeolian Sand was the only geomorphic surface observed in the group. See Figure 9.3.

For Cluster 2, the major hierarchical clustering connectivity happened to occur on 5 out of 9 dust source soil locations that pertained to this group. Sand prevailed as the soil texture category for these sites. Similarly, Loamy Sand and Sandy Loam were the soil texture types that resulted to lesser presence in the group (provided from 4 source sites). 55.6% (5/9), 22.2% (2/9), and 22.2% (2/9) were the percentages calculated for Sand, Loamy Sand, and Sandy Loam soil texture categories, respectively. After applying the U. S. General Soil Map Data criteria, Patricia, Portales, Acuff, Brownfield, and Gomes were the soil names that were allotted to 4, 2, and 1 source sites of the Southern High Plains region under investigation and from which hierarchical clustering bounded these sites to Cluster 2. 44.45% (4/9), 22.22% (2/9), and 33.33% (3/9) were the percentages computed for Patricia, and Portales, besides the same percent amount (11.11% each) to Acuff, Brownfield, and Gomes soil textures, correspondingly. Like Cluster 1, Non-Irrigated farmland activity was the main land use class, which in conjunction with Mixed, (appearing to be a regular land use activity), involved the land use classes in this group. As a result, 66.7%, and 33.3% totaled the percentages to both Non-Irrigated Farmland and Mixed land use classes, individually.

Dust source sites included on Cluster 2 were mapped by using the ESRI ArcGIS ArcMap version 10.1. As a result, it was perceived that dust source sites containing this group were observed to be widely spread from the central to the southeast part areas of the Southern High Plains region.

As expected, Aeolian Sand was the only geomorphic surface observed in the group. See Figure 9.3.

An interesting hierarchical clustering connectivity occurred in Cluster 3. Here, the group containing 13 dust source sites from which the unique land use class observed was Irrigated Farm widely spread into a total of 9 soil names, nonetheless. No characteristic soil name groups were possible to detect since the soil name classes were not different in presence among each other.

After categorizing the soil name types by following the U.S. General Soil Map Data criteria, Patricia, Amarillo and Brownfield counted identical site quantities (15.38% each), as well as Acuff with equivalent presence of dust sources related to those of Arvana, Olton, Portales, Simona, and Springer (7.69% each) soil names, computed 23.08% (3/13), 30.76% (4/13) and 46.14% (6/13) total percentages based on 3, 4, and 6 dust source sites, in that particular order. Sand was the main soil texture category for these sites from earlier Laser Diffraction research analysis. Similarly Loamy Sand and Sandy Loam were barely present in the group (comprising 4 dust sites). These texture categories computed, 69.23% (9/13), 23.08% (3/13), and 7.69% (1/13) total percentages for Sand, Loamy Sand, and Sandy Loam soil textures categories.

Dust source sites comprising Cluster 3 were then mapped by using the ESRI ArcGIS ArcMap version 10.1, resulting in a wide spread for the sites within the Central area of the Southern High Plains region.

As expected, Aeolian Sand was the unique geomorphic surface observed in this group. See Figure 9.3.

Hierarchical clustering resulted from Cluster 4 comprised 12 dust source sites from which the sole land use class observed was Range. Nonetheless a total of 11 soil names were detected within this group, however. Like Cluster 3, specific soil name groups were significantly associated with this group.

U. S. General Soil Map Data criterion was followed to categorize soil names. Amarillo was found in 2 source sites, and with one each Arvana, Berda, Brownfield, Church, Clovis, Hindman, Pep, Reagan, Reeves, and Spantara (8.33% each) soil names, resulting in 16.67% (2/12), and 80.33% (10/12) based on 2 and 10 dust source sites, respectively. Loamy Sand and Sand comprised the soil texture categories for this group. Each texture category comprised 6 dust source sites based on earlier data on Particle Size Distribution. Consequently, 50% was computed to each Loamy Sand and Sand soil textures categories.

ESRI ArcGIS ArcMap version 10.1 was used to examine the dust source sites that comprised Cluster 4. Results mapped these sites on the southeast and northwest (New Mexico section), as well as the New Mexico southwest (minimal site presence observed) areas of the Southern High Plains region.

As expected, Aeolian Sand was the unique geomorphic surface observed into this Cluster. See Figure 9.3.

In Cluster 5, highest hierarchical clustering connectivity occurred on 7 out of 11 dust source sites in this group. Sand was the main soil texture category for these dust sites. Similarly, Loamy sand soil texture was regularly observed. 63.64% (7/11), and 36.36% (4/11) represented the totaled percentages for Sand and Loamy Sand soil texture categories. After performing the U. S. General Soil Map Data criteria, Amarillo was found on 5 source sites, with single occurrences of Ector, Maljama, Midessa, Potter, Sotim, and Springer (9.09% each) soil names, which led to 45.45% (5/11), and 54.54% (6/11) calculated percentages based on 5 and 6 dust source sites, accordingly. Mixed and Range land use categories were observed commonly when compared to those of Irrigated farm and Non-Irrigated farm (9.09% each) land use categories, causing these two first land use classes mentioned above to be taken as main for this group (land use activity observance). As a result, 45.45% (5/11), 36.36% (4/11), and 18.18% (2/11) totaled percentages computed on 5, 4, and 2 dust source sites, in that order.

ESRI ArcGIS ArcMap version 10.1 was used to examine the dust source sites comprising Cluster 5. Results plotted these sites in the southeast and central, as well as southwest (New Mexico) areas of the Southern High Plains region.

As expected, Aeolian Sand was the main geomorphic surface observed on this Cluster, but Loess and Alluvial geomorphic surfaces were detected in a single dust source site each, obtaining 81.82% (9/11), 9.09% (1/11), and 9.09% (9/11) totaled percentages for Aeolian Sand, Loess, and Alluvial geomorphic surfaces. See Figure 9.3.

Hierarchical clustering in Cluster 6 comprised 6 out of 10 dust sources sites into this group. Silt Loam was the majority soil texture. Loam, Clay Loam, and Silty Clay Loam soil texture categories appeared on a minor basis. Consequently, 60% (6/10), 20% (2/10), and 40% (4/10) computed the total percentages for Silt Loam, Loam, as well as Clay Loam and Silty Clay Loam (20% each) soil texture categories. After performing the U. S. General Soil Map Data Criteria, Reagan was observed on 3 source sites, as well as single occurrences of Arch, Arno, Bigetty, Glendale, Pantex, Portales, and Pullman (10% each) soil names, which led to 30% (3/10), and 70% (7/10) totaled percentages based on 3, and 7 dust source sites, respectively. Mixed and Range land use categories were observed as well as Irrigated farm and Non-Irrigated farm land use categories. Therefore, this cluster suggested the presence of activities directly related to the four land use categories mentioned above. As a result, 30% (3/10), 30% (3/10), 20% (2/10) and 20% (2/10) calculated percentages were found on 3, 3, 2, and 2 dust sources sites comprised to this group, correspondingly.

ESRI ArcGIS ArcMap version 10.1 plotted the dust source sites of Cluster 6 on the southeast, northeast, and southwest (New Mexico) areas of the Southern High Plains region under investigation.

As expected, Aeolian Sand was the major geomorphic surface observed in this Cluster, Alluvial and Loess geomorphic surfaces were detected on dust sources of this group however, leading to 50% (5/10), 30% (3/10), and 20% (2/10) total percentages for Aolian Sand, Alluvial and Loess geomorphic surfaces. See Figure 9.3.

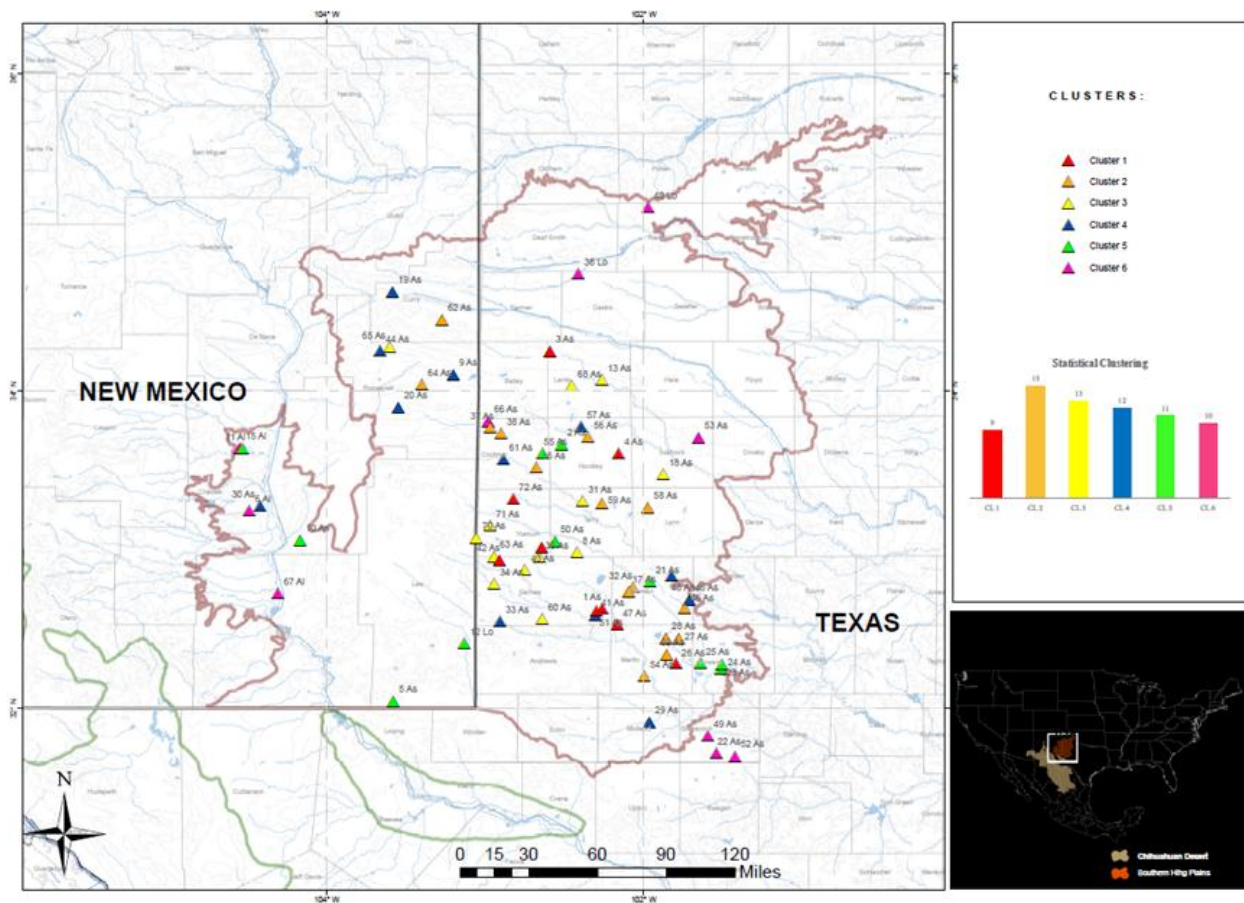


Figure 9.3 – SHP ArcGIS Clustering Map 1.

Southern High Plains region: Geographical Information System Clustering Map. A total of 70 cases plotted into 6 clustering layers resulting from the dust source sites cluster statistical analysis to notice relativeness between site cases and regional area sections.

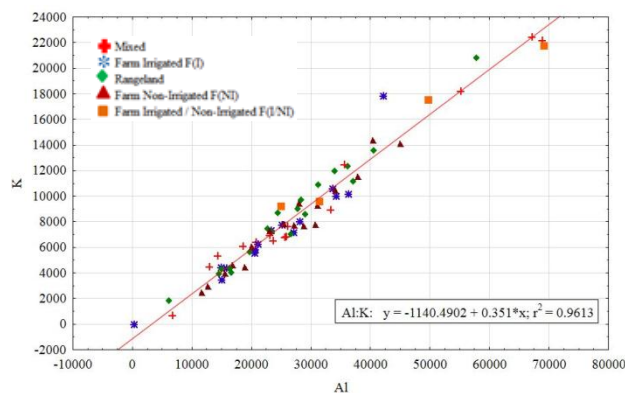
9.1.3 Narrowing Variables

Pearson's correlation coefficient was examined to obtain dependence relationship between two variables (linear correlations observation). Dust Source Sites as well as elemental concentrations were the two variables of this project under study comprising the Cases and Variables matrix for multivariate analysis. That was defined statistically as a (Rows x Column) database spreadsheet equal to (70 x 23). After dividing the covariance of the 2 variables mentioned above by the product of their standard deviations, strength of linear dependence between these two variables were created. By selecting a not only maximum likelihood method with pairwise correlation, but also Pearson's correlation values (p value) of 0.05, 0.001, and 0.0001, significance levels were obtained after completion of multivariate statistical analyses. Table 9.1 shows the correlation coefficients at significance levels.

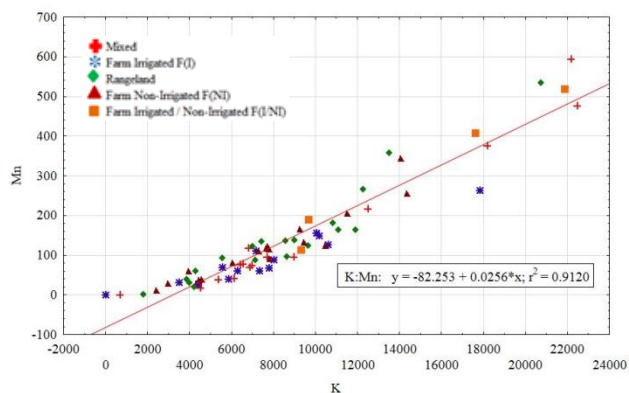
Pearson's correlation statistical analysis specified that correlation coefficient with values of 1 imply that a linear equation have an ideal relationship between (Row x Colum). Therefore, after correlation scrutiny on (Rows x Column) matrix, strong correlation coefficients at (p value) of 0.0001 were found for Al:K, Al:Mn, and Pb:Ga concentrations. 0.9805, 0.9505, and 0.8989, were the correlation coefficient values obtained after computing the two-elemental variable sets mentioned above, correspondingly. Moreover, detailed linear regression scatter plots resulted with r^2 values of 0.9613, 0.9034, and 0.9409 (See Figure 9.4). On the contrary, Si showed sole dependence with Ge, with a correlation value of 0.7723 (See Table 9.10).

Resuming from Pearson's correlation analysis, K, Mn, and Ga concentrations were screened out from the (Row x Column) matrix, but linked to Al because of their strong correlations. Unlike Si, where minor correlation relationships between elemental concentrations

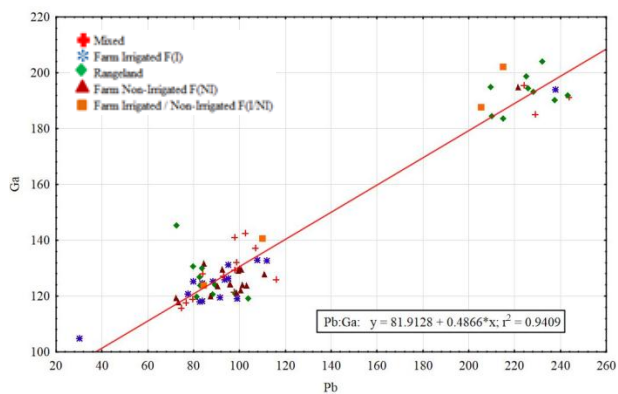
were observed, they were also separated from the database spreadsheet matrix. These 4 elements were not taken into account on the subsequent statistical analysis performed in this project.



4(a) K:Al scatter plot



4(b) K:Mn scatter plot



4(c) Pb:Ga scatter plot

Figure 9.4 – 2D scatter plots of K:Al, K:Mn, and Pb:Ga

4(a) scatter plot of K against Al; (4b) scatter plot of Mn against K; and (4c) scatter plot of Ga against Pb.

9.1.3.1 Discussions after variables reduction

In conclusion, homogeneous well separated subsets were found after hierarchical divisive clustering examination. Each cluster was chosen according to a selection criterion and continued till all clusters comprised single objects. The refined original matrix after correspondence analysis completion determined 54 dependent continuous variables to be examined next by Principal Component Analysis. This polished matrix included two particle size data variables, one naturally occurring soil property variable, sixteen elemental concentrations values, thirty soil name categories, and five land use classes. Figure 9.5 showed 5 dendograms connectivity after performing the minimum variances methodology: **(1)** Fe – Al – Ti – Cs – Ba – P - Silt – Clay – Rb – Cr – Mg – Ca – TOC – Sr; **(2)** Spantara – Reeves – Clovis – Berda – Church – Hindman – Pep; **(3)** Pb – As – Cu – Acuff – Patricia – Range – Mixed – Rural – Amarillo; **(4)** Olton – Simona – Springer – F[Ni] – Arvana – Brownfield – Zr – Ge –Abilene; and **(5)** Sotim – Pullman – Potter – Maljama – Pantex – Portales – F[I] – Reagan – Gomes. Therefore, 48 out of 54 variables resulted with hierarchical clustering connectivity on closer and farther correlation characteristics. Midessa, Arno, Bigetty, Glendale, Ector, and Reeves soils did not show clustering.

In Cluster 1, strong subset connectivity was observed between Fe-Al-Ti-Cs-Ba-P first-elemental group associated to moderate cluster linkage of the Rb-Cr-Mg-Ca-Sr second group including TOC, and Silt and Clay particle size data variables.

Spantara, Reeves, Clovis, Berda, Chuch, Hindman, and Pep soils included on Cluster 2 exposed distant hierarchical connectivity to those from Cluster 4, Olton, Simona, Springer, Arvana, Brownfield, and Abilene. Minimal connectivity was shown between Clusters 1, 2, and 4, from which Non Irrigated Farmland could be considered the main land use class that impacted

the presence of these elements comprised in the different soil names previously mentioned above. Most importantly, Cluster 3 suggested that anthropogenic metals, Cu, Pb, and As may be associated with Range, Rural, and Mixed land use activities located on Patricia, Acuff, and Amarillo soils. After discerning Cluster 5, Irrigated Farmland land use may have provided a source of these anthropogenic metals, especially from Gomes, Reagan, Portales, Maljama, Potter, Sotim and Pullman soils.

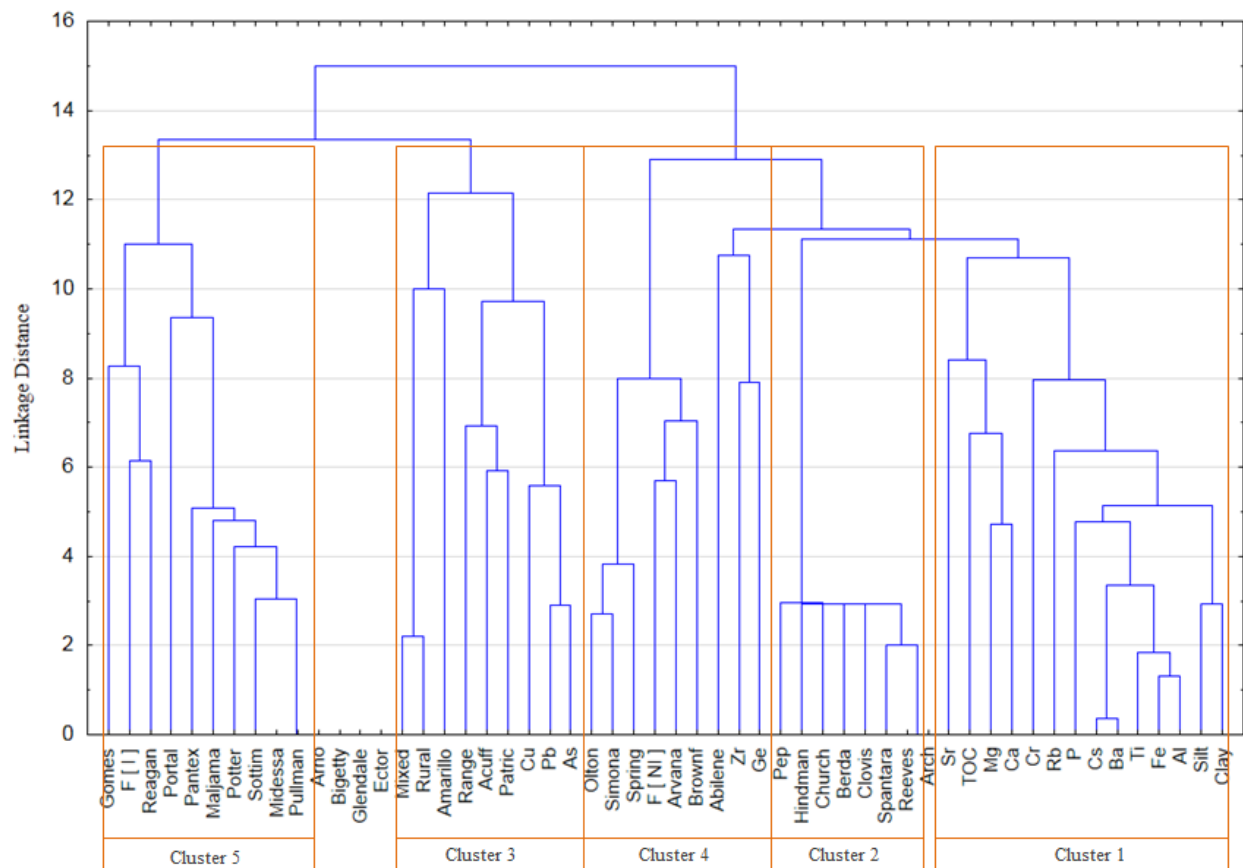


Figure 9.5 – Tree diagram of 54 variables with complete linkage and geometric distance.

9.1.4 Narrowing Cases Observations

Systematic relation between variables was used for data simplification. Correspondence analysis examined two way variables to find size of correspondence between the rows and the columns database spreadsheet. This exploratory data analytic technique shortened complex data and exposed relationships schemed on graphical display of row and column points concentrated in biplots. Therefore, the table of numerical information of the database was transformed into a graphical presentation, in which each row and column was denoted as a point. Because the data matrix of this study was sufficiently large, correspondence analysis aided noticing structural associations among the variables categories (elemental concentrations confined on columns) and cases (dust source sites contained on rows) impossible to observe either by visual scrutiny or simple statistical analysis. Better yet, column and row geometries maintained similar interpretations, easing scrutiny and discovery of relationships. The results of correspondence analysis are presented next on graphs exemplifying the configurations of points in projection planes. From the column graph, Si resulted with undistinguishable profile distribution because of its proximity with the origin. Elements that had similar profiles were perceived on five sets of plotted points sited away from the origin, but close to each other: (1) Pb, Ga, Cu, Rb, and As; (2) Ge, Zr, and Cr; (3) K, Fe, Al, and Ti; (4) P, Ba, and Cs; and (5) Mg and TOC. Some values which did not enhance fundamentally to the inertia of each axis, were virtually undistinguishable from the average profile; confined in this interpretation were Mn, Silt, Clay, Sr, and Ca. (See Figure 9.6). Sets of plotted points situated away from the origin, but close to each other have similar profiles. Pb, Ga, Cu, Rb, and As plotted points as well as K, Fe, Al, and Ti, P, Ba, and Cs.

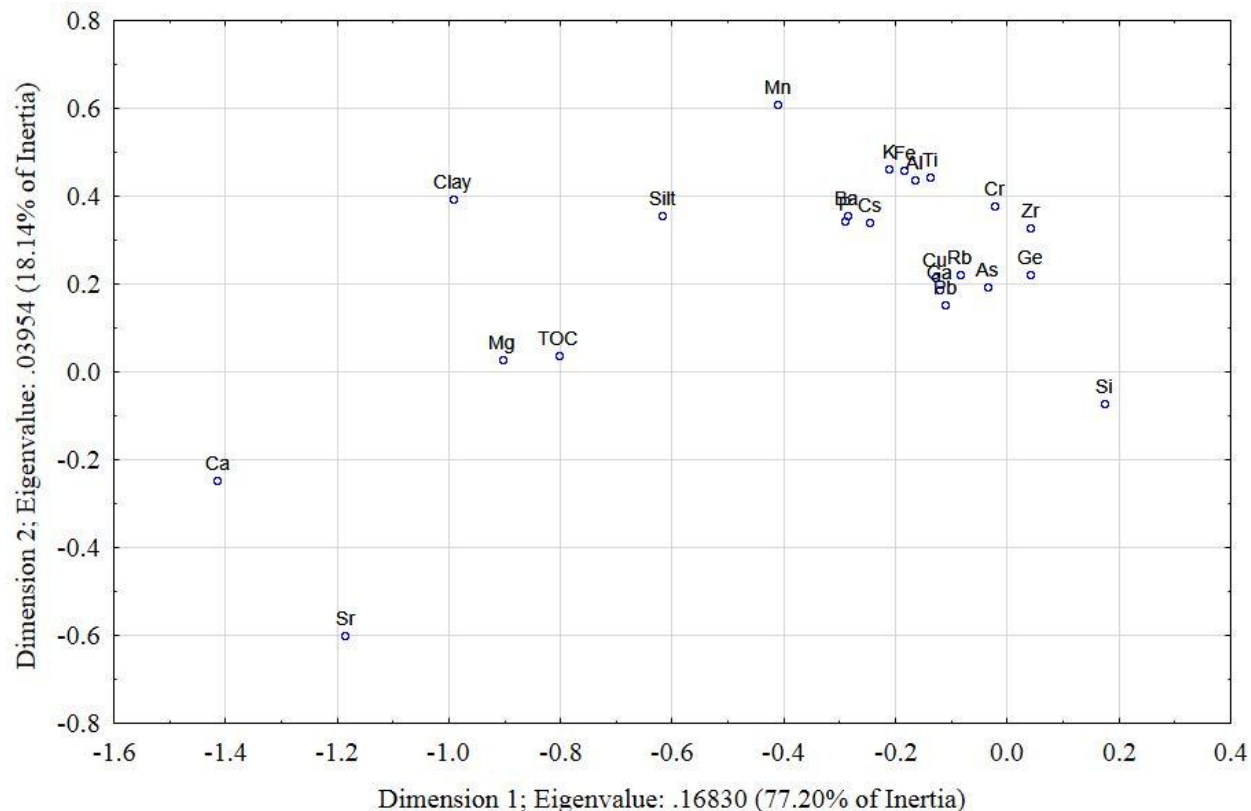
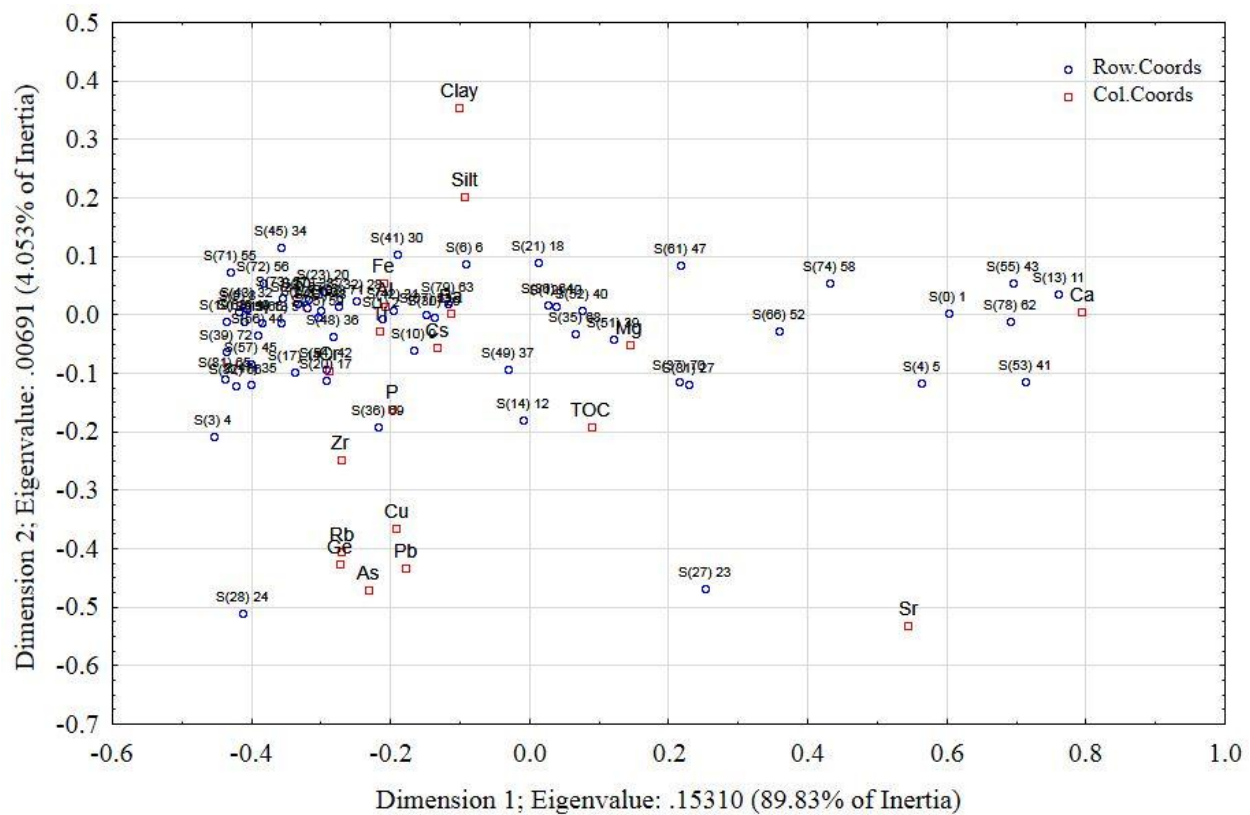


Figure 9.6 – 2D Plot of Column Coordinates Part 1.

Dimension: 1 x 2. Input Table (Rows x Columns): 70 x 23. Standardization: Row and Column profiles.

From row graph, S(25) 21, S(64) 50, S(68) 54, and S(33) 29 dust source sites did not contribute to the inertia of each axis, causing to be considered identical to the average profile. It was observed also that S(59) 46, S(2) 3, S(76) 60, S(77) 61, S(29) 25, S(26) 22, and S(18) 15 dust sites were sited away from the origin, but close to each other. The remaining 59 dust sites were all considered and included in a single group with homogeneous profile distribution because of their proximity to the origin. (See Figure 9.7).

distance between column points, but not the distance between row points and column points. However, it was reasonable to deduce the comparative locations of one point of one set with respect to all the points of the other set.



9.1.4.1 Discussions after cases reduction

As previously stated, linkage relativeness to the potential wind-erosion of soils during dust storms were attained when performing hierarchical divisive clustering with similar (short and large Euclidean) distances. Similar to Elemental Concentrations section, the refined original matrix after correspondence analysis conclusion determined 59 dependent continuous cases to be examined next in Principal Component Analysis. Hence, 59 cases fitted hierarchical clustering connectivity on closer and farther correlation characteristics after divisive clustering inspection assenting Ward's criterion. Figure 9.9 revealed 6 hierarchical clusters after cluster analysis assessment: **(1)** S(62)48 – S(52) 40 – S(67) 53 – S(79) 63 – S(42) 31 – S(74) 58 – S(36) 69 – S(20) 17 – S(72) 56 – S(66) 52 – S(82) 66 – S(57) 45 – S(30) 26 – S(3) 4 – S(48) 36 – S(17) 14 – S(1) 2; **(2)** S(73) 57 – S(9) 8 – S(49) 37 – S(81) 65 – S(39) 72 – S(35) 68 – S(75) 69 – S(15) 13 – S(80) 64 – S(38) 71 – S(21) 18 – S(78) 62; **(3)** S(56) 44 – S(63) 49 – S(28) 24 – S(19) 16 – S(32) 28 – S(34) 32 – S(31) 27 – S(27) 23 – S(4) 5 – S(14) 12; **(4)** S(50) 38 – S(71) 55 – S(34) 67 – S(51) 39 – S(54) 42 – S(47) 35 – S(65) 51 – S(22) 19 – S(10) 9 – S(23) 20 – S(37) 70; **(5)** S(41) 30 – S(45) 34 – S(12) 10 – S(13) 11 – S(6) 6; and **(6)** S(53) 41 – S(0) 1 – S(55) 43 – S(61) 47. As a result, 59 dust source sites under examination located on the Southern High Plains region showed hierarchical clustering connectivity into closer and farther correlation characteristics after subsets explorative process analysis.

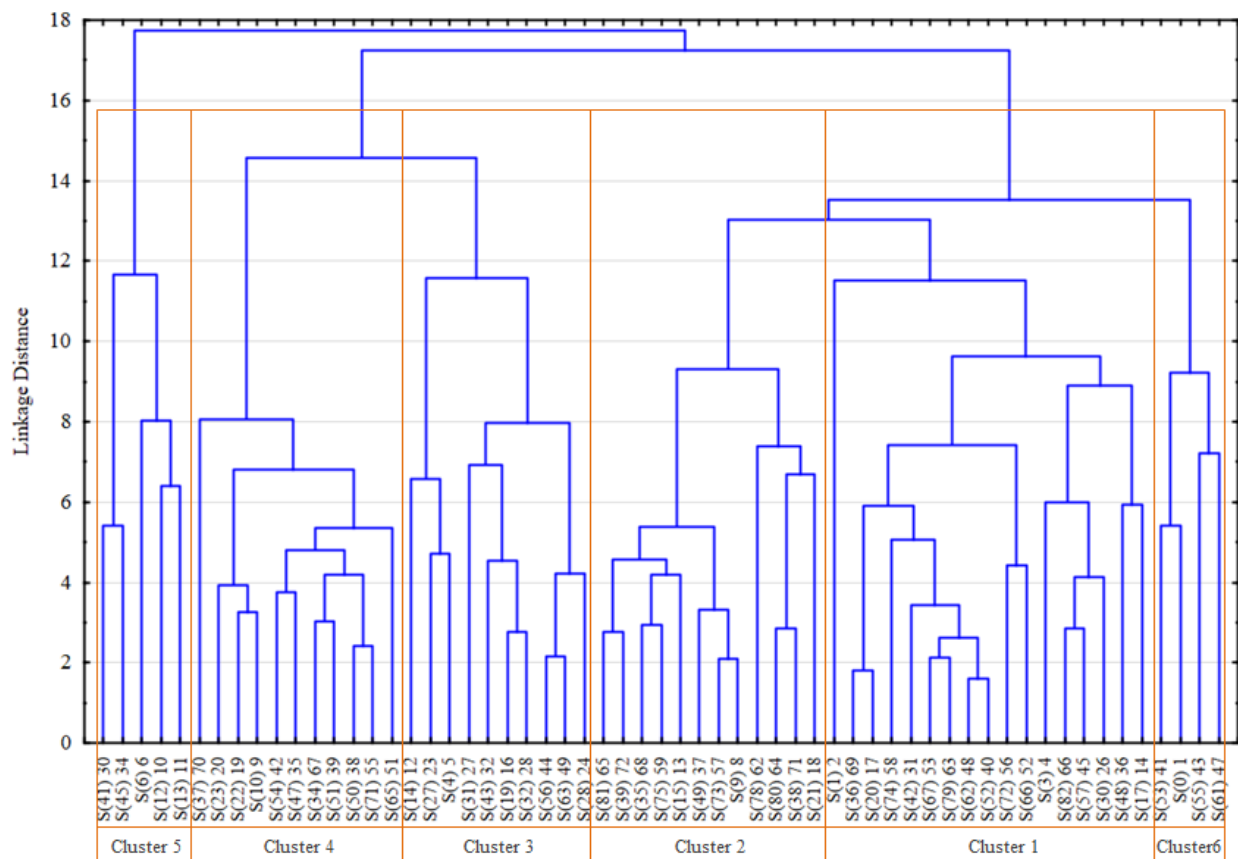


Figure 9.9 – Tree diagram of 59 cases with complete linkage and geometric distance.

Cluster 1 from dust source sites statistical analysis comprised 17 dust sites having Sand (found on 9 sites) as the main soil texture from particle size distribution analysis. Loamy Sand and Sandy Loam soil textures proceeding from 6 and 2 source sites were involved in this cluster, in that order. 52.94% (9/15), 35.29% (6/17), and 11.76% (2/17) were the computed percentages for Sand, Loamy Sand, and Sandy Loam soil texture categories. In addition, soil names were identified by following the U.S. General Soil Map Data criteria. Based on that, Amarillo resulted to be the typical soil for this group totalizing 52.94% (9/17) of the entire site amount. Patricia was a regular soil computing 23.53% (4/17) site volume. Abilene, Acuff, and Brownfield soils

were occasional due to their infrequent presence in this group calculating 23.53% (4/17); Acuff and Brownfield soils were detected in only one site (5.88% each), whereas Abilene was observed on two sites causing 11.76%. Non-Irrigated farmland activity was the main land use class which in conjunction with Mixed, Irrigated/Non Irrigated farmland, and Irrigated farmland land use classes (occasional land use activities), encompassed the land uses classes taken into account for this Cluster. As a result, values of 70.59% (12/17), 23.52% (4/17), and 5.88% (1/17) totaled percentages were computed for Non-Irrigated farmland, Mixed besides Irrigated/Non Irrigated farmland (11.76% each), and Irrigated farmland, based on 12, 2, 2, and 1 dust source sites, correspondingly.

Dust source sites comprised in Cluster 1 were then mapped on ESRI ArcGIS ArcMap version 10.1. Sites were located on Southeast, Central, and Northwest areas of the Southern High Plains region. Dust source sites were more commonly concentrated in the Southeast area, however.

As expected, Aeolian Sand was the unique geomorphic surface observed in this group. See Figure 9.10.

Hierarchical clustering connectivity on Cluster 2 included 12 dust source sites where Sand prevailed as the conventional soil texture (found on 8 sites). As with Cluster 2, Loamy Sand and Sandy Loam soil textures were present in 3 and 1 source sites in this cluster, accordingly. 66.67% (8/12), 25.00% (3/12), and 8.33% (1/12) were the calculated percentages for Sand, Loamy Sand, and Sandy Loam soil texture categories. Next, soil names were classified by following the U.S. General Soil Map Data Criteria. No consistent soil name characterized this Cluster but Patricia as well as Amarillo and Brownfield (16.67% each) were consistent soils in the group; similarly, Acuff ,Olton, Portales, Simona, and Springer soils (8.33% each) were

classified. All soils mentioned before, computed 25.00% (3/12), 33.34% (4/12), and 41.65% (5/12) totaled percentages based on 3, 4, and 5 dust source sites, accordingly. Irrigated Farmland was the unique land use class observed in this Cluster, but widely categorized in 8 soil names previously described, nonetheless.

ESRI ArcGIS ArcMap version 10.1 was used examining the dust source sites that shaped Cluster 2. Results mapped these sites on the Central area of the Southern High Plains, mostly.

As expected, Aeolian Sand was the sole geomorphic surface observed into this Cluster. See Figure 9.10.

Sand was the main soil texture category for the 10 dust source sites comprised in Cluster 3 in accordance with hierarchical clustering connectivity. After performing the U.S. General Soil Map Data Criteria in this group, Amarillo characterized the main soil name in this group while Maljama, Midessa, and Potter (10% each) were present. All soils mentioned above, computed 70% (7/10), and 30% (3/10) totaled percentages based on 7, and 3 dust source sites.

Mixed and Range land use classes were comprised in this Cluster. These two land use classes computed 70% (7/10), and 30% (3/10) based on 7 and 3 source sites, respectively.

Dust source sites comprised in Cluster 3 were mapped by using ESRI ArcGIS ArcMap version 10.1. Sites were located on the Southeast, Central and Southwest (far west Texas) areas of the Southern High Plains region.

9 out of 10 dust sour sites were Sand geomorphic surface characterized. Loess surface was detected at 1 site. See Figure 9.10.

In Cluster 4, an interesting hierarchical clustering connectivity could be discussed. Here, the group comprised 11 dust source sites from which the unique land use class observed was Range widely classified into 10 soil names.

After categorizing the soil name types by following the U.S. General Soil Map Data criteria, Amarillo, Arvana, Berda, Brownfield, Church, Clovis, Hindman, Pep, Reagan, and Spantara (9.09% each), computed 18.18% (2/11) and 80.81% (9/11) totaled percentages based on 2, and 9 dust source sites, in that particular order.

Dust source sites included in Cluster 4 were mapped on ESRI ArcGIS ArcMap version 10.1, resulting in a narrowed outcome of the sites which were located within Northwest and Southwest (New Mexico) as well as Southeast areas of the Southern High Plains region.

As expected, Aeolian Sand was the unique geomorphic surface characterized in this group. See Figure 9.10.

Hierarchical clustering connectivity on Cluster 5 involved 5 dust source sites where Sandy Loam and Silt Loam (40% each), and Loam soil textures characterized the sites of this group, computing 80% (4/5), and 20% (1/5) totaled percentages based on 4 and 1 dust source sites. Like Cluster 4, no specific soil names were possible to detect since the soil name classes were not different on presence number between each other after analyzing the U. S. General Soil Map Data criteria. Therefore, Bigetty, Ector, Pantex, Pullman, and Sotim soil names, calculating 100% (5/5) totaled percentages based on 5 dust sources sites. Range, Mixed, and Non Irrigated farmland involved the land use classes observed in this Cluster. As a result, values of 80% (4/5) and 20% (1/5) totaled percentages were computed for both Range and Mixed (40% each) as well as 20% to Non Irrigated farmland land use classes based on 2, 2, and 1 dust source sites, respectively.

Dust source sites included in Cluster 5 were mapped on ESRI ArcGIS ArcMap version 10.1. Sites were located on Northeast and Southwest areas of the Southern High Plains region.

Aeolian Sand, and Alluvial with Loess (40% each) were the geomorphic surfaces detected in this group, computing 10% (1/5), and 80% (4/5) totaled percentages based on 1 and 4 dust source sites. See Figure 9.10.

Ward's analysis included 4 dust source sites in Cluster 6 where Loam, Loamy Sand, Sand, and Silt Loam soil textures (25% each) characterized the sites for this group, and computing 100% totaled percentages based on 5 source sites. U. S. General Soil Map Data criteria characterized Gomes, Patricia, Portales, and Reagan (25% each) soil names included in this Cluster. In addition, Non Irrigated Farmland and Mixed land use classes comprised the land use classes on this Cluster, resulting 75% (3/4), and 25% (1/4) total percentages for these two land use classes mentioned above based on 3 and 1 dust source sites, accordingly.

ESRI ArcGIS ArcMap version 10.1 mapped source sites of Cluster 6 that were located on the Southeast area of the Southern High Plains region.

As expected, Aeolian Sand was the unique geomorphic surface observed in this group. See Figure 9.10.

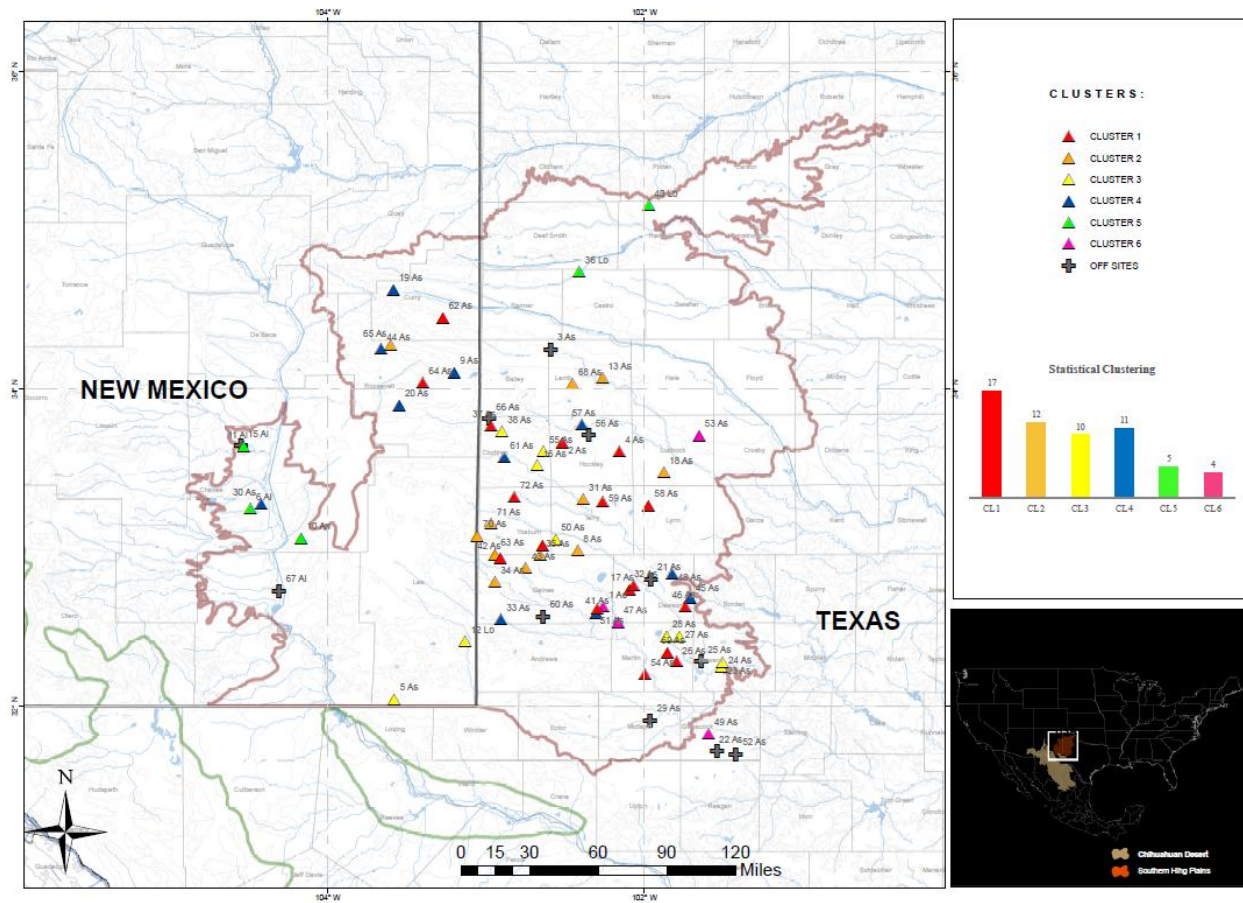


Figure 9.10 – SHP ArcGIS Clustering Map 2.

Southern High Plains region: Geographical Information System Clustering Map. A total of 59 cases plotted into 6 clustering layers resulting from the Dust Source Sites cluster statistical analysis to notice relativeness between site cases and regional area sections.

9.2 Principal Component Analysis

Principal Component Analysis was introduced with the two following aims: (1) Eliminate redundant information by obtaining a small number of variables that make it easier to apply other multivariate statistical techniques subsequently; and (2) Obtain uncorrelated variables that represent the structure of the original collection of variables in an optimal way.

Refined original elemental concentration matrix (comprising Inductively Coupled Plasma Optical Spectrometry, ICP-OES data) that resulted after correspondence analysis completion, determined 59 cases to be examined under the ordination analysis called Principal Component Analysis (PCA) with Varimax normalized rotation (orthogonal rotation methodology). This rotation on PCA produced a change of coordinates that maximized the sum of the variances of the squared loadings. That was, every single value was well described by a linear combination. Varimax rotation ($R_{VARIMAX}$), is mathematically described as:

$$R_{VARIMAX} = \arg \max_R \left(\sum_{j=1}^k \sum_{i=1}^p (AR)_{ij}^4 - \frac{\gamma}{p} \sum_{j=1}^k \left(\sum_{i=1}^p (AR)_{ij}^2 \right)^2 \right)$$

Factors marked by high loadings from some variables and low loadings for others, resulted when clearer patterns of loadings were created after rotating the Varimax algorithms. Loadings with patterns ≥ 0.70 were considered excellent and loading patterns ≤ 0.32 were considered very poor. Principal factors that resulted with eigenvalues ≥ 1.0 were retained. In due course, after Principal Component Analysis, variables with high loadings (correlations) were observed on different factors.

9.2.1 Ordination analysis on original correlation matrix

Table 9.1 provides the variance of the first eight Varimax rotated (orthogonal rotation methodology), principal components resulted after analysis completion on the correlation matrix. It was seen that the eight components contained nearly 88% of the total variation, where the eight components provided with a 2.50 value of variance.

The eigenvalues determined the number of principal components that were necessary. This number depended on the amount of variation in the data. Since the principal components were ordered according to importance (the first principal component explained the largest part of the variance), it was sufficient to determine both few first principal components that contained the amount of variation larger than a certain percentage (often 90%), and the few last principal components to detect extreme observations.

Table 9.1 – SHP elemental coefficients Factors on original database

Factor	Eigenvalue	Percent Variance	Cumulative Percent Variance
1	12.6427	23.4124	23.4124
2	10.7446	19.8974	43.3098
3	8.8971	16.4760	59.7859
4	6.0795	11.2583	71.0441
5	3.3469	6.1979	77.2421
6	2.6020	4.8186	82.0606
7	1.6055	2.9731	85.0337
8	1.3510	2.5018	87.5355

Coefficients for the eight Factors: Southern High Plains elemental and dust source sites statistical characterization. Complete dataset matrix formed by 54 x 59 variables and cases, in that particular order.

As shown in Table 9.2, Factor 3 computed 39/54 parts of positive correlations between the 54 sources having its highest loadings (top value above 0.9) in variables Al, Ti, Fe, Ba, and Cs. The second uppermost loading values (first correlation loading above 0.8) were found on Factors 5, 4, and 2, totalizing 28/54, 23/54, and 23/54 parts of positive correlations, accordingly. Factor 5 represented Pb, As, and Cu peak loading variables values. Factor 4 obtained its greatest loadings on Irrigated Farm, Gomes, Reagan, and P variables. Range, Acuff, Patricia, and Olton variables computed the highest loadings for Factor 2, resulting with 31/54 parts of positive correlation. Factor 7 contained the loadings just above the 0.7 p-value limit selected for this statistical analysis. Sr, Ca, Mg, and TOC were the peak loading values for this Factor. However, Factor 7 totalized 40/54 parts of positive correlations. Factors 1 and 6 resulted with their uppermost loading value above 0.5. Amarillo, Rural, and Mixed, as well as Portales, Non Irrigated Farmland, Brownfield, and Maljama, were the variables comprised in these two Factors, computing 30/54, and 34/54 parts of positive correlations, respectively. Finally, Factor 8, calculated 28/54 parts of positive correlation totalizing the poorest loadings (above 0.3) value on Clay and Silt variables.

Different variables were comprised on more than one Factor loading group due to their peak correlation values. It is important to mention that top five robust correlation values were considered to be described and/or classified in the factor loading mentioned in this section.

As noted on Figure 9.8, parts of positive loading values were computed based on the Factor statistical analysis outcomes implemented on complete database matrix enclosing 54 variables and 59 cases.

Table 9.2 – Topmost Factor loading values on original database.

Variable	Factor 1	Variable	Factor 2	Variable	Factor 3
Amarillo	0.56826 *	Range	0.82775 *	Al	0.977668
As	0.34361 **	Acuff	0.69467	Ti	0.972985
Rural	0.305742	Patricia	0.66114 *	Fe	0.966495
Pb	0.26580 **	Portales	0.50821 **	Ba	0.930025
Mixed	0.251927	Olton	0.395595	Cs	0.92627 *
Variable	Factor 4	Variable	Factor 5	Variable	Factor 6
F [I]	0.876893	Pb	0.89532 *	Portales	0.54019 *
Gomes	0.726806	As	0.86521 *	Reagan	0.47898 **
Reagan	0.66044 *	Cu	0.826901	F [NI]	0.328863
Amarillo	0.32260 **	Range	0.25335 **	Brownfield	0.301878
P	0.159546	Portales	0.22918 ****	Maljama	0.11318
Variable	Factor 7	Variable	Factor 8		
Sr	0.779879	Patricia	0.34848 **		
Ca	0.741771	Reagan	0.28517 ***		
Mg	0.611816	Clay	0.283929		
TOC	0.557697	Portales	0.26971 ***		
Cs	0.23150 **	Silt	0.267352		
Strong to weak loading values:					
* First positive correlation		*** Third positive correlation			
** Second positive correlation		**** Fourth positive correlation			

Factor loading values Varimax normalized from 54-variable matrix. Extraction: Principal components. Loadings are marked at p-values > .700000.

9.2.2 Detecting Outliers

The first few principal components of the 54 predictor variables were plotted in an effort to detect outliers. Plots for the first two principal components are reproduced in Figure 9.11. Roughly judging their significance, no outliers were present on elemental concentration variables, and therefore, the data were approximately multivariate normal. Soil name variables were, in the other hand, situated distant from the origin, but not so far away as to be considered in outlying positions on the plot. An interesting aspect of this figure is that the anthropogenic metals were observed grouped comparable to that of the correspondence analysis results, suggesting that Rural, Mixed and Range land use classes may impact the presence of these metals within the Southern High Plains region. Factor loadings were considered small enough (correlation values > 1.0) to state that there was no suspicion of any incorrect or influential observation in this analysis in producing blatant cases.

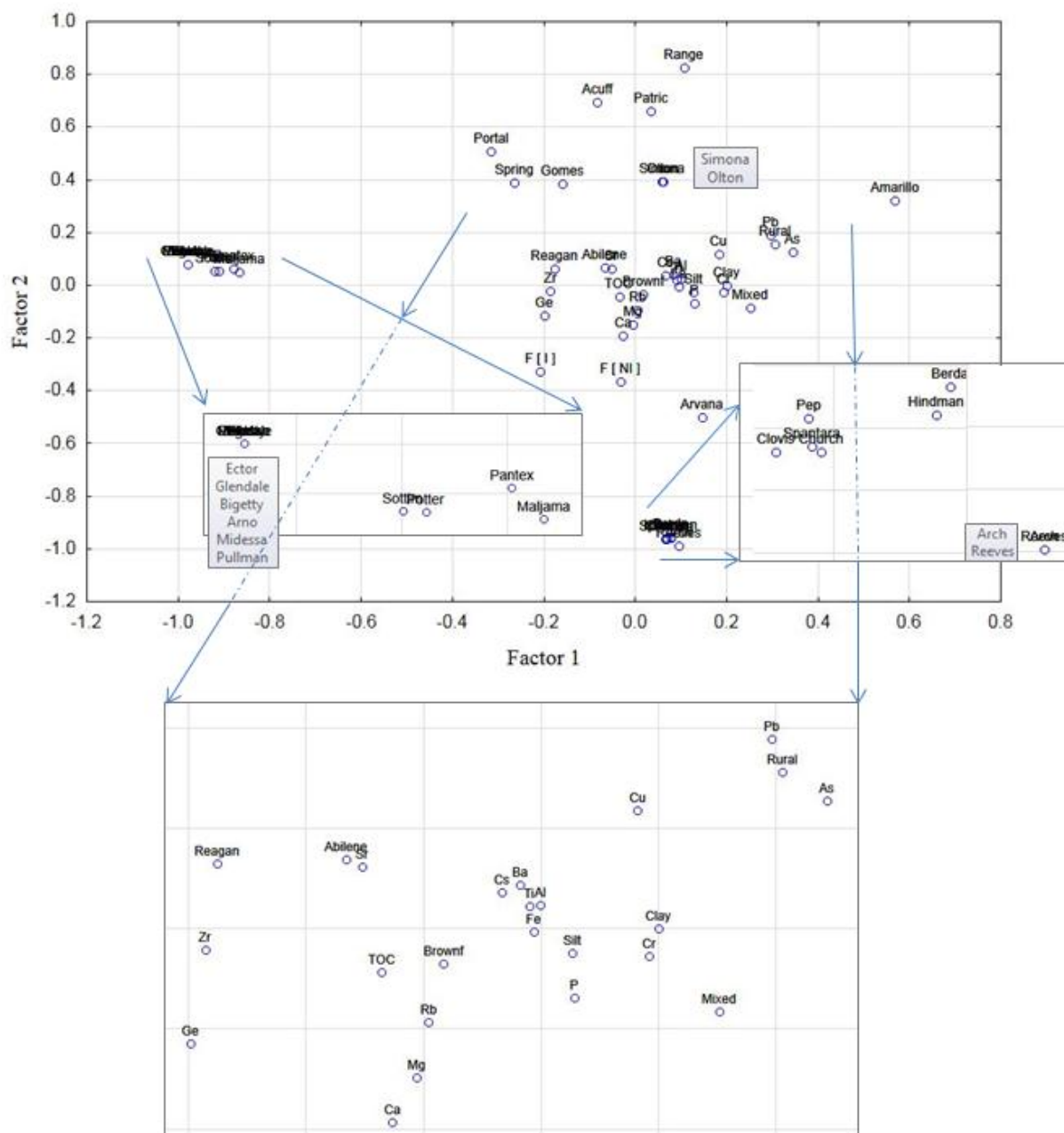


Figure 9.11 – Factor loadings: Factor 1 vs Factor 2 on original database.

Rotation: Varimax normalized. Extraction: Principal components.

9.2.3 Ordination analysis on reduced correlation matrix

Principal component analysis was performed again, once reducing the database matrix enclosing both Elemental Concentrations and Land Use class variables to notice any observations (considered as outliers with respect to the correlation structure of the data) on the last few principal components.

Potential outliers (observations that were different from, or inconsistent with, the remainder of the data set), were identified after Principal Component Analysis completion. However, outliers sometimes may come from observations that did not produce extreme values on any of the original variables, but considered still as outliers because they did not follow the correlation configuration of the rest of the data. Ultimately, additional information which was not available in plots of the original variables, were perceived in the last few principal components, after studying the outliers that resulted from these principal components. In other words, the last few principal components identified outliers with respect to the original variables.

After eliminating the Soil Name variables, the principal components become strong, shortening the effect of outliers on both first few and the last few principal components.

Table 9.3 delivered the variance of the first five Varimax rotated (orthogonal rotation methodology) principal components resulting after analysis completion of the reduced correlation matrix. It was perceived that the five components contained nearly 80% of the total variation, where the fifth component impacted the variance with a 6.52 value.

Table 9.3 – SHP metallic coefficients Factors on reduced database

Factor	Eigenvalue	Percent Variance	Cumulative Percent Variance
1	10.0237	41.7655	41.7655
2	3.4779	14.4910	56.2566
3	2.1253	8.8556	65.1121
4	1.8493	7.7056	72.8177
5	1.5653	6.5221	79.3398

Percent variance explained by successive principal components (factors). Eigenvalues and percent variance explained by the 5 principal components. Five factors contained nearly 79.4% of the entire variance, which was sufficient to give a good idea of the data structure.

Table 9.4 provided the topmost correlation loading values resulting from the Factors (elemental concentrations and land use land class variables). It was observed that Factors 3, 1, and 2 totalized 14/24, 22/24, and 17/24 parts of positive correlations of the 24 variables, starting their highest values (above 0.9), on Mixed, Rural, and Silt, as well as Al, Ti, Fe, Ba, and Cs, and Pb, As, Cu, Range, and Clay variables, in that particular order. Second primary loading values (top value above 0.8) were noted on Factor 4, computing 18/24 of positive correlation on Ca, Mg, TOC, and Sr. Finally, Non Irrigated Farmland and Zr were the variables comprised on Factor 5, that totaled 13/24 parts of correlation (main positive p-value above 0.7).

Some variables resulted being considered on more than one Factor loading group because of their peak values. At this time, for simplicity purposes, the strongest correlation value of every single variable was considered to be mentioned and/or classified in the Factor loading descriptions mentioned above.

As displayed in Figure 9.11, parts of positive correlations were calculated based on the Factor statistical analysis results performed on the complete database matrix which was formed by 24 variables in 59 cases.

Table 9.4 – Topmost Factor loading values on reduced database.

Variable Factor 1		Variable Factor 2		Variable Factor 3	
Al	0.97041	Pb	0.925819	Mixed	0.98734
Ti	0.96540	As	0.866381	Rural	0.98629
Fe	0.96102	Cu	0.81534 *	Cu	0.12441 **
Ba	0.90171	Range	0.57224 *	Sr	0.09165 **
Cs	0.89584 *	Clay	0.234162	Silt	0.08334
Variable Factor 4		Variable Factor 5			
Ca	0.83582 *	F [NI]	0.78590		
Mg	0.70671	Zr	0.23556		
TOC	0.68637	Range	0.16879 **		
Sr	0.65072 *	Sr	0.08559 ***		
Cs	0.34787 **	Ca	0.06038 **		

Strong to weak loading values:

* First positive correlation *** Third positive correlation

** Second positive correlation

Factor loading values Varimax normalized from 24-variables matrix. Extraction: Principal components. Loadings are noted at p-values > .700000.

9.2.3.1 Detecting disrupted observations

Principal Component Analysis detected observations that disrupted the correlation structure enforced by the bulk of the data, which were not irregular with respect to individual variables. Three groups identified in Figure 9.12 were located near the edge of the factor 2 vs. factor 4 plot: the anthropogenic metals comprised on Group 1, and the calcareous carbonate associated elements included on Group 2. Group 3 represented not outliers but a group which data were approximately normally multivariate classified.

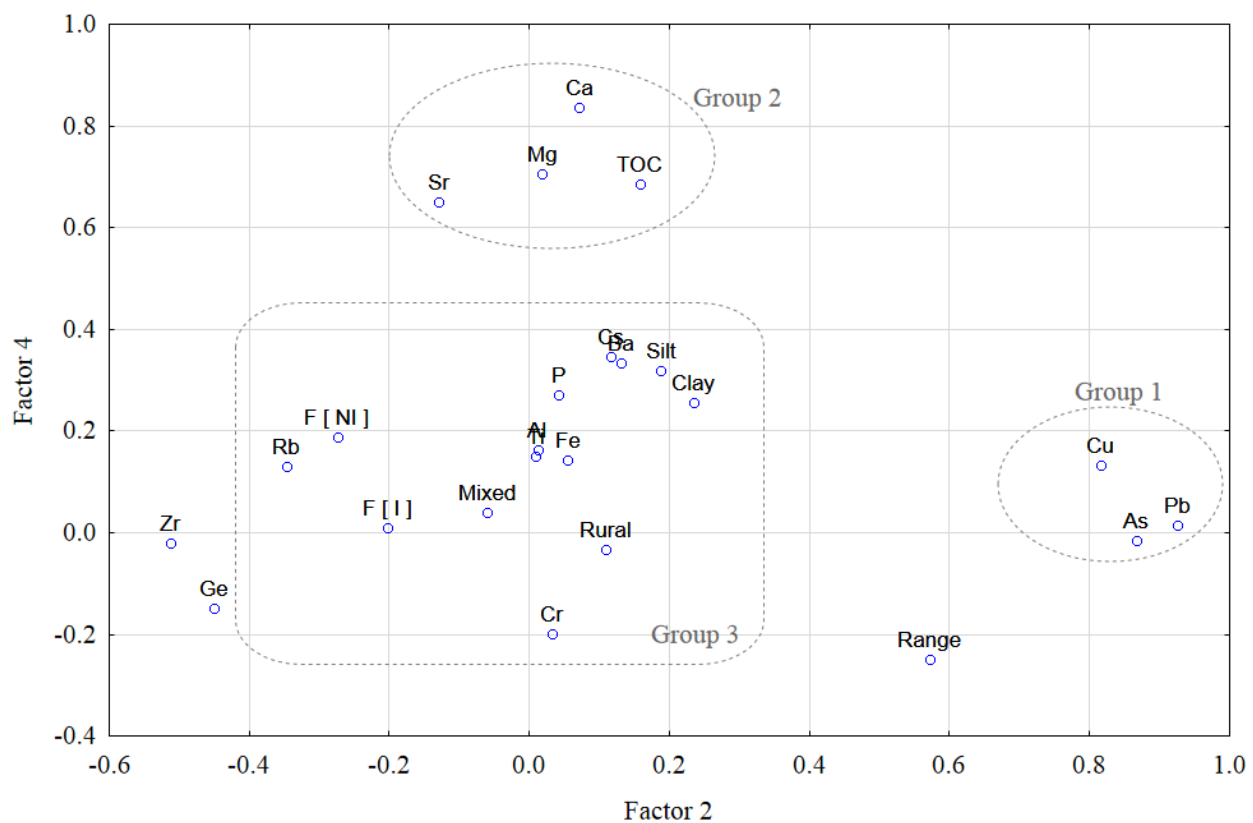


Figure 9.12 – Factor loadings: Factor 2 vs Factor 4 on reduced database.

Southern High Plains formation data: plot of observations with respect to the first few factor 2 and the last few factor 4 plot. Reduced database matrix conformed of 24 variables and 59 cases.

9.2.3.2 Eliminating disrupted observations

In this study, it was perceived that few observations were sufficiently dissimilar from the rest, as a result of a relative small sample size, that caused the outliers to impact strongly the last few principal components. As displayed on Figure 9.13, three groups were gathered together at different factor loading values, but a total of 9 cases in outlying position on plot were considered as blatant cases, and these observations were considered as extreme cases because they were outlying plotted on the 3 and 4 last few principal components.

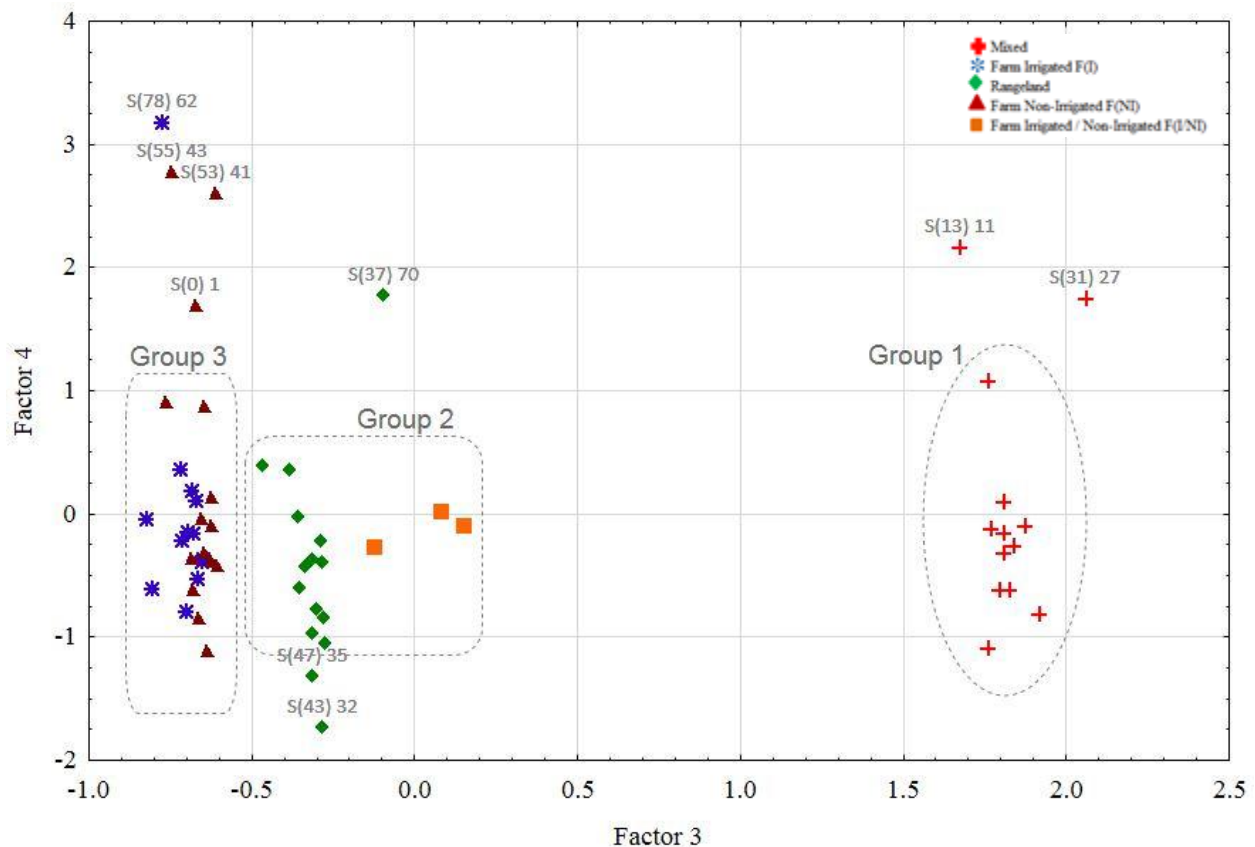


Figure 9.13 – Factor loadings: Factor 3 vs Factor 4 on reduced database.

Southern High Plains formation data: scattering plotting of observations with respect to 3 vs. 4 last few factors. Distinguished extreme cases are observed. Reduced database matrix conformed of 24 variables and 59 cases.

9.2.4 Final ordination analysis on reduced correlation matrix

Principal Component Analysis was then repeated without these nine observations, and the results of the regression were well changed. The number of Principal Components remained the same, and as is shown in Figure 9.14, four groups were gathered together after scatter plotting 2 vs. 4 factor loading values that resulted from the regression analysis performed on the reduced database matrix.

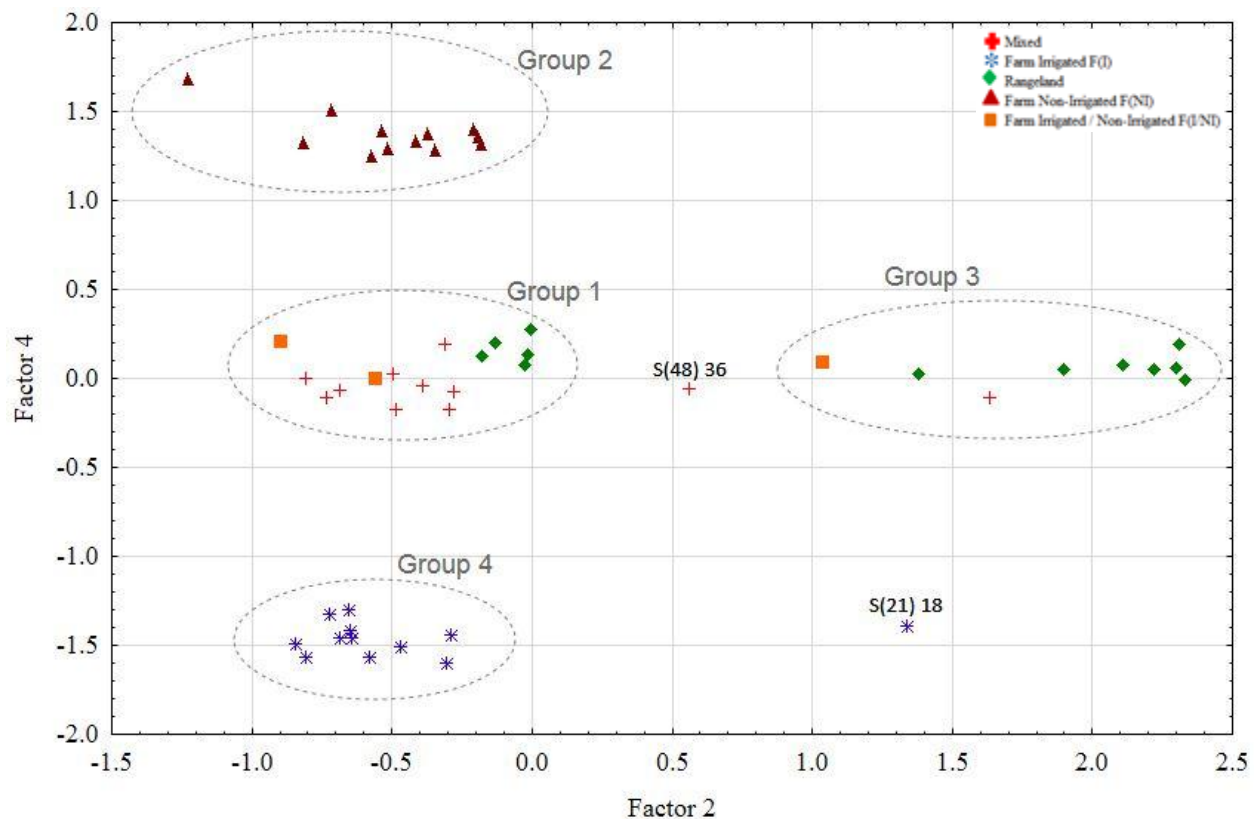


Figure 9.14 – Factor loadings: Factor 2 vs Factor 4 on final reduced database.

Southern High Plains formation data: scatter plotting of observations with respect to 2 vs. 4 last few factors. Reduced database matrix conformed of 24 variables and 50 cases.

In addition to the results of the regressions which were well changed, the variance of the first five principal components was improved from 79.4% to 83.9%, and the five components impacted positively the variance from 6.52% to 5.49% values (See Table 9.5).

Table 9.5 – SHP metallic coefficients Factors on final reduced database

Factor	Eigenvalue	Percent Variance	Cumulative Percent Variance
1	11.3846	47.4359	47.4359
2	3.6518	15.2158	62.6517
3	2.1492	8.9551	71.6069
4	1.6466	6.8607	78.4675
5	1.3182	5.4926	83.9602

Percent variance explained by successive principal components (factors). Eigenvalues and percent variance explained by the 5 principal components. Five factors contained nearly 84% of the entire variance.

Principal Component Analysis performed on final reduced database matrix, defined 4 factor loading groups with 16, 12, 9, and 11 cases representing individual sites that formed Groups 1, 2, 3, and 4, respectively. It was noted that both S(21) 18 and S(48) 36 did not fit properly any of these groups (See table 9.6).

Table 9.6 – SHP elemental concentration Factors on final reduced database

Group 1	Group 2	Group 3	Group 4	No Group
S(61) 47	S(30) 26	S(6) 6	S(38) 71	S(21) 18
S(17) 14	S(52) 40	S(12) 10	S(80) 64	S(48) 36
S(28) 24	S(62) 48	S(10) 9	S(9) 8	
S(32) 28	S(74) 58	S(22) 19	S(15) 13	
S(63) 49	S(79) 63	S(23) 20	S(39) 72	
S(65) 51	S(3) 4	S(4) 5	S(49) 37	
S(45) 34	S(20) 17	S(27) 23	S(66) 52	
S(71) 55	S(36) 69	S(1) 2	S(73) 57	
S(50) 38	S(42) 31	S(14) 12	S(75) 59	
S(51) 39	S(57) 45		S(81) 65	
S(34) 67	S(67) 53		S(35)68	
S(41) 30	S(82) 66			
S(72) 56				
S(56) 44				
S(19) 16				
S(54) 42				

Groups formed after last repeated Principal Component Regression Analysis excluding the nine extreme cases [S(78) 62, S(55) 43, S(53) 41, S(0) 1, S(37) 70, S(47) 35, S(43) 32, S(13) 11, and S(31) 27]. Groups resulted from Factor 2 vs. Factor 4 scattering plot.

9.2.5 Mapping factors loading groups

Dust source sites included on factor loading groups (Table 9.6), were then mapped on ESRI ArcGIS ArcMap version 10.1, resulting to a wide spread of the sites which were located within the Central area of the Southern High Plains, causing no observation of a strong spatial relation between groups (See Figure 9.15).

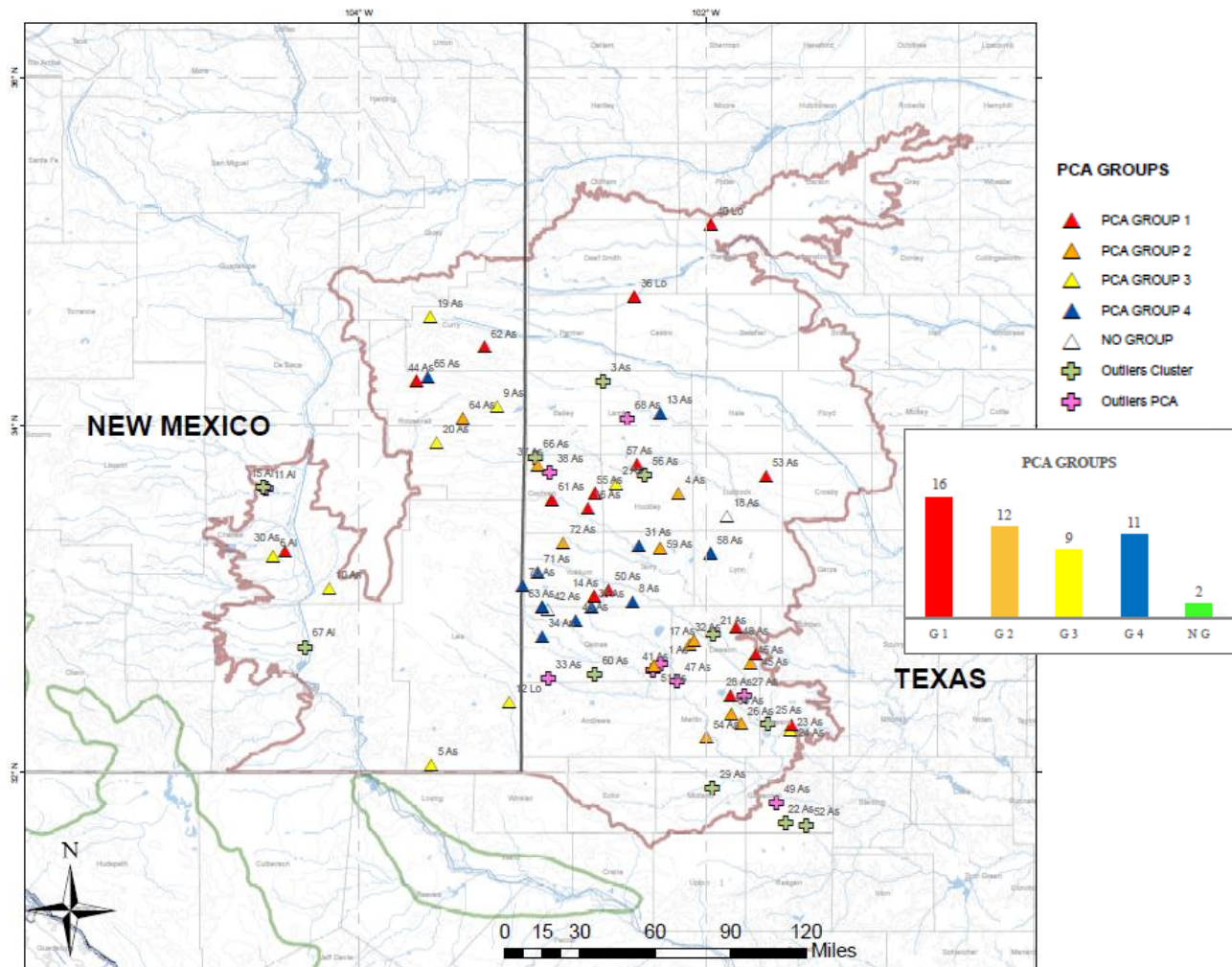


Figure 9.15 – SHP ArcGIS final factorial loading Map.

Southern High Plains region: Geographical Information System factors Map. A total of 50 cases plotted into 4 loading groups resulting from the reduced database matrix after principal component analysis, noticing relativeness between site cases and regional area sections.

9.2.6 Conclusions

Principal Component analysis concluded a satisfactory analysis of multivariate data after creating patterns that characterized both the elemental concentrations and the dust source sites. In addition, the similarity of the variables and cases were determined. Moreover, clustering algorithms achieved the best statistical classification. It must be mentioned, Principal Component Analysis corroborated the connectivity results acquired previously from Cluster Analysis, a prelude statistical technique to the application of multivariate statistical methods, from which the homogeneity of a set of data was attained.

As previously stated, the dataset matrix was reduced on observations when performing hierarchical connectivity methodology. Then, the dataset matrix was reduced once more on principal components excluding nine observations/cases. At this point, the principal components became strong, causing to shorten the effect of outliers on the last few principal components, considered as the major blatant case producers (See Table 9.7).

Table 9.7 – Ordination Analysis Final Dataset Groups

CLUSTER	PCA	FINAL DATASET GROUPS			
CASES	CASES	GROUP 1	GROUP 2	GROUP 3	GROUP 4
S(2) 3	S(43) 32	S(61) 47	S(30) 26	S(6) 6	S(38) 71
S(18) 15	S(47) 35	S(17) 14	S(52) 40	S(12) 10	S(80) 64
S(25) 21	S(0) 1	S(28) 24	S(62) 48	S(10) 9	S(9) 8
S(26) 22	S(37) 70	S(32) 28	S(74) 58	S(22) 19	S(15) 13
S(29) 25	S(31) 27	S(63) 49	S(79) 63	S(23) 20	S(39) 72
S(33) 29	S(13) 11	S(65) 51	S(3) 4	S(4) 5	S(49) 37
S(59) 46	S(78) 62	S(45) 34	S(20) 17	S(27) 23	S(66) 52
S(64) 50	S(53) 41	S(71) 55	S(36) 69	S(1) 2	S(73) 57
S(68) 54	S(55) 43	S(50) 38	S(42) 31	S(14) 12	S(75) 59
S(76) 60		S(51) 39	S(57) 45		S(81) 65
S(77) 61		S(34) 67	S(67) 53		S(35) 68
		S(41) 30	S(82) 66		
		S(72) 56			
		S(56) 44		NO GROUP	
		S(19) 16		S(21) 18	
		S(54) 42		S(48) 36	

Cases observed on Cluster and Principal Component Analyses listed on first two columns. Final dataset groups resulted from last principal component examination on final reduced dataset. Final dataset groups included on table resulted from Factor comparison.

Table 9.8 – Factorial ordination analysis on original dataset matrix
Factor loadings (Varimax normalized) on a 54-variable matrix. Extraction: Principal components. (Marked loadings are red-inked noted at p-values >.700000).

Variable	Factor 1	Factor 2	Factor 3	Factor 4	Factor 5	Factor 6	Factor 7	Factor 8
Clay	0.19980	0.00012	0.849602	-0.038370	0.081438	0.032079	0.071303	0.283929
Silt	0.12645	-0.02467	0.875297	-0.036508	0.100589	-0.021713	0.114465	0.267352
Al	0.09913	0.02344	0.977668	0.042109	0.018772	-0.034997	0.028527	-0.063682
As	0.34361	0.12803	0.042830	0.059829	0.865211	0.045227	0.008952	0.014228
Ba	0.08178	0.04377	0.930025	-0.033309	0.162040	0.039433	0.217292	-0.052182
Ca	-0.02684	-0.19263	0.399935	-0.114046	0.166713	0.079431	0.741771	0.035893
Cr	0.19211	-0.02740	0.674651	0.008531	0.146856	-0.011055	-0.223530	-0.366766
Cs	0.06663	0.03680	0.926269	-0.025991	0.155288	0.050458	0.231504	-0.060103
Cu	0.18235	0.11797	0.305268	0.025914	0.826901	-0.087418	0.075702	0.178975
Fe	0.09426	-0.00345	0.966495	0.073704	0.064723	-0.043922	-0.005387	-0.035198
Ge	-0.19886	-0.11472	0.174238	-0.042294	-0.039511	-0.016209	-0.014688	-0.805456
Mg	-0.00631	-0.14850	0.674266	-0.015872	0.102667	0.048004	0.611816	-0.018356
P	0.12836	-0.06918	0.868126	0.159546	-0.001000	0.107717	0.121437	0.071664
Pb	0.29580	0.18895	0.069896	0.071136	0.895323	0.052232	0.030158	0.083715
Rb	0.00432	-0.09313	0.864191	0.020085	-0.242803	-0.018850	0.052688	-0.297520
Sr	-0.05253	0.06227	0.131231	-0.034991	-0.089231	-0.117818	0.779879	-0.178013
Ti	0.09024	0.02291	0.972985	-0.018130	0.031350	-0.045915	0.017643	-0.063931
Zr	-0.18621	-0.02150	0.591277	-0.190385	-0.329377	-0.111550	-0.056934	-0.328616
TOC	-0.03590	-0.04356	0.557317	-0.026970	0.110109	0.076943	0.557697	0.237971
Ector	-0.98001	0.08021	-0.101091	0.052537	-0.073803	0.075320	0.008190	-0.040628
Glendale	-0.98001	0.08021	-0.101091	0.052537	-0.073803	0.075320	0.008190	-0.040628
Bigetty	-0.98001	0.08021	-0.101091	0.052537	-0.073803	0.075320	0.008190	-0.040628
Armo	-0.98001	0.08021	-0.101091	0.052537	-0.073803	0.075320	0.008190	-0.040628
Midessa	-0.98001	0.08021	-0.101091	0.052537	-0.073803	0.075320	0.008190	-0.040628
Portal	-0.31602	0.50821	0.206621	-0.028976	0.229178	0.540194	0.078436	0.269790
Patric	0.03358	0.66114	-0.014716	-0.049163	0.137113	-0.284029	-0.030598	0.348477
Amarillo	0.56826	0.32185	-0.115512	0.322601	-0.118998	-0.046546	-0.161093	-0.316962
Reagan	-0.17616	0.06544	0.195944	0.660443	0.220201	0.478983	0.050110	0.285165
Brownf	0.01714	-0.03478	0.006750	-0.814694	0.089061	0.301878	-0.017364	0.137910
Arvana	0.14570	-0.49942	0.005754	-0.778179	-0.030651	-0.263143	0.040114	0.088343
Spring	-0.26496	0.39131	-0.006949	-0.804302	-0.080320	-0.237614	0.007921	0.023716
Acuff	-0.08261	0.69467	0.028456	-0.065965	0.191217	-0.607480	-0.007896	0.148628
Simona	0.05741	0.39391	0.009607	-0.846214	0.023255	-0.240775	0.020027	0.011894
Olton	0.06139	0.39560	0.006840	-0.841990	0.005576	-0.239160	0.145398	0.044874
Gomes	-0.15860	0.38504	0.004621	0.726806	0.127775	-0.430664	0.022879	0.117066
Abilene	-0.06632	0.06957	-0.017755	0.067485	-0.232809	0.062386	0.201973	-0.400306
Arch	0.09582	-0.98963	0.023851	0.034081	-0.026899	0.002627	0.011450	0.021857
Church	0.06904	-0.96387	0.012048	0.031820	0.047809	0.005796	0.007140	0.016516
Spantara	0.06833	-0.96287	0.025034	0.031563	0.033646	0.004291	-0.007877	0.019898
Clovis	0.06561	-0.96382	0.041472	0.030225	0.047815	0.002458	-0.013742	-0.003598
Reeves	0.09582	-0.98963	0.023851	0.034081	-0.026899	0.002627	0.011450	0.021857
Berda	0.07870	-0.95342	0.019429	0.039778	-0.060108	0.003485	0.119936	-0.009136
Pep	0.06808	-0.95855	0.011831	0.034200	-0.044486	0.006059	0.020585	0.022563
Hindman	0.07759	-0.95794	-0.002343	0.036484	-0.054398	0.010197	0.012112	0.053001
Pantex	-0.87851	0.06245	-0.002583	0.030954	-0.162767	0.097571	-0.003972	-0.028388
Maljama	-0.86638	0.04982	-0.287273	0.029883	0.007630	0.113180	0.080365	-0.055255
Pullman	-0.98001	0.08021	-0.101091	0.052537	-0.073803	0.075320	0.008190	-0.040628
Sottim	-0.91979	0.05332	0.020595	0.030377	-0.164563	0.016103	-0.018163	-0.040938
Potter	-0.91097	0.05281	-0.079495	0.031043	-0.169593	0.021615	-0.014523	-0.045091
Rural	0.30574	0.15586	0.026565	-0.077275	0.031988	-0.902750	0.017939	0.048719
Mixed	0.25193	-0.08296	0.018490	-0.062538	-0.038415	-0.900544	0.024718	0.017484
F [I]	-0.20783	-0.32795	0.007279	0.876893	-0.050970	0.079018	-0.042676	0.026530
Range	0.10601	0.82775	-0.040282	-0.003832	0.253350	0.104198	0.015737	0.016935
F [NI]	-0.03199	-0.36418	0.014688	-0.819034	-0.152250	0.328863	0.016494	-0.055369
Expl.Var	10.27742	10.81453	9.679185	6.001777	3.035793	3.379464	2.168252	1.912749
Prp.Totl	0.19032	0.20027	0.179244	0.111144	0.056218	0.062583	0.040153	0.035421

Table 9.9 – Factorial ordination analysis on reduced dataset matrix

Factor loadings (Varimax normalized) on a 24-variables matrix. Extraction: Principal components. (Marked loadings are red-inked noted at p-values > .700000).

Variable	Factor 1	Factor 2	Factor 3	Factor 4	Factor 5
Clay	0.802516	0.234162	0.020362	0.256533	0.014778
Silt	0.810101	0.187928	0.083345	0.319301	0.003326
Al	0.970414	0.011765	0.048421	0.162549	-0.029352
As	0.110218	0.866381	0.043463	-0.014359	-0.021061
Ba	0.901707	0.131508	-0.006613	0.335094	0.053134
Ca	0.287292	0.070684	-0.058185	0.835821	0.060378
Cr	0.769983	0.032088	0.007827	-0.199450	0.040564
Cs	0.895842	0.116967	-0.020828	0.347868	0.044700
Cu	0.316795	0.815339	0.124405	0.133790	-0.047069
Fe	0.961015	0.054736	0.041185	0.142091	-0.063642
Ge	0.268374	-0.450231	-0.037927	-0.148498	0.044498
Mg	0.588740	0.018519	-0.058476	0.706711	-0.007115
P	0.838113	0.042101	-0.092254	0.271873	-0.163582
Pb	0.123213	0.925819	0.009794	0.015616	-0.032958
Rb	0.870550	-0.346774	0.003803	0.131522	-0.012363
Sr	0.065460	-0.129729	0.091653	0.650716	0.085588
Ti	0.965399	0.009248	0.057101	0.151171	0.039062
Zr	0.595431	-0.512812	0.031644	-0.019191	0.235559
TOC	0.438060	0.157529	-0.054554	0.686367	-0.008805
Rural	0.042786	0.108567	0.986286	-0.033326	0.028252
Mixed	0.017395	-0.060546	0.987336	0.038886	-0.029201
F [I]	-0.004505	-0.203056	-0.197076	0.009266	-0.939618
Range	0.026063	0.572235	-0.132634	-0.248748	0.168792
F [NI]	-0.031407	-0.273933	-0.236454	0.189368	0.785896
Expl.Var	8.949723	3.491778	2.121742	2.835303	1.643014
Prp.Totl	0.372905	0.145491	0.088406	0.118138	0.068459

Table 9.10 – Restricted maximum likelihood correlation coefficients of selected elemental concentrations.

	Clay	Silt	Al	As	Ba	Ca	Cr	Cs	Cu	Fe	Ga	Ge	K	Mg	Mn	P	Pb	Rb	Sr	Si	Ti	Zr	TOC
Clay	1	.8260***	.6875***	.1363	.7103***	.7250***	.2940*	.7039***	.3686*	.7037***	.2767*	-.1597	.7102***	.7900***	.7580***	.7894***	.1065	.4797***	.4029**	-.2132	.6149***	.0248	.7829***
Silt		1	.8045***	.2718*	.8384***	.6623***	.4350**	.8287***	.5055***	.8110***	.4110**	-.1249	.8248***	.5661***	.8786***	.8380***	.2620*	.5755***	.2913*	-.1629	.7883***	.1574	.7698***
Al			1	.1846	.8704***	.3921**	.7103***	.8700***	.3682*	.9883***	.2417*	.1996	.9805***	.4175**	.9505***	.8528***	.1238	.8003***	.0579	.1101	.9687***	.4701***	.4810***
As				1	.3534*	.2698*	.2526*	.3559*	.8014***	.2032	.8878***	.1832	.2610*	.1387	.1753	.1245	.8989***	-.2253	.2129	.0914	.2004	-.1857	.1985
Ba					1	.6170***	.5747***	.9987***	.5360***	.8578***	.4274**	.1014	.8698***	.5763***	.8493***	.7876***	.3114*	.6206***	.2690*	.0244	.8658***	.3624*	.6720***
Ca						1	.0876	.6175***	.4380**	.3975**	.3720*	-.1985	.4219**	.8092***	.4573***	.5690***	.2441*	.1787	.6837***	-.2401*	.3446*	-.1351	.8540***
Cr							1	.5764***	.3012*	.6916***	.2250	.3549*	.6825***	.1267	.6003***	.4997***	.1844	.5693***	-.0857	.2516*	.7023***	.4347**	.1904
Cs								1	.5353***	.8561***	.4184**	.1308	.8667***	.5737***	.8406***	.7818***	.3049*	.6132***	.2675*	.0450	.8648***	.3704*	.6694***
Cu									1	.3882**	.8771***	.0141	.4512***	.3241*	.4092**	.3184*	.8506***	-.0677	.2922*	-.0262	.3828*	-.1423	.4054*
Fe										1	.2702*	.1648	.9948***	.4245**	.9528***	.8502***	.1511	.7749***	.0469	.0865	.9683***	.4556***	.4857***
Ga											1	-.1402	.3479*	.2349	.2975*	.2406*	.9700***	-.1674	.2605*	-.0996	.2534*	-.2935*	.3312*
Ge												1	.1184	-.1106	.0180	-.0157	-.0641	.2079	-.0775	.7723***	.2240	.5360***	-.1927
K													1	.4320**	.9550***	.8530***	.2296	.7250***	.0594	.0556	.9631***	.4135**	.5059***
Mg														1	.4702***	.5616***	.0891	.2543*	.6778***	-.1648	.3521*	-.0352	.7582***
Mn															1	.8893***	.1613	.7443***	.1172	-.0311	.9434***	.3807*	.5472***
P																1	.1070	.6618***	.1752	-.0844	.8044***	.2318	.6828***
Pb																	1	-.2704*	.1753	-.0229	.1496	-.2791*	.2102
Rb																		1	-.0113	.1849	.7635***	.5247***	.2624*
Sr																			1	-.0872	.0315	-.1365	.5007***
Si																				1	.1262	.4508***	-.2218
Ti																					1	.5913***	.4377**
Zr																						1	-.0299
TOC																							1

* Significant at the 0.05 Level; ** Significant at the 0.001 level; *** Significant at the 0.0001 level

Chapter 10

Summary and Conclusions

10.1 Particle Size Distribution

Malvern Mastersizer laser diffraction particle size analysis concluded that dust source soils from the Chihuahuan Desert region were less sandy in texture when compared to dust source soil samples from the Southern High Plains region. Soil texture classifications of the two regions were obtained after plotting the granulometric data results that resulted from the average of the three consecutive analytical runs for each sample in the soil texture triangle and in accordance to the United States Department of Agriculture's soil texture grain size limit classification. That is to say, and by observing Figure 10.1, it may be concluded that:

(1). 38% of the bulk samples from the Chihuahuan Desert MEX region fitted into the two sand size related intervals (23% from sand texture-, and 15% from sandy loam-intervals) after particle size distribution examination.

Clay, clay loam, loam, silt loam, silty clay, and silty clay loam comprised the remaining soil texture classes acquired in this region with computed percentages values of 4%, 4%, 4%, 31%, 7%, and 12%, correspondingly.

(2). From the USA part of the Chihuahuan Desert, 69% of the bulk samples from this region fitted into the three sand size related intervals (19% from loamy sand-, 38% from sand-, and 12% from sandy loam-intervals) once particle distribution examination was concluded.

Loam and silt loam soil texture classes in this region comprised values of 8%, and 23% in that particular order.

(3). The Southern High Plains region dust source soils are predominantly sandy textured. From Figure 10.1, it could be implied that 85% of the bulk samples from this region fitted into the three sand size related intervals (24% from loamy sand-, 51% from sand-, and 10% from sandy loam-intervals) after laser particle examination. Clay loam, loam, silt loam, and silty clay loam involved the remaining soil texture classes in this region with percentages of 1%, 3%, 10%, and 1%, respectively.

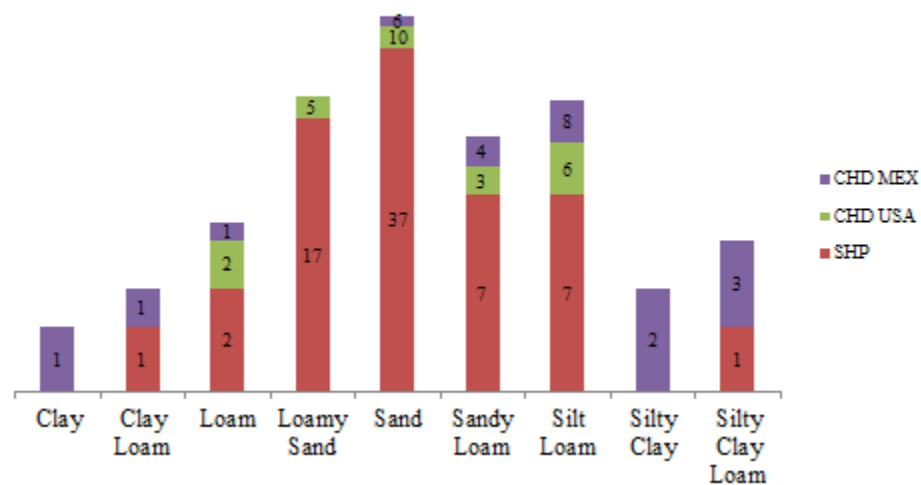


Figure 10.1 – Soil Texture classification resulted from USDA texture triangle. Granulometric data results obtained from Particle Size Distribution analysis. Chart presented at logarithmic scale.

Figure 10.2 illustrates a LANDSAT satellite image of the region under study reflecting dryland areas that are mostly found on the Chihuahuan Desert region.

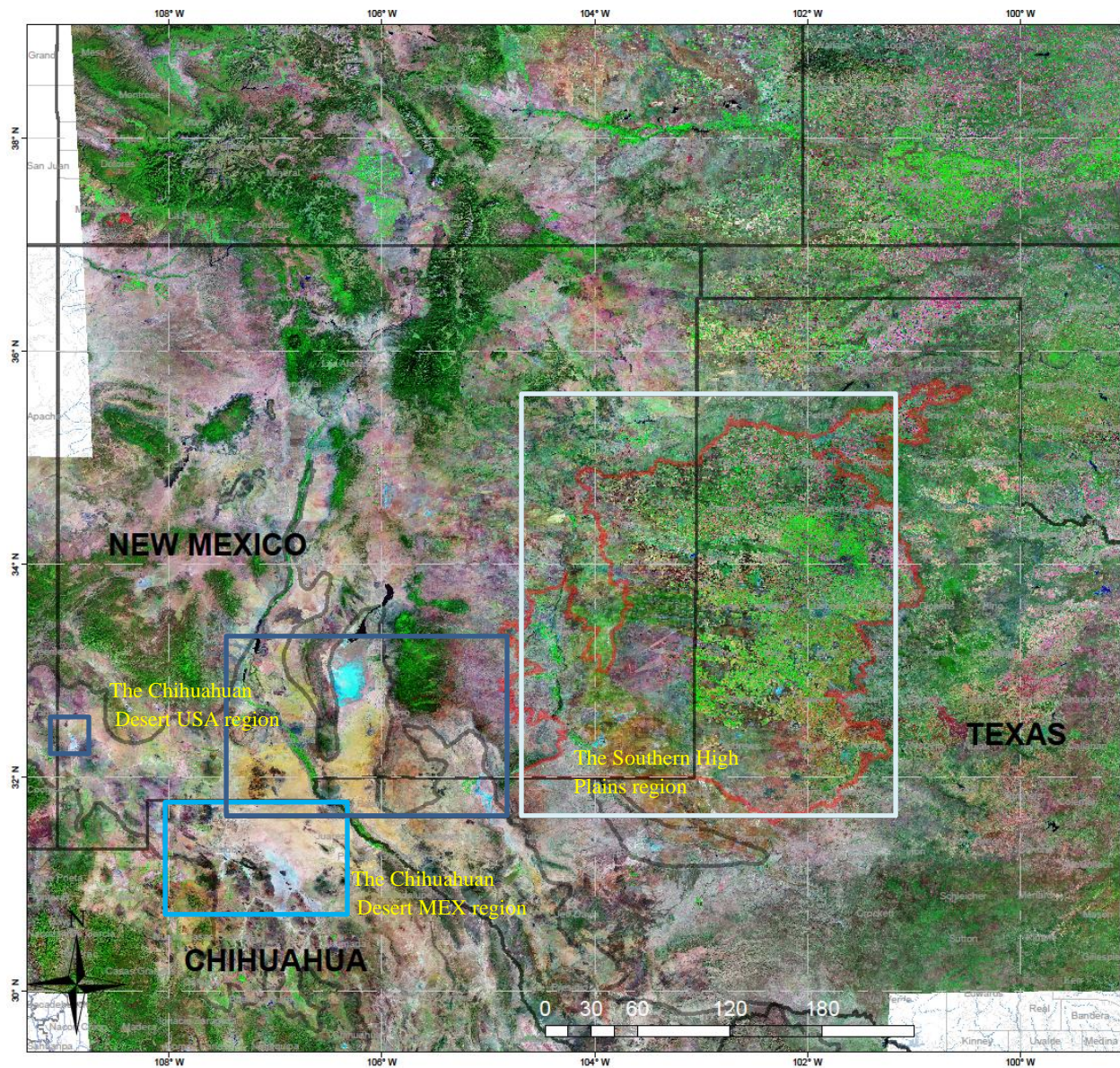


Figure 10.2 – Satellite imagery: The Chihuahuan Desert and Southern High Plains regions.

10.2 Land use codes and Land use categories association

Land use codes were created for a total of 125 sites from which dust plumes were perceptible on true color Moderate Resolution Imaging Spectroradiometer ([MODIS](#)) imagery from both the Terra and Aqua satellites during dust event days. Field verification and air photo interpretation activities settled the land use classification after examining the geomorphic classification alongside the geomorphic modifiers codes established on the [Bullard et al. \(2008\)](#) procedure.

After completing the land use classification process, a total of 28 unique land use classes characterized the samples from the Southern High Plains (west Texas and eastern New Mexico), the Chihuahuan Desert USA region (southern New Mexico and far west Texas), and the Chihuahuan Desert MEX region (northern Chihuahua). See Figure 10.3.

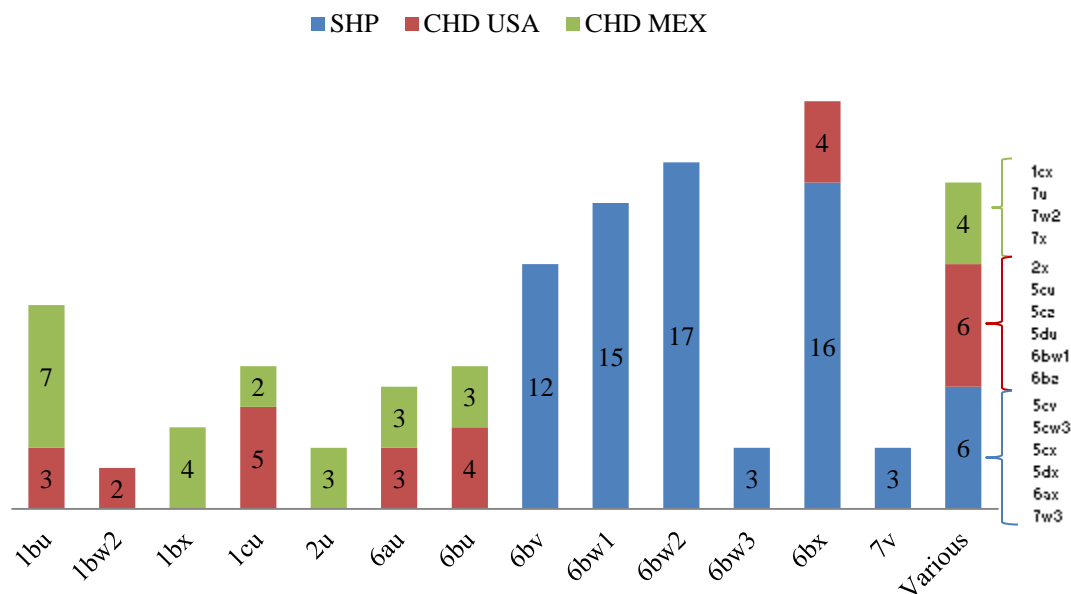


Figure 10.3 – Land Use Codes of 125 dust source sites.

Defining that every soil sample was associated with a dust event, then land use categories were directly related to dust production. As can be seen on Figure 10.4, all of the dust source sites that were involved in this project were comprised within five land use categories: Rangeland, Irrigated-, Non Irrigated-, Irrigated/Non Irrigated-farmlands, and Mixed land. The highest dust emission percentage value appeared to occur on Range land use, with a calculated percent value equal to 24.8%. Non Irrigated farmland category with a calculated percentage value of 16% was the second dust producer land use category. Dust production calculated percentage values equal to 14.4% and 12.8% from Mixed and Irrigated Farm land use categories were the third and fourth land use categories that influenced dust production in the regions. Only Irrigated / Non Irrigated farm land use category with a calculated percentage value below 5% was the minor land use category associated with dust production within the region.

It is important to mention that the bulk of soil samples categorized in the Unknown land use category group, were formed by not only dust source sites from eastern New Mexico that were located on military restricted areas limited the ability in characterizing in detailed these sites, but also the main samples taken from the Chihuahuan Desert MEX region were collected from playa basin sections commonly located on undisturbed land areas with scarce agriculture activity, and with no appreciable anthropogenic disturbance of soil observed.

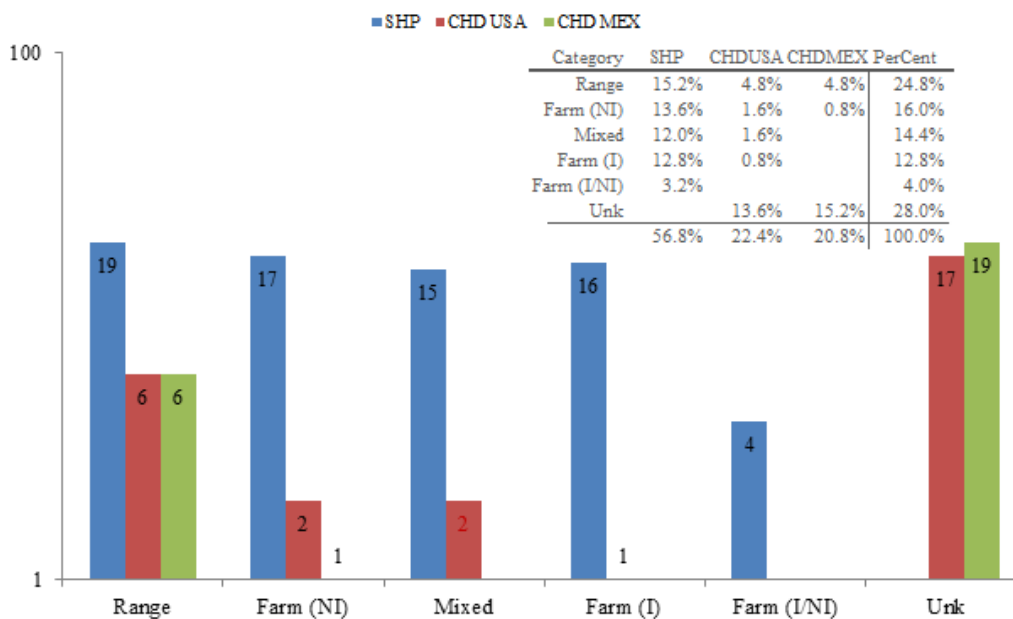


Figure 10.4 – Land Use Categories of 125 dust source sites.

Range and Non Irrigated farm land use categories delivered the main portion of dust source sites, covering almost 25% of the dust sources under study. In addition, Range was the only land use category observed in all the three regions under investigation.

Geomorphic Classification was established after land use categorization. Aeolian sand, alluvial, caliche, loess and playa comprised the geomorphic classes observed in the region under examination. From Figure 10.5, Aeolian Sand resulted as the geomorphic surface that categorized more than 50% of the total dust source soil samples (67.2% of dust emission sources). Playa was the geomorphic surface found in more than a half of the total soil samples taken from the Chihuahuan Desert MEX region. Playa surface resulted with a calculated percentage value of 43.4% for all the dust source soil samples collected across the entire Chihuahuan Desert region.

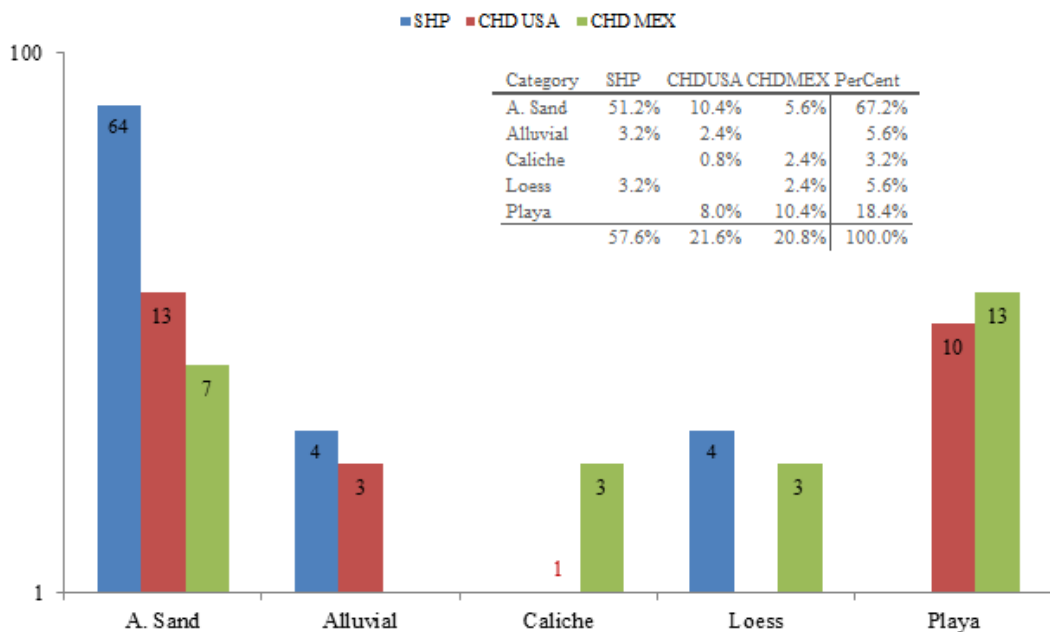


Figure 10.5 – Geomorphic surfaces of 125 dust sources sites.

Aeolian sand surface provided the highest number of samples for both the Southern High Plains and the Chihuahuan Desert USA regions, covering roughly 50% of the sources included in this project. Playa surface sources are found the most in northern Chihuahua.

In conclusion, no single land use category or geomorphic surface dominated the production of blowing dust within the three regions, the Southern High Plains (west Texas and eastern New Mexico), the Chihuahuan Desert USA (southern New Mexico and far west Texas), and the northern Chihuahua Desert MEX regions. As for land use and geomorphic classifications, no single land use category or single geomorphic surface dominated dust production across the regions under examination. However, it was implied that both aeolian sand as well as playa surfaces formed proportionally more dust plumes than other geomorphic surface types.

Aeolian sand surface dominated the west Texas and eastern New Mexico, i.e., the Southern High Plains region. Playa, aeolian sand, and caliche geomorphic surfaces comprised the bulk of the samples in the northern Chihuahua, southern New Mexico and far west Texas (the Chihuahuan Desert region).

10.3 Mineral Composition

Mineral composition was accomplished by X-ray diffraction (XRD) analysis. Individual digitized pattern process was completed on 83 bulk soil samples from the Southern High Plains (west Texas and eastern New Mexico), the Chihuahuan Desert USA (southern New Mexico and far west Texas), and the northern Chihuahua (the Chihuahuan Desert MEX) regions. After performing automated searching followed by manual searching (visual selection analysis) to acquire the best answer from a considerable number of match options, mineral compositions from X-ray diffractometry matched a total of 14 minerals with the majority of the strong reflections of the individual digitized pattern soil sample results:

- (1) Calcite, syn (Calcium Carbonate) [CaCO_3 PDFTM-2 card No. 5-0586],
- (2) Sodium Plagioclase Ordered (Sodium Aluminum Silicate) [$\text{NaAlSi}_3\text{O}_8$ PDFTM-2 card No. 9-0466],
- (3) Gypsum, syn (Calcium Sulfate Hydrate) [$\text{CaSO}_4 \cdot 2\text{H}_2\text{O}$ PDFTM-2 card No. 33-0311],
- (4) Dolomite (Calcium Magnesium Carbonate [$\text{CaMg}(\text{CO}_3)_2$ PDFTM-2 card No. 36-0426],
- (5) Calcite, magnesian (Calcium Magnesium Carbonate) [$(\text{Ca}, \text{Mg})\text{CO}_3$ PDFTM-2 card No. 43-0697],
- (6) Quartz, syn (Silicon Oxide) [SiO_2 PDFTM-2 card No. 46-1045],
- (7) Calcite (Calcium Carbonate) [CaCO_3 PDFTM-2 card No. 47-1743],

- (8) Calcium Plagioclase (Anorthite, sodian, ordered) $[(\text{Ca}, \text{Na})(\text{Al}, \text{Si})_2\text{Si}_2\text{O}_8]$ PDFTM-2 card No. 9-0465],
- (9) Sodium Plagioclase (Albite, disordered) $[\text{Na}(\text{Si}_3\text{Al})\text{O}_8]$ PDFTM-2 card No. 10-0393],
- (10) Calcium Plagioclase (Anorthite, sodian, ordered) $[(\text{Ca}, \text{Na})(\text{Al}, \text{Si})_2\text{Si}_2\text{O}_8]$ PDFTM-2 card No. 20-0528],
- (11) Muscovite 2M_2 (Potassium Sodium Aluminum Silicate Hydroxide) $[(\text{K}, \text{Na})_2\text{Al}(\text{Si}, \text{Al})_4\text{O}_{10}(\text{OH})_2]$ PDFTM-2 card No. 34-0175],
- (12) Muscovite (Muscovite, vanadian barian)
 $[(\text{K}, \text{Ba}, \text{Na})_{0.75}(\text{Al}, \text{Mg}, \text{Cr}, \text{V})_2(\text{Si}, \text{AlV})_4\text{O}_{10}(\text{OH}, \text{O})_2]$ PDFTM card No. 46-1409],
- (13) Halite, syn (Sodium Chloride) $[\text{NaCl}]$ PDFTM card No. 5-0628], and
- (14) Orthoclase barian (Potassium Barium Aluminum Silicate) $(\text{K}, \text{Ba}, \text{Na})(\text{Si}, \text{Al})_4\text{O}_8$ PDFTM card No. 19-002.

Minerals found in the samples from the Southern High Plains, the Chihuahuan Desert USA, and the Chihuahuan Desert MEX regions are shown on Table 10.1, Table 10.2, and Table 10.3, accordingly.

Table 10.1 – Concentration in percent on SHP soil sources.

Sample	Quartz	Calcite	Gypsum	Dolomite	Calcium Plagioclase
S(1) 2	100%				
S(4) 5	100%				
S(10) 9	100%				
S(12) 10	100%				
S(14) 12	100%				
S(22) 19	100%				
S(23) 20	100%				
S(27) 23	100%				
S(38) 71	100%				
S(44) 33	100%				
S(45) 34	100%				
S(49) 37	100%				
S(51) 39	100%				
S(54) 42	100%				
S(65) 51	100%				
S(72) 56	100%				
S(81) 65	100%				
S(2) 3	77%	23%			
S(13) 11	79%	21%			
S(18) 15	70%	30%			
S(21) 18	96%	4%			
S(26) 22	57%	43%			
S(37) 70	76%	24%			
S(53) 41	94%	6%			
S(59) 46	44%	56%			
S(78) 62	88%	12%			
S(29) 25	58%		42%		
S(33) 29	84%		16%		
S(76) 60	28%	57%		15%	
S(77) 61	48%	41%		11%	
S(6) 6	81%	3%			17%

Quartz (PDF™ card No. 46-1045), Calcite (PDF™ card No. 47-1743), Gypsum (PDF™ card No. 33-0311), Dolomite (PDF™ card No. 36-0426), and Calcium Plagioclase (PDF™ card No. 9-0465) records comprised the soil mineralogy of the SHP region.

Table 10.2 – Concentration in percent on Chihuahuan Desert USA soil sources.

Sample	Quartz	Gypsum	Calcite	Sodium Plagioclase	Muscovite	Dolomite	Calcium Plagioclase
D 1K U	100%						
DU 1.5 K M	100%						
RL-MV-60B	100%						
RL-MV-62A	100%						
Sh 1K M U	100%						
Sh 400 M	100%						
Dune Surface		100%					
Hammock		100%					
Salt Flat S2		100%					
Salt Flat S36		100%					
Salt Flat S56		100%					
SPHA BOT		100%					
WS Dune		100%					
WS Interdune		100%					
Coordinates	87%		13%				
McGregor	91%		9%				
Old Coe Lake	64%		36%				
Well 9	95%		5%				
Doña Ana	63%		1%	36%			
WRJG 006	76%		13%	10%			
WRJG 001	44%			56%			
Jornada Scrap	79%			21%			
WRJG 007	21%		22%		58%		
Well 15	81%		6%		13%		
Tula G	16%	84%					
Blue House	4%	56%				40%	
INBA	63%						37%

Quartz (PDF™ card No. 46-1045), Gypsum (PDF™ card No. 33-0311), Calcite (PDF™ card No. 5-0586), Sodium Plagioclase (PDF™ card No. 10-0393), Muscovite 2M2 (PDF™ card No. 34-0175), Dolomite (PDF™ card No. 36-0426), and Calcium Plagioclase (PDF™ card No. 20-0528) records contained the soil mineralogy of the CHD USA region.

Table 10.3 – Concentration in percent on Chihuahuan Desert MEX soil sources.

Sample	Quartz	Calcite	Sodium Plagioclase	Orthoclase	Halite	Dolomite
COR 009	100%					
SMD 002	100%					
SMD 003	100%					
SMD 026	100%					
ASC 001	33%	67%				
COR 001	74%	26%				
COR 010	66%	34%				
DBM 001	59%	42%				
GV 002	52%	48%				
LPAL 005	37%	63%				
LF 004	54%	46%				
COR 004	66%		35%			
COR 008	89%		11%			
HWY 45	62%		39%			
TLG 001	33%		67%			
LSM 002	75%	12%	13%			
LSM 003	73%	11%	16%			
SELP 003	29%	55%	16%			
LG 004	17%	44%	40%			
COR 005	35%	28%	37%			
LDP 001	55%	6%	39%			
CLP 001	21%	66%			14%	
COR 002	69%	16%			16%	
ASC 002				20%	80%	
ASC 003	66%				34%	
CLP 002	49%	42%				9%

Quartz (PDF™ card No. 46-1045), Calcite (PDF™ card No. 5-0586), Sodium Plagioclase (PDF™ card No. 9-0466) - (PDF™ card No. 10-0393), Halite (PDF™ card No. 5-0628), and Dolomite (PDF™ card No. 36-0426) records denoted the soil mineralogy of the CHD MEX region.

10.4 Standardized value range analysis

As shown in Table 10.4, standardized values of elemental concentration analysis provided five dust source sites which were outliers considered after correspondence statistical analysis. Highest standardized values of Pb, As, K, Ba-Cs, and Ca-Mg-Sr sets were found on S(2) 3, S(29) 25, S(59) 46, S(26) 22, and S(76) 60 soil sites, respectively. Top standardized concentration values for: (a) Lead proceeded from a site surrounded by farmhouses where center pivots were present. In addition, Pb uppermost standardized value was localized on *Mixed* (where farmland, rangeland, urban, and rural development were perceived) land use class, (b) Arsenic came from a site where both petroleum production and dry farmland were noticed. Moreover, As peak standardized value was found on Rangeland area, (c) Potassium derived from both Irrigated-, and Non-irrigated-farmland. What is more, K highest standardized value approached from Mixed land use class, (d) Barium and Cesium originated from Non-irrigated farmland, and (e) Calcium, Magnesium, and Strontium came from Irrigated farmland.

Mn-Ti-Zr, Al-Cr-Fe-P-Rb, and Ge-Si elemental sets obtained their highest standardized values on S(45) 34, S(41) 30, and S(38) 71 dust source sites, but they were not considered outliers because their standardized data behaved approximately multivariate normal. Therefore, S(45) 34 and S(41) 30 sites were included in Group 1 of the Principal Component Analysis statistical analysis. Likewise, S(38) 71 dust source site was comprised in Group 4 of the Principal Component Analysis results. Moreover, uppermost standardized values of Mn-Ti-Zr were localized on Mixed land use class; Al-Cr-Fe-P-Rb provided its highest standardized value from Irrigated / No Irrigated farmland land use class. The Ge-Si set provided its maximum standardized value from Irrigated farmland area.

An unique case occurred with Copper which highest standardized value was observed on S(48) 36 soil site localized on Mixed land use class where farmland, rangeland, urban, and rural development were detected. Statistical observations of this site in particular appeared plotted distant from the origin but not far away enough to be perceived into an outlying position in Principal Component analysis.

Table 10.4 – Statistical Analysis Results.

CORRESP. Outliers	PCA Outliers	FINAL DATASET GROUPS			
SITES	SITES	GROUP 1	GROUP 2	GROUP 3	GROUP 4
S(2) 3	S(43) 32	S(61) 47	S(30) 26	S(6) 6	S(38) 71
S(18) 15	S(47) 35	S(17) 14	S(52) 40	S(12) 10	S(80) 64
S(25) 21	S(0) 1	S(28) 24	S(62) 48	S(10) 9	S(9) 8
S(26) 22	S(37) 70	S(32) 28	S(74) 58	S(22) 19	S(15) 13
S(29) 25	S(31) 27	S(63) 49	S(79) 63	S(23) 20	S(39) 72
S(33) 29	S(13) 11	S(65) 51	S(3) 4	S(4) 5	S(49) 37
S(59) 46	S(78) 62	S(45) 34	S(20) 17	S(27) 23	S(66) 52
S(64) 50	S(53) 41	S(71) 55	S(36) 69	S(1) 2	S(73) 57
S(68) 54	S(55) 43	S(50) 38	S(42) 31	S(14) 12	S(75) 59
S(76) 60		S(51) 39	S(57) 45		S(81) 65
S(77) 61		S(34) 67	S(67) 53		S(35) 68
		S(41) 30	S(82) 66		
		S(72) 56			
		S(56) 44		NO GROUP	
		S(19) 16		S(21) 18	
		S(54) 42		S(48) 36	
		<div style="border: 1px dashed orange; display: inline-block; width: 15px; height: 10px; vertical-align: middle;"></div> Sites with highest standardized values			

Explicit sites resulting from Correspondence and Principal Component statistical analyses are comprised on first two columns. Final dataset groups were obtained after principal component statistical examination. Final dataset groups included in the table arose from Factor comparison.

The values of As, Cu, Ga, and Pb through all soil texture classes were inconsistent and comprised their peak standardized values on Sandy Loam texture class. Al, Fe, K, Mn, P, and Ti high standardized values were found on Silty Clay Loam soil texture class. Highest standardized concentration values for Ca, Mg, and Sr occurred on Clay Loam soil texture. Ba, Cr, Cs, and Zr peak standardized concentration values matched the Silt Loam soil texture. Ge, and Rb highest standardized values were observed on Loam soil texture class. Silicon uppermost standardized value fitted on Loamy Sand Texture. No peak standardized values were observed in the Sand soil texture, causing to not include this soil texture class in Table 10.5.

Table 10.5 – Standardized values: relationships among elemental concentrations and sites

Element	Highest Z			Range of Z values for soil texture					
	Value	Site	Sample	Clay Loam	Loam	Loamy Sand	Sandy Loam	Silt Loam	Silty Clay Loam
Al	3.00	36	S(41) 30	0.61	1.98	0.22	0.01	1.78	2.85
As	2.28	25	S(29) 25	-0.37	0.22	0.27	1.00	0.29	-0.35
Ba	3.62	22	S(26) 22	1.98	1.47	0.16	0.13	2.02	1.91
Ca	3.89	66	S(76) 60	3.89	0.42	-0.13	0.57	1.27	2.88
Cr	3.38	36	S(41) 30	-0.64	0.54	0.10	0.05	1.25	1.01
Cs	3.60	22	S(26) 22	1.95	1.42	0.19	0.15	1.98	1.98
Cu	2.47	42	S(48) 36	0.55	0.21	0.21	1.13	0.78	0.42
Fe	2.88	36	S(41) 30	0.80	2.06	0.15	0.09	1.76	2.79
Ga	2.16	6	S(6) 6	0.14	-0.13	0.36	1.10	0.55	0.00
Ge	2.02	34	S(38) 71	-0.83	0.64	0.33	-0.59	-0.27	-0.43
K	2.83	52	S(59) 46	0.73	1.95	0.17	0.18	1.76	2.83
Mg	6.69	66	S(76) 60	6.69	0.55	-0.05	0.35	0.76	1.25
Mn	3.42	40	S(45) 34	0.93	1.76	0.03	0.07	2.05	2.53
P	3.33	36	S(41) 30	1.60	0.67	0.16	-0.04	2.01	3.16
Pb	2.09	3	S(2) 3	-0.84	-0.25	0.35	1.09	0.25	-0.40
Rb	3.24	36	S(41) 30	0.36	2.20	0.16	-0.44	1.43	1.87
Sr	4.23	66	S(76) 60	4.23	-0.10	0.01	0.58	0.02	0.17
Si	1.93	34	S(38) 71	-1.45	-0.10	0.27	-0.60	-0.49	-0.96
Ti	3.39	40	S(45) 34	0.14	1.70	0.24	0.01	1.93	2.13
Zr	2.76	40	S(45) 34	-1.05	0.47	0.19	-0.71	0.90	-0.02

10.5 Ordination Analysis

Hierarchical clustering connectivity, correspondence analysis, and principal component analysis were the ordination statistical techniques used in this study. Master dataset matrix was designed by including two particle size data variables (clay and silt), one naturally occurring soil property variable (total organic carbon, TOC), twenty elemental concentrations in parts per million [ppm]: Al, As, Ba, Ca, Cr, Cs, Cu, Fe, Ga, Ge, K, Mg, Mn, P, Pb, Rb, Si, Sr, Ti, and Zr, and thirty soil name categories: Abilene, Acuff, Amarillo, Arch, Arno, Arvana, Berda, Bigetty, Brownfield, Church, Clovis, Ector, Glendale, Gomes, Hindman, Maljama, Midessa, Olton, Pantex, Patricia, Pep, Portales, Potter, Pullman, Reagan, Reeves, Simona, Sotim, Spantara, and Springer, that in association to irrigated-, no irrigated-, irrigated/no irrigated-farmland types, as well as mixed, and range land use classes. The aim of ordination analysis consisted in exploring relations and linkage between variables and their impact to the potential wind erosion of soils during dust events.

10.5.1 Preliminary Statistical Relationship

As shown in Figure 10.6, cluster analysis exhibited five hierarchical clusters that provided a preliminary statistical relationship (short and large Euclidean distances) between the fifty eight variables master dataset matrix:

- (1) K-Fe-Al-Ti-Mn-Cs-Ba-P-Silt-Rb-Cr-Mixed-Rural,
 - (2) Pep-Hindman-Berda-Reeves-Clovis-Spantara-Church-Arch,
 - (3) Olton-Simona-Spring-Non irrigated farmland-Brownfield-Arvana-Si-Ge-Zr-Abilene,
 - (4) Pantex-Pullman-Maljama-Potter-Sotim-Portales-Irrigated farmland-Reagan-Gomes,
- and

(5) Pb-Ga-As-Cu-Patricia-Acuff-Range-TOC-Ca-Mg-Clay-Sr-Amarillo

Hierarchical clustering connectivity was not observed on Midessa, Arno, Bigetty, Glendale, and Ector soils, after explorative data mining process completion.

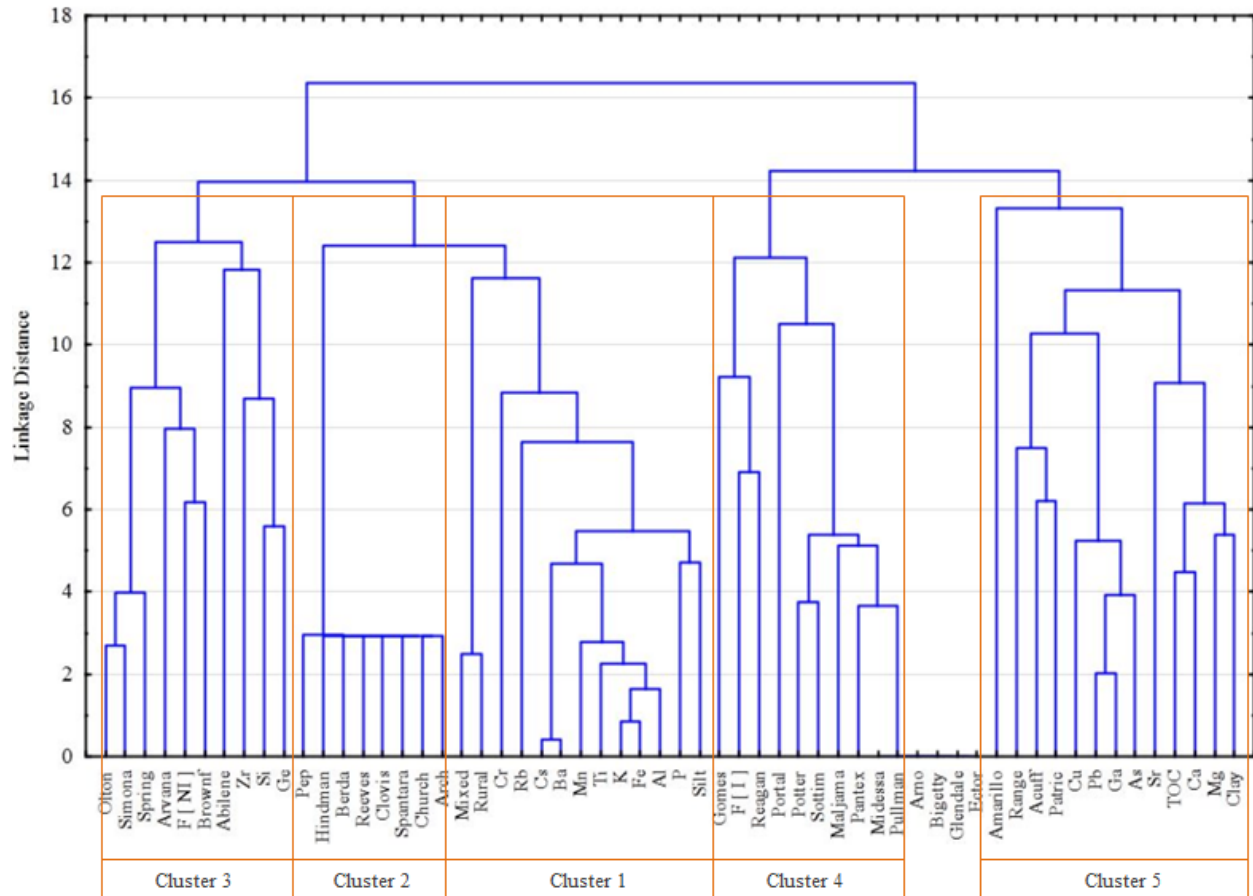


Figure 10.6 – Preliminary Statistical Relationship.

Tree Diagram of 58 variables with complete linkage and geometric distances.

Ward's analysis on Cluster 5 suggested the existence of a probable affinity among the anthropogenic-related metals Pb, Ga, As, and Cu as well as the calcareous elements Ca and Mg which shaped a strong association with total organic carbon, TOC, and Clay variables. Furthermore, Range land use class in this cluster (on Patricia, Acuff, and Amarillo soils), was the principal land use class that was perhaps impacted from activities that may have generated the anthropogenic related metals mentioned above. Furthermore, an affinity between the elemental concentrations of the elements comprising cluster 5 could not only be associated with the Clay soil fraction, but also prone to dispersion across the region (compared to those that comprised the rest of the elemental concentrations under statistical analysis), being carried away on the fine particle fraction emitted from fugitive dust storm sites. Thus, the metallic concentrations of the sites that comprised this hierarchical cluster perhaps continued to be suspended into the atmosphere long enough to be transported long distances.

10.5.2 Refining Statistical Relationship

Pearson's correlation analysis screened out K, Mn, Ge, and Si concentration variables from the master dataset matrix. Correspondence analysis performed in the refined matrix provided not only homogeneous but also well separated subsets after hierarchical divisive clustering examination. This polished matrix included two particle size fractions, one naturally occurring soil property, sixteen elements, thirty soil name categories, and five land use classes.

As shown in Figure 10.7, cluster analysis exhibited five dendograms with connectivity after minimum variance examination on the fifty-four variables refined dataset matrix:

- (1) Fe-Al-Ti-Cs-Ba-P-Silt-Clay-Rb-Cr-Mg-Ca-TOC-Sr,
- (2) Spantara-Reeves-Clovis-Berda-Church-Hindman-Pep,

- (3) Pb-As-Cu-Acuff-Patricia-Range-Mixed-Rural-Amarillo,
- (4) Olton-Simona-Springer-F(NI)-Arvana-Brownfield-Zr-Ge-Abilene, and
- (5) Sotim-Pullman-Potter-Maljama-Pantex-Portales-F(I)-Reagan-Gomes.

Midessa, Arno, Bigetty, Glendale, Ector, and Reeves soils did not show relative clustering.

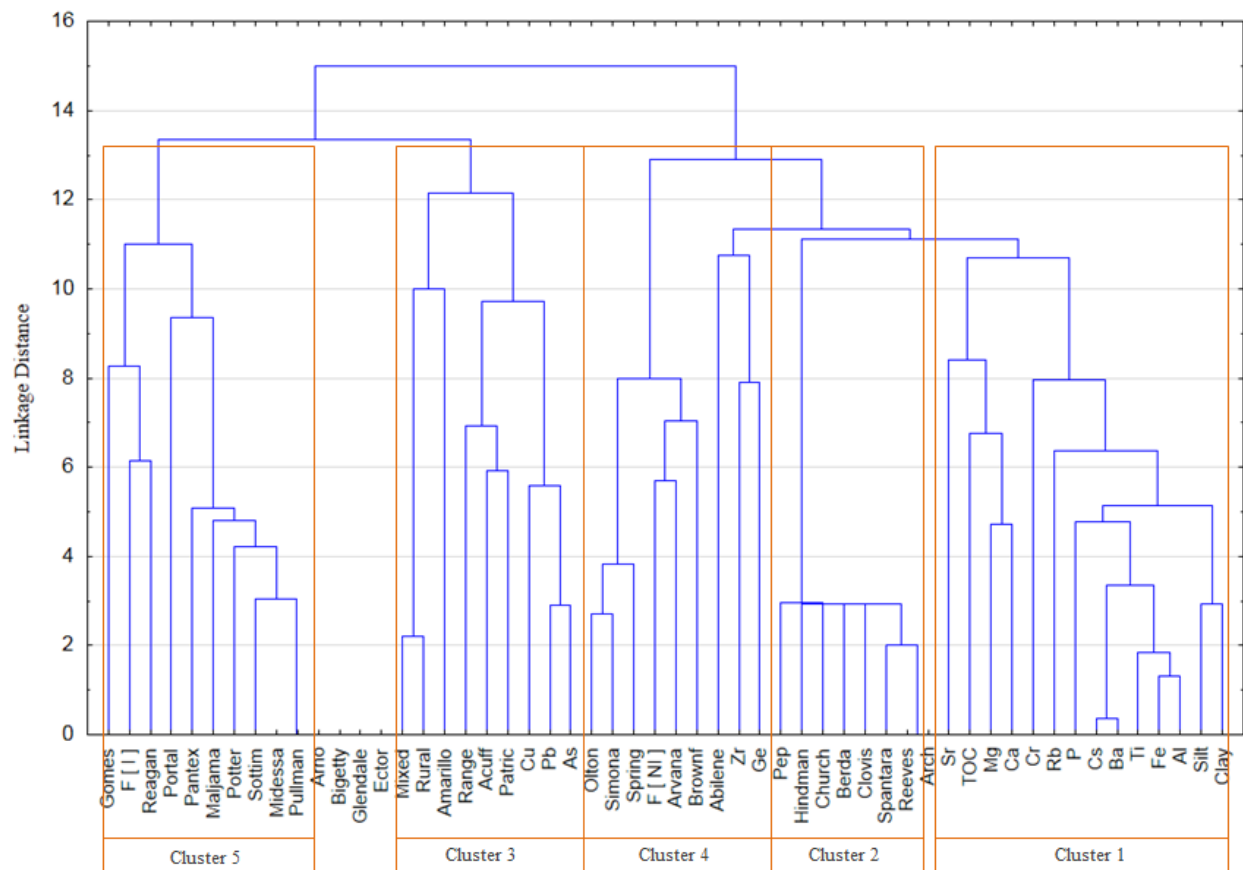


Figure 10.7 – Refined Statistical Relationship.

Tree diagram of 54 variables with complete linkage and geometric distance.

Ward's analysis on Cluster 3 suggested that anthropogenic metals, Cu, Pb, and As, may be directly impacted from Range, Rural, and Mixed land use activities located on Patricia, Acuff, and Amarillo soils. After discerning Cluster 5, Irrigated farmland land use might be considered as an indirect provider of these metals, especially from Gomes, Reagan, Portales, Maljama, Potter, Sotim, and Pullman soils.

10.5.3 Narrowing Statistical Relationship

Correspondence analysis aided noticing structural associations among the variables categories (elemental concentrations confined on columns) and cases (dust source sites contained on rows) that were impossible to observe either by visual scrutiny or simple statistical analysis. Elemental concentrations that had similar profile distribution were perceived on column graph. Likewise, dust source sites with similar profile distribution were observed on row graph.

After observing both column and row graphs, K, Mn, Ga, and Ti concentration values, besides S(25) 21, S(64) 50, S(68) 54, S(33)29, S(59) 46, S(2) 3, S(76) 60, S(77) 61, S(29) 25, S(26) 22, and S(18) 15 dust source sites were removed from the master dataset matrix to determine the probability of global association between rows and columns.

Correspondence analysis then provided a chart in which row and column coordinates were summarized in a single plot, shown in Figure 10.8. From this chart, not only the distances between row points, but also the distances between column points can be deduced, but not mixing the distance between row points and column points, however.

10.5.4 Principal Component Analysis

Principal component analysis eliminated redundant information by obtaining a small number of variables that made it easier to apply on other multivariate statistical techniques. Uncorrelated variables that represented the structure of the original collection of variables in an optional way were obtained after performing the Principal Component statistical technique.

Refined master dataset matrix (including Inductively Coupled Plasma Optical Spectrometry, ICP-OES data) after correspondence analysis completion, comprised fifty nine variables to be examined under the ordination analysis known as Principal Component Analysis (PCA) with Varimax normalized rotation (orthogonal rotation methodology).

A total of 88% of total variation was embraced within eight factors after principal component examination's first attempt. Since the principal components were ordered according to importance (first principal component described the largest part of the variance), it was adequate to determine the first few principal components that contained large amounts of variation (often 90%), and the few last principal components that contained usually extreme observations. An interesting aspect observed in Figure 10.9 that plotted the first two principal components, was that the anthropogenic metals As, Pb, and Cu, were observed grouped-comparable with those of the correspondence analysis results, suggesting that Rural, Mixed, and Range land use classes were statistically predicted to associate with the presence of these anthropogenic metals within the Southern High Plains region. Soil name variables were, on the other hand, the observations situated distant from the origin, but not that far away to classify them as outliers.

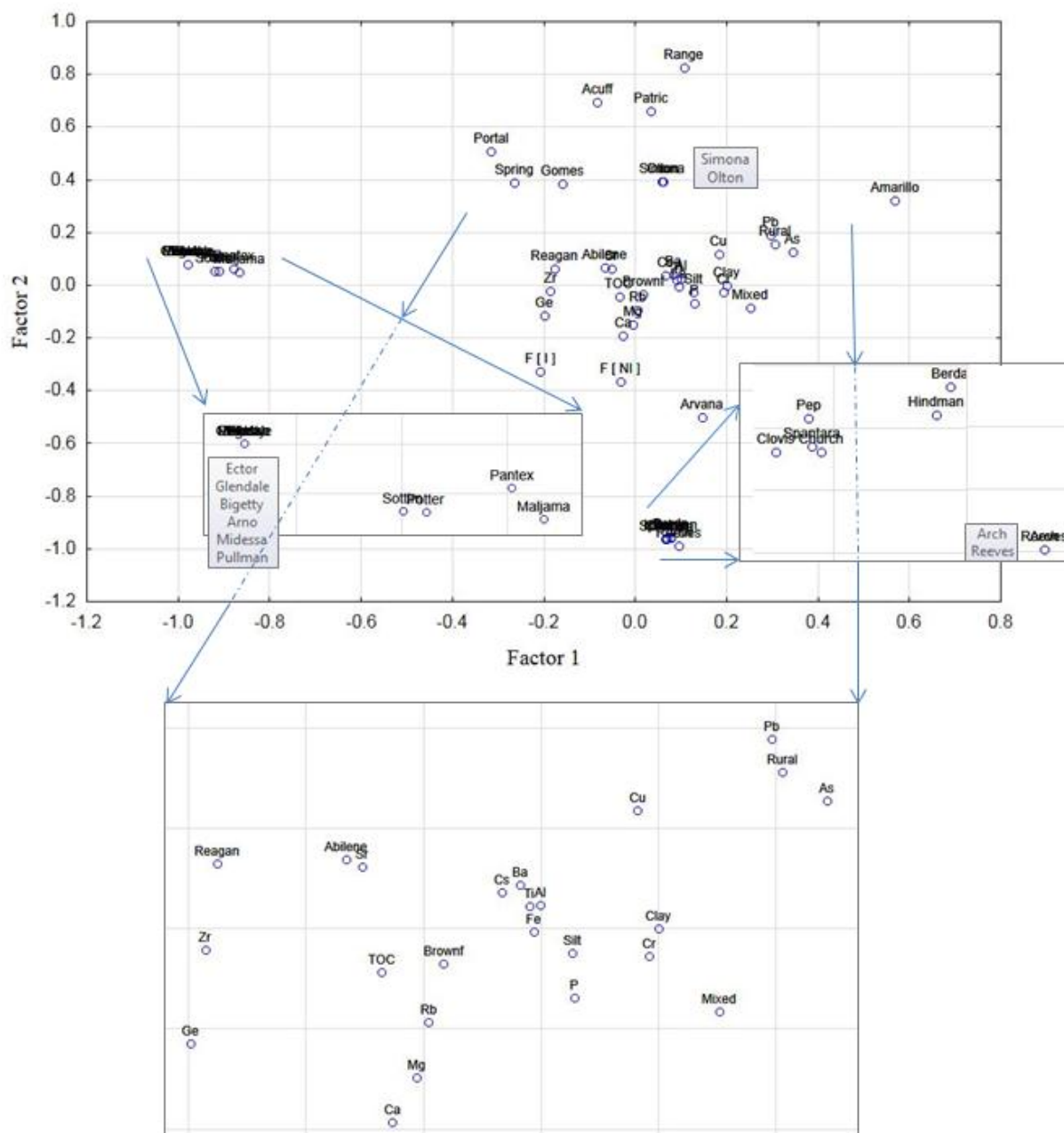


Figure 10.9 – PCA factor loadings. First attempt results.

Factor 1 vs Factor 2 on original database.

The second attempt on Principal Component Analysis examination computed a percentage value nearly to 80% of total variance distributed on five factors (See Table 10.6). After removing the Soil Name variables from the reduced master dataset matrix, the principal components became stronger, shortening the effect of outliers on both first few and the last few principal components. Moreover, the last few principal components identified outliers that did not follow apparently the correlation configuration of the rest of the data.

Table 10.6 – PCA factor loading values

Variable Factor 1		Variable Factor 2		Variable Factor 3	
Al	0.97041	Pb	0.925819	Mixed	0.98734
Ti	0.96540	As	0.866381	Rural	0.98629
Fe	0.96102	Cu	0.81534 *	Cu	0.12441 **
Ba	0.90171	Range	0.57224 *	Sr	0.09165 **
Cs	0.89584 *	Clay	0.234162	Silt	0.08334
Variable Factor 4		Variable Factor 5			
Ca	0.83582 *	F [NI]	0.78590		
Mg	0.70671	Zr	0.23556		
TOC	0.68637	Range	0.16879 **		
Sr	0.65072 *	Sr	0.08559 ***		
Cs	0.34787 **	Ca	0.06038 **		

Strong to weak loading values:

* First positive correlation

Factor loading values Varimax normalized from 24-variables reduced master dataset matrix. Extraction: Principal components. Loadings are noted at p-values > .700000.

Observations that disrupted the correlation structure enforced by the bulk of the data were perceived when plotting the last few components. As displayed in Figure 10.10, it was observed that three groups gathered together at different factor loading values, but a total of nine samples [S(78) 62, S(55) 48, S(53) 41, S(0) 1, S(37) 70, S(47) 35, S(43) 32, S(13) 11, and S(31) 27], were located at outlying position in the plot causing to be classified as extreme cases because of their behavior after plotting factor 3 vs. factor 4 last few principal components.

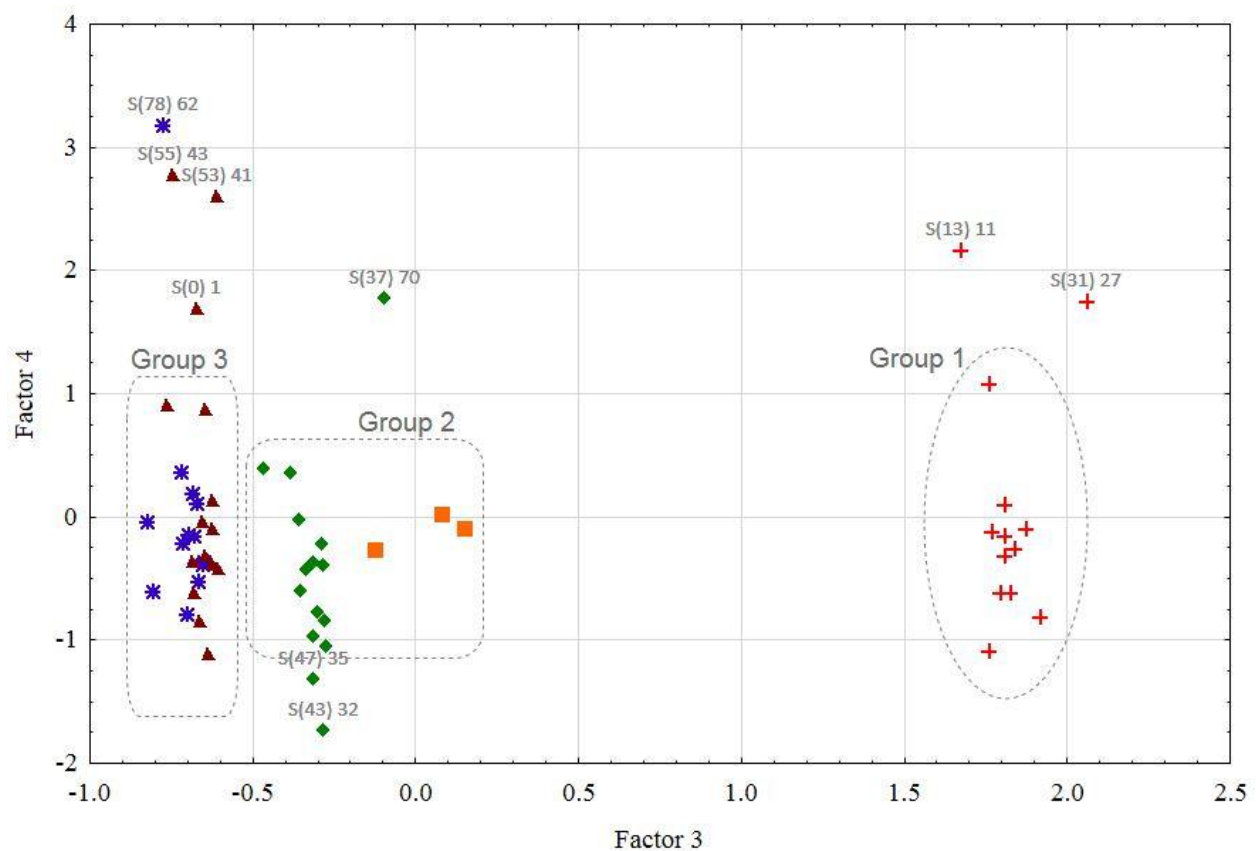


Figure 10.10 – PCA. Factor 3 vs. Factor 4 on Reduced master database matrix.

Southern High Plains formation data. Scatter plotting of observations with respect to factors 3 vs. 4 . Distinguished extreme cases are observed. Reduced master database matrix conformed by 24 variables (elemental concentrations and land use) and 50 cases (dust source sites).

The third attempt on Principal Component Analysis results computed a percentage value of nearly 84% of total variance distributed on five factors (See Table 10.7). After screening out the nine dust source sites that were considered obvious cases from the reduced master dataset matrix, the principal components results of the regression were noticeably changed. The number of Principal Components remained the same, and as is shown in figure 10.11, four groups gathered together after scattered plotting 2 vs. 4 factor loading values after regression analysis completion on the reduced master database matrix.

Table 10.7 – PCA Final factor loading values

Factor	Eigenvalue	Percent Variance	Cumulative Percent Variance
1	11.3846	47.4359	47.4359
2	3.6518	15.2158	62.6517
3	2.1492	8.9551	71.6069
4	1.6466	6.8607	78.4675
5	1.3182	5.4926	83.9602

Southern High Plains elemental coefficients factors resulted from reduced master database matrix. Percent variance explained by successive principal components (factors). Eigenvalues and percent variance explained by the 5 principal component. Five factors contained nearly 84% of the entire variance.

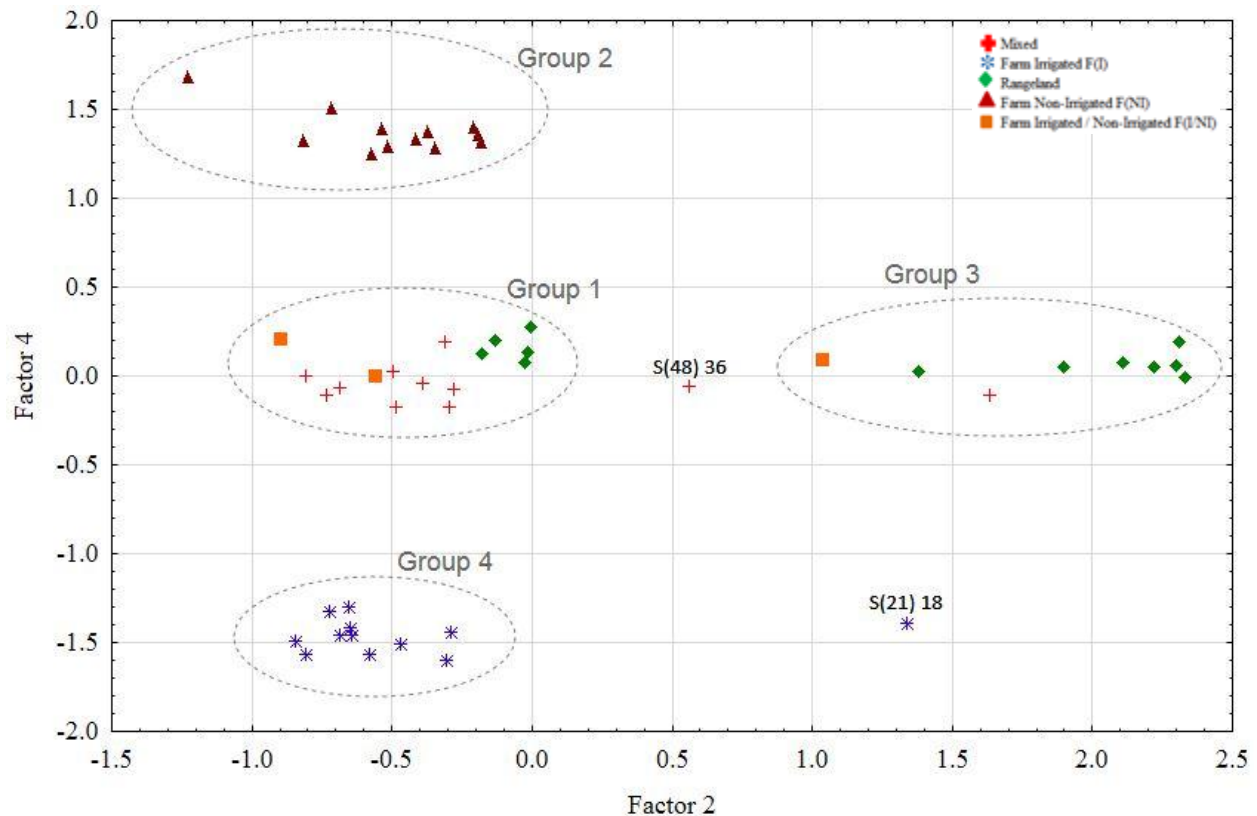


Figure 10.11 – PCA. Factor 2 vs. Factor 4 on reduced master database matrix.

Southern High Plains formation data: scatter plotting of observations with respect to factors 2 vs. 4. Reduced master database matrix conformed by 24 variables (metal concentrations and land use classes) and 50 cases (soil sites).

As reflected on Table 10.8, Principal component analysis on the final reduced database matrix, defined 4 factor loadings groups with sixteen, twelve, nine, and eleven cases (dust source sites) that were comprised into 1, 2, 3, and 4 component groups, accordingly. It was noted that both S(21) 18 and S(48) 36 cases did not fit properly on any of these groups.

Table 10.8 – PCA. Component Groups for dust source sites. Final attempt.

Group 1	Group 2	Group 3	Group 4	No Group
S(61) 47	S(30) 26	S(6) 6	S(38) 71	S(21) 18
S(17) 14	S(52) 40	S(12) 10	S(80) 64	S(48) 36
S(28) 24	S(62) 48	S(10) 9	S(9) 8	
S(32) 28	S(74) 58	S(22) 19	S(15) 13	
S(63) 49	S(79) 63	S(23) 20	S(39) 72	
S(65) 51	S(3) 4	S(4) 5	S(49) 37	
S(45) 34	S(20) 17	S(27) 23	S(66) 52	
S(71) 55	S(36) 69	S(1) 2	S(73) 57	
S(50) 38	S(42) 31	S(14) 12	S(75) 59	
S(51) 39	S(57) 45		S(81) 65	
S(34) 67	S(67) 53		S(35)68	
S(41) 30	S(82) 66			
S(72) 56				
S(56) 44				
S(19) 16				
S(54) 42				

Groups formed after the principal component analysis final attempt. S(78) 62, S(55) 43, S(53) 41, S(0) 1, S(37) 70, S(47) 35, S(43) 32, S(13) 11, and S(31) 27 dust source sites were statistically considered extreme cases and therefore they were removed from the final reduced database matrix.

10.6 Connectivity Results Acquirement

Standardized value range exploration, Pearson's correlation coefficient as well as ordination analysis techniques used in this study concluded a satisfactory multivariate data examination. Principal component analysis statistical technique verified the connectivity results previously acquired from Cluster and Correspondence analyses; these were prelude statistical methods to the subsequent application of multivariate statistical methods from which the homogeneity of a set of data (final reduced database matrix) was attained.

The key important procedure to mention is that the original database matrix was reduced on observation in both, the columns (representing elemental concentrations, land use classes, and soil names categories) and the rows (characterizing dust source sites) when performing hierarchical connectivity methodology, as well as cluster, correspondence and principal component analyses. Table 10.9 shows the outstanding cases that were observed (after standardized range exploration, among correspondence and principal component analyses) and separated from statistical analysis on second attempts.

Table 10.9 – PCA. Connectivity Results Acquirement.

CORRESPONDENCE	PCA	FINAL DATASET GROUPS					
SITES	SITES	GROUP 1	GROUP 2	GROUP 3	GROUP 4		
S(2) 3 <i>Q+C</i>	S(43) 32	S(61) 47	S(30) 26	S(6) 6 <i>Q+C+CP</i>	S(38) 71 <i>Q100</i>		
S(18) 15 <i>Q+C</i>	S(47) 35	S(17) 14	S(52) 40	S(12) 10 <i>Q100</i>	S(80) 64		
S(25) 21	S(0) 1	S(28) 24	S(62) 48	S(10) 9 <i>Q100</i>	S(9) 8		
S(26) 22 <i>Q+C</i>	S(37) 70 <i>Q+C</i>	S(32) 28	S(74) 58	S(22) 19 <i>Q100</i>	S(15) 13		
S(29) 25 <i>Q+G</i>	S(31) 27	S(63) 49	S(79) 63	S(23) 20 <i>Q100</i>	S(39) 72		
S(33) 29 <i>Q+G</i>	S(13) 11 <i>Q+C</i>	S(65) 51 <i>Q100</i>	S(3) 4	S(4) 5 <i>Q100</i>	S(49) 37 <i>Q100</i>		
S(59) 46 <i>Q+C</i>	S(78) 62 <i>Q+C</i>	S(45) 34 <i>Q100</i>	S(20) 17	S(27) 23 <i>Q100</i>	S(66) 52		
S(64) 50	S(53) 41 <i>Q+C</i>	S(71) 55	S(36) 69	S(1) 2 <i>Q100</i>	S(73) 57		
S(68) 54	S(55) 43	S(50) 38	S(42) 31	S(14) 12 <i>Q100</i>	S(75) 59		
S(76) 60 <i>Q+C+D</i>		S(51) 39 <i>Q100</i>	S(57) 45		S(81) 65 <i>Q100</i>		
S(77) 61 <i>Q+C+D</i>		S(34) 67	S(67) 53		S(35) 68		
		S(41) 30	S(82) 66				
		S(72) 56 <i>Q100</i>					
		S(56) 44		NO GROUP			
		S(19) 16		S(21) 18 <i>Q+C</i>			
		S(54) 42 <i>Q100</i>		S(48) 36			
<i>Q100</i> Quartz at 100% <i>Q+C</i> Quartz+Calcite <i>Q+G</i> Quartz+Gypsum <i>Q+C+D</i> Quartz+Calcite+Dolomite <i>Q+C+CP</i> Quartz+Calcite+Calcium Plagioclase		<div> <div></div> Sites with highest standardized values </div>					

Blatant cases observed on correspondence and principal component analyses are listed in first two columns. Final dataset groups resulted from the last principal component examination on final reduced database matrix. Final dataset groups included in the table arose from the factor comparison.

Connectivity results derived from table 10.9 were that:

(1) Final dataset groups were formed after Principal component analysis final attempt. S(43) 32, S(47) 35, S(0) 1, S(37) 70, S(31) 27, S(13) 11, S(78) 62, S(53) 41, and S(55) 43 dust source sites listed in second column of Table 10.9, were statistically considered extreme cases and therefore they were removed from final reduced database matrix.

(2) Important to notice is that S(2) 3, S(18) 15, S(25) 21, S(26) 22, S(29) 25, S(33) 29, S(59) 46, S(64) 50, S(68) 54, S(76) 60, and S(77) 61 dust source sites were removed from the correspondence analysis performed earlier in this study because they were considered outlier observations. Moreover, higher standardized values for Pb, Ba-Cs, As, K, Ca-Mg-Sr elemental groups were obtained from S(2) 3, S(26) 22, S(29) 25, S(59) 46, and S(76) 60 dust source sites. As explained earlier, these soil sites were removed from the original database matrix after correspondence analysis examination considered them as outlier cases.

(3) Likewise, Mn-Ti-Zr, Al-Cr-Fe-P-Rb, and Ge-Si sets had their topmost standardized value from S(45) 34, S(41) 30, and S(38) 71 dust source sites. These sites were included on the final reduced database matrix due mainly that their elemental concentration values were approximately multivariate normal.

(4) Copper concentration proceeding from S(48) 36 soil site produced its single observation situated distant from the origin, but not that far away to be considered to either being comprised in a singular final dataset group nor being perceived as a blatant case.

(5) Mineralogical characterization resulting from X-Ray Diffraction analysis comprised the Quartz 100% dust source sites on the final dataset groups 3, 2, and 4. Quartz + Calcite; Quartz + Gypsum; and Quartz + Calcite + Dolomite mineral sets were characterized on dust source sites that were not considered in the principal component analysis, final attempt.

10.6.1 Box Plot Analysis

Box plot descriptive statistics analysis was performed to display differences between elemental concentration values (dependent; continuous variables) and land use classes (predictor; categorical variable) to indicate the degree of dispersion and skewness in the data in order to identify outliers.

After Box plot analysis completion, it is observed from Table 10.10 that not only final dataset groups 4, and 2 were connectivity localized on Non Irrigated farm and Irrigated Farm land use classes comprising a total of twenty three dust source sites. Final dataset groups 1 and 3 were spread within Mixed, Range, and Irrigated/No Irrigated farm land use classes.

Table 10.10 – Box Plot. Connectivity Results Acquirement.

MIXED		FARM (I)		RANGE		FARM (NI)		FARM (I/NI)	
S(14) 12	G3	S(9) 8	G4	S(4) 5	G3	S(3) 4	G2	S(1) 2	G3
S(17) 14	G1	S(15) 13	G4	S(6) 6	G3	S(20) 17	G2	S(41) 30	G1
S(19) 16	G1	S(35) 68	G4	S(10) 9	G3	S(30) 26	G2	S(72) 56	G1
S(28) 24	G1	S(38) 71	G4	S(12) 10	G3	S(36) 69	G2		
S(32) 28	G1	S(39) 72	G4	S(22) 19	G3	S(42) 31	G2		
S(45) 34	G1	S(49) 37	G4	S(23) 20	G3	S(52) 40	G2		
S(56) 44	G1	S(66) 52	G4	S(27) 23	G3	S(57) 45	G2		
S(61) 47	G1	S(73) 57	G4	S(34) 67	G1	S(62) 48	G2		
S(63) 49	G1	S(75) 59	G4	S(50) 38	G1	S(67) 53	G2		
S(65) 51	G1	S(80) 64	G4	S(51) 39	G1	S(74) 58	G2		
		S(81) 65	G4	S(54) 42	G1	S(79) 63	G2		
				S(71) 55	G1	S(82) 66	G2		

Final dataset groups 4 (G4) and 2 (G2) with excellent connectivity results between Irrigated and Non-Irrigated farm land use classes.

Ordination analysis techniques provided several elemental concentration sets with similar profiles that generally became graphically sited away from origin, but close to each other. As-Pb-Cu-Cr, and K-Fe-Al-Ti elemental sets were observed in all the ordination analysis techniques applied in this project.

Connectivity results of As-Pb-Cu-Cr, and K-Fe-Al-Ti metallic sets were then performed on the four final dataset groups by comparing the mean value of these concentrations. Figure 10.12 includes the descriptive statistics for every single final dataset group.

Likewise, by observing the mean comparison of these elements in Figure 10.13, it was deduced that the major mean concentration values of the As-Pb-Cu-Cr metallic set were found in the final dataset group 3. Likewise, main mean concentration values of the K-Fe-Al-Ti set were observed in the final dataset group 1.

Descriptive Statistics (Spreadsheet in Group 1 BOX PLOT)				
	Mean	Std.Dev	Minimum	Maximum
Clay	3.4	3.90	0.0	11.4
Silt	17.7	19.02	0.0	60.7
Al	31392.9	18233.64	6672.8	69017.8
As	14.2	1.66	11.1	16.8
Ba	25.0	15.65	0.0	58.0
Ca	5660.0	8543.50	430.0	34451.4
Cr	2.9	1.99	0.1	7.2
Cs	26.5	14.27	1.9	56.3
Cu	3.5	0.69	2.4	5.2
Fe	12554.4	7591.40	2140.3	28248.3
Ga	12.7	0.82	11.6	14.2
Ge	73.6	6.23	62.6	83.6
K	9566.7	6093.87	696.7	22162.4
Mg	3061.3	2220.97	640.8	7828.8
Mn	168.1	174.76	0.0	594.2
P	367.7	192.64	223.3	955.5
Pb	9.1	1.15	7.5	11.0
Rb	56.6	4.00	50.5	64.9
Sr	50.0	44.42	0.0	151.3
Si	255123.7	45013.81	138438.6	329088.9
Ti	1832.5	999.73	440.3	4235.1
Zr	25.3	7.56	13.1	42.7
TOC	9.2	6.35	1.7	23.2

(a)

Descriptive Statistics (Spreadsheet in Group 2 BOX PLOT)				
	Mean	Std.Dev	Minimum	Maximum
Clay	2.0	1.70	0.0	5.4
Silt	10.3	8.88	0.2	31.8
Al	23392.7	7836.57	11616.8	34132.8
As	14.6	1.23	12.8	16.8
Ba	20.1	7.19	7.7	29.9
Ca	7026.9	8681.21	331.3	31826.7
Cr	2.8	1.22	0.8	5.1
Cs	22.3	6.62	11.0	31.1
Cu	3.1	0.31	2.5	3.7
Fe	9075.5	3331.64	4275.9	13960.4
Ga	12.4	0.42	11.8	13.0
Ge	77.0	6.99	67.4	91.4
K	6542.0	2719.98	2431.0	10447.8
Mg	2347.0	947.88	944.3	3782.0
Mn	86.3	49.75	10.5	164.8
P	289.5	55.48	221.3	412.7
Pb	9.4	1.13	7.2	11.1
Rb	55.8	1.73	53.0	57.6
Sr	36.8	18.53	6.9	63.2
Si	273668.9	57061.50	183852.5	367573.0
Ti	1460.5	472.78	721.9	2107.0
Zr	24.0	7.57	13.0	41.8
TOC	8.7	8.51	0.2	31.4

(b)

Descriptive Statistics (Spreadsheet in Group 3 BOX PLOT)				
	Mean	Std.Dev	Minimum	Maximum
Clay	3.9	5.48	0.0	17.6
Silt	16.4	13.01	1.4	46.0
Al	26020.0	15019.01	6243.6	57871.2
As	21.9	1.34	20.2	24.0
Ba	26.0	11.41	5.5	46.2
Ca	8511.0	5760.74	3438.3	17794.2
Cr	2.9	0.65	2.1	4.2
Cs	27.3	10.41	8.7	45.8
Cu	6.2	0.59	5.7	7.3
Fe	10563.1	6805.77	2074.0	25104.0
Ga	19.2	0.64	18.4	20.4
Ge	69.7	5.11	61.2	76.7
K	8918.4	5572.28	1833.5	20768.6
Mg	3150.2	2096.96	1233.7	8165.4
Mn	138.2	161.83	0.0	533.5
P	347.8	203.67	179.8	862.8
Pb	22.6	1.20	20.5	24.3
Rb	53.5	2.69	49.9	58.9
Sr	69.7	32.77	29.3	138.9
Si	233294.5	33276.35	173746.1	273191.0
Ti	1600.0	859.54	463.2	3401.0
Zr	17.0	5.26	8.4	23.9
TOC	10.2	4.61	4.4	20.1

(c)

Descriptive Statistics (Spreadsheet in Group 4 BOX PLOT)				
	Mean	Std.Dev	Minimum	Maximum
Clay	1.2	0.65	0.4	2.4
Silt	8.1	5.20	2.7	20.0
Al	24024.0	6403.66	14808.9	34228.2
As	14.2	1.61	11.4	17.2
Ba	19.0	5.84	10.5	29.2
Ca	5599.1	5713.86	587.8	17271.2
Cr	2.7	0.85	1.0	4.0
Cs	21.6	5.49	13.7	30.9
Cu	3.2	0.36	2.5	3.7
Fe	9583.8	2442.69	6363.5	14015.3
Ga	12.5	0.51	11.8	13.3
Ge	76.7	9.91	59.9	93.7
K	7033.7	2028.16	4405.0	10591.0
Mg	2528.0	854.91	1272.4	4435.2
Mn	76.4	41.48	25.3	157.1
P	356.0	123.27	262.9	647.0
Pb	9.2	1.11	7.7	11.2
Rb	55.6	1.72	53.2	58.8
Sr	39.9	17.23	13.7	71.0
Si	275179.8	87091.18	107264.7	380575.6
Ti	1424.1	322.43	955.5	1954.2
Zr	22.2	4.50	14.3	27.6
TOC	7.1	3.74	3.1	16.4

(d)

Figure 10.12 – Box Plot Descriptive Statistics for final dataset groups.

Letters (a), (b), (c), and (d) referencing final dataset groups 1, 2, 3, and 4, respectively.

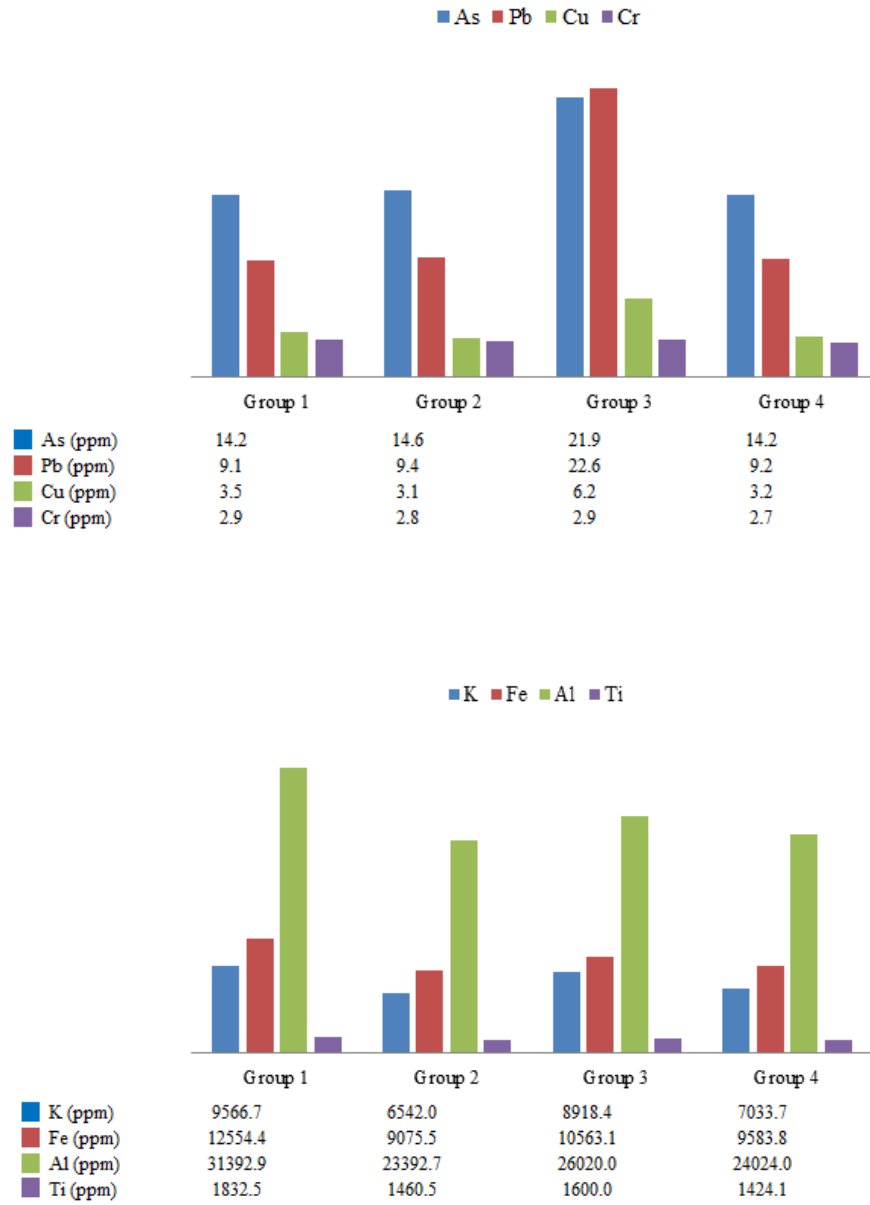


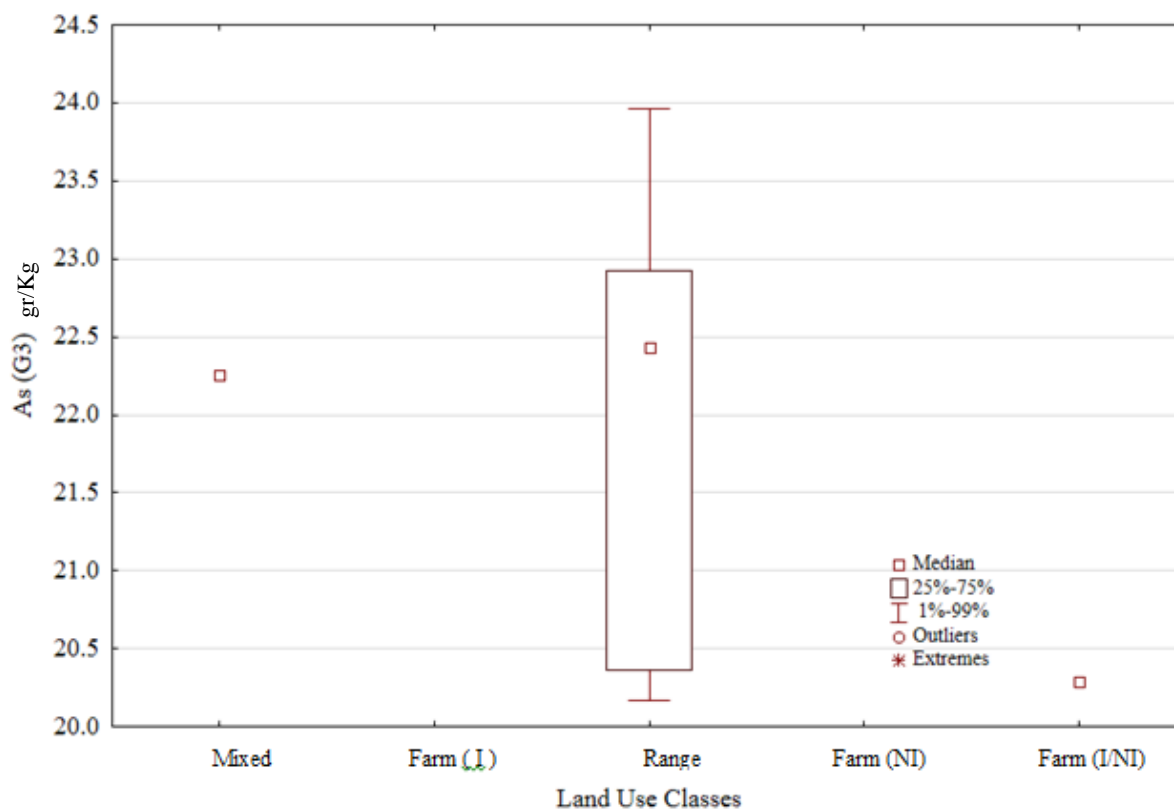
Figure 10.13 – Box Plot Mean concentration values charts.

As-Pb-Cu-Cr and K-Fe-Al-Ti sets obtained their highest mean values from final dataset groups 3 and 1 respectively.

As previously mentioned before, final dataset groups 1 and 3 were spread within Mixed, Range, and Irrigated/No Irrigated farm land use classes. Box Plot of the As-Pb-Cu-Cr set was then individually group analyzed by land use classes. Moreover, the main dust source sites for the elemental set mentioned above were contained within the Range land use class. Figure 10.14 shows the box plot of Arsenic, Lead, Copper, and Chromium concentrations by land use classification.

Box plot analysis of the K-Fe-Al-Ti elemental set was independently group analyzed by land use classes. Therefore, the highest concentration dust source sites for this set were comprised between the Range and Mixed land use classes. Figure 10.15 presents the box plot of Potassium, Iron, Aluminum, and Titanium concentration by land use classification.

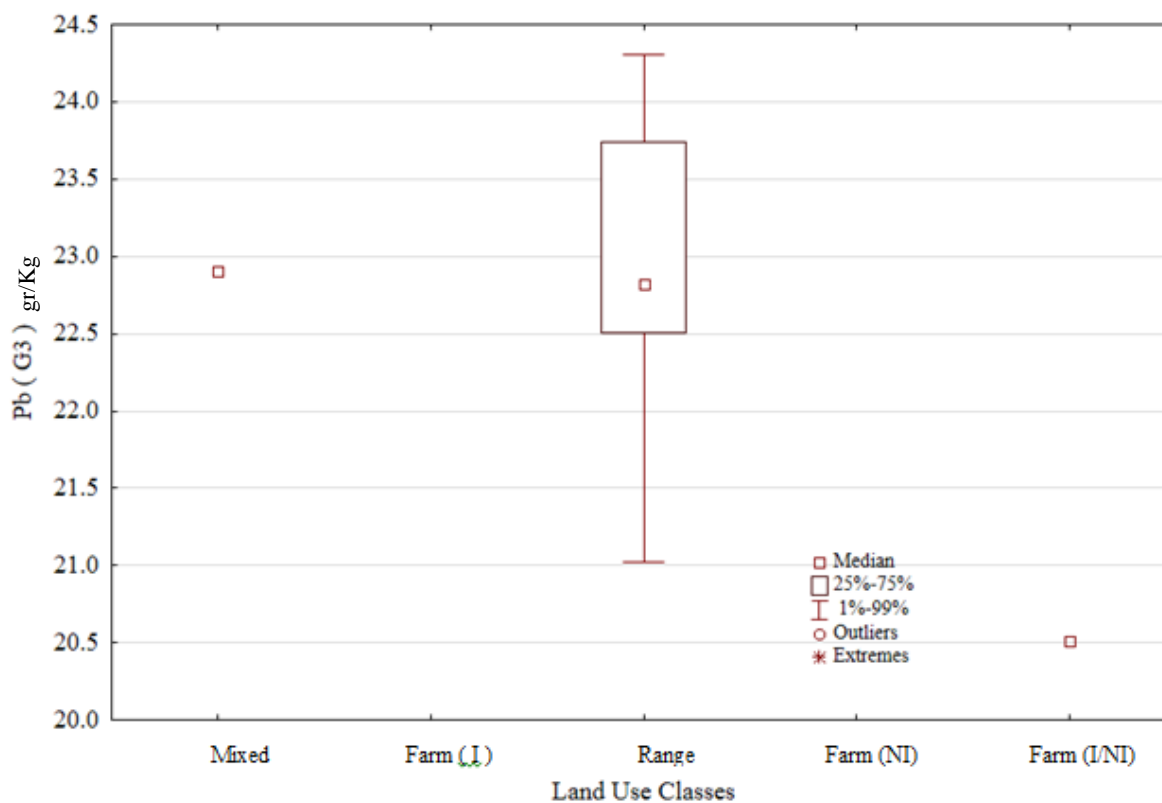
Mixed	Farm (I)	Range	Farm (NI)	Farm (I/NI)
S(14) 12		S(6) 6 S(12) 10 S(10) 9 S(22) 19 S(23) 20 S(4) 5 S(27) 23		S(1) 2



1 Case		7 Cases		1 Case	
Median=	22.2545	Median=	22.4312	Median=	
25%=		25%=	20.3625	25%=	
75%=		75%=	22.9233	75%=	
1%=		1%=	20.1673	1%=	
99%=		99%=	23.9628	99%=	

Figure 10.14 – Box Plot of Arsenic grouped by land use classes.

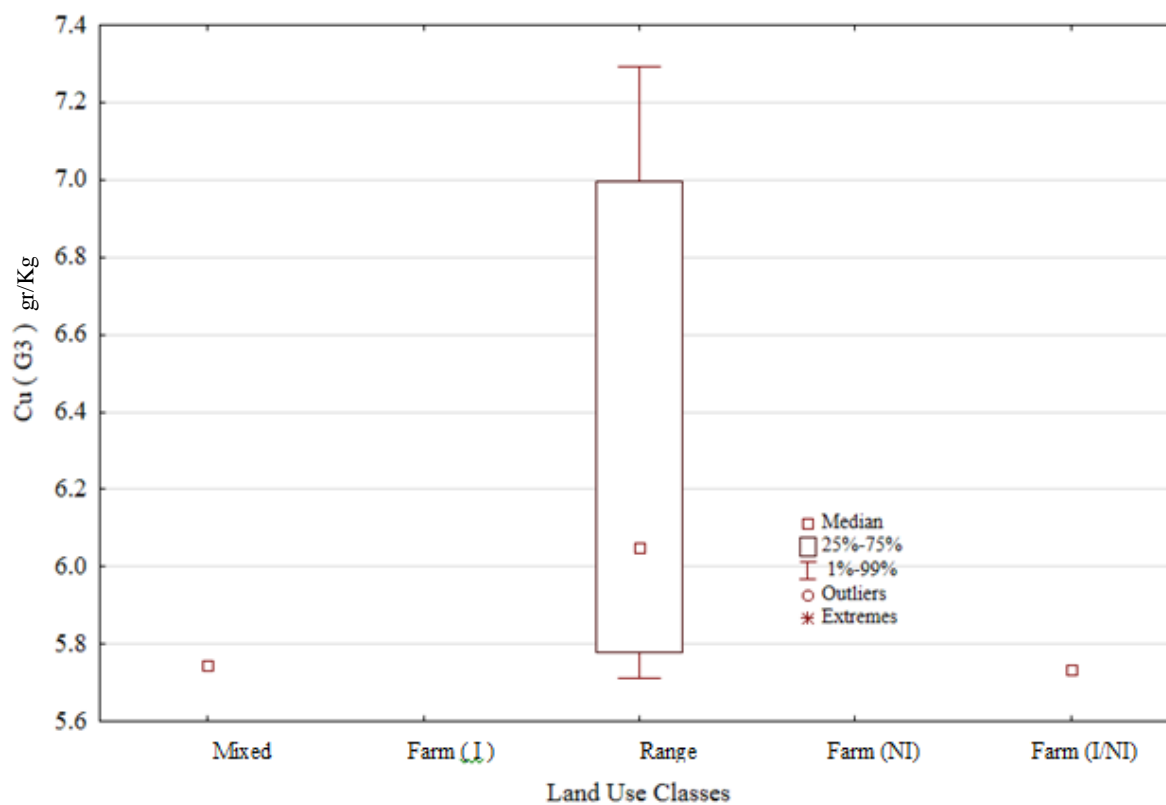
Mixed	Farm (I)	Range	Farm (NI)	Farm (I/NI)
S(14) 12		S(6) 6 S(12) 10 S(10) 9 S(22) 19 S(23) 20 S(4) 5 S(27) 23		S(1) 2



1 Case		7 Cases		1 Case
Median= 22.9011		Median= 22.825		Median= 20.509
25%=		25%= 22.5064		25%=
75%=		75%= 23.7403		75%=
1%=		1%= 21.0226		1%=
99%=		99%= 24.3069		99%=

Figure 10.14 (Cont.) – Box Plot of Lead grouped by land use classes.

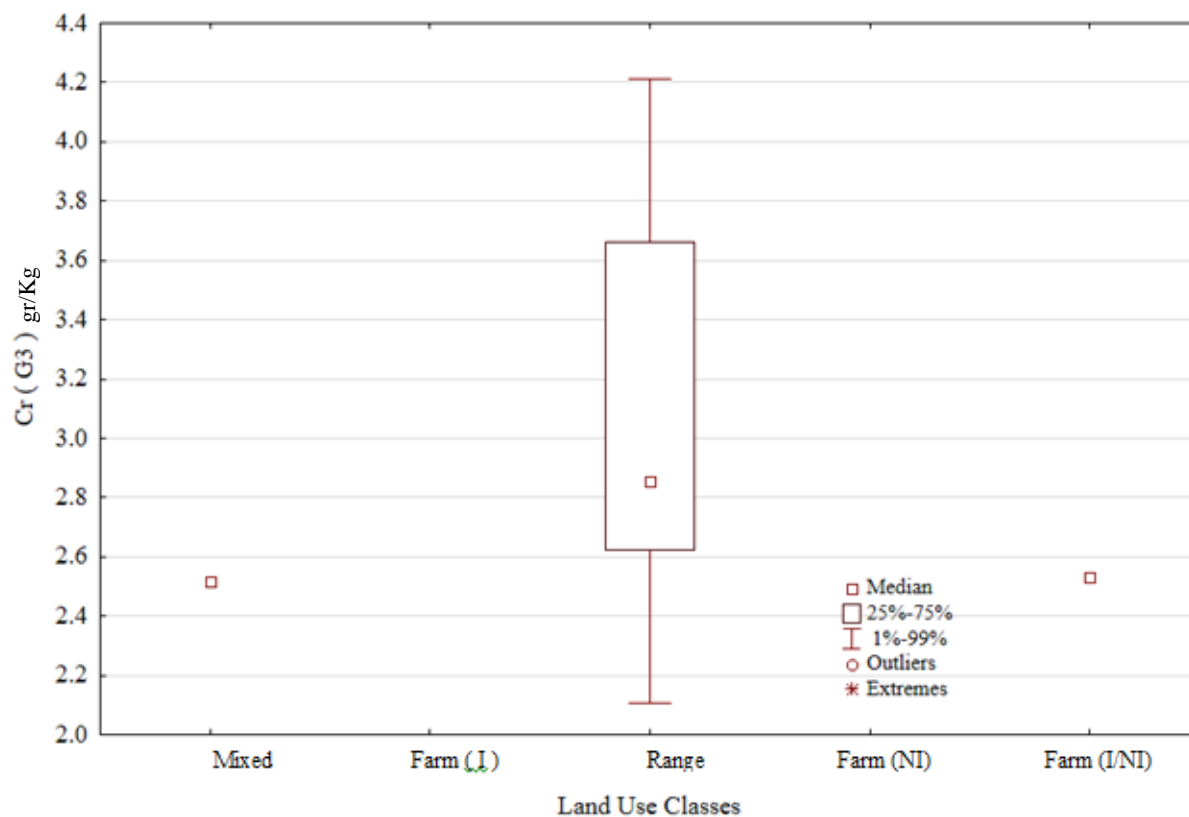
Mixed	Farm (I)	Range	Farm (NI)	Farm (I/NI)
S(14) 12		S(6) 6 S(12) 10 S(10) 9 S(22) 19 S(23) 20 S(4) 5 S(27) 23		S(1) 2



1 Case		7 Cases		1 Case
Median= 5.77405		Median= 6.0503		Median= 5.73332
25%= 5.77405		25%= 5.77916		25%= 5.73332
75%= 5.77405		75%= 6.997		75%= 5.73332
1%= 5.77405		1%= 5.71227		1%= 5.73332
99%= 5.77405		99%= 7.29214		99%= 5.73332

Figure 10.14 (Cont.) – Box Plot of Copper grouped by land use classes.

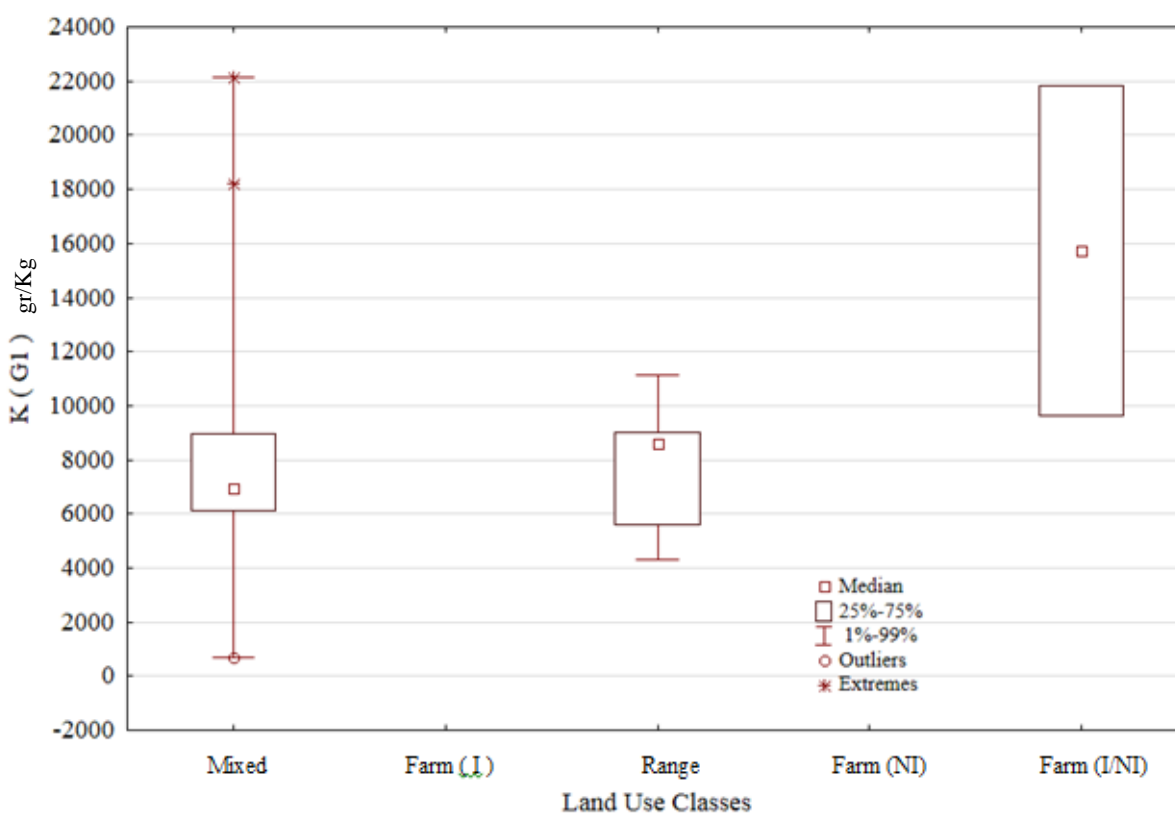
Mixed	Farm (I)	Range	Farm (NI)	Farm (I/NI)
S(14) 12		S(6) 6 S(12) 10 S(10) 9 S(22) 19 S(23) 20 S(4) 5 S(27) 23		S(1) 2



1 Case		7 Cases		1 Case	
Median=	2.5156	Median=	2.8565	Median=	2.5294
25%=		25%=	2.6215	25%=	
75%=		75%=	3.6627	75%=	
1%=		1%=	2.1063	1%=	
99%=		99%=	4.2118	99%=	

Figure 10.14 (Cont.) – Box Plot of Chromium grouped by land use classes.

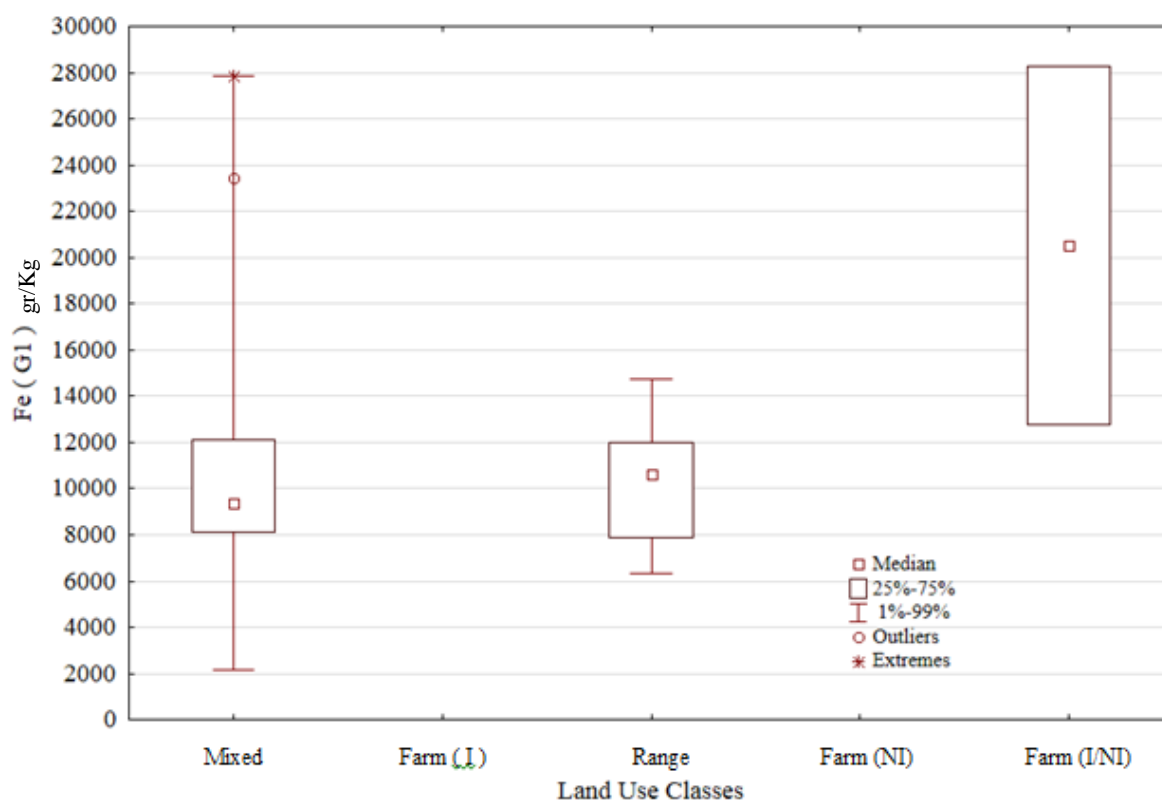
Mixed	Farm (I)	Range	Farm (NI)	Farm (I/NI)
S(61) 47		S(71) 55		S(41) 30
S(17) 14		S(50) 38		S(72) 56
S(28) 24		S(51) 39		
S(32) 28		S(34) 67		
S(63) 49		S(54) 42		
S(65) 51				
S(45) 34				
S(56) 44				
S(19) 16				



9 Cases		5 Cases		2 Cases	
Median=	6949.81	Median=	8582.04	Median=	15743
25%=	6099.7	25%=	5605.21	25%=	9659.11
75%=	8948.7	75%=	9016.63	75%=	21826.8
1%=	696.67	1%=	4307.34	1%=	9659.11
99%=	22162.4	99%=	11131.2	99%=	21826.8

Figure 10.15 – Box Plot of Potassium grouped by land use classes.

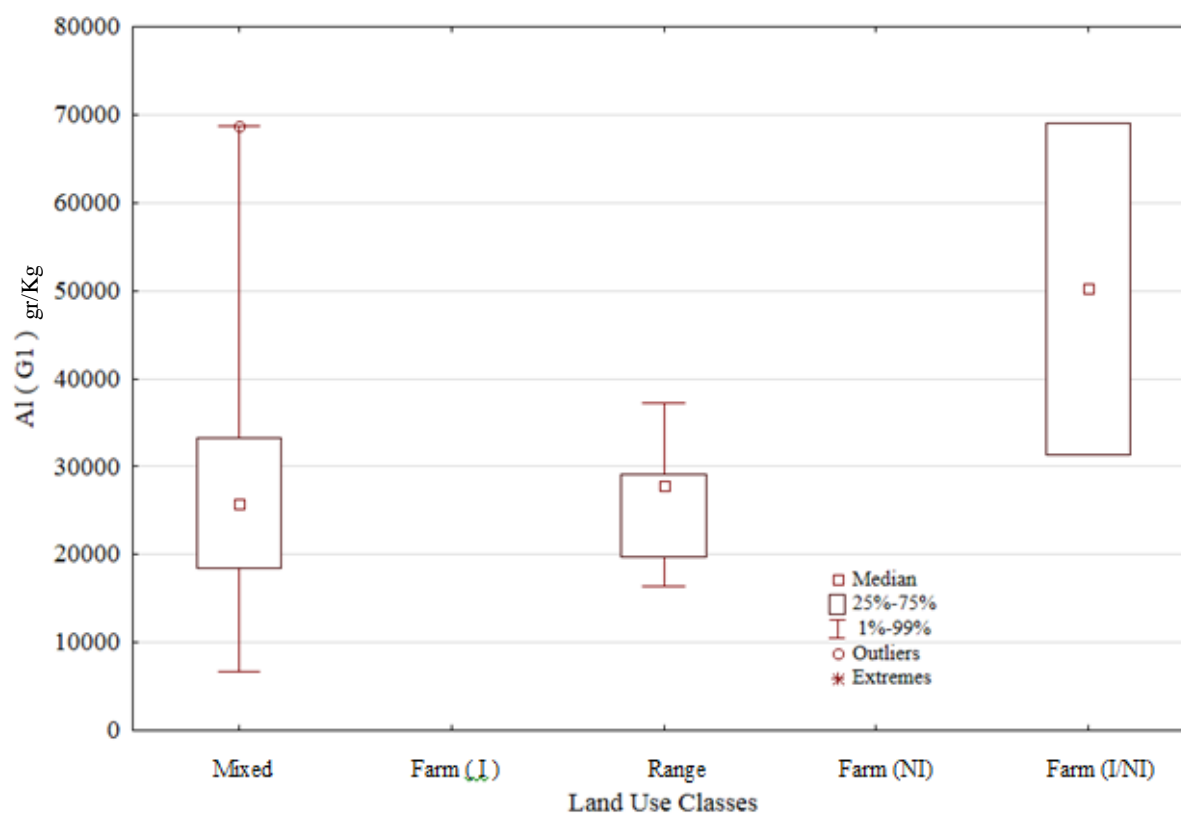
Mixed	Farm (I)	Range	Farm (NI)	Farm (I/NI)
S(61) 47		S(71) 55		S(41) 30
S(17) 14		S(50) 38		S(72) 56
S(28) 24		S(51) 39		
S(32) 28		S(34) 67		
S(63) 49		S(54) 42		
S(65) 51				
S(45) 34				
S(56) 44				
S(19) 16				



9 Cases		5 Cases		2 Cases	
Median=	9380.3	Median=	10610.5	Median=	20512.3
25%=	8095.03	25%=	7872.29	25%=	12776.3
75%=	12133.3	75%=	12014.5	75%=	28248.3
1%=	2140.32	1%=	6355.68	1%=	12776.3
99%=	27875.5	99%=	14717.8	99%=	28248.3

Figure 10.15 (Cont.) – Box Plot of Iron grouped by land use classes.

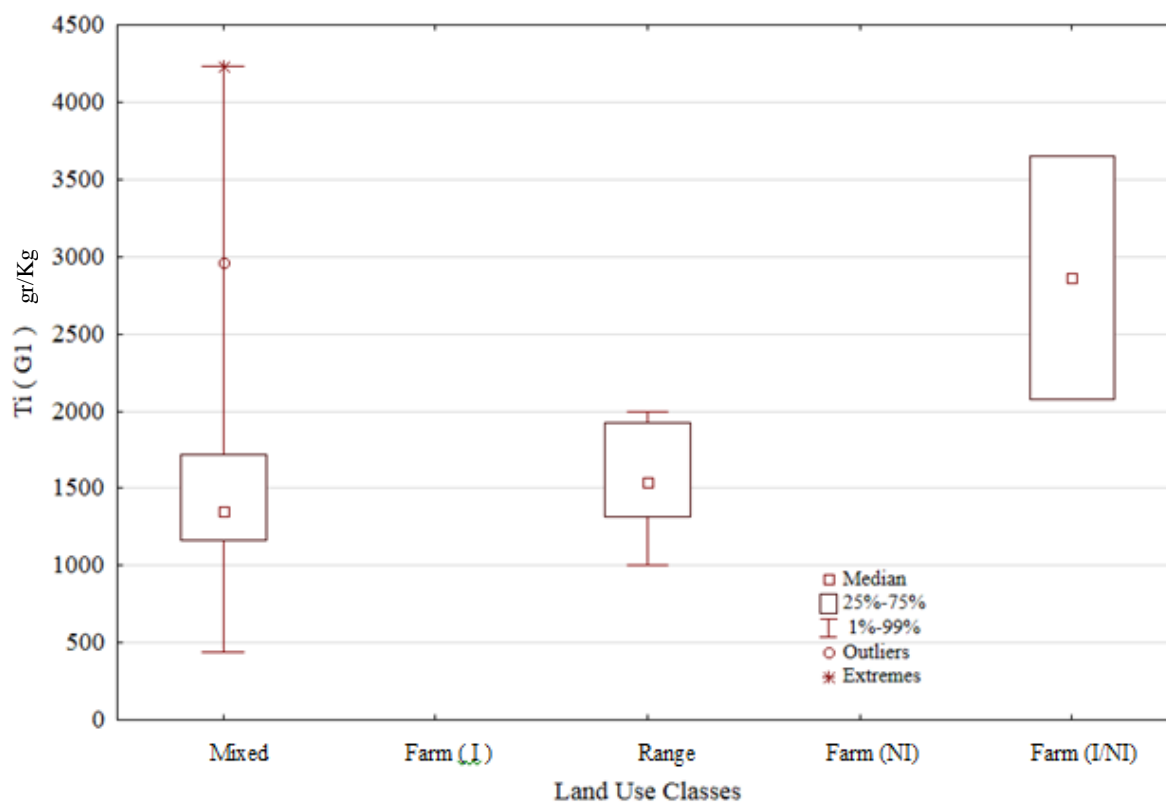
Mixed	Farm (I)	Range	Farm (NI)	Farm (I/NI)
S(61) 47		S(71) 55		S(41) 30
S(17) 14		S(50) 38		S(72) 56
S(28) 24		S(51) 39		
S(32) 28		S(34) 67		
S(63) 49		S(54) 42		
S(65) 51				
S(45) 34				
S(56) 44				
S(19) 16				



9 Cases		5 Cases		2 Cases	
Median=	25761.2	Median=	27849.9	Median=	50192.9
25%=	18521.6	25%=	19794.3	25%=	31367.9
75%=	33309.7	75%=	29129.7	75%=	69017.8
1%=	6672.84	1%=	16482.2	1%=	31367.9
99%=	68782.8	99%=	37182.6	99%=	69017.8

Figure 10.15 (Cont.) – Box Plot of Aluminum grouped by land use classes.

Mixed	Farm (I)	Range	Farm (NI)	Farm (I/NI)
S(61) 47		S(71) 55		S(41) 30
S(17) 14		S(50) 38		S(72) 56
S(28) 24		S(51) 39		
S(32) 28		S(34) 67		
S(63) 49		S(54) 42		
S(65) 51				
S(45) 34				
S(56) 44				
S(19) 16				



9 Cases		5 Cases		2 Cases	
Median=	1356.37	Median=	1543.81	Median=	2862.65
25%=	1162	25%=	1312.4	25%=	2078.42
75%=	1719.1	75%=	1920.57	75%=	3646.87
1%=	440.31	1%=	998.603	1%=	2078.42
99%=	4235.11	99%=	1996.76	99%=	3646.87

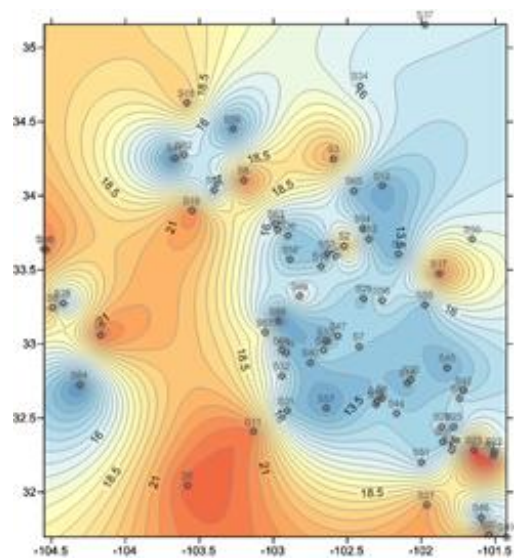
Figure 10.15 (Cont.) – Box Plot of Titanium grouped by land use classes.

10.6.2 Contour Plotting

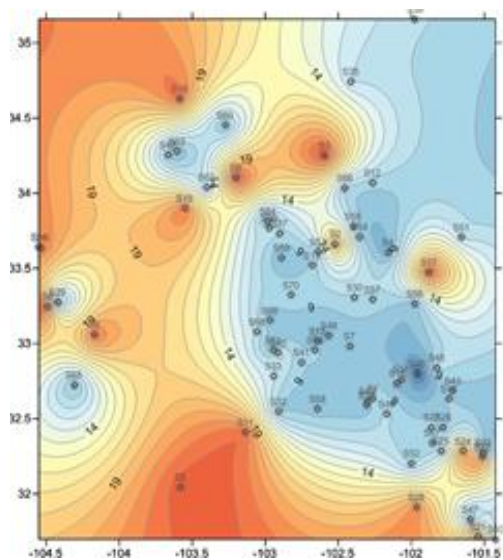
Concentrations of As-Pb-Cu-Cr and K-Fe-Al-Ti sets were contour plotted by using Surfer, a grid based mapping program that interpolates irregularly spaced XYZ data into a regularly spaced grid.

As previously deducted in this study, the As-Pb-Cu-Cr set was connectively linked to Range land use class. Concentrations of this elemental set that were obtained from Inductively Coupled Plasma Optical Emission Spectrometry analysis were then contoured in Surfer, showing connectivity between these likely-anthropogenically-associated metallic elements. See Figure 10.16. The highest concentrations of these metals appeared to be found in the far west Texas region.

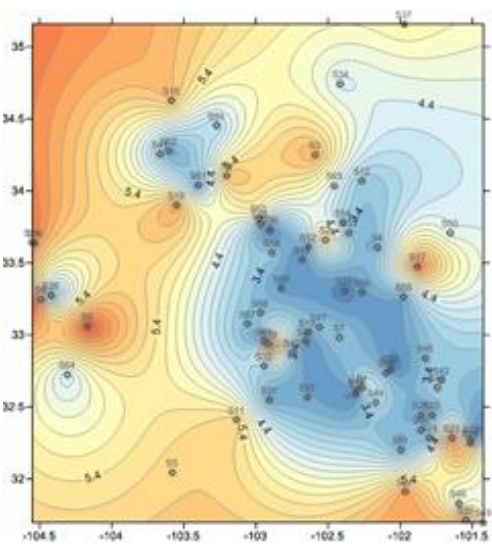
Similarly, K-Fe-Al-Ti were connectively linked to Mixed and Range land use classes. Concentrations of these elements obtained from Inductively Coupled Plasma Optical Emission Spectrometry examination were then contoured in Surfer software package, showing a good affinity between these elements. See Figure 10.17. Highest concentrations of these elements appeared to be located in the northeast region.



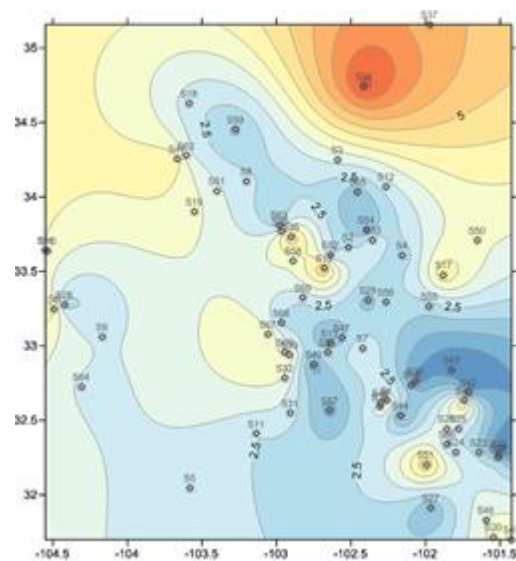
Arsenic



Lead

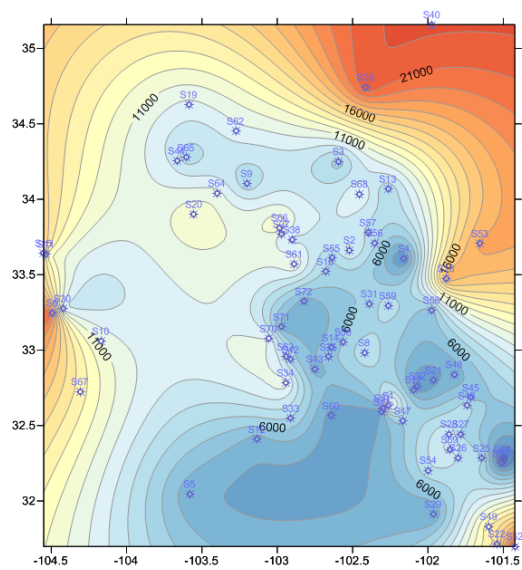


Copper

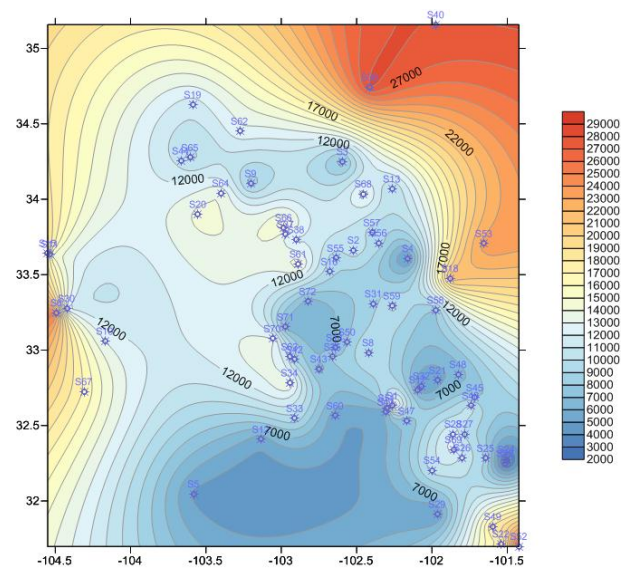


Chromium

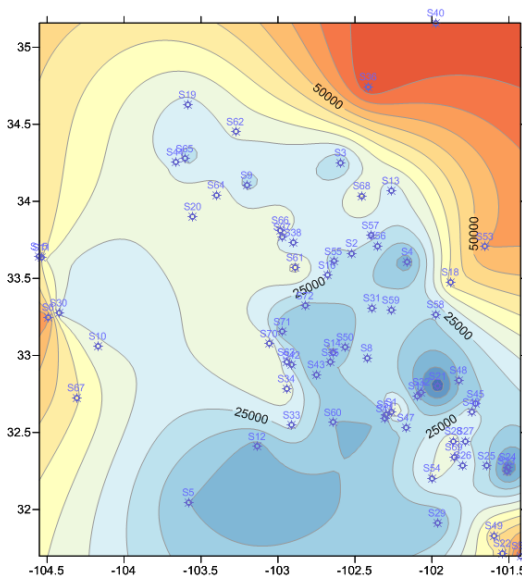
Figure 10.16 – Contoured Mapping of the As-Pb-Cu-Cr metallic set.



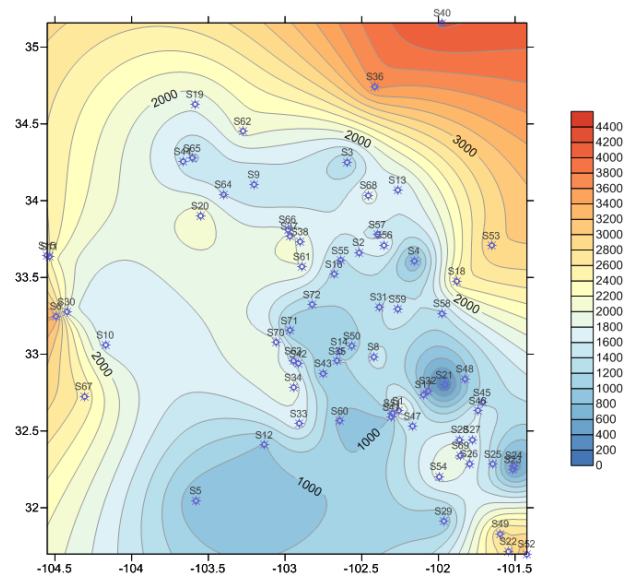
Potassium



Iron



Aluminum



Titanium

Figure 10.17 – Contoured Mapping of the K-Fe-Al-Ti metallic set.

References Cited

- Allen, B. L., B. L. Harris, K. R. Davis, and G. B. Miller, 1972: *The Mineralogy and Chemistry of High Plains Playa Lake Soils and Sediments*, Prepared for Office of Water Resources Research, U. S. Department of the Interior. Agronomy Department, Texas Tech University. 75 pp.
- Arimoto, R., 2001: *Eolian dust and climate: relationships to sources, tropospheric chemistry, transport and deposition*. *Earth-Science Reviews*, **54**, pp 29-42.
- Ashbaugh, L. L., O. M. Carvacho, M. S. Brown, J. C. Chow, J. G. Watson, and K. C. Magliano, 2003: *Soil sample collection and analysis for the Fugitive Dust Characterization Study*. *Atmospheric Environment*, **37**, pp 1163- 1173.
- Bach, A. J., and A. J. Brazel, 1996: *Temporal and Spatial Aspects of Blowing Dust in the Mojave and Colorado Deserts of Southern California 1973-1994*. *Physical Geography*. **17**, pp 329-353.
- Baddock, M. C., T. E. Gill, J. E. Bullard, M. Dominguez Acosta, and N. I. Rivera Rivera, 2011: [*Geomorphology of the Chihuahuan Desert based on potential dust emissions*](#). *Journal of Maps*, **7**, pp 249-259.
- Bale, A. J., 1996: *In situ laser optical particle sizing*. *Journal of Sea Research*, **36**, pp 31-36.
- Batjes, N. H., 1996: *Total Carbon and Nitrogen in the Soils of the World*. *European Journal of Soil Science*, **47**, pp. 151- 163.
- Bolin, B., 1981: *Carbon Cycle Modelling*. John Wiley and Sons, 390 pp.
- Bomar, G. W., 1983: *Texas Weather*. Austin: University of Texas Press.
- Brazel, A. J., and W. G. Nickling, 1986: *The Relationship of Weather Types to Dust Storm Generation in Arizona (1965-1980)*. *International Journal of Climatology*, **6**, pp 255-275.
- Bullard, J. E., M. C. Baddock, G. McTainsh, and J. Leys, 2008: *Sub-basin scale dust source geomorphology detected using MODIS*. *Geophysical Research Letters*, **35**, DOI: 10.1029/2008GL033928.
- Bullard, J. E., S. P. Harrison, M. C. Baddock, N. Drake, T. E. Gill, H. McTainsh, and Y. Sun, 2011: *Preferential dust sources: a geomorphological classification designed for use in global dust-cycle models*. *Journal of Geophysical Research*, **116**, F04034.
- Buurman, P., K. de Boer, and T. Pape, 1997: *Laser diffraction grain-size characteristics of Andisols in perhumid Costa Rica: the aggregate size of allophane*. *Geoderma*, **78**, pp 71-91.

Castiglia, P. J., and P. J. Fawcett, 2006: *Large Holocene lakes and climate change in the Chihuahuan Desert. Geology*, **34**, pp 113-116.

Clausnitzer, H., and M. J. Singer, 1999: *Mineralogy of Agricultural Source Soil and Respirable Dust in California. Journal of Environmental Quality*, **28**, pp 1619-1629.

Court, A., and J. F. Griffiths, 1982: *Thunderstorm Morphology and Dynamics. Thunderstorm climatology*, pp 11-52. Washington: U.S. Department of Commerce. 603 pp.

Cousins, I. T., A. J. Beck, and K. C. Jones, 1999: *A review of the processes involved in the exchange of semi-volatile organic compounds (SVOC) across the air-soil interface. The Science of the Total Environment*, **228**, pp 5-24.

Dixon, J. B., and D. G. Schulze, 2002: *Soil Mineralogy with Environmental Applications*. Soil Science Society of America.

Dominguez-Acosta, M., T. E. Gill, and P. Peinado, 2010: *Geochemical Characterization of an Aeolian Corridor in Northern Chihuahua, Mexico. Actas del INAGEQ (Instituto Nacional de Geoquímica, Mexico)* **16**, pp 198-209.

Dominguez Acosta, M., 2009: *The Pluvial Lake Palomas - Samalayuca Dunes System*, Ph. D. Dissertation, Geological Sciences, University of Texas at El Paso, 278 pp.

Douglas, M. W., R. A. Maddox, and K. Howard, 1993: *The Mexican Monsoon. Bulletin of the American Meteorological Society*, **6**, pp 1665-1677.

Engelbrecht, J. P., and E. Derbyshire, 2010: Airborne Mineral Dust. *Elements*, **6**, pp 241-246.

Finger, L. W., 1989: *Synchrotron powder diffraction. Modern powder diffraction*, **20**, pp 307 - 331.

Gill, T. E., 1996: *Eolian sediments generated by anthropogenic disturbance of playas: human impacts on the geomorphic system and geomorphic impacts on the human system. Geomorphology*, **17**, pp 207-228.

Gill, T. E., M. Dominguez Acosta, and N. I. Rivera Rivera, 2008: *The Lake Palomas Basin: Dust Engine of the Chihuahuan Desert. Geological Society of America Abstracts and Programs*, **40**, p. 78.

Gill, T. E., J. E. Stout, and P. Peinado, 2009: *Composition and Characteristics of Aerosols in the Southern High Plains of Texas (USA). American Institute of Physics Conference Proceedings*, **1099**, pp 255-258.

Gill, T. E., R. J. Vet, P. Biscaye, E. Bleiweiss, and M. P. Shaw, 2006: *Recurrent transcontinental dust transport from southwestern North America to Canada*, Abstracts of the Sixth International Conference on Aeolian Research. University of Guelph, Ontario Canada. p. 150.

Gillette, D. A., 1999: *A qualitative geophysical explanation for "hot spot" dust emitting source regions*. *Contributions to Atmospheric Physics*, **72**, p. 67-77.

Grande-López, R., and A. Gómez-González, 1971: *Estudio de los suelos del ejido Salitral de Carrera, municipio de Villa de Ramos, S.L.P.: dictámen Técnico*. San Luis Potosí. Universidad Autónoma de San Luis Potosí. Instituto de Investigación de Zonas Desérticas, pp 10.

Grave, P., L. Lisle, and M. Maccheroni, 2005: *Multivariate comparison of ICP-OES and PIXE/PIGE analysis of east Asian storage jars*. *Journal of Archaeological Science*, **32**, pp 69-80.

Hai, C., C. Yuan, G. Liu, X. Li, F. Zhang, and X. Zhang, 2008: *Research on the Components of Dust Fall in Hohhot in Comparison with Surfaces Soil Components in Different Lands of Inner Mongolia Plateau*. *Water Air and Soil Pollution*, **190**, pp 27-34.

Henrickson, J., and R. M. Straw, 1976: *A gazetteer of the Chihuahuan Desert Region: A supplement to the Chihuahuan Desert flora*. Los Angeles: California State University.

Holliday, V. T., 1989: *The Blackwater Draw Formation (Quaternary): a 1.4-plus-m.y. Record of Eolian Sedimentation and Soil Formation on the Southern High Plains*. *Geological Society of America Bulletin*, **101**, pp 1598-1607.

Holliday, V. T., 1991: *The geologic record of wind erosion, eolian deposition, and aridity on the Southern High Plains*. *Great Plains Research*, **1**, pp 6-25.

INEGI: Instituto Nacional de Estadística y Geografía.
http://mapserver.inegi.org.mx/data/inf_e1m/?s=geo&c=979

IPCC., 1990: *Climate Change: The IPCC Scientific Assessment*, 410 pp.

Janugani, S., V. Jayaram, S. D. Cabrera, J. G. Rosiles, T. E. Gill, and N. I. Rivera Rivera, 2009: *Directional Analysis and Filtering for Dust Storm Detection in NOAA-AVHRR imagery*. Algorithms and Technologies for Multispectral, Hyperspectral and Ultraspectral imagery XV. *Proceedings of the SPIE* **7334**, 73341g, doi: 10.1117/12.820235, 12 pp.

Johnson, E., 1986: *Late Pleistocene and Early Holocene Paleoenvironments on the Southern High Plains (USA)*. *Geographie Physique et Quaternaire*, **40**, pp 249-261.

Johnson, W. C., 1965: *Wind in the Southwestern Great Plains*. US Department of Agriculture, Conservation Research Report 6.

Lee, J. A., M. C. Baddock, M. J. Mbuh, and T. E. Gill, 2012: *Geomorphological and land cover characteristics of aeolian dust sources in west Texas and eastern New Mexico, USA*. *Aeolian Research*, **3**, pp 459- 466.

Lee, J. A., T. E. Gill, K. R. Mulligan, M. Dominguez Acosta, and A. E. Pérez, 2009: *Land use/land cover and point sources of the 15 December 2003 dust storm in southwestern North America*. *Geomorphology*, **105**, pp 18-27.

Lee, J. A., K. E. Moffett, B. L. Allen, R. E. Peterson, and J. M. Gregory, 1994: *Environmental controls on blowing dust direction at Lubbock, Texas, U.S.A*. *Earth Surface Processes and Landforms*, **19**, pp 437-449.

Levy, J. I., T. Dumyahn, and J. D. Spengler, 2002: *Particulate matter and polycyclic aromatic hydrocarbon concentrations in indoor and outdoor microenvironments in Boston, Massachusetts*. *Journal of Exposure Analysis and Environmental Epidemiology*, **12**, pp 104-114.

Levy, J. I., D. H. Bennett, S. J. Melly, and J. D. Spengler, 2003: *Influence of traffic patterns on particulate matter and polycyclic aromatic hydrocarbon concentrations in Roxbury, Massachusetts*. *Journal of Exposure Analysis and Environmental Epidemiology*, **13**, pp 364-371.

Lunderberg, J. M., R.J. Bartlett, A.M. Behm, C. Contreras, P.A. DeYoung, N.L. Hoogeveen, A.J. Huisman, G.F. Peaslee, and J.K. Postma, 2008: *PIXE as complement to trace metal analysis of sediments by ICP-OES*. *Nuclear Instruments and Methods in Physics Research Section B*, **266**, pp 4782-4787.

Mahowald, N. M., R. G. Bryant, J. Del Corral, and L. Steinberger, 2003: *Ephemeral Lakes and Desert Dust Sources*. *Geophysical Research Letters*, **30**, 1074. doi: 10.1029/2002/GO16041.

Makra, L., I. Borbély-Kiss, E. Koltay, and Y. Chen, 2002: *Enrichment of desert soil elements in Takla Makan dust aerosol*. *Nuclear Instruments and Methods in Physics Research Section B*, **189**, pp 214-220.

McGinnies, W. G., B. J. Goldman, and P. Paylore, 1970: *Deserts of the world*. Tucson: University of Arizona Press.

Medellin-Leal, F., 1982: *Reference Handbook on the Deserts of North America*. The Chihuahuan Desert. Gordon L. Bender (Ed.). Greenwood Press. First Edition. pp 321-381.

Menzel, N., P. Scharamel, and K. Wittmaack, 2002: *Elemental composition of aerosol particulate matter collected on membrane filters, a comparison of results by PIXE and ICP-AES*. *Nuclear Instruments and Methods in Physics Research Section B*, **189**, pp 94-99.

Mernet, J. M., 2005: *Is it still possible, necessary and beneficial to perform research in ICP-atomic emission spectrometry?* *Journal of Analytical Atomic Spectrometry*, **20**, pp 11-16.

Neal, J. T., 1975: *Playa Surface as Indicators of Environment*. Playas and Dried Lakes, J. T. Neal (Ed.), Halsted Press, New York, pp 363-368.

Novlan, D. J., M. Hardiman, and T. E. Gill, 2007: *A synoptic climatology of blowing dust events in El Paso, Texas from 1932 - 2005* J3.12, 13 pp. 16th Conference on Applied Climatology, American Meteorological Society, January 2007, San Antonio, TX, preprint in digital format, <http://ams.confex.com/ams/pdfpapers/115842.pdf>.

Orgill, M. M., and G. A. Sehmel, 1976: *Frequency and diurnal variation of dust storms in the contiguous U.S.A.* *Atmospheric Environment*, **10**, pp 813-825.

Perez, A. E., 2008: *Application of Integrated Remote Sensing and GIS Technologies to Geoenvironmental Issues in Far West Texas and Southern New Mexico*, Ph. D. Dissertation, Geological Sciences, University of Texas at El Paso, 321 pp.

Pope, C. A., and D. W. Dockery, 2006: *Health Effects of Fine Particulate Air Pollution: Lines that connect.* *The Journal of the Air & Waste Management Association*, **56**, pp 709-742.

Prospero, J. M., 1999: *Long-range transport of mineral dust in the global atmosphere: Impact of African Dust on the environment of the southeastern United States.* *Proceedings of the National Academy of Sciences*, **96**, pp 3396-3403.

Prospero, J. M., P. Ginoux, O. Torres, S. E. Nicholson, and T. E. Gill, 2002: *Environmental characterization of global sources of atmospheric soil dust identified with the NIMBUS 7 total ozone mapping spectrometer (TOMS) absorbing aerosol product.* *Reviews of Geophysics*, **40**, pp 2-1 - 2-31.

Reeves, C. C. J., 1976: *Quaternary stratigraphy and geologic history of Southern High Plains, Texas and New Mexico.* *Quaternary Stratigraphy of North America*. Mahany, W. C. (Ed.), pp 215-234. Stroudsburg, Pennsylvania. Dowden, Hutchinson, and Ross.

Rice, K. C., 1999: *Trace-element concentrations in streambed sediment across the conterminous United States.* *Environmental Science and Technology*, **33**, pp 2499-2504.

Rivera Rivera, N. I., T. E. Gill, M. P. Bleiweiss, and J. L. Hand, 2010: *Source characteristics of hazardous Chihuahuan Desert dust outbreaks.* *Atmospheric Environment*, **44**, pp 2457-2468.

Rivera Rivera, N. I., T. E. Gill, K. A. Gebhart, J. L. Hand, M. P. Bleiweiss, and R. M. Fitzgerald, 2009: *Wind modeling of Chihuahuan Desert dust outbreaks.* *Atmospheric Environment*, **43**, pp 347-354.

Rogers, D. M., 1969: *A Morphological and Mineralogical Study of the Pullman Soil*. M.S. Thesis, Soil Science, Texas Technological College. Lubbock, Texas, 102 pp.

Rojo, A., 2010: *Granulometry and Geochemistry of Dust Emission from Owens (Dry) Lake California*. Ph. D. Dissertation, Environmental Science and Engineering, University of Texas at El Paso, 135 pp.

Schulze, D. G., and P. M. Bertsch, 1995: *Synchrotron X-Ray Techniques in Soil, Plant, and Environmental Research*. *Advances in Agronomy*, **55**, pp 1- 66.

Smodis, B., 2007: *Investigation of trace element atmospheric pollution by nuclear analytical techniques at a global scale: Harmonised approaches supported by the IAEA*. *Journal of Environmental Management*, **85**, pp 121-128.

Sokolik, I. N., and O. B. Toon, 1996: Direct Radiative Forcing by Anthropogenic Airborne Mineral Aerosols. *Nature*, **381**, pp 681-683.

Sperazza, M., J. M. Moore, and M. S. Hendrix, 2004: *High-resolution particle size analysis of naturally occurring very fine grained sediment through laser diffractometry*. *Journal of Sedimentary Research*, **74**, pp 736-743.

Stefánsson, A., I. Gunnarsson, and N. Giroud, 2007: *New methods for the direct determination of dissolved inorganic, organic and total carbon in natural waters by Reagent-Free Ion Chromatography and inductively coupled plasma atomic emission spectrometry*. *Analytica Chimica Acta*, **582**, pp 69-74.

Stout, J. E., 2001: *Dust and environment in the Southern High Plains of North America*. *Journal of Arid Environments*, **47**, pp 425-441.

Stout, J. E., and J. A. Lee, 2003: *Indirect evidence of wind erosion trends on the Southern High Plains of North America*. *Journal of Arid Environments*, **55**, pp 43-61.

Suzuki, K., K. Maeda, Y. Sasa, A. Okada, K. Sakamoto, and T. Ozawa, 1993: *Application of PIXE to source identification of Kosa aerosol: analysis of desert soils in China*. *Nuclear Instruments and Methods in Physics Research Section B*, **75**, pp 317-320.

Trabalka, J. R., and D. E. Reichle, 1986: *Changing Carbon Cycle: A Global Analysis*. Oak Ridge National Laboratory.

Walters, J. P., 1988: *Variation, Classification, Genesis, and Mineralogy of Soils in the Sandhills of Yoakum, Cochran, and Terry Counties, Texas*. M. S. Thesis, Soil Science, Texas Tech University. Lubbock, Texas. 199 pp.

Wania, F., and D. Mackay, 1995: *A global distribution model for persistent organic chemicals*. *Science of the Total Environment*, **160-161**, pp 211-232.

Washington, R., M. Todd, N. J. Middleton, and A. S. Goudie, 2003: *Dust-Storm Source Areas Determined by the Total Ozone Monitoring Spectrometer and Surface Observations*. *Annals of the Association of American Geographers*, **93**, pp 297-313.

Wigner, K. A., and R. E. Peterson, 1987: *Synoptic climatology of blowing dust on the Texas South Plains, 1947-84. Journal of Arid Environments*, **13**, pp 199-209.

Wilson, W. E., and H. H. Suh, 1997: *Fine Particles and Coarse Particles: Concentration relationship relevant to epidemiological studies. Journal of Air & Waste Management Association*, **47**, pp 1238-1249.

WSS: Web Soil Survey. <http://websoilsurvey.nrcs.usda.gov/app/HomePage.htm>

Zhang, B., H. S. Cheng, B. Ma, Q. H. Li, P. Zhang, F. X. Gan, and F. J. Yang, 2005: *PIXE and ICP-AES analysis of early glass unearthed from Xinjiang, China. Nuclear Instruments and Methods in Physics Research Section B*, **240**, pp 559-564.

Zobeck, T. M., 2004: *Rapid particle size analyses using laser diffraction. Applied Engineering in Agriculture*, **20**, pp 633-639.

Appendix A

X-Ray Diffraction Peak ID Reports

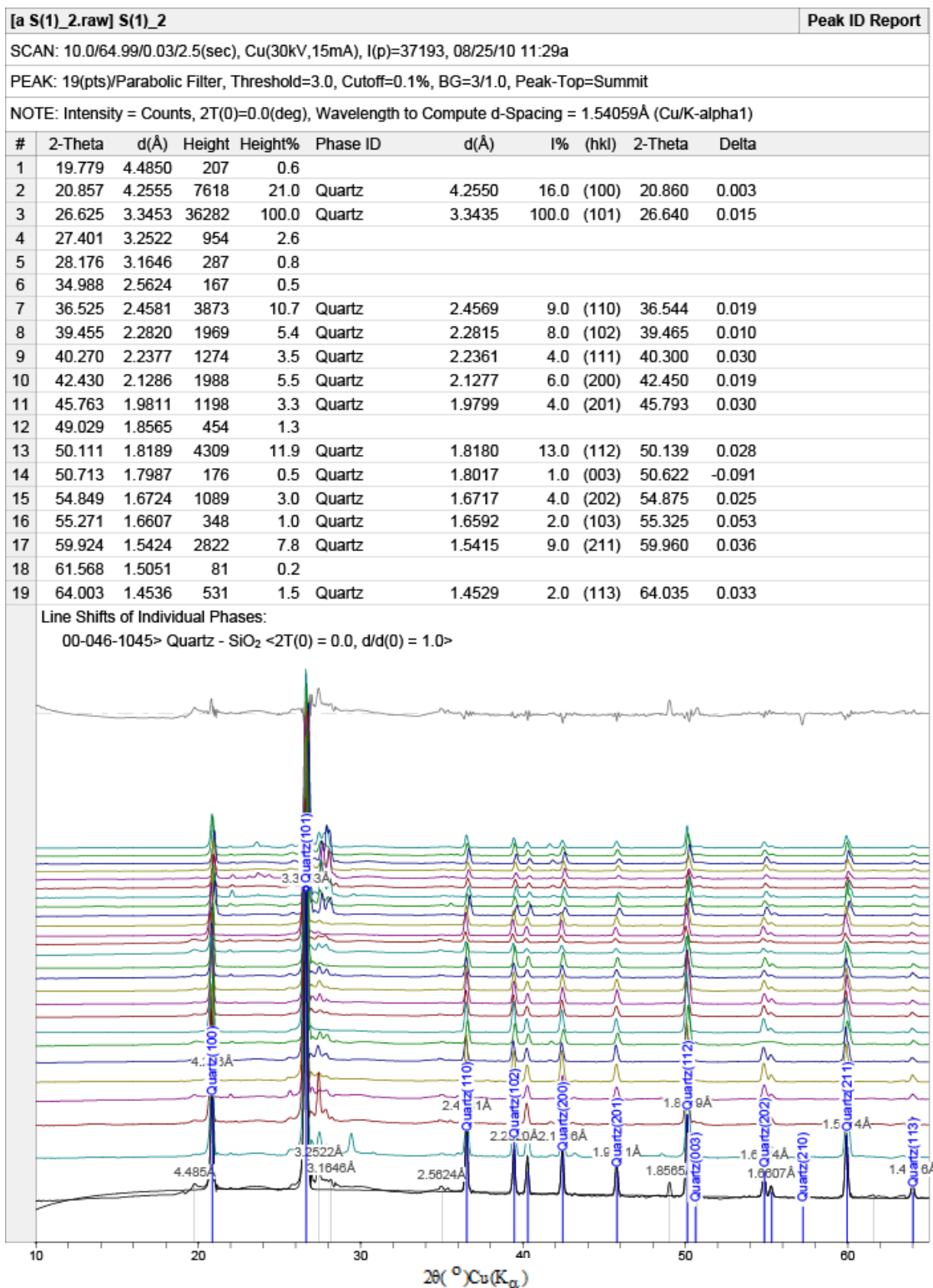


Figure A.1 – Quartz Peak ID Report.

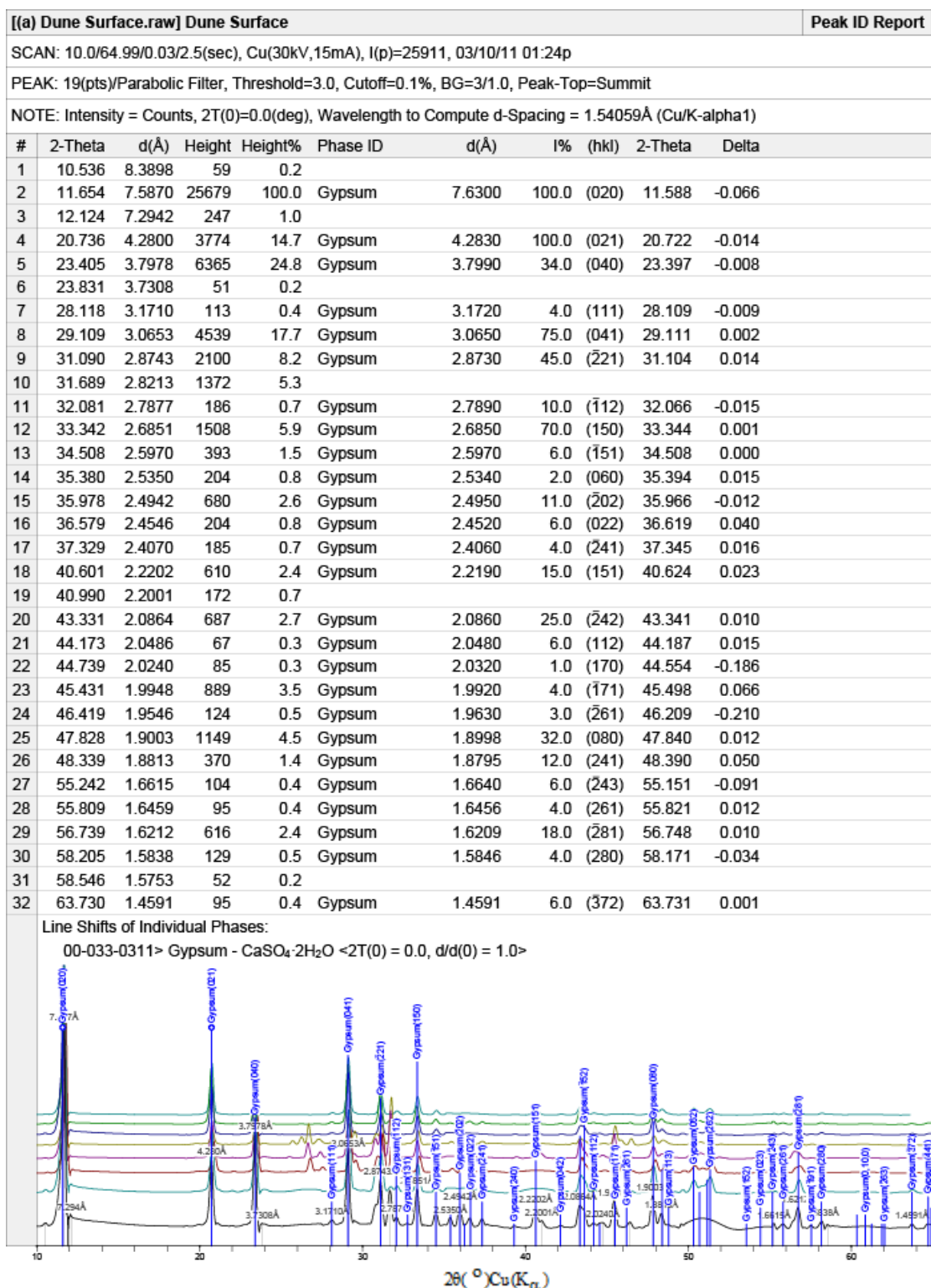


Figure A.2 – Gypsum Peak ID Report.

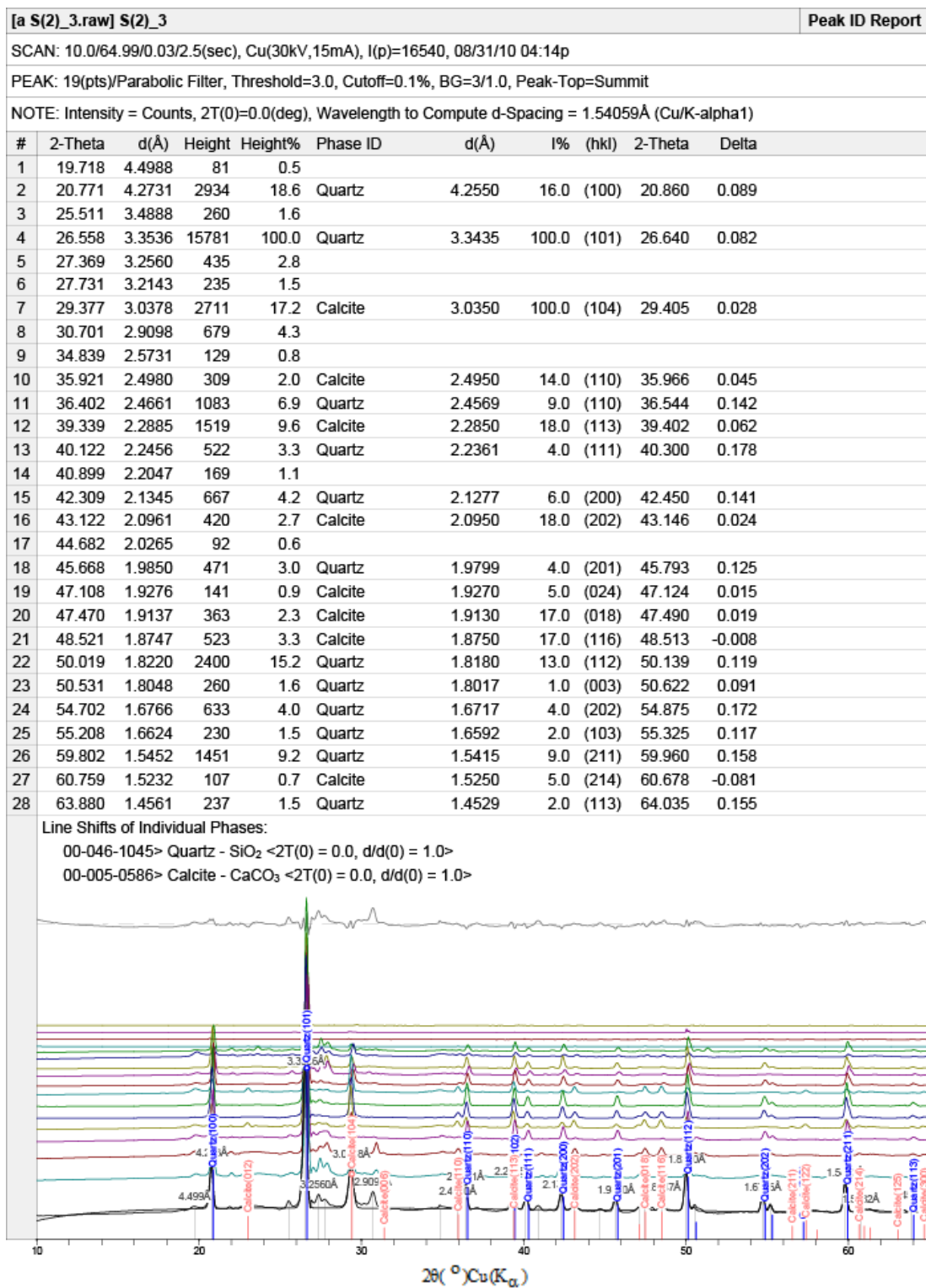


Figure A.3 – Quartz + Calcite Peak ID Report.

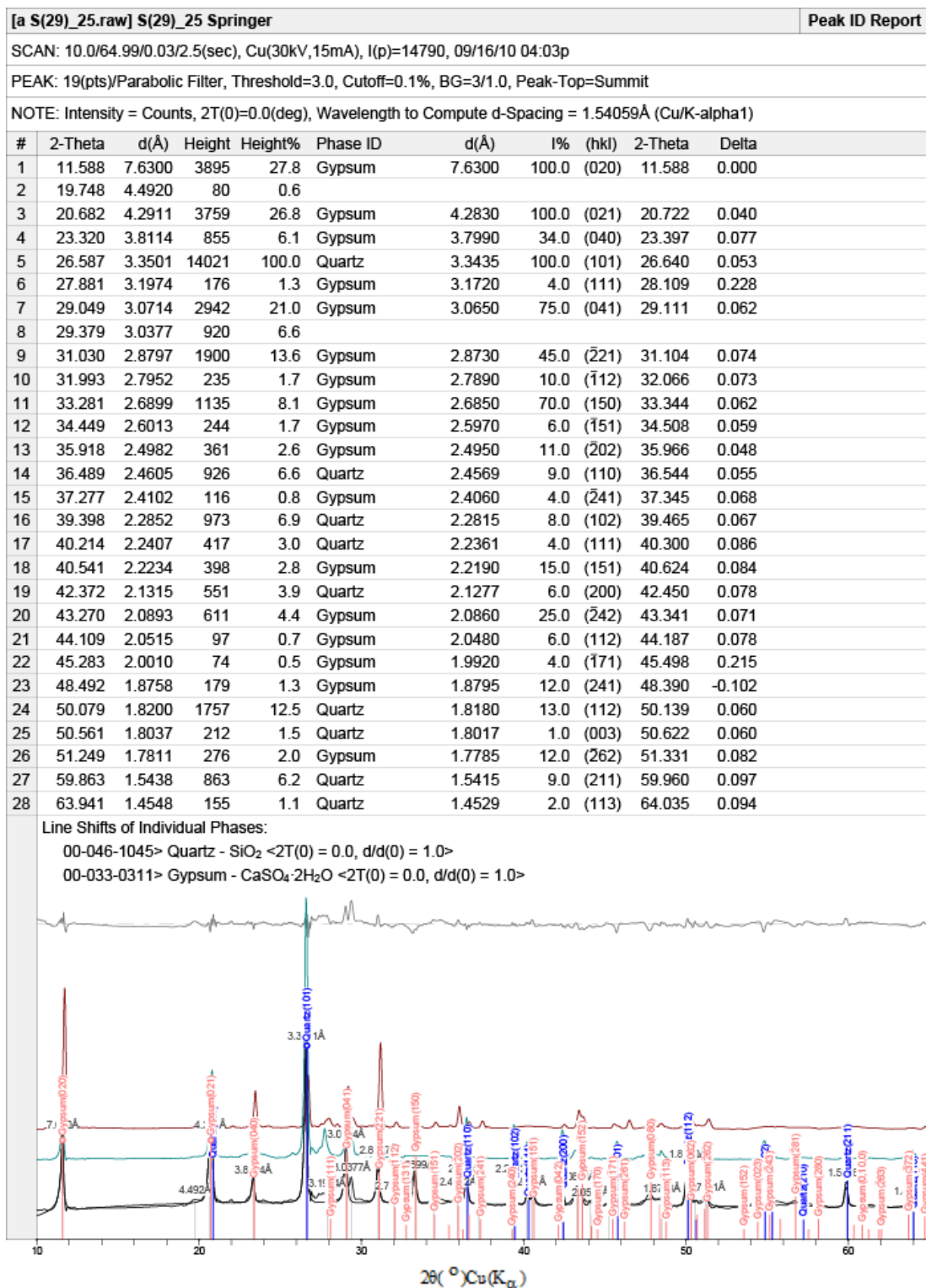


Figure A.4 – Quartz + Gypsum Peak ID Report.

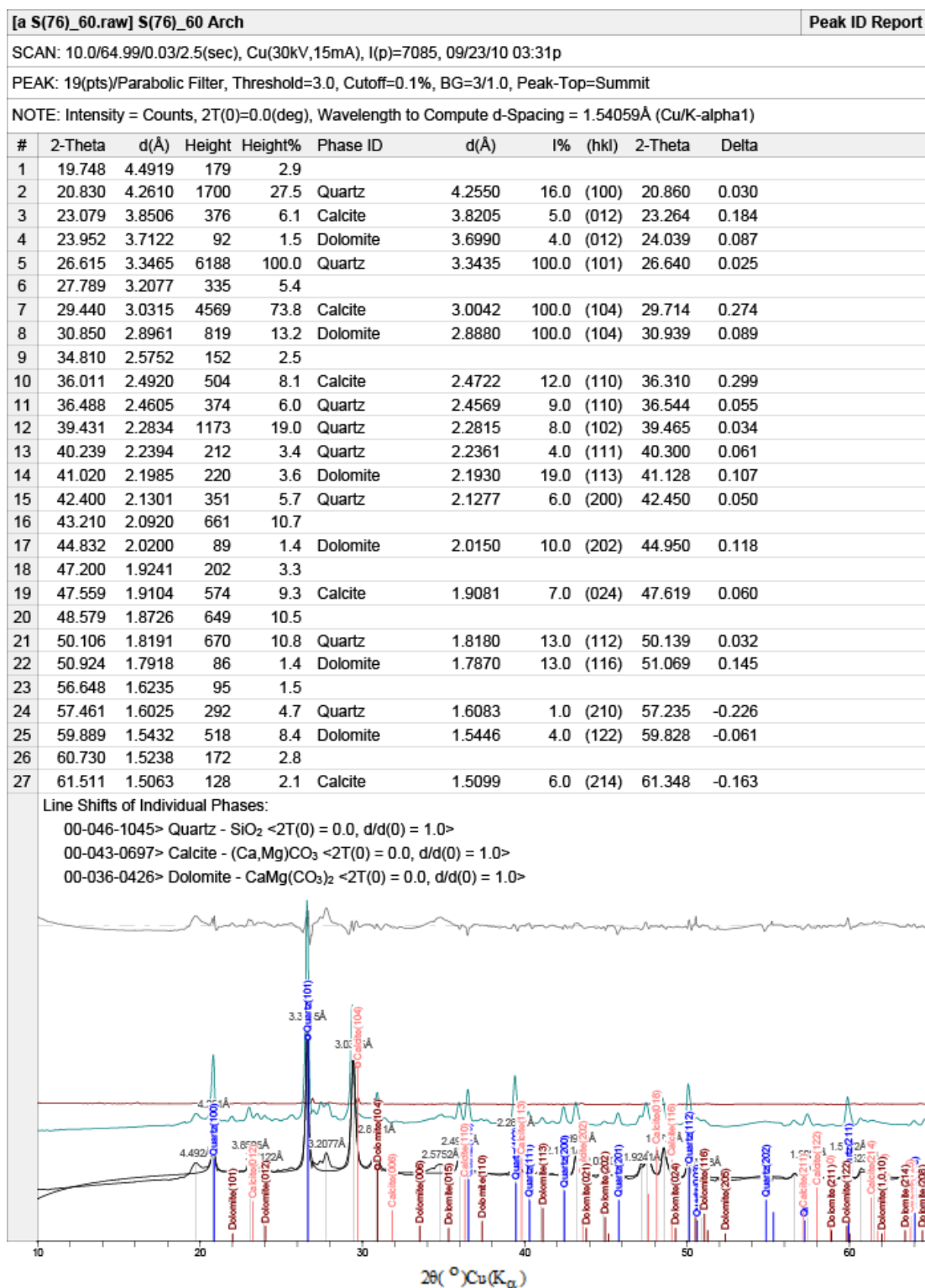


Figure A.5 – Quartz + Calcite Magnesian + Dolomite Peak ID Report.

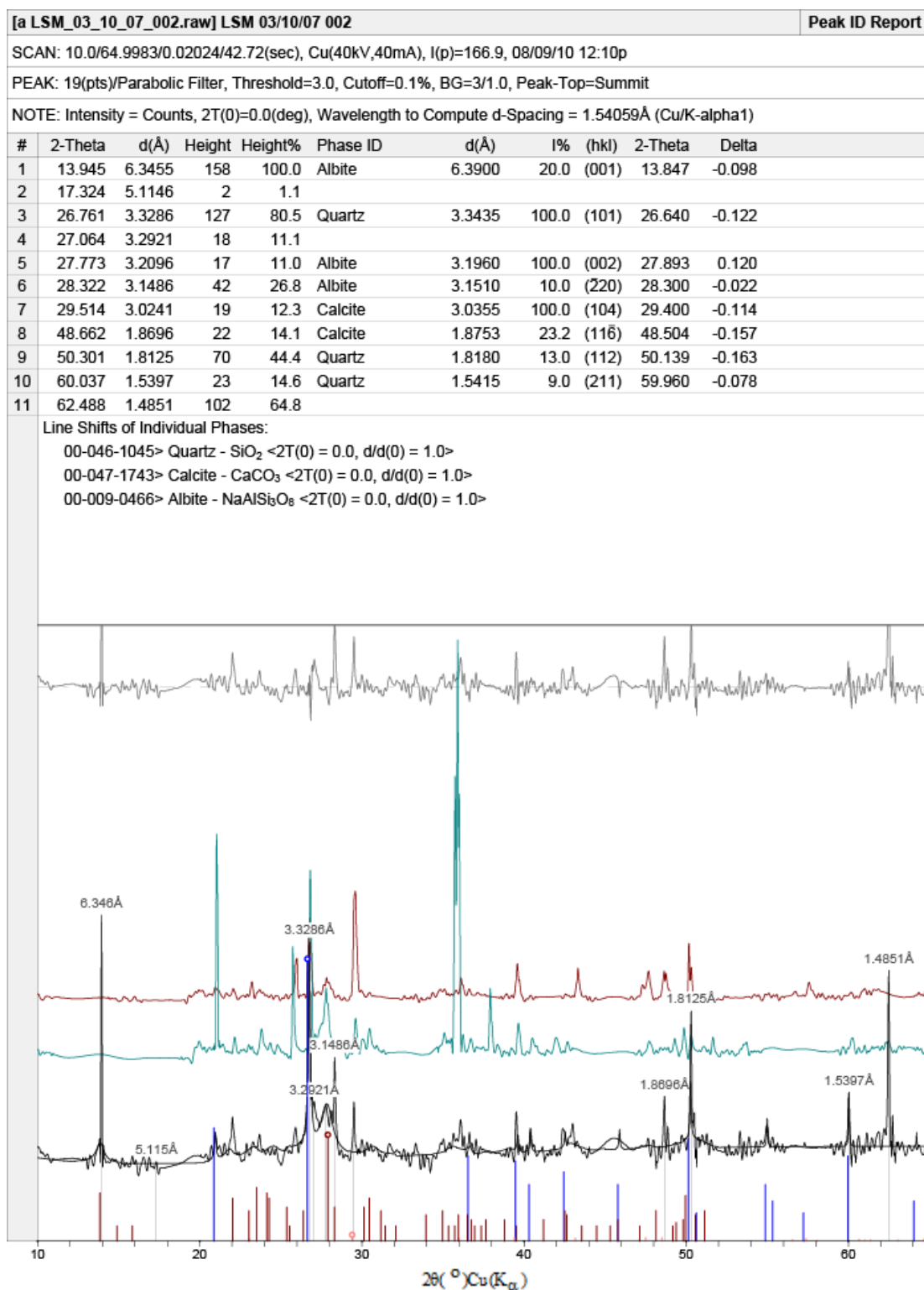


Figure A.6 – Quartz + Calcite + Sodium Plagioclase Peak ID Report.

Curriculum Vita

Porfirio Peinado Coronado was born on September 15, 1967 in Los Mochis, Sinaloa, México. The second son of Refugio Coronado Osuna and José Peinado Ramírez, Porfirio concluded his high school studies at the Centro de Bachillerato Tecnológico Industrial y de Servicios 43 in Los Mochis, Sinaloa, in the year 1985. He entered the Instituto Tecnológico de Los Mochis in the year of 1985, where he obtained a degree in chemical sciences, with a minor in industrial engineering in May of 1989. Porfirio entered the graduate program at UTEP in Environmental Engineering in the fall of 2005, and obtained his masters of science degree in December 2007, presenting a thesis entitled “Water quality factors affecting the restoration of the Río Grande: El Paso/Juárez Region.” During his graduate studies he continued working in the Civil Engineering and Geological Science departments as a teaching and research assistant. Porfirio entered the Environmental Science and Engineering Doctoral program at UTEP in spring 2008, where he continued working as a teaching and research assistant. Porfirio has presented his doctoral research at several conferences in the U.S. and Mexico.

Permanent address: Bosque Bonito 7139

Fraccionamiento Tecnológico, Ciudad Juárez, Chih., Méx. C.P. 32500

Email: pilocoronado@hotmail.com